Determining The Excited State Properties of Novel Aryleneethynylenes

COOMBS, BENJAMIN,ALEXANDER

Determining The Excited State Properties of Novel Aryleneethynylenes

Benjamin Alexander Coombs

A Thesis presented for the degree of
Doctor of Philosophy

Supervised by Dr Andrew Beeby
Department of Chemistry
University of Durham
England

July 2010

Determining The Excited State Properties of Novel Aryleneethynylenes

Abstract

The first chapter introduces the area of phenyleneethynylenes. The parent of the novel systems presented here, 1,4-bis(phenylethynyl)benzene (**BPEB**), is an extended π–conjugated system, known for its interesting structural, optical and electronic properties. Derivatives of this system have demonstrated great potential in the field of organic electronics, particularly as components in OLEDs, PV cells and molecular wires. An introduction to the phenyeneethynylenes and fundamentals of various photophysical properties is presented, along with a brief overview of several synthetic methodologies available for the preparation of arylethynylenes. In Chapter 2 the equipment and methods used for the determination of the excited state properties of the compounds are discussed.

The preparations and excited state study of a series of thiophene–based aryleneethynylene oligomers are reported in Chapter 3. This chapter begins with a short review of thiophene based molecules followed by a discussion of the synthetic procedures available for the preparation of the various dibromoheteroarene cores. The work presented here has allowed comparisons to be drawn with the photophysical and structural properties of the known 2,5-bis(phenylethynyl)thiophene, upon modification of the central thiophene core. Oligomers containing an oxidised thiophene (thiophene-1,1-dioxide) displayed significantly red–shifted absorption and emission bands compared to those of the parent and derivatives, indicating significant ICT in the excited state. Furthermore, the lifetimes of the thiophene-1,1-dioxide systems were significantly longer than those of the non–oxidised derivatives, resulting in much higher rates of fluorescence decay (k_f). Quantum yields for this series of thienyl arylethynylenes varied from 3 % to 43 %. Several systems featuring peripheral substituents (OMe and CN) were prepared to probe the effect of electron donating and withdrawing groups on the photophysical properties of the oligomers. Also, two of the oligomers prepared featured a break in the conjugation across the thiophene derivative and one of these molecules exhibited phosphorescence upon

cooling to 77 K, allowing direct measurement of the triplet energy.

Chapter 4 begins with a short review of the diazole heterocycles, to illustrate the potential applications of these systems. The novel oxygen-containing diazoles were compared to their sulfur–containing analogues, which have been reported previously in the literature. The benzofurazan and benzothiadiazole–based oligomers have been appended with peripheral substituents in the form of electron–donating and electron–withdrawing groups (R = H, *t*–Bu, OMe, NH_2, CO_2Me and CN), in an attempt to monitor the effect of increasing electron donation and electron withdrawing effects on these already electron–deficient oligomeric systems. 2,5-bis(Phenylethynyl)-1,3,4-oxadiazole exhibited high energy absorption and emission maxima, as well as relatively narrow absorption and emission profiles, in contrast to the broad profiles of the other electron–deficient systems. The benzofurazan series exhibited broad, unstructured emission profiles, yet all systems displayed two distinct absorption bands. Fluorescence quantum yields of these compounds were generally very high; for 4,7-bis(4-*t*-butylphenylethynyl)benzofurazan, $\phi_f = 0.96$. All benzofurazan and benzothiadiazole arylethynylenes displayed fluorescence lifetimes of several nanoseconds.

Chapter 5 presents a comparison of the photophysical properties of selected molecules from Chapters 3 & 4 and **BPEB**, as well as suggestions for future work.

All novel systems have been purified and characterised using typical methods (^{1}H and ^{13}C NMR spectroscopy, accurate mass spectrometry, melting point, and elemental analysis and crystallographic structure determination where possible) and their excited state properties have been probed using photophysical methods (including room and low temperature UV–vis absorption and fluorescence spectroscopy and fluoresence quantum yields and lifetime). *Ab initio* calculations have afforded optimised geometries which have been compared to molecular structures determined using X–ray diffraction and vibrational spectroscopy. TD–DFT calculations have been used to rationalise the observed photophysical spectra, helping with assignment of bands in the fluorescence spectra, aiding the determination of states responsible for absorption and emission.

Declaration

The work in this thesis is based on research carried out under the supervision of Dr Andrew Beeby, in the Department of Chemistry, University of Durham, England. No part of this thesis has been submitted elsewhere for any other degree or qualification and it is all my own work unless referenced to the contrary in the text.

Acknowledgements

Through-out the last three and a half years, I have been lucky enough to work with so many great people and a lot of them have become more than just colleagues over this time.

I would like to extend my warmest thanks to my supervisor Dr. Andrew Beeby, who has guided me and offered sage words of advice over the course of this PhD (or a beer in The Vic). Secondly, thanks to Dr. Lars-Olof Pålsson for all his help with photophysics and general support, and Prof. Paul Low and Dr. Mark Fox for their help with cyclic voltammetry. For fruitful discussions regarding crystallography, I must thank my friends Dr Michael Probert and Dr Hazel Sparkes, and for equally helpful discussions regarding DFT calculations my thanks go to Dr Michael Peach.

Now for my thanks to the cast and crew of CG 7/11. To Lucas, Adam, Squirrel and Geri, and all the fourth years; it was a pleasure to work with you. I also append to this list the honorary group–members Robek and Kate, for all the coffee mornings.

Furthermore, I must thank all my other friends in the department, past and present: in the GS lab (Ian, Jess, Chris and Matt) the PJL lab (Neil, Phil and Jules), the PWD lab (Pippa, Antonis and Dan), CG1 (Nick, John D., Jonathon S., Marie, Kathryn, Matt, Marvis, Pete, Lisa, Louise, Pierpaulo and Will), XRD (Hazel and Mike) and the IRC (Seb, Greg, Will, Dave and Barry).

Also, a huge thank you goes out to the various service departments that I have begged and pleaded to do the impossible and have always endeavoured to make me look better than I am — Alan, Catherine, Ian and Neil from NMR; Mike, Lara, Jackie and Dave in Mass Spec; Judith and Craig in CHN; Hazel and Amber in

crystallography; Malcolm and Pete the Glass Blowers (handy to have a lab near!); Neil, Scott and Jim (mechanical work–shop); Barry, Omer and Kelvin (electrical workshop); and all the other lab–technicians and attendants, including the Stores' folks (Liz, Tony, Phil, Jeff and Gary), and Miriam, Claire, Jean and Joan. And never forgetting the department secretary, Andrew Unwin, for chats on everything from f–stops to iPhones.

On a personal note, I give never–ending thanks to my family; Mum, Dad and Vic, thank you for your enduring support — both emotional and financial!

Lastly, to Alice, without whom the last three years would have been a great deal harder. You have helped me in so many ways, and made it so much fun Al, thank you.

Abbreviations

Å	Angstrom, 1×10^{-10} m
A	Absorption
antTT	Thieno[3,2-*b*]thiophene (*anti* conformation)
antXTT	Thieno[3,2-*b*]thiophene (*anti* conformation; non conjugated)
ASAP	Atmospheric Solids Analysis Probe
ASCII	American Standard Code for Information Interchange
Bf	Benzofurazan
BHJ	Bulk heterojunction
BPE	bis(Phenylethynyl)-
BPEAn	9,10-bis(Phenylethynyl)anthracene
BPEantTT	2,5-bis(Phenylethynyl)thieno[3,2-*b*]thiophene
BPEantXTT	3,6-bis(Phenylethynyl)thieno[3,2-*b*]thiophene
BPEB	1,4-bis(Phenylethynyl)benzene
BPEBf	4,7-bis(Phenylethynyl)benzofurazan
BPEBtd	4,7-bis(Phenylethynyl)benzothiadiazole
BPEEDOT	2,5-bis(Phenylethynyl)-3,4-ethylenedioxythiophene
BPEEDOTO$_2$	2,5-bis(Phenylethynyl)-3,4-ethylenedioxythiophene-1,1-dioxide
BPET	2,5-bis(Phenylethynyl)thiophene
BPETd	2,5-bis(Phenylethynyl)-1,3,4-thiadiazole
BPETO$_2$	2,5-bis(Phenylethynyl)thiophene-1,1-dioxide
BPEOx	2,5-bis(Phenylethynyl)-1,3,4-oxadiazole
BPEsynTT	2,5-bis(Phenylethynyl)-3,4-dimethylthieno[2,3-*b*]thiophene

BPyEBtd	4,7-bis(4-Pyridylethynyl)benzothiadiazole
bs	Broad singlet
Btd	Benzothiadiazole
BuLi	Butyl lithium
c	Concentration
calcd.	Calculated
CL	Chemiluminescence
cm^{-1}	Reciprocal centimeters
CN	Cyano
CO_2Me	Methylester
CP–MAS	Cross Polarised Magic Angle Spinning
cps	Counts per second
CV	Cyclic voltammetry
d	Doublets
DCM	Dichloromethane
dd	Doublet of doublets
°C	Degrees, celsius
δ	Chemical shift
ΔE	Change in energy
DFT	Density Functional Theory
DMD	Dimethyldioxirane
DMF	Dimethylformamide
DMSO	Dimethylsulfoxide
DNA	Deoxyribonucleic acid
DTT	Dithienothiophene
$E_{1/2}$	Half wave potential
ECHB	Electron conducting hole blocking
EDO	Ethylenedioxy-
EDOT	3,4-Ethlenedioxythiophene
$EDOTO_2$	3,4-Ethylenedioxythiophene-1,1-dioxide
EI	Electron ionisation

EL	Electroluminescence
EPA	Solvent mixture of ethanol/2-methylbutane/diethylether (2:5:5)
E_{pa}	Anodic peak potential, in Volts
E_{pc}	Cathodic peak potential, in Volts
ε	Extinction coefficient
ϵ	Dielectric constant
EQE	External quantum efficiency
E_{red}	Reduction potential, in Volts
ES	Electrospray
ESD	Estimated standard deviation
eV	Electron Volts
f	Oscillator strength
FcH	Ferrocene
FEM	Field effect mobility
FET	Field effect transistor
FRET	Fluorescence resonance energy transfer
g	Gram
GC	Gas Chromatography
GC MS	Gas Chromatography Mass Spectrometry
GPC	Gel Permeation Chromatography
h	Plancks constant, 6.63×10^{-34} m^2kgs^{-1}
HMPT	Hexamethylphosphorous triamide
HOMO	Highest occupied molecular orbital
Hz	Hertz
I_0	Incident intensity
I_t	Transmitted intensity
IC	Internal conversion
ICT	Intramolecular/internal charge transfer
IP	Ionisation potential
I_p	Peak current
IR	Infrared

ISC	Intersystem crossing
ITO	Indium tin oxide
IUPAC	International Union of Pure and Applied Chemistry
JY	Jobin-Yvon
K	Kelvin
k_f	Rate of radiative decay
k_{IC}	Rate of internal conversion
k_{nr}	Rate of non–radiative decay
l	Path length
L	Litres
λ	Wavelength, in nm
λ_{max}	Maximum wavelength
LCD	Liquid Crystal Display
LDA	Lithium diisopropylamide
LE	Locally excited
LED	Light Emitting Device (or Diode)
LUMO	Lowest unoccupied molecular orbital
M	Molar, concentration
m	Multiplet
M.P.	Melting point
MALDI	Matrix–Assisted Laser Desorption/Ionisation
m-CPBA	*meta*-Chloroperoxybenzoic acid
MEH-PPV	Poly[2-(2-ethylhexyloxy)-5-methoxy-1,4-phenylenevinylene]
mg	Milligram, 1×10^{-3} grams
MHz	Megahertz, 1×10^{3} Hz
μs	Microseconds, 1×10^{-6} seconds
mL	Millilitres, 1×10^{-3} litres
mmol	Millimoles, 1×10^{-3} moles
MNBDA	4-(N -Methylamino)-7-nitro-2,1,3-benzooxadiazole
mol	Moles
mol%	Percentage by mole

MS	Mass spectrometry
μ	Transition dipole moment
mV	Millivolts, 1×10^{-3} Volts
n	Refractive index
n/a	not available
NBD	4-Nitrobenzooxadiazole/4-nitrobenzofurazan
NBS	N-Bromosuccinimide
n-BuLi	n-Butyl Lithium
ND	Neutral density
NH_2	Amino
NIS	N-Iodosuccinimide
nm	Nanometer, 1×10^{-9} m
NMe_2	N,N-Dimethylamino
NMP	N-Methyl-2-pyrrolidone
NMR	Nuclear Magnetic Resonance
NO_2	Nitro
$\bar{\nu}$	Frequency, in cm^{-1}
O.D.	Optical density
OLED	Organic Light Emitting Device (or Diode)
OMe	Methoxy
Ox	1,3,4-Oxadiazole
P3HT	Poly(3-hexylthiophene)
PAE	Poly(aryleneethynylene)
PAV	Poly(arylenevinylene)
PBD	2-(4-Biphenylyl)-5-(4-*tert*-butylphenyl)-1,3,4-oxadiazole
PBTCT	Poly(2,5-bis(3-alkylthiophen-2-yl)thieno[2,3-b]thiophene
PBTTT	Poly(2,5-bis(3-alkylthiophen-2-yl)thieno[3,2-b]thiophene
PCBM	Phenyl C_n-butyric acid methyl ester
PEDOT	Poly(3,4-ethylenedioxythiophene)
PET	Photoinduced electron transfer
ϕ	Quantum yield

PL	Photoluminescence
PLED	Polymer Light Emitting Device (or Diode)
PLQY	Photoluminescent quantum yield
PMMA	Poly(methyl methacrylate)
PPA	Polyphosphoric acid
PPE	Poly(phenyleneethynylene)
PPV	Poly(phenylenevinylene)
ps	Picoseconds, 1×10^{-12} seconds
PSS	Poly(styrene sulfonic acid)
PV	Photovoltaic
RAM	Random Access Memory
RDS	Rate determining step
s	Seconds
S_0	Singlet ground state
S_n	Singlet excited state
SAM	Self Assembled Monolayer
SBD-F	Ammonium-7-fluorobenzo-2-oxa-1,3-diazole-4-sulfonic acid
STM	Scanning Tunnelling Microscope
SWNT	Single walled nanotube
synTT	Thieno[2,3-*b*]thiophene (*syn* conformation)
T	Thiophene
t	Triplet
T_0	Triplet ground state
T_n	Triplet excited state
TAC	Time-to-Amplitude Converter
τ	Lifetime
t-Bu	*tert*-Butyl
TCSPC	Time Correlated Single Photon Counting
Td	1,3,4-Thiadiazole
TD-DFT	Time Dependent Density Functional Theory
TFAA	Trifluoroacetic anhydride

TFT	Thin Film Transistor
THF	Tetrahydrofuran
TLC	Thin Layer Chromatography
TMSA	Trimethylsilylacetylene
TMSCl	Chlorotrimethylsilane
TNT	Trinitrotoluene
TO_2	Thiophene-1,1-dioxide
TR^3	Time Resolved Resonance Raman
UHP	Ultra high purity
UV	Ultraviolet
V	Volts
v/v	Volume/volume
vis	Visible
VR	Vibrational relaxation

Contents

List of Figures

Nomenclature System

Most of the systems presented in this work consist of the bis(phenylethynyl)– motif, and as such have the prefix:

BPE –

To this is appended the abbreviation for the relevant heterocycle using, where possible, literature precedents for abbreviating the name. Thus, thiophene is appreviated to **T**, giving, for 2,5-bis(phenylethynyl)thiophene;

BPET

and 2,5-bis(phenylethynyl)thiophene-1,1-dioxide becomes:

BPETO$_2$

Several systems in Chapter 4 don't feature the standard bis(phenylethynyl)-heterocycle motif. However, these are named using a similar convention to that described above. For instance 4-(phenylethynyl)benzofurazan becomes:

PEBf

And 1,4-bis(benzofurazanethynyl)benzene becomes:

BBfEB

For systems which feature peripheral substituents, such as electron–donating and withdrawing groups, the nomenclature system appends a standard abbreviation for these systems on to the end of the code. Thus, 4,7-bis(4-methoxyphenylethynyl)-benzofurazan becomes:

BPEBf.OMe

where **OMe** represents the methoxy substituent. Unsubstituted derivatives do not feature a suffix, *i.e.* **BPEX.H** is denoted **BPEX**.

This nomenclature has also been applied to several systems described in the literature. These are listed in the table of abbreviations, but will not be outlined in **bold**.

For a complete list of the compounds abbreviated titles refer to Appendix A on the laminated card, which also includes chemical structures and IUPAC names.

Things should be made as simple as possible, but not any simpler.

Albert Einstein (1879—1955)

1

The Excited State Properties of Highly Conjugated Molecules

1.1 Introduction

Highly conjugated molecules feature a system of saturated and unsaturated carbon-carbon bonds. Electrons in these compounds are effectively free to move around the molecule, delocalized in a π–electron 'cloud'. This affords molecules in possession of such a system interesting and useful optical and electronic properties. They absorb and emit electromagnetic radiation at useful wavelengths, such as in the visible and ultra–violet (UV) region. Furthermore, under the right conditions, they can conduct charge. These two functions have led to a significant amount of research into the properties of myriad conjugated species in an attempt to exploit them in applications as diverse as luminescent biological sensors and molecular scale wires.

1,4-bis(Phenylethynyl)benzene (Figure 1.1, **BPEB**) is an aryleneethynlene, and one example of a compound which exhibits the properties described above. It is a highly conjugated compound consisting of phenyl–ethynyl repeating units. It possesses an extended delocalized π–electron system and a linear, rigid molecular structure. These properties have afforded it great potential in the aforementioned applications, and as such a great deal of literature exists on phenylethynyl-type oligomeric systems.

Figure 1.1: 1,4-bis(Phenylethynyl)benzene (**BPEB**).

The work presented in this thesis demands a review of the literature pertaining to phenylethynylene systems. This chapter will therefore introduce phenylethynylenes and their potential applications, including as components of organic light emitting diodes and photovoltaic cells, and as molecular wires. This will be followed by a brief introduction to the photophysical investigation of the excited states of these systems and the use of DFT methods to understand experimental observations. This chapter is concluded by a review of several synthetic routes to the acetylene–containing systems.

1.2 Organic electronics

One area of nanotechnology that has caught the attention of the main stream media is that of molecular, or even organic, electronics. 'Organic electronics' is an umbrella term for organic compounds which have been designed with the intention of being incorporated into some device which will ultimately perform an electronic–based task. Electronic conduction through a non–metal–containing compound is possible through extended π–conjugation. In 1977 polyacetylene was shown to conduct electrical charge, albeit with doping. [1] This was the first example of a conducting polymer – a semiconductor. One of, if not *the*, most important uses of semiconductors is in the manufacture of computer chips.

1.2.1 Conductors, semiconductors and insulators

In a metallic material valence electrons are said to occupy molecular orbitals delocalised throughout the solid, according to the tight-binding approximation. [2] In a metal the molecular orbitals can be considered to form a continuous band. The simplified band structure of a metal is presented in Figure 1.2. At T= 0 K only the lower half of the band is filled with electrons, but at temperatures above absolute zero electrons can be excited into empty orbitals lying just above in energy, purely by thermal motion of the atoms. These mobile electrons give rise to conduction. Paradoxically, heating of a metal lowers the conductivity, as thermal excitation of the atoms causes more collisions of the electrons. This lowers their efficiency at conducting charge. A metallic conductor experiences a decrease in conductivity with temperature increase.

In an insulator, the valence and conduction band are separated by a gap – a *band–gap* – that is too large to allow population of the conduction band, rendering it non–conducting.

Unlike a metal, a semiconductor experiences an *increase* in conduction with increased temperature. At T = 0 K the bands are not continuous and the valence band and conduction band are separated by a band–gap, similar to an insulator. However, as the temperature is increased electrons can be excited across the gap,

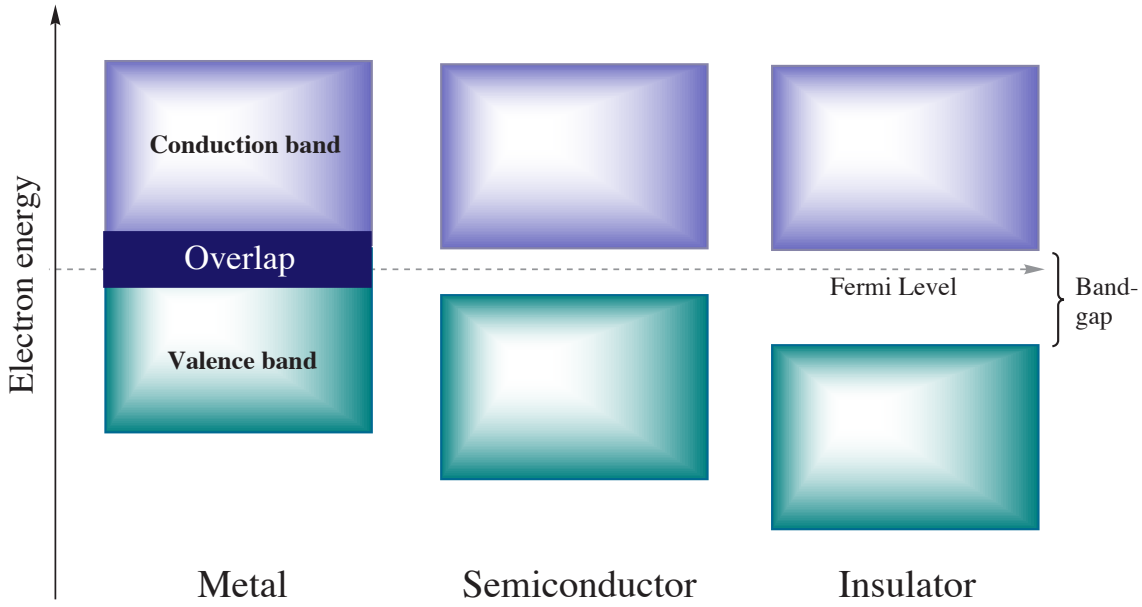

Figure 1.2: Schematic representing band–gap of a metal, semiconductor and insulator.

occupying the empty orbitals in the upper band. The material is now a conductor.

As well as using temperature to improve semiconductivity, dopants – or 'impurities' – may be used to increase the number of free charge carriers (electrons or holes) in the semiconductor:

- a dopant with fewer electrons than the host forms a narrow band capable of accepting electrons from the host, enabling mobile holes to conduct charge – a **p–type** semiconductor
- a dopant containing more electrons that the host forms a band capable of donating electrons to the conduction band, enabling the mobile electrons to conduct charge – an **n–type** semiconductor

Semiconductors in computer chips

Today's computers use a microprocessor – a 'chip' – composed of billions of silicon–based transistors (see Figure 1.3). The transistor is a component in an electronic circuit which can be used to amplify or switch electronic signals. This allows a transistor to act as a switch, with the electronic signal either 'on' (1) or 'off' (0).

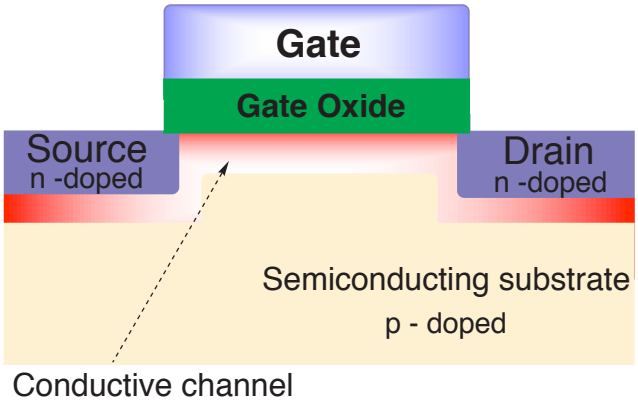

Figure 1.3: Schematic of a basic field effect transistor.

Currently transistors are built on silicon substrates, produced by photolithography; a process which uses high intensity UV light to etch a photo–resistive layer on a semiconducting material. The photo–resist layer is exposed to light through a masking layer, which acts as a template. Consequently, selected areas of the resist layer are degraded by light, washed away, allowing for the semiconductor – a silicon wafer – underneath to be patterned according to the template. This advanced form of lithography has allowed features to be cut accurately at the nanometer scale. Intel's Atom processor has features photolithographically cut to 45 nm, and the recently announced next–generation will have 32 nm features.

These improvements in technology have afforded chip–manufacturers the ability to continually increase the transistor–density of their processors. This is referred to as **Moore's Law**, after Dr G E Moore,[1] who first realised the potential for silicon chip design. In 1965 he published an article in the journal Electronics [3] in which he foresaw a year–on–year increase in transistor density. He predicted that approximately every 18 months the transistor–density would double. This prediction has driven the industry's roadmap for the past 40 years to continually improve manufacturing techniques.

While it has usually been the engineering and improved lithographic technology that have been responsible for the manufacture of ever–smaller silicon–based transistors, quantum tunnelling effects are now impeding further improvements. As

[1]Originally a director at the Research and Development Laboratories of Fairchild Camera and Instrument Corporation's Semiconductor division, Dr. G. E. Moore went on to found Intel, the world's premier computer processing chip designer and manufacturer

decreasing transistor dimensions force a commensurate shrinkage of their features, the gate–oxide layer – a thin strip of insulating material separating the gate electrode from the source and drain electrodes – is becoming so thin it is possible for electrons to tunnel through, negating the insulating nature of the material.

This problem has meant that, in order to avoid deviating from Moore's Law, different materials are being examined and investigated for possible solutions. Non-organic solutions include the use of metals with higher insulating properties, such as hafnium, which would allow a continuation of Moore's Law.

Organic components of electronic circuits have been prepared and published in the literature, and all rely on their ability to conduct charge. Of those, conjugated polymers are technically proconductors and as mentioned above, for polyacetylene, require doping to oxidise or reduce the proconductor to a conductor. [4] This allows them to be classified as organic semiconductors. Without dopants the conjugated organic molecule acts as an insulator.

Figure 1.4: Picture of an OLED–based screen now commercially available.

Since the discovery of polyacetylene's potential as a semiconductor, different compounds and dopants have been investigated, molecules and deposition techniques developed and improved, and now organic polymers are in use as field–effect transistors in various applications, including molecular wires, photovoltaic cells, and organic light emitting diode (OLED) displays (see Figure 1.4). The use of organic

electronics may well afford, in the future, engineers the ability to build electronic devices from single molecules. This "bottom–up" approach could enable the manufacture of infinitesimally small electronic components, likely unobtainable using conventional "top–down" methods.[2]

1.2.2 The bigger picture

The myriad of electronic capabilities of organic compounds necessitates, where possible, a bottom-up approach to the engineering of devices as well as the intelligent design of compounds, at the molecular level, to fully harness and help exploit a compounds natural properties. Two such fields of research which are seeing potentially enormous benefit from technologies based on materials and devices which are cheap to synthesize and process at the bulk scale are OLED screens (see Figure 1.4 and section 1.3.1, page 8) and organic photovoltaic cells (see section 1.3.2, page 10).

The optical properties of these compounds are similarly deserving of investigation and exploitation. Electroluminescence in organic compounds is the phenomenom responsible for emission of light from OLEDs (see Figure 1.5). Furthermore, photoluminescent–active 'fluorophores' can be attached to binding species to form biological sensors, detectors and probes, capable of altering the emission upon binding of an analyte.

In the next section a review of selected literature is presented, which describes attempts to harness the excited state properties of various highly conjugated compounds in several areas of science. The review will not be exhaustive as this is one of the most prolifically and fervently researched areas of materials science – there are several excellent reviews by Bunz, [5] Swager, [6, 7] and Michl [8] available on arylethynylenes and their properties and applications – so presented here are selected articles to demonstrate the potential applications of aryleneethynylene–based materials.

[2] In 1959 Richard P. Feynman gave a lecture entitled "There's plenty of room at the bottom", in which he reasoned that their current scope for miniaturization was nothing compared to what was technically possible. Feynman is regarded by many as the father of nanotechnology.

1.3 Applications of highly conjugated molecules

Yamamoto and co–workers were among the first to publish on the optical properties of various aryleneethynylene polymers. [9] Yamamoto's work was initiated by an interest in polymers with high π–conjugation. Several different poly(aryleneethynylene) (PAE) type polymers – which had received significantly less interest than the structurally similar poly(arylenevinylene) (PAV) polymers up until then – were synthesised using Sonogashira cross–coupling methods. In solution the polymer PPE exhibited a bluish–purple fluorescence, yet no conduction was observed. Further work by Yamamoto on thiophene–containing arylethynylenes is presented later (section 3.1.6, page 62).

In the early 1990's Burroughes *et al.* published their work on the development of a light emitting diode. [10] This work was important because the emissive layer was composed of poly(phenylenevinylene) and heralded the start of research into OLEDs.

1.3.1 OLEDs

Organic electroluminescence (EL) is the phenomenon being utilised in the application of OLEDs. EL is the emission of light due to the passage of current through an organic material. In an electroluminescent device, electrons are injected into the lowest unoccupied molecular orbital (LUMO) of the organic material forming radical anions. Electrons are also removed from, or holes injected into, the highest occupied molecular orbital (HOMO) to form radical cations. When an electric field is applied these charges move towards each other, hopping from molecule to molecule in the polymeric material and, upon combining, form a local excited state. This excited state can be either singlet or triplet in nature, in the ratio of 1:3 respectively.[3] In organic polymeric materials only the singlet state emits light.

As shown in Figure 1.5 a typical OLED has at least three layers, but often four,

[3]Due to this inherent 25% efficiency limitation, many recent organic OLEDs also incorporate a heavy metal, such as iridium [11] to enhance spin–orbit coupling. This allows intersystem crossing (ISC, see section 1.4.1, page 19), which affords radiative decay from a triplet state. These will not be considered in this review.

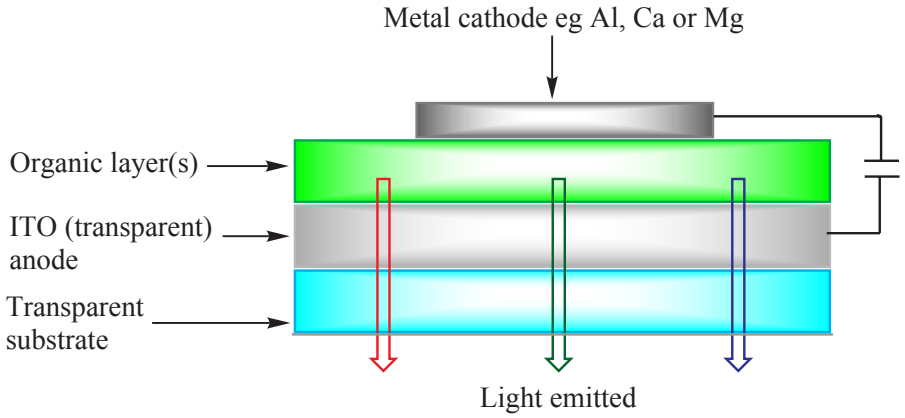

Figure 1.5: Illustration of a basic OLED.

comprised of:

- a cathode – injector of electrons;
- a conducting polymer sandwiched in the middle – the tunable and interesting part (see Figure 1.5, GREEN layer);
- a layer which confines charge carriers (within the GREEN layer, but a separate component to the emissive layer);
- a transparent anode (typically indium tin oxide) – injector of holes.

Brown *et al.* used the conducting polymer poly(phenylenevinylene) (PPV) in such a device (employing an oxadiazole derivative for charge–carrier confinement - see section 4.2.1). [12] PPV is a polymer of repeating phenyl rings linked through a vinylene moiety (see Figure 1.6a).

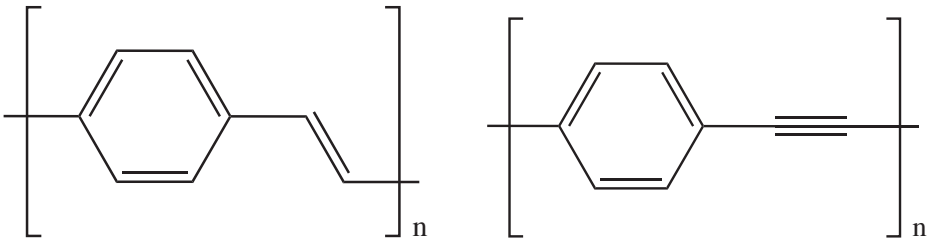

(a) Poly(phenylenevinylene) (PPV) (b) Poly(phenyleneethynylene) (PPE)

Figure 1.6: Monomers of the structurally similar polymers.

The structural similarities with PPE (Figure 1.6b) are clear, however, the aryl-ethynylene bond causes it to perform poorly as a conductor. Swager highlighted

the concern over the conduction of phenyleneethynylene–based polymers, explaining that poly(phenyleneethynylenes) (PPEs) contain a greater alternation in bond lengths (triple–single as well as double–single), compared with their vinyl-linked analogue (double–single only). [13] This increased alternation increases the band gap whilst decreasing the band width, thus requiring the PPEs to be doped to display high conductivities.

Examples exist in the literature of OLEDs that have been developed incorporating aryleneethynylene-based compounds. Bryce and co-workers investigated the inclusion of 2,5-di(aryleneethynyl)pyrazine derivatives, prepared using Sonogashira cross–coupling techniques, as a dopant in a single layer device with MEH-PPV as the emissive layer. Bryce reported enhanced external quantum efficiencies of 0.07%, attributed to the electron-transporting ability of the pyrazine system. [14] Adachi and co–workers developed diphenyl substituted bis(phenylethynyl)benzene systems using a double-elimination protocol; coupling dialdehydes with β–substituted sulfones. These systems exhibited blue emission for use in OLEDs, which are seen as the most problematic colour emitter due to their high energy. [15]

1.3.2 Organic photovoltaic devices

Organic photovoltaic devices promise the delivery of cheap energy, harvested from solar rays using robust and flexible cells. The most promising system is based on the bulk heterojunction (BHJ) device. [16, 17] The BHJ works by photoexcitation of an electron–rich species, generating an exciton – an electron–hole pair. This pair diffuses to the interface of the donor–acceptor composite within the active – *i.e.* semiconducting – layer of the BHJ, where the pair can dissociate and act as free charge carriers to transport charge to the appropriate electrodes (see Figure 1.7).

A BHJ device requires semiconducting polymers with a low enough band gap to harness the energy of photons in the solar spectrum, between 1.6 – 1.8 eV (669 nm – 775 nm). This dictates that polymers with band–gaps in the near-IR *i.e.* 1.3 – 1.5 eV (827 nm – 954 nm) are required as the active component in solar cells; to absorb the available energy and, through processes within the photovoltaic cell, generate charge. [17] A second material, typically a fullerene derivative such as [6,6]-

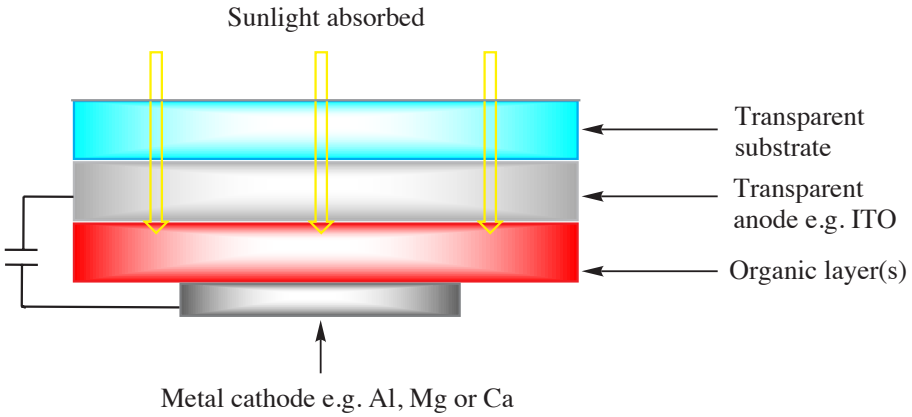

Figure 1.7: Schematic of basic organic photovoltaic cell.

phenyl C_{61}-butyric acid methyl ester (PCBM), acts as the charge acceptor, requiring its LUMO to be below that of the semiconducting polymer layer in order to enable electron transfer. Alteration of the fullerene derivative has been shown to play a part in improving the overall efficiency of these devices. Mühlbacher *et al.* demonstrated a 3 % improvement by swapping $PC_{61}BM$ with $PC_{71}BM$. [17] The polymer layer can also be tuned and this is thought to show the most promise for application in a PV cell (see section 4.3.2).

Chen and co-workers [18] recently published the development of a PV device incorporating a PPE/carbon nanotube composite. In order to exploit the superior performance of single walled nanotubes (SWNT) over PCBM composites as the electron accepting unit within the active layer, Chen synthesized a polymer based on a substituted poly(phenyleneethynylene) system (Figure 1.8). This acted as the donor component, which was designed to over–come the solubility issues of SWNTs through favourable π–stacking interactions. Relative to the bench–mark octyl–substituted polythiophene derivative, a power conversion efficiency improvement of 0.03 % was observed, although the relatively narrow absorption band of the PPE derivative prohibited superior device performance. Chen suggested further derivatisation of the PPE unit would be able to circumvent this. The development of polymers for application in PV devices is discussed in more detail later (see section 4.3.2).

The performance of phenyleneethynylene polymers as the emissive component in devices such as OLEDs and photovoltaic cells is not as promising as that displayed by

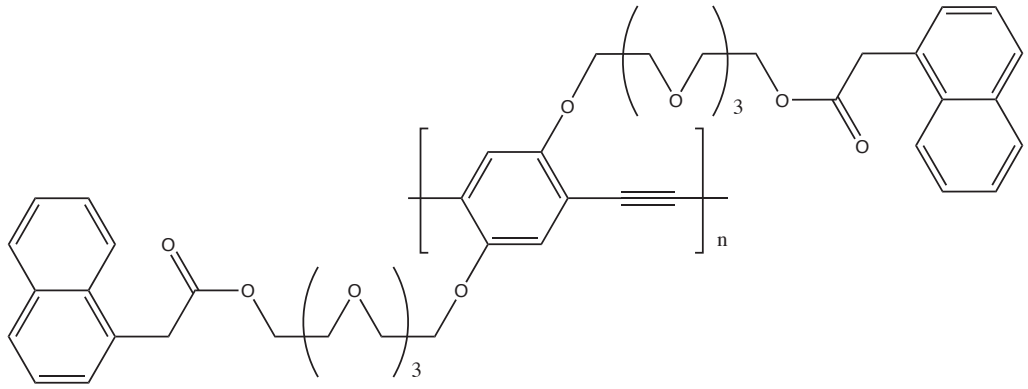

Figure 1.8: PPE—based electron rich unit featured with SWNT in the composite organic active layer of the PV device reported by Chen *et al.*.

systems containing iridium complexes (for OLEDs) and copolymer systems featuring electron-rich/poor units for BHJs (see section 4.3.2). Consequently further work is needed on the derivatisation of PPEs to tune them for use in devices to optimise performance. However, their ability to conduct charge and ease of functionalisation has led them to be superb molecular-wire candidates.

1.3.3 Application as charge transfer devices

The rigid and linear nature of the PPE structure affords it good applicability as the simplest component of an electrical circuit; the wire. Tim Swager first reported use of the poly(phenyleneethynylene) (PPE) molecular wire motif as a means to 'interconnect' multiple receptors, in an effort to enhance the sensitivity of a chemosensor. [19] Using a cyclophane–based receptor to bind paraquat, the monomeric species was compared to the polymeric species; the polymeric system exhibited a 65–fold improvement in sensitivity over the monomeric system.

Since this first success, Swager has developed an effective sensor for the explosive trinitrotoluene (TNT). The pentiptycene moieties (see Figure 1.9), whilst preventing excimer formation and π–stacking, have also been shown to be remarkably sensitive to trace quantities of the volatile vapours from TNT. Upon detection, the polymers fluorescence is quenched, with the polymeric nature of the detector greatly increasing sensitivity. This occurs because of rapid energy transfer in the molecule; if there is detection in any monomer unit then fluorescence of the whole molecule is disrupted.

Furthermore only detection of the desired analyte affects the molecule's emission, since the bulky pentiptycene moiety prevents quenching by aggregation. [20, 21]

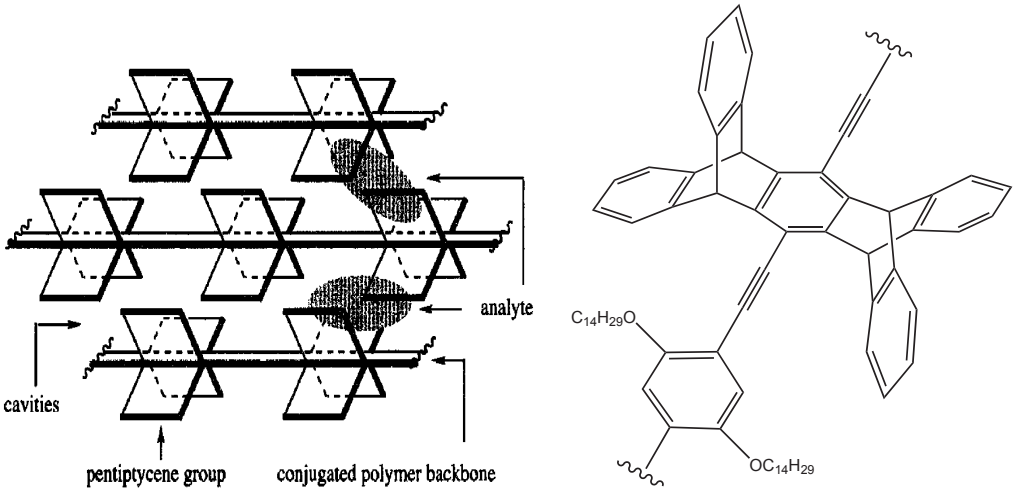

Figure 1.9: Swager's pentiptycene–containing arylethynylenes used for the detection of TNT.**??**

This work by Swager and Yang has prompted two reviews, written by members of Swager's group, on the ability of these molecular wires to produce signal gain, leading them to be termed amplifying fluorescent polymers. [6, 7] It is posited that the signal gain is due to the transportation of electronic excited states, *i.e.* excitons, as opposed to electrons or holes, as seen in conventional electronic circuits.

J M Tour's "Molecular Electronics" [22] provides an excellent introduction to the ideology behind molecular devices but also describes several techniques used to measure the conductivities of molecular wires. The first method, with long molecular wires straddled over gold–coated probes which had been lithographically printed at a separation of 100 Å, was reported to be unreliable. A second method was described, where molecular 'alligator clips' (thioacetates) were used to attach single molecules to a metal surface. This exploited the predilection of sulfur for gold; by attaching thioacetate groups to the end of wire candidates the wire was bound through the sulfur moiety to the gold. This technique was further improved with collaborators Paul Weiss and David Allara, [23] who helped address the need to measure the conductivity of a single molecular wire by insertion at the grain–boundaries of a self assembled monolayer (SAM) of insulating dodecanethiol on gold. The gold then acted as an electrode allowing the tip of a scanning tunnelling microscope (STM) to

be passed across the surface, registering a change in current when over the molecular wire candidate (see Figure 1.10).

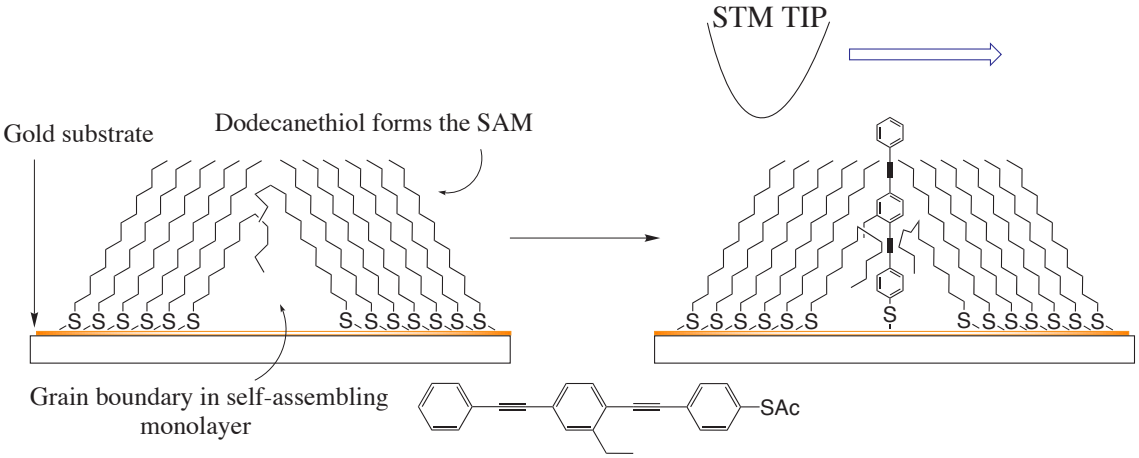

Figure 1.10: Schematic to demonstrate the insertion of a molecular wire within the SAM at the grain boundary, and then the measurement of conduction through the molecular wire by scanning tunnelling microscopy, adapted from Tour's paper. [22]

A third method was also discussed, using a mechanically controlled break junction. [24] By attaching a strip of gold to a silicon wafer and forcing it to bend, Tour, in collaboration with M A Reed, forced a break–junction in the strip of gold, allowing control of the tip–to–tip distance. This method of control allowed manipulation at the sub-atomic level and enabled direct measurement of charge–transport across a single molecule of benzene, bonded through sulfur, to the gold.

Reed and Tour collaborated to prepare systems functionalised with various nitro and amine moieties, which allowed the systems to act as electronically programmable memory devices *i.e.* RAM storage devices, based on single molecules (see Figure 1.11). [25] The device consisted of a SAM of the material which was sandwiched between two gold electrodes using molecular 'alligator clips' of thioacetate connected to gold. The device was operated by storage of high or low conductivity, with the application of a voltage converting low conductivity to high conductivity, with this high conductivity state being a stored bit (of information).

Whilst these articles have demonstrated applications for the described properties of these molecules, they have not explained how these molecules came to possess these properties. Beeby *et al.* have recently published several papers on work

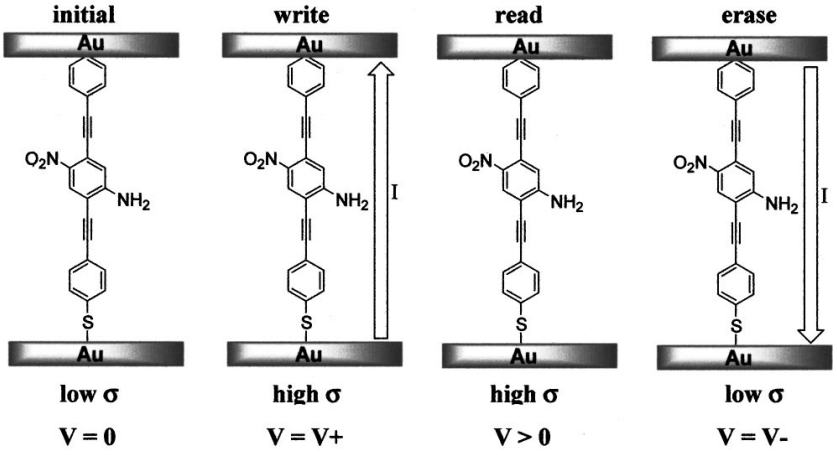

Figure 1.11: RAM storage devices based on single molecules by Reed *et al.* [25]

intended to elucidate the origins of these systems' properties based upon a knowledge of their excited state behaviours. [26, 27]

Excited state studies on bis(arylethynyl)benzene

Work conducted by Beeby *et al.* has attempted to ascertain the structure of **BPEB** in the excited state. It was thought to adopt a quinoidal/cumulenic configuration in the excited state, as predicted by Sluch *et al.* using *ab initio* calculations. [28] However, using time resolved resonance Raman spectroscopy (TR^3), Beeby *et al.* have shown that there is significant acetylene character in the S_1 excited state of **BPEB**, challenging this supposition. [26] The effects of twisting these molecular wire candidates has been highlighted by Cornil *et al.*, [29] who suggested that a twist of the central ring in the three ring system leads to a 'switch off' of conductance. Tour and co-workers have queried this conclusion, however, by demonstrating that alteration of the hybridization at the molecule–surface connection caused changes in conduction in their systems. [30]

To further understand and clarify the effects on twisting of the photophysical properties of the aryleneethynylene systems, Beeby *et al.* reported the preparation of several aryleneethynylene oligomers, heavily–substituted with *tert*–butyl groups, with anthracene as the central aryl group (see Figure 1.12). [27] Synthesis was by Sonogashira cross–coupling of various *tert*–butyl–substituted phenylacetylenes with dibromoanthracene. This produced compounds with an enforced orthogonal twist

in the oligomer backbone and thus potentially limited π—π interactions *c.f.* the unsubstituted parent BPEAn. This featured only a 24.7 ° twist (from crystallographic data analysis) in the terminal rings relative to the central group in the solid state, and close contact between adjacent anthracene moieties, suggesting π—π interactions. Significant configurational change in the excited state is indicated as

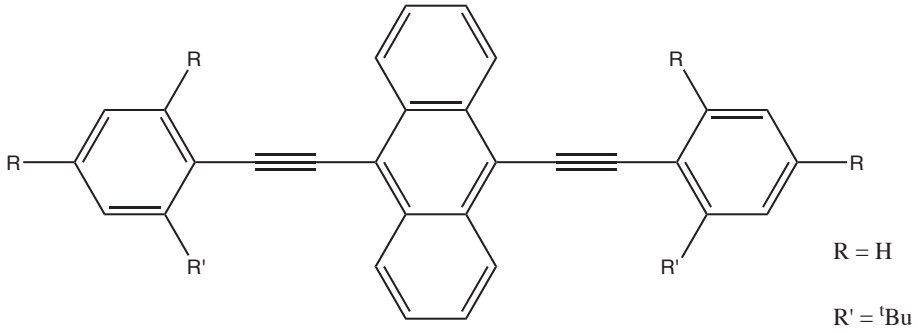

Figure 1.12: 9,10-bis(Phenylethynyl)anthracene, BPEAn, prepared by Beeby *et al.*.

the emission spectrum of the unsubstituted derivative is not the mirror–image of the absorption spectrum. This is expected for these compounds as rotation about the triple bond is possible (see section 1.4). This is also the case for the structure featuring one *tert*–butyl group, suggesting that the barrier to rotation is similarly low in this compound. Both of these systems were studied by optical spectroscopy at 77 K, revealing increased vibrational structure as well as showing the absorption spectra to be a mirror image of the emission spectra, indicating the low temperature and viscous solvent were enforcing planarity in the ground state (see section 1.4.6). However, a derivative featuring *tert*–butyl groups in the phenyl rings' *ortho*–positions showed increased vibrational structure in the absorption spectrum, yet a relatively broad emission band. At low temperature the absorption spectra showed no significant change, yet the emission profile featured enhanced vibrational fine structure and a general blue shift. It was thus demonstrated that at room temperature the compounds – including those featuring sterically demanding substituents – were susceptible to a degree of planarisation. This was only inhibited by dissolution at low temperature in rigid glasses.

1.4 Photophysical methods to elucidate excited state properties of molecules

Conjugated organic molecules typically exhibit luminescence, be it by photo-excitation (photoluminescence, PL), chemical excitation (chemiluminescence, CL), or electrical excitation (electroluminescence, EL). Various applications of these properties have been discussed so far *e.g.* OLEDs using EL and biosensors using CL or PL, which are attributable to the optical and electronic properties of the material. These properties are in turn attributable to the nature of the excited state.

Luminescence spectroscopy allows the excited electronic states to be probed, providing information about the electronic structure *e.g.* the HOMO and LUMO energy levels of the molecule. In the following section an explanation of what and how photophysical measurements can be made to probe the excited state is given, along with what the results from these measurement can help deduce about the compound and the nature of its excited states.

1.4.1 Excitation and the Jablonski diagram

In order for a compound to absorb light, the electric field of the light must interact with a dipole of the molecule, a so–called transition dipole moment, μ. This is different to the permanent ground state dipole of the compound, which is due to a displacement of the electrons' negative charge away from the positive charge of the nuclei. The transition dipole moment describes the displacement of this electronic charge during the transition, *e.g.* $S_n \leftarrow S_0$, and only lasts for the duration of the transition.

The size of the transition dipole moment is related to the oscillator strength, f, of the transition such that:

$$f \propto \mu^2 \tag{1.1}$$

where the oscillator strength, in the classical theory of light as a wave, represents the probability or intensity of an electronic transition. Thus, the oscillator strength is also related to the extinction coefficient, ε, a measure of a chemical's absorption

of light, at a given wavelength, by:

$$f = 4.3 \times 10^{-9} \int \varepsilon \, \mathrm{d}\bar{\nu} \tag{1.2}$$

which indicates that the oscillator strength is also proportional to the integral of the absorption spectrum of a molecule,[4] as a plot of extinction coefficient against wavenumber. This is taken further by:

$$k_f = 3 \times 10^{-9} \bar{\nu}_0^2 \int \varepsilon \, \mathrm{d}\bar{\nu} = \bar{\nu}_0^2 f \tag{1.3}$$

which relates the radiative rate constant to the molar extinction coefficient, and thus also to the oscillator strength. [31] The molar extinction coefficient, ε, is obtained from the absorption, A, of a compound at a known concentration. The Beer-Lambert equation shows that:

$$A = log_{10}\left(\frac{I_o}{I_t}\right) = \varepsilon.c.l \tag{1.4}$$

where A is defined as the logarithm of the intensity of incident light, I_0, divided by the intensity of transmitted light, I_t, and as the product of ε, concentration, c, and path length, l.

A molecule will only absorb electromagnetic radiation of discrete energies which correspond to transitions between energy states for that molecule; the difference in energy, ΔE between the ground state, S_0, of energy E_1 and excited state, S_n, of energy E_2 (Equation 1.5). This can be shown to correspond to a wavelength of light using Equation 1.6, where h is Planck's constant, ν is the frequency of the light and c is the speed of light.

$$\Delta E = |E_2 - E_1| \tag{1.5}$$

$$\Delta E = h\nu = h\frac{c}{\lambda} \tag{1.6}$$

Under normal conditions the ground state is described by the lowest vibration state of the lowest electronic state, the HOMO. This arrangement of electrons determines the nuclear geometry of the molecule. The Born-Oppenheimer approximation dic-

[4]Strictly this is for each transition, *i.e.* $S_1 \leftarrow S_0$, $S_2 \leftarrow S_0$, but often these have a degree of overlap.

tates that an electronic transition takes place within a stationary nuclear framework which does not change during the period of excitation, *i.e.* the molecule does not vibrate during the electronic transition, which is effectively instantaneous ($< 10^{-15}$ s). In accordance with the Franck–Condon principle the promoted electron must populate a state with vibrational levels most closely resembling that of the ground state molecular geometry. Thus, as a photon is absorbed by the molecule, its energy is converted instantaneously (10^{-15} s) into an electronic excitation energy which changes the electronic configuration, and therefore distribution, about the nuclei. However, the nuclei are not displaced and it takes time, of the order of a vibrational frequency, for them to reconfigure to the equilibrium geometry for the new electronic configuration. The absorption transition is shown on the Jablonski diagram (Figure 1.13), as a vertically ascending arrow (blue).

The multiplicity of the excited state can be either singlet or triplet, depending on the overall spin of the electrons within the molecule. If the electrons are parallel, *i.e.* S = 1, the state is termed triplet, and if antiparallel, *i.e.* S = 0, the state is termed singlet. As the Jablonski diagram illustrates, the ground state of a molecule is singlet, and termed S_0. Excited singlet states are termed S_1, S_2, S_3...S_n. The lowest energy triplet state of an organic molecule is typically still an excited state, and thus termed T_1, with higher energy states termed T_2, T_3...T_n. Additionally, due to electron-electron repulsions, triplet states are lower in energy than singlet states; a stipulation from Hund's first rule. *N.B.* For optical transitions the selection rule is $\Delta S = 0$; this is relaxed slightly in molecules due to spin–orbit coupling.

The Jablonski Diagram

In the Jablonski[5] diagram (Figure 1.13) the vertical axis corresponds to energy, with higher energy states located at the top. The horizontal axis corresponds to a change in the nature of the electronic state. There are several groups of states, S_0, S_1, S_2 and T_1, characterised by horizontal black lines, and several grey lines above. The grey lines represent vibrational levels within the excited state, termed manifolds.

[5]Professor Alexander Jablonski is regarded by many as the father of fluorescence spectroscopy, and it is he who the diagram is named after. [33]

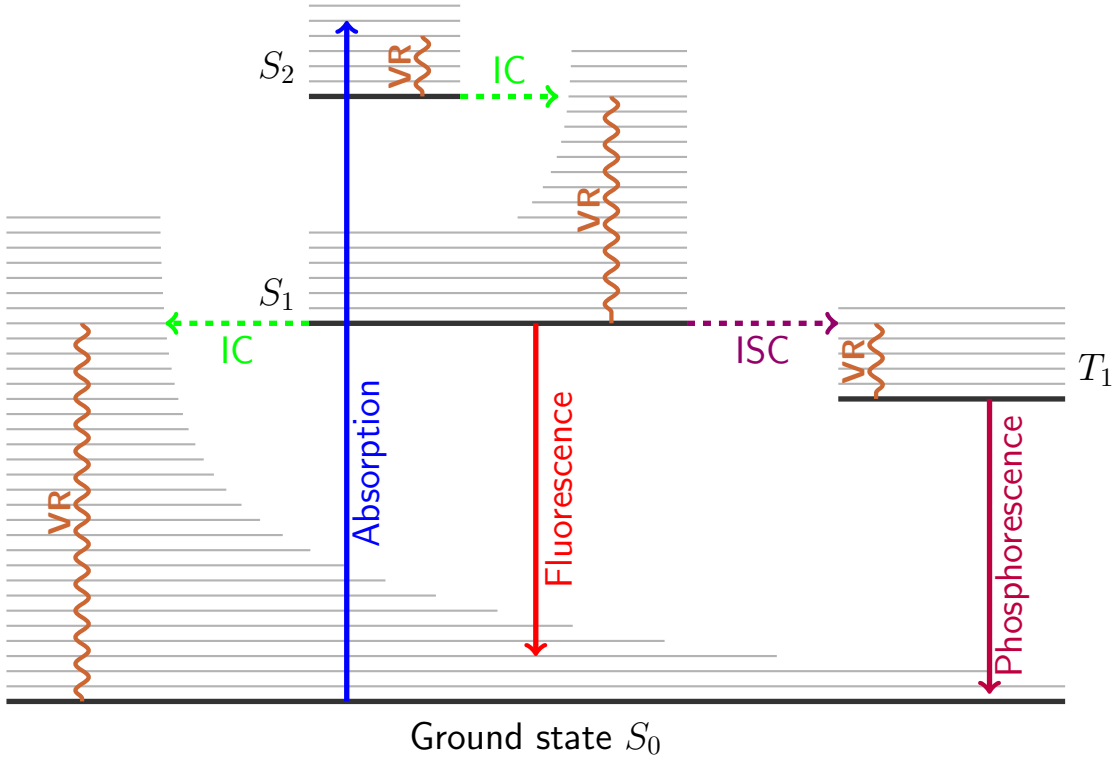

Figure 1.13: Jablonski Diagram, adapted from [32] demonstrating the transitions between excited states.

There are several vertical lines depicted which all, as the axis dictates, pertain to an energy change. The vertical blue line, discussed above, describes an absorption process. The vertical nature of the line helps portray the instantaneous nature of the absorption event. The orange lines, within the manifolds of the various states, depict vibrational relaxation (VR) and are also essentially instantaneous (10^{-12} s). Decay to lower excited states of the same multiplicity uses the process of internal conversion, IC, depicted in the Jablonski diagram as a green horizontal arrow. Access to a triplet state from a higher energy singlet state (*e.g.* $T_1 \leftarrow S_1$) is through a process called intersystem crossing, ISC, depicted by a purple horizontal arrow in the diagram. Although this is technically a spin–forbidden transition ($\Delta S \neq 0$), most molecules display some evidence of triplet state population.

Formation of the triplet state and the ramifications

When an excited state is generated, the multiplicity, S, can be either 0 or 1. The multiplicity $S = 0$ requires $M_s = 0$, *i.e.* there is only one ('singlet') orientation of the

paired spins contributing to the multiplicity. However, for S = 1 quantum mechanics requires three degenerate sublevels corresponding to the quantum numbers M_S = -1, 0 and +1, hence the term 'triplet'. This 3:1 triplet–singlet ratio is problematic in the preparation of OLEDs, as it enforces a 25 %–maximum efficiency in organic systems. For this reason, heavy metals including iridium [11] and platinum have been complexed with ligands to induce the S↔T ISC by a spin–orbit coupling mechanism, and hence improve phosphorescence yields.

1.4.2 The excited state

As the Jablonski diagram illustrates, once a compound is in an excited state, there are several paths by which it can relax. Kasha's Rule states that emission is independent of excitation wavelength, *i.e.* even with excitation into a higher electronic and/or vibrationally excited state, processes (VR and IC) will conspire such that the molecule is left in the lowest vibrational level of the S_1 manifold, before the emission process takes place *i.e.* $k_{IC}(S_2 \rightarrow S_1) >> k_{IC}(S_1 \rightarrow S_0)$ and $k_f > k_{IC}(S_1 \rightarrow S_0)$.[6] Decay to the ground state is not always to the lowest vibrational level, and as such emission spectra often feature vibrational fine structure. These processes result in emissions to the ground state that are lower in energy than the absorption event. This can be observed experimentally by comparing an absorption spectrum to the emission spectrum of the same compound; the emission spectrum is at lower energy. This difference is known as the Stokes Shift, and is defined as the energy gap between the 0,0 transitions of the emission and absorption spectra, which is often, but not always, the difference between the maxima of the two spectral profiles.

The spectra in Figure 1.14 illustrate the difference in energy between absorption and emission profiles. Figure 1.14 also demonstrates the similarity between the absorption and emission profiles; in rigid aromatic hydrocarbons they are often mirror images of each other. Typically the emission spectrum is the mirror image of the $S_1 \leftarrow S_0$ absorption transition. This is due to the similarity between the vibrational spacings for the ground and excited states, as derived from the Franck Condon

[6] There are some exceptions to this rule, known to display emission from the S_2 state, *e.g.* Azulene.

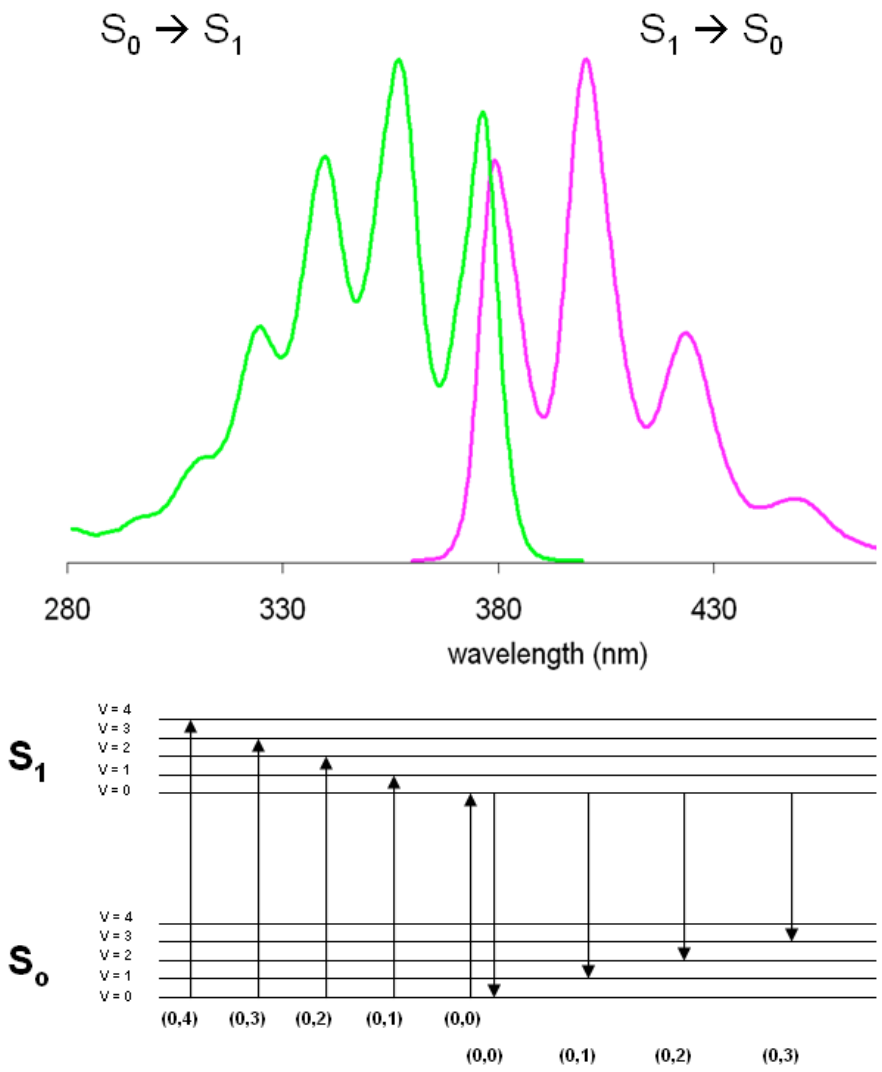

Figure 1.14: Graphic to demonstrate the mirror–image nature of absorption and emission spectral profiles for anthracene, a rigid hydrocarbon. Data from Dr A. Beeby.

principle.

1.4.3 Relaxation processes

Radiative decay from the lowest excited singlet state, S_1, is termed fluorescence and it is the most common form of emission for organic molecules, termed fluorophores. Fluorescence is a $S_0 \leftarrow S_1$ transition, where $\Delta S = 0$. Therefore it is an allowed transition, hence the fluorescence lifetimes are fast (see section 1.4.4). Emission from a state of different multiplicity to the ground state *i.e.* where $\Delta S \neq 0$, is a spin forbid-

den process and is termed phosphorescence. The use of heavy atoms such as bromine and iodine as well as transition metals can, to an extent, circumvent this selection rule (*vide supra*). Due to the lower energy of the triplet state, phosphorescence is at a much lower energy than fluorescence.

1.4.4 Quantum yields and lifetimes

The two most important properties of a fluorophore are the quantities that describe the intensity and duration of fluorescence. These properties are defined by the fluorescence quantum yield, ϕ_f, and the fluorescence lifetime, τ_f, respectively. The quantum yield is simply a ratio of the photons emitted and absorbed:

$$\phi_f = \frac{\text{number of photons emitted}}{\text{number of photons absorbed}} \tag{1.7}$$

i.e. if 100 photons are absorbed and only 50 are emitted, the compound exhibits a quantum yield of 0.5. The fluorescence lifetime, τ_f, is a very important property of a fluorophore as it governs the time available for detection of the fluorophore. Radiative emission from a singlet excited state typically takes 10^{-12}—10^{-7}s (ps and ns *e.g.* pyrene, τ_f = 500 ns). Radiative emission from a triplet state is a spin forbidden transition. This is echoed in the phosphorescent lifetime, τ_p, which can range from 10^{-6} to 10^{0} s (μs, ms and s); considerably longer than for fluorescence. Knowing values for these two properties allows calculation of a third property, the rate of fluorescence, k_f. The quantum yield can be described as a ratio of the rates of radiative emission (k_f) and all excited state relaxation processes (k_f + k_{nr}):

$$\phi_f = \frac{k_f}{k_f + k_{nr}} \tag{1.8}$$

The lifetime can be described as the reciprocal of all the rates of relaxation from the excited state:

$$\tau_f = \frac{1}{k_f + k_{nr}} \tag{1.9}$$

Equation 1.9 can be substituted into Equation 1.8 and rearranged so that:

$$k_f = \frac{\phi_f}{\tau_f} \tag{1.10}$$

Coefficients of the rate of emission (k_f) depend upon the absorption intensity. Strong absorption for $S_1 \leftarrow S_0$, for instance, would result in a fast rate for the reverse process. The opposite of this is also true *i.e.* for a forbidden absorption transition, the rate of fluorescence for the reverse process will be low. [31, 33]

1.4.5 Solvent effects

Different solvents have different polarities, an electric dipole over the molecule of solvent, quantified by the dielectric constant, ϵ. Water is highly polar ($\epsilon = 80$), alkanes such as hexane ($\epsilon = 1.88$) are non polar.

Due to the instantaneous nature of absorption relative to the rate of solvent molecule relaxation, absorption spectra are rarely affected by changes in solvent polarity.[7] However, fluorescence occurs only after the solvent molecules have had a chance to reorient about the fluorophore; hence emission spectra often exhibit changes depending upon solvent polarity, especially for fluorophores which feature a slight ground state dipole.

Typically, in excited states, molecules experience larger dipole moments, μ_E, and as such these are stabilised by polar solvents. The result of this is increasingly red-shifted emission with increased solvent polarity; solvents of increased polarity stabilise the increased dipole of the excited state. This leads to *solvatochromism* in the emission spectrum, the term used to define a change in colour of a compound's emission with solvent.

Specific solvent effects can also affect the emission spectra, such as with solvents containing groups capable of H–bonding with an appropriate fluorophore. Furthermore, for compounds featuring electron–rich and electron–poor regions – affording them some degree of charge–transfer – excitation can result in the fluorophore form-

[7] In some materials with a polar ground state, polar solvents can act to stabilise the ground state, *e.g.* benzophenone.

ing an internal charge transfer (ICT) state which is more readily stabilised by dissolution in higher polarity solvents. Hence the ICT may be the lowest energy state in the polar solvent whereas in non–polar solvents a locally-excited (LE) state is lowest in energy.

The measure of the effect of solvent change on the absorption and emission characteristics of a fluorophore is performed using the Lippert equation:

$$\Delta\bar{\nu} = \frac{2\Delta f}{hca^3}(\mu_E - \mu_G)^2 + k \tag{1.11}$$

where h is Planck's constant, c is the speed of light, and $\Delta\bar{\nu}$ is the difference between the absorption maxima and emission wavelength in wavenumbers. Δf is defined as:

$$\Delta f = \frac{\epsilon - 1}{2\epsilon + 1} - \frac{n^2 - 1}{2n^2 + 1} \tag{1.12}$$

and describes the orientation polarizability, which is in turn defined by the change in dielectric constant, ϵ and the refractive index, n of the solvent. a is the radius of the cavity, and μ_E and μ_G describe the dipole moments in the excited and ground states respectively. The constant, k, accounts for energy losses from vibrational effects, as emission rarely occurs to the lowest vibrational state of the S_0 manifold.

Figure 1.15 shows a Lippert plot demonstrating the linearity of Δf against $\Delta\bar{\nu}$ for several aryleneethynylene systems prepared and studied by an earlier group member, Dr K S Findlay. These plots allowed determination of μ_e, using a calculated value for the ground state dipole moment.

1.4.6 Low temperature spectroscopy

As well as the radiative relaxation pathways already discussed, molecules in the excited state can undergo a variety of non–radiative relaxation processes. The rates of these processes (namely IC and ISC) can be minimised by cooling the sample, which has two effects. Some rates are lowered sufficiently by the low temperature to become small relative to the rate of emission (k_f). Additionally, the rigidity of the sample has the effect of physically prohibiting motions, including selected

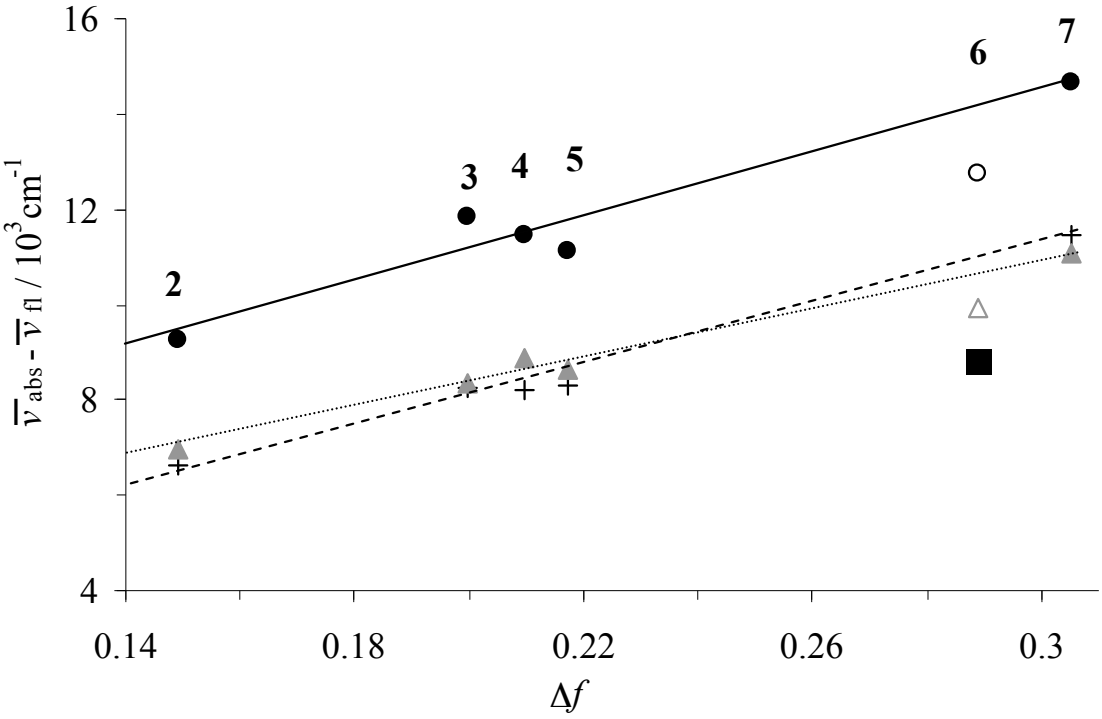

Figure 1.15: Example of a Lippert plot, taken from the thesis of Dr K S Findlay, reproduced with permission. [34]

vibrations, twists and stretches and diffusion–based quenching processes, which can lead to attenuated non–radiative decay rates. Combined, these restrictions can act to increase radiative emission by decreasing non–radiative means of relaxation. It can also lead to observation of appreciable phosphorescent decay due to the inability of oxygen to quench triplet formation.

For the freely–rotating ethynylene–containing systems considered in this work, the effect of cooling the sample into a rigid organic glass at 77 K affords elucidation of the absorption and fluorescence spectra of the favoured planar state. This presents as spectra featuring a high degree of vibrational fine coupling with enhanced 0,0 bands due to the increased population of the planar (lowest energy) conformation. This is in contrast to the typically broad and featureless spectra, characteristic of the averaging of all rotamers available in solution for these types of compounds at room temperature.

Enforced planarity also acts to increase effective conjugation length in multi–arene systems. This can present interesting photophysics, such as colour changes

(see Figure 4.38 on page 176 and the accompanying text).

1.5 The use of density functional theory calculations in this work

The use of *ab initio* calculations to rationalise and help understand experimental observations has become commonplace in the literature today. From their inception using Hartree–Fock theory, through the improvements brought with Semi–empirical and Correlated–ion methods, first principles calculations are now routinely performed using density functional theory, DFT. By considering just the electron density of a molecule, this theory affords accurate predictions of numerous properties including the geometries of chemical structures, vibrational modes, reaction barriers, shielding constants for a given magnetic pertubation, electric dipole moments for a given electric field pertubation, and excited state energies due to electromagnetic radiation.

Throughout this thesis (see sections 3.1.1, 4.2.2 and 4.3) references are discussed which have cited the use of *ab initio* calculations to explain observed properties.

1.6 Synthetic Routes

This introduction has thus far served as a review of the properties and potential applications of oligoaryleneethynylenes, in an attempt to illustrate why they are important in the field of electro-optic materials. In discussing these facts, aspects of their synthesis have been mentioned, although not examined in any depth.

As was covered at the start (see section 1.1), aryleneethynylenes are aromatic species joined together by ethynylene linkages. The synthesis of systems of this type can be achieved *via* several routes, with the Sonogashira cross–coupling reaction being, by far, the easiest, most efficient, and robust method. For the sake of thoroughness, what follows will introduce several other methods of introducing a C—C triple bond, before considering the Sonogashira methodology.

1.6.1 The halogenation–dehydrohalogenation method

This is the original route, requiring synthesis of 1,4-bis(phenylvinyl)benzene first. This is subsequently brominated which opens up each double bond. Dehydrobromination with base allows formation of the triple bonds. [35]

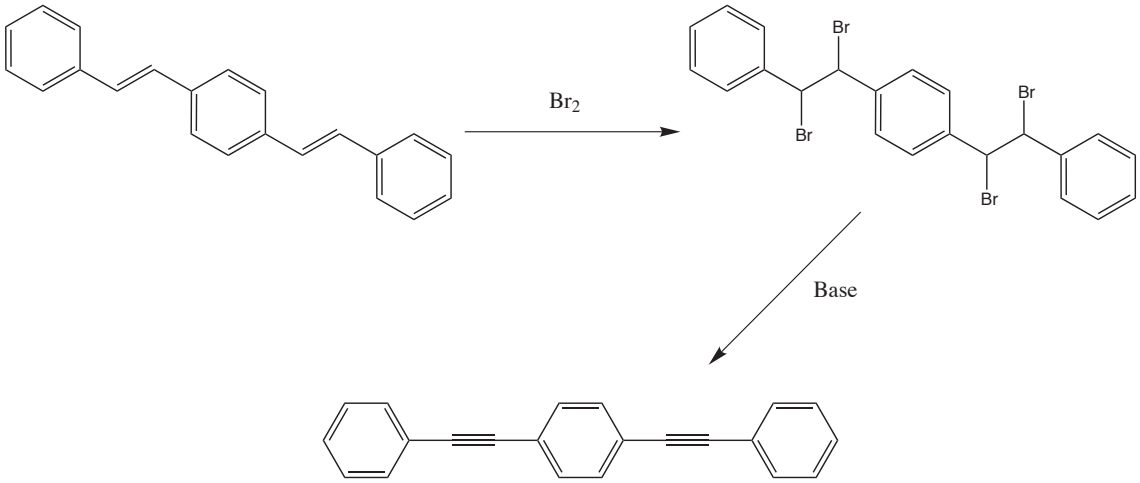

Figure 1.16: Early preparative route of BPEB, adapted from [8].

1.6.2 The Stephens-Castro method

In 1963 Stephens and Castro published a copper–mediated coupling reaction allowing coupling of arylacetylenes with aryl halides to form tolan (see Figure 1.17). A copper acetylide could be prepared by treatment of the arylacetylene in ethanol with copper iodide in ammonia solution. This could then be reacted with an aryliodide, in refluxing pyridine under nitrogen, to generate tolan. The route was not versatile enough to allow usage of *ortho*–substituted aryliodides, as this caused a cyclization reaction to dominate.

1.6.3 The double elimination method

This synthetic route (Figure 1.18) was mentioned earlier (see page 10), as it was used by Adachi for preparation of various substituted BPEB–based systems as blue fluorophores in OLEDs. [15]

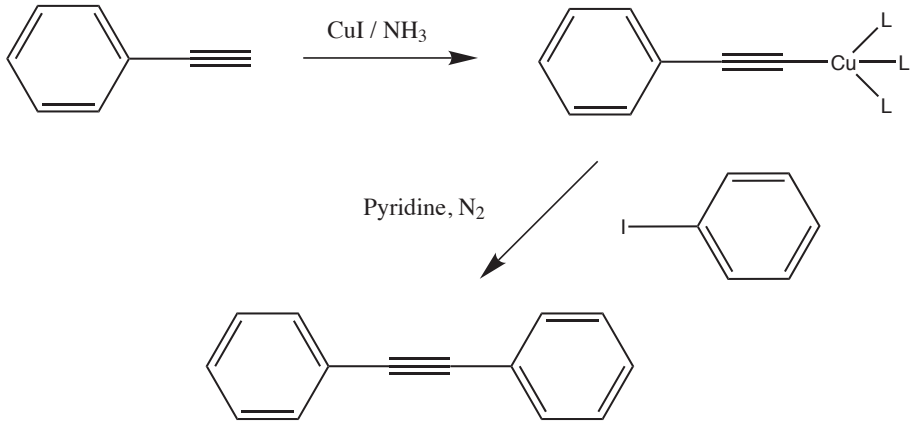

Figure 1.17: Formation of tolan, using the Stephens-Castro method, adapted from Castro *et al.* [36]

1.6.4 The Sonogashira cross–coupling reaction

Citing the Stephens-Castro coupling of copper-arylacetylenes with iodoarenes [36,37] as being potentially 'limited by the violent reaction conditions' and other difficulties [38], Kenichi Sonogashira, Nobue Hagihara and Yasuo Tohda published their method for substituting an acetylenic hydrogen by various arylhalides, under mild conditions. It required catalytic amounts of bis(triphenylphosphine)palladium dichloride and the co–catalyst cuprous iodide, stirred in diethylamine under an atmosphere of nitrogen. Their reported reaction was allowed to stir for six hours, at room temperature, and produced an 85 % yield.

The Sonogashira cross–coupling methodology can afford coupling between terminal alkynes and aryl (or sometimes alkenyl) halides and triflates (sp—sp^2 hybridized carbons). It proceeds with the use of two catalytic species, copper(I) iodide and, most commonly, bis(triphenylphosphine)palladium dichloride, stirred together with base, under a rigorously maintained inert atmosphere. Other palladium–based catalysts are available, and their use is dependent upon the intended target compound. For simplicity, and due to the nature of the work being considered in this review, this introduction will only refer to arylhalides (*c.f.* alkenylhalides).

The catalytic cycle (see Figure 1.19) is similar to that of other cross–coupling methods; in particular the Suzuki–Miyaura cross coupling of arylboronates with arylbromides, and, to a lesser extent, the Heck cross–coupling of vinyl groups with vinyl, benzyl or arylhalides. The finer points are discussed below.

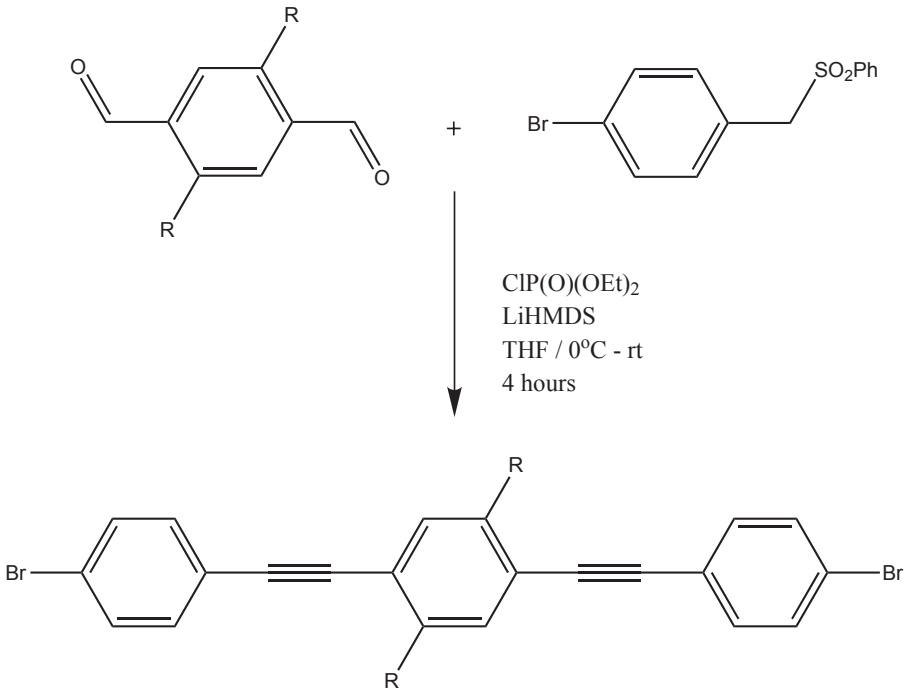

Figure 1.18: Preparative route for substituted BPEB systems involving double elimination of dialdehyde with β–sulfone, adapted from Mao *et al.*. [15]

Reduction of Pd(II) to Pd(0)

Bis(triphenylphosphine)palladium dichloride is the catalyst precursor in the Sonogashira reaction. It provides a source of the active species Pd(0). In $PdCl_2(PPh_3)_2$ palladium is in the 2+ oxidation state, thus stable in air for short time periods facilitating use and storage. This means, however, a reduction is required before it can act catalytically. This is seen in section 1 of Figure 1.19 of the cycle. The amine base, copper(I) and the acetylene moiety generate a copper acetylide. Transmetallation transfers two equivalents of the alkynyl to the palladium species (Figure 1.19, step A). The alkynyl groups are subsequently lost, through reductive elimination, as the diiyne, leaving the active Pd(0) species as $Pd(PPh_3)_2$ (Figure 1.19, step B). Nguyen *et al.* have shown that the reduction is fast relative to the next step, implying the arylhalide will not cross–couple until all of the palladium(II) is reduced to palladium(0). [39] This highlights the need for thorough Schlenk line (or other inert atmosphere) techniques. If oxygen is present during the reaction the diiyne is formed catalytically as any Pd(0) generated is oxidised back to Pd(II). Only one equivalent of diiyne should be produced during a typical cross coupling

reaction involving the bis(triphenylphosphine)palladium dichloride catalyst precursor; any more indicates oxygen was present during the reaction. If it is thought the target compound and the diiyne by–product could prove difficult to separate, tetrakis(triphenylphosphine)palladium can be used. Palladium(0) is present in this catalyst without the need for reduction and thus no diiyne should be generated. However, handling of this catalyst must done be under nitrogen to prevent its oxidation.

Oxidative Addition

As the aryl halide is introduced the Pd(0) essentially attacks the arylhalide as a nucleophile, resulting in a *trans* oxidative addition (section 2 of Figure 1.19, step C) across the square planar complex. This step is deemed the rate determining step (RDS) and as such several variables can be tuned to afford shorter reaction times. The arylhalide can be made more reactive by using a more labile halogen or by substitution with an electron–withdrawing moiety. Either case would reduce the strength of the C—X bond, increasing the rate of the oxidative addition.

The Copper Cycle

Scheme 3 in Figure 1.19 illustrates a suggested copper–catalyst cycle [40], and is largely similar to that expected to happen in scheme 1 (step A). The amine (triethylamine in this instance) is not considered basic enough to remove the acetylenic proton, hence the π–coordinating alkyne–Cu complex indicated at the bottom of the cycle [41]. Step E illustrates the formation of the copper acetylide which, through transmetallation (step D) with the arylhalide–bound palladium species, binds *trans* to the aryl group, displacing the halide, reforming $Cu^{+}X^{-}$.

Reductive Elimination

With both aryl groups now ligated across the square planar palladium complex, trans–cis isomerization brings the aryl groups *cis* to one another (step F). Reductive elimination (step G) affords the desired product, as well as reforming the active catalyst.

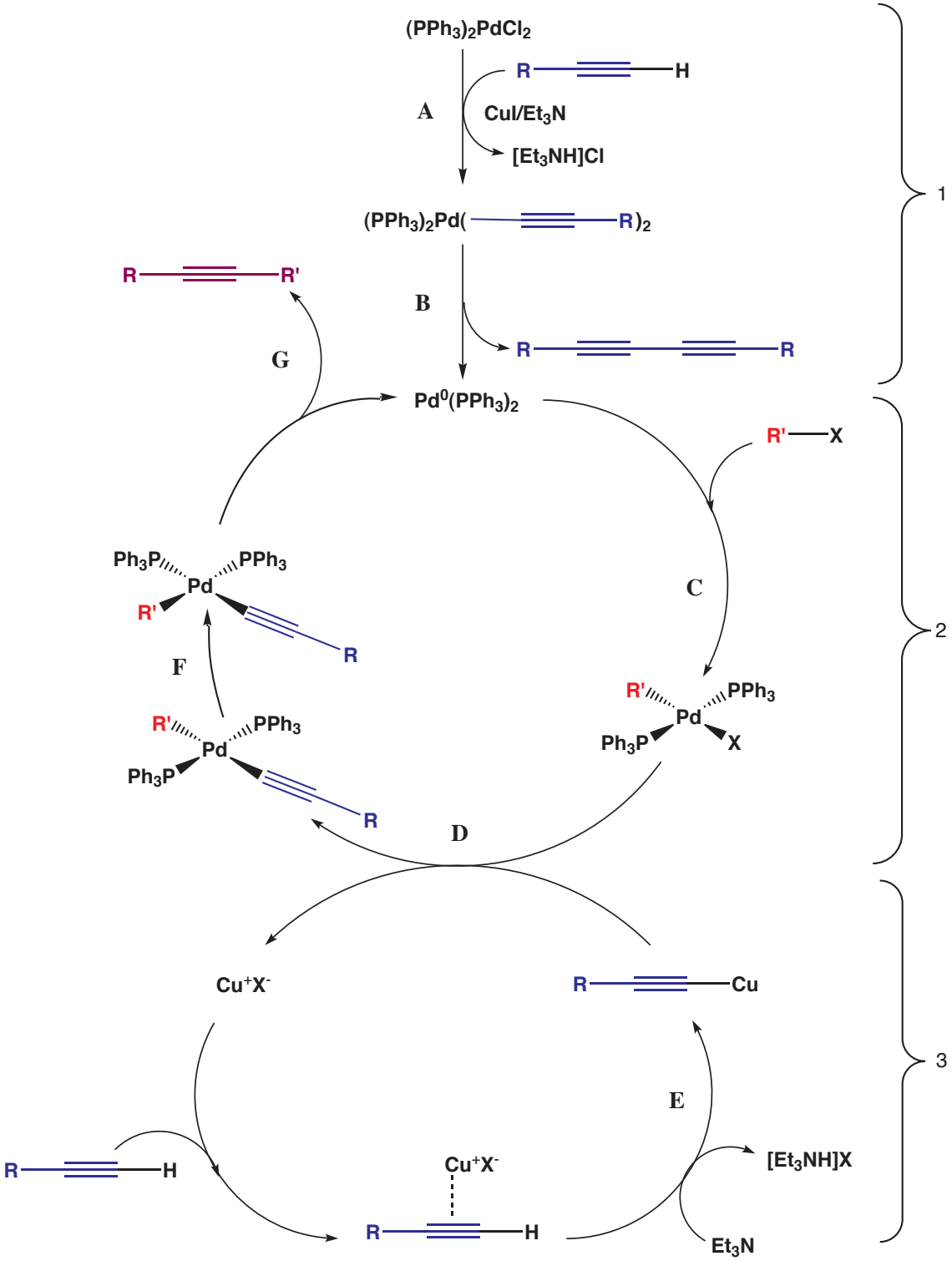

Figure 1.19: The Sonogashira cross–coupling cycle. Adapted from [38].

1.7 Aims and Objectives

This chapter has aimed to provide an introduction to oligomeric phenylethynylene systems, including an overview of their potential applications. These have been shown to be attributable to phenylethynylenes excited state properties, which have been examined and explained.

The aims of this work are to investigate the use of different heterocycles in the bis(arylethynyl)-arene motif and to see what effect alteration of the heterocycle has on the overall photophysical properties. Work by previous group members [34, 42] has demonstrated that alteration of the central ring system in a 3–ring arylethynylene oligomer has the greatest effect on the photophysical properties of the molecule *c.f.* outer rings, or addition of substituents. This work constitutes the synthesis of various di–halogenated heterocycles and their cross–coupling with different arylacetylenes to afford novel aryleneethynylene three–ring oligomers. These materials are purified and characterised, and their photophysical properties investigated. Two systematic variations will be monitored in the work presented here:

- the effect on the aryleneethynylenes' excited state properties upon the alteration of the heterocycle
- appendage of electron donation and withdrawing substituents.

Furthermore, the heterocycles under consideration will be derivatives of two of the most common heterocycles researched in the field of organic electronics, thiophene and oxadiazole.

Using DFT methods, optimised geometries will be compared to crystallographic data, allowing comparison of bond lengths and angles. Energy and TD–DFT calculations will be used to help understand observed photophysical properties and Raman spectra.

This work is important because an understanding of the excited state properties of an oligomeric system has been shown to be instrumental in predicting properties of the bulk polymer. [43] On a practical side, the relatively small oligomer is easier to deal with than a polymeric system, and derivatisations can be made with comparative ease, affording facile tuning of a compound's properties.

2

Experimental Methods

2.1 Introduction

This chapter will serve as an introduction to the experimental methods or equipment used in the determination of excited state properties. Photophysical measurements are the primary method and as such this chapter will introduce the different equipment and techniques used in measuring absorption, excitation and emission spectra at room and low temperature, and determining extinction coefficients, quantum yields, and lifetimes. Also included is information pertaining to the electrochemical apparatus and the software and methods used in performing the DFT calculations.

2.2 UV-vis absorption spectroscopy

2.2.1 Absorption spectra

An absorption spectrum is a plot of absorption against wavelength (nm) or wavenumber (cm^{-1} – less common due to modern spectrometer settings).

An ATI Unicam UV-2 spectrophotometer was used to record absorption spectra of samples in solution and glasses. These were performed at appropriate concentrations, in quartz cuvettes, over an appropriate wavelength range, against a reference cell containing pure solvent.

For each extinction coefficient reported herein, three samples were prepared with weights accurate to ± 0.05 mg, and solutions made up in volumetric flasks with the appropriate solvent. Serial dilution of each solution to obtain 2–3 values with an optical density (O.D.) < 1.1 afforded three sets of data which were plotted, using Microsoft Excel, as Abs_{max} *vs* concentration. Linear trend lines could be applied to this data, fit through the origin, supplying the extinction coefficient for each sample. An average could be calculated, which is the quoted value of ε (see Tables 3.5 and 4.4).

2.3 Fluorescence spectroscopy

2.3.1 Fluorescence spectra

Fluorescence emission spectra were obtained as a plot of intensity of fluorescence against wavelength (nm) with a constant bandwidth (nm). Fluorescence excitation spectra were obtained by measuring intensity of emission as a function of excitation wavelength (nm). An excitation spectrum presents, for dilute solutions subject to no inner–filter effects *i.e.* $A_{max} < 0.1$, a spectrum identical to the absorption spectrum, albeit with a 1000–fold increase in sensitivity.

Although wavelength is not linear with respect to energy (*c.f.* cm^{-1}) the spectrometers used for the work presented here determine the data as intensity against wavelength with constant bandwidth (in nm), so for consistency this has been maintained throughout.

2.3.2 Fluorescence spectrometer

Fluorescence excitation and emission spectra were obtained using the Jobin-Yvon Horiba Fluorolog 3-22 Tau-3 spectrofluorimeter (see Figure 2.1), detecting at 90 ° to the illumination source.

To avoid inner-filter effects dilute solutions with ~ 0.1 O.D. (in a 10 mm cuvette) were measured. The parameters for each reading were adjusted to ensure a linear detector response (< 1000000 cps). Spectra obtained were corrected for the light source and spectral response of the spectrometer, and converted to ASCII or text format for presentation and plotting in Microsoft Excel or Origin.

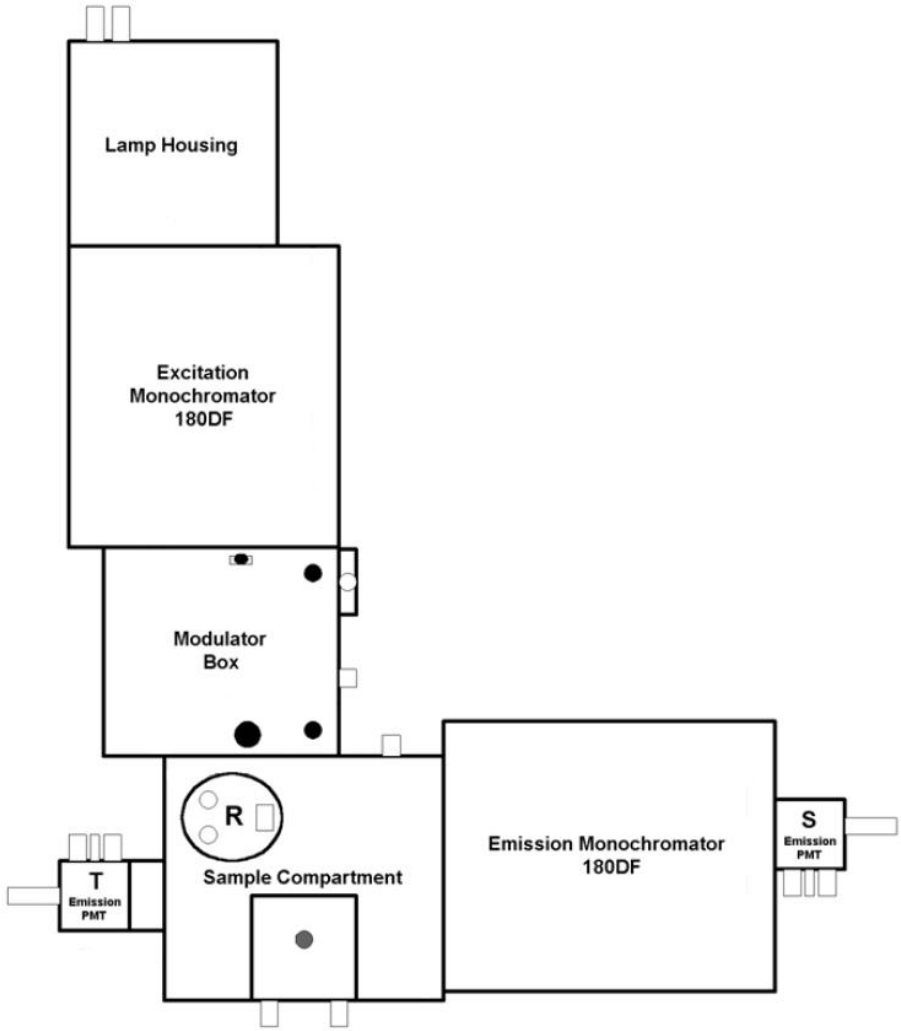

Figure 2.1: Schematic of the JY Horiba Fluorolog 3-22 Tau-3 Spectrometer. Image adapted from the JY Horiba Fluorolog manual.

2.4 Low temperature spectroscopy

Both the ATI Unicam UV-2 and the JY Horiba Fluorolog spectrometers are adapted to hold a cryostat. Spectra presented in this thesis were obtained at 298 K and 77 K by dissolving the sample in EPA (a solvent mixture of diethyl ether, 2-methylbutane, and ethanol; in the ratio 5:5:2 respectively, and see section 1.4.6).

All low temperature measurements were taken using an Oxford Instruments DN 1704 Optical Cryostat, with liquid nitrogen cooling (see Figure 2.2). Thermostatic control was provided by an Oxford Instruments ITC 601 temperature controller. Samples were allowed to 30 minutes to equilibriate at the given temperature prior to spectroscopic measurements.

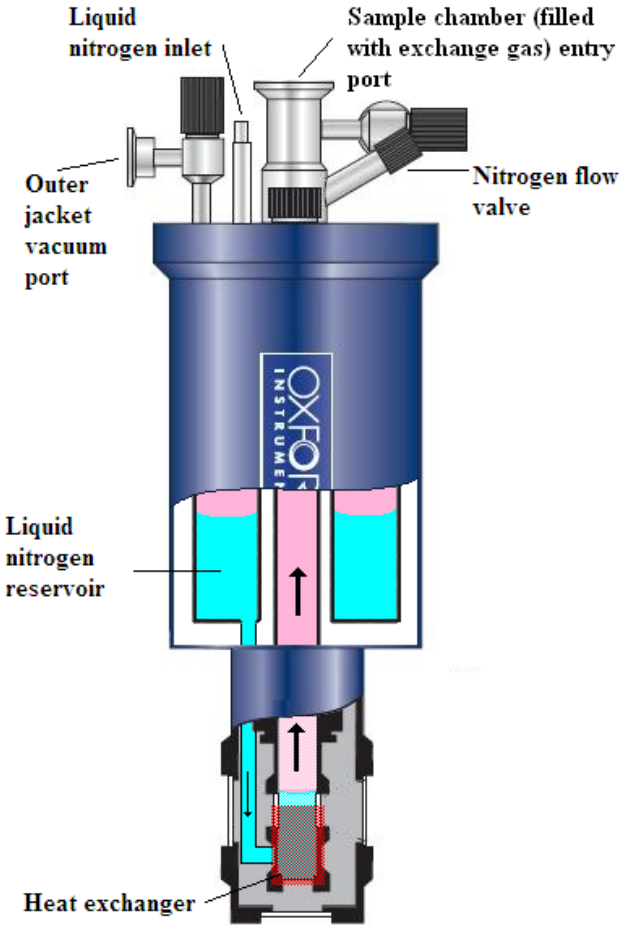

Figure 2.2: Schematic of the Oxford Instruments DN 1704 Optical Cryostat, used to obtain low temperature spectra. Image adapted from [44].

2.5 Quantum yield determination

Two methods were employed for determination of photoluminescence quantum yields (PLQYs). Several PLQYs were obtained using a Labsphere® optical Spectralon® integrating sphere (100 mm diameter), with accessories made from Spectralon® (baffle) and Teflon® (sample holder). The cuvettes used were homemade quartz cylinders (8 mm diameter). The integration sphere allows use of the *absolute* method for determination of a PLQY. A second method, the *comparative* method, was also used for PLQY determination.

The Comparative Method [45]

A solution of a novel fluorophore was prepared with an absorbance of 0.1 O.D.. The UV-vis absorbance spectrum and then the emission spectrum were measured. The absorption at the excitation wavelength was recorded and plotted against the integral of the emission spectrum. The sample was then diluted four times and the procedure repeated for each dilution. The graph of integrated fluorescence intensity against absorbance was a linear plot, through the origin. At no point during the experiment were spectrometer parameters (*e.g.* slit widths) altered. A suitable (*i.e.* spectrally similar) fluorescent standard was chosen – fluorescein in 0.1 M sodium hydroxide ($\phi_f = 0.95 \pm 0.03$ at $\lambda_{ex} = 496$ nm), quinine sulfate in 0.1 M sulfuric acid ($\phi_f = 0.58$ at $\lambda_{ex} = 350$, $\phi_f = 0.53 \pm 0.02$ at $\lambda_{ex} = 366$) or rhodamine 101 in ethanol ($\phi_f = 1.0$ at $\lambda_{ex} = 450$–465 nm) [33] – and prepared with a 0.1 O.D.. The same procedure is applied to the standard, allowing the plotting of a second linear graph, also through the origin. A comparison of the gradients ($\mathbf{Grad}_{X,ST}$), accounting for the refractive index of the solvent (n) of these two plots affords determination of the PLQY, see equation 2.1.

$$\Phi_X = \Phi_{ST} \left(\frac{Grad_X}{Grad_{ST}} \right) \left(\frac{n_X^2}{n_{ST}^2} \right) \tag{2.1}$$

Problems with this system are the reliance on the fluorescent standard, a problem at longer wavelengths due to limited availability, and the need for so many measurements; not only time consuming, but also a source of error.

The Absolute Method [46]

The absolute method measures the loss of intensity of excitation of a sample (*i.e.* its absorption), negating the need for a reference sample – immediately halving the number of measurements required. The principle depends on collection of all the emitted radiation from a sample, hence the high reflectivity (Spectralon®, reflectance > 99 %) of the inner surface of the sphere. Three different measurements were required for each quantum yield; $\mathbf{Ex}_{solvent}$, the integrated luminesence from direct excitation of the solvent at x nm, reading intensity response from x ± 5 nm; $\mathbf{Ex}_{prod}$, the integrated luminesence from the direct excitation of the product at x nm, reading intensity response from x ± 5 nm; and $\mathbf{Em}_{prod}$, the integrated luminesence of the emission spectrum of the product, excited at x nm. The quantum yield Φ_F is calculated by;

$$\Phi_F = \frac{Em_{prod} \times ND}{Ex_{solvent} - Ex_{prod}} \tag{2.2}$$

The high intensity of the excitation profiles necessitates use of a neutral density gauze filter (typically 2 %), ND.

2.6 Lifetime measurements

Fluorescence lifetime, τ_f, measurements were made using the time correlated single photon counting (TCSPC) method. A description of the process can be found in Lakowicz. [33] Very briefly, the sample is excited by a fast-repetition light source. Equipment parameters are adjusted so that the detection rate is ≤ 1 % that of the laser repetition rate. The time between the excitation pulse and emission detection is recorded as such:

- an excitation pulse (start time) excites the sample and a signal is passed on to a time–to–amplitude converter (TAC);
- the TAC initiates a voltage ramp; this converts the start time to a voltage which increases linearly with time;
- detection of a photon of emission stops the voltage ramp;

- the voltage ramp of the TAC is proportional to the time difference of the excitation and emission pulses;
- this is repeated many times, allowing evolution of a histogram representative of the decay profile;
- due to high repetition light sources the reverse of this process is usually employed, whereby the emission pulse starts the TAC voltage ramp, and the excitation pulse acts as the stop signal.

The data is fit by iterative reconvolution and non-linear least-squares analysis of the convolved data (see Figure 2.3). The measured decay is thus fit to a theoretical decay, allowing determination of the lifetime from:

$$I(t) = \sum_{i=0}^{n} a_i exp\frac{-t}{\tau_i} \tag{2.3}$$

where I(t) is the intensity of light at time t, τ_i is the lifetime, and a_i is a pre-exponential factor, mainly relevant for situations where there are several fluorophores in the solution and can thus be normalized to 1. [33]

Excitation was by either pulsed IBH NanoLED diode (371 or 396 nm) or Coherent Verdi–pumped MIRA–D Titanium–Sapphire laser (300 nm) – the excitation wavelength and thus the light source was determined by samples' absorption spectra – with a cavity dumper. Emission was collected at 90° to the excitation source, and emission wavelength was selected by a Jobin Yvon Triax 190 monochromator. Fluorescence was recorded over a minimum of 10 000 counts in the peak channel of the pulse height analyser. A dilute suspension of Ludox® silica in water was used to obtain an instrument response function. The time per channel was changed depending upon the sample's response. The Solver function within Microsoft Excel was used to fit the data. The compounds' lifetimes were adjudged as accurate by reduced χ^2, weighted residuals (see Figure 2.3, black) and the Durbin–Watson parameter.

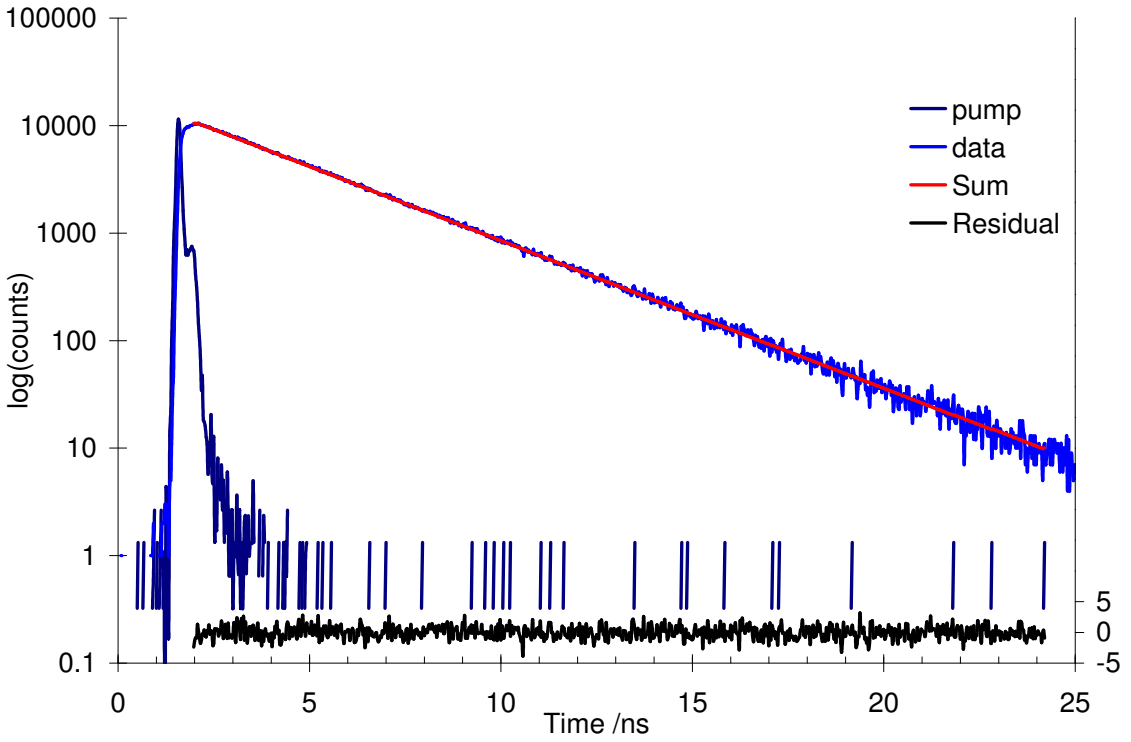

Figure 2.3: Fluorescence decay data and fit as obtained using TCSPC method on 4,7-bis(phenylethynyl)-benzofurazan (**BPEBf**) in toluene, $\lambda_{ex} = 396$ nm, $\tau_f = 3.1$ ns.

2.7 Electrochemical analysis

Electrochemical methods have been employed for analysis of various novel compounds under an applied potential difference.

The example CV plot (Figure 2.4a) is that of the novel arylethynylene **BPEBf.-OMe**, prepared for this thesis, against the standard ferrocene (wave not shown). The positions labelled are indicative of different properties;

- I_p = peak current.
- $E_{1/2}$ = half wave potential for the process.

2.7.1 Electrochemical measurements

Cyclic voltammograms were recorded ($\nu = 100$ mV s^{-1}) from 0.1 M Bu_4NPF_6, CH_2Cl_2 solutions $\sim 1 \times 10^{-4}$ M in analyte using a gas–tight single–compartment three–electrode cell: a Pt disk working electrode, a Pt wire counter electrode, and a

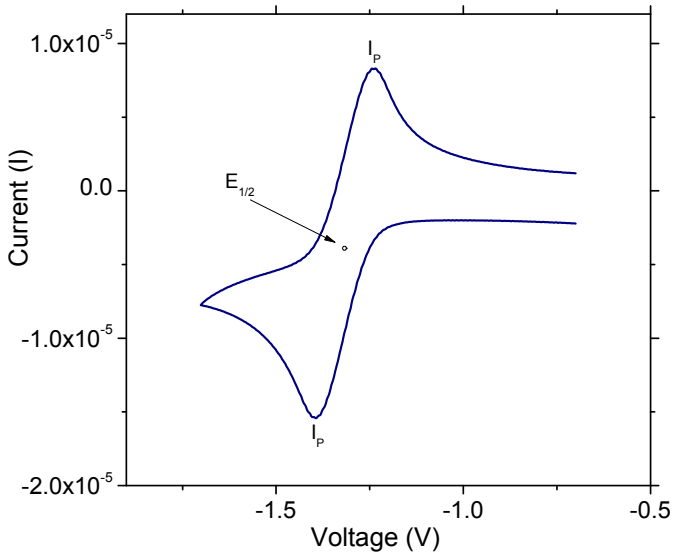

(a) Cyclic voltammogram exhibiting the reversible reduction of **BPEBf.OMe** in DCM with Bu_4NPF_6, scanning at 100 mVs^{-1}, referenced to the FcH/FcH^+ couple (0.00V).

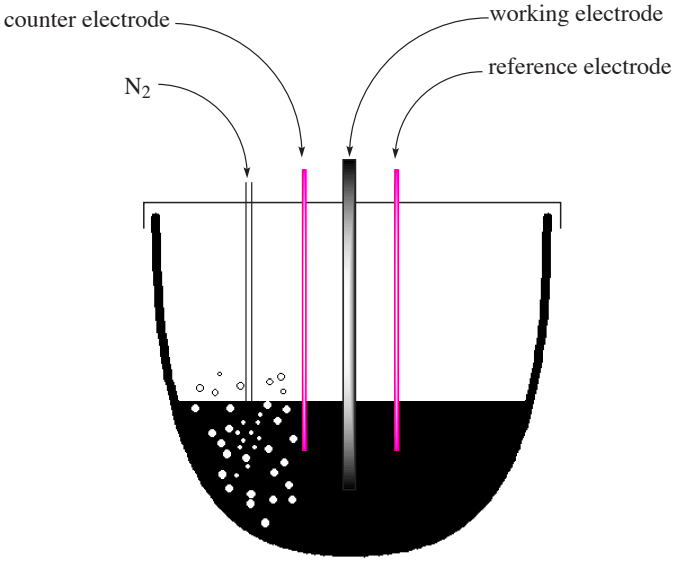

(b) Schematic of typical 3–electrode cell for typical controlled–potential experiment.

Figure 2.4: Typical cyclic voltammogram and 3–electrode electrochemical cell.

Pt wire pseudoreference electrode (see Figure 2.4b). The data was collected on an Autolab PG–STAT 30 potentiostat. The working electrode was polished with alumina paste before each scan. All redox potentials are reported with reference to an internal standard of the ferrocene/ferrocenium couple (FcH/FcH^+ = 0.00 V). UV–vis spectroelectrochemical experiments were performed at room temperature with an airtight OTTLE cell equipped with Pt minigrid working and counter electrodes,

a Ag wire reference electrode, and CaF_2 windows using a Perkin-Elmer Lambda 900 spectrometer.

2.8 Computational modelling

DFT calculations were performed on all systems prepared in this thesis using the Gaussian 03W package (Revision -E.01), [47] in conjunction with the visualisation package GaussView (4.1.2 release). Optimised structures were first obtained using the B3LYP functional [48–52] with the 6-31G(d) basis set. The geometries obtained were then used in both frequency and time-dependent DFT (TD-DFT) calculations, allowing prediction of Raman vibration stretches and electronic excitation energies.

In the work presented here, all systems were optimised employing the B3LYP functional, as stated above. However, the basis set used will not achieve the true answer obtainable by this functional; a larger basis set is required. Furthermore, all systems were simulated in the gas–phase, to allow comparisons with work reported in the literature, with no consideration of solvation.

Whilst the use of DFT calculations is ubiquitous in the literature today, and its implementation is undoubtedly useful, it must be used cautiously, with critical assessment of the information it offers. There is an intrinsic error associated with using B3LYP and a (relatively) small basis set. Geometries will be affected by the lack of solvation to varying degrees. The frequencies are obviously dependent on the geometry, but also we have used the harmonic approximation that states that the frequencies are simply the 2^{nd} derivative of the energy with respect to a given normal coordinate. To obtain full anharmonic frequencies requires one to solve the nuclear Schrődinger equation, which is incredibly computationally demanding on large systems such as those presented in this work (although possible on small systems such as diatomics).

Determination of the Raman intensities involved the use of static polarisabilities *i.e.* independent of the frequency of the applied radiation, rather than dynamic polarisabilities. Dynamic polarisabilities can be simulated, but again, it is very computationally demanding. B3LYP is relatively poor at simulating polarisabilities.

However, because it is consistently poor, it gives relatively reliable Raman intensities once a known correction is applied.

Valence excitation energies are quite accurately described (in a large basis set); excitation energies may be artificially high by the use of a small basis set although this is offset, to some extent, by the fact that all systems were simulated in the gas–phase, thereby negating effects on energies from solvents. Oscillator strengths will be affected by this failure to account for solvation effects though.

3

Aryleneethynylenes Containing Thiophene Derivatives

3.1 Introduction to thiophene and its derivatives

3.1.1 The interest in thiophene

Perhaps the most commonly researched molecules seen in the literature regarding organic semiconducting materials are oligo– and poly–thiophenes. Thiophene–based oligomers are highly conjugated units of repeating thienyl rings. They are renowned for their high chemical stability and fluorescence, as well as for their redox properties, and ease with which they can be functionalised, allowing easy tuning of their electronic properties. Moreover, they are relatively cheap as the starting materials are isolated during petroleum distillation. [53] Unsubstituted oligothiophene is a p–type semiconductor; it has been shown consistently throughout the literature [54–58] that thiophene–based polymers and oligomers host spectacular charge transporting properties, as demonstrated by the high field effect mobilities (FEMs) they exhibit.

In 1986 Tsumara *et al.* reported the first use of an organic macromolecule, polythiophene, as a semiconductor in an organic field effect transistor (FET). [54] Prepared from the electrochemical polymerization of 2,2'-bithiophene, a carrier mobility of 10^{-5} $cm^{-2}V^{-1}s^{-1}$ was achieved for this material. Two years later poly(3-hexylthiophene) (P3HT) was shown to be capable of a charge carrier mobility of 10^{-5} – 10^{-4} $cm^{2}V^{-1}s^{-1}$, a 10–fold increase on the charge mobility of polythiophene films. [55] In the early 1990's D. Fichou *et al.* reported impressive charge mobilities exhibited by a series of oligothiophenes of different chain lengths (three to eight thienyl units). The oligomer consisting of six units – hexathiophene – showed the largest carrier mobility, at 10^{-3} $cm^{2}V^{-1}s^{-1}$. [56, 57]

Preparation techniques and problems

Polymeric semiconducting films are not ideal for use in FET devices due to the very nature of polymers; the distribution of chain lengths can vary and disorder of molecules in the film can cause poor contact between surfaces, lowering FEM values and conductivities. To realise high charge–transfer efficiencies *i.e.* high carrier mobilities, high ordering in samples is essential.

This necessitates the avoidance of defects and grain–boundaries during sample

preparation, which was achieved by means of direct electrochemical polymerisation of precursors onto electrode surfaces. [54, 59]

Capping of oligothiophenes at their most reactive positions – the α and β (*1* and *2* positions) carbons[1] – was investigated in an attempt to improve regularity of molecular structure. In a communication Bäuerle [43] explained how end–capped oligomers can act as good models for polythiophene, with the advantage that undesirable reactions are limited during their production. Since end–capping can lead to a change in the molecules properties, and hence reduced efficiency of a compound, different means of controlling ordering have been investigated, including sample preparation/deposition techniques. P3HT was deposited as a Langmuir Blodgett film and incorporated as the organic layer in an FET. [60] Bao *et al.* reported spin coating and solution casting P3HT. [59] Flash evaporation was used to afford a totally organic FET device containing α,ω-dihexylhexathiophene (Figure 3.1) as the semiconducting layer. [61] This molecule was used due to its reported ability

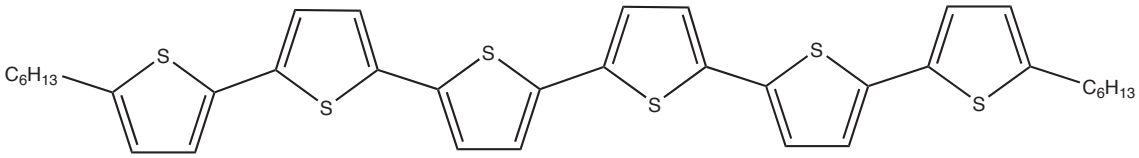

Figure 3.1: α,ω-Dihexylhexathiophene.

to self–organise into films. It was synthesised with the aim of creating self–induced stacking molecules; long alkyl chains act to increase the propensity of the molecule to organise itself spatially in stacks, hence increasing the regularity of the bulk structure. It is considered a fact that the spatial arrangement of molecules in polymeric films affects the bulk properties. To prove the improved efficiency upon ordering of films, a comparison of charge mobilities of the unsubstituted and hexyl–substituted sexithiophene films was undertaken which revealed that addition of the alkyl group prompted a 25–fold increase in carrier mobility. [62] By 1998 the carrier mobilities reported for a polymeric thiophene derivative reached between 0.1 $cm^{-2}V^{-1}s^{-1}$ (P3HT) and 0.23 $cm^{-2}V^{-1}s^{-1}$ (for α,ω-dihexyl-quarterthiophene) but largely the

[1] A second type of capping is discussed later (section 3.1.3) where the *3* and *4* positions of the thiophene ring are capped to avoid side chain polymerization and other undesirable side products

improvements had stagnated. Only recently a paper reported a carrier mobility of 0.1 $cm^{-2}V^{-1}s^{-1}$ for poly(3-pentylthiophene). [63] In a report reviewing the highest FEMs for various organic materials between 1983 and 2000, thiophene based polymers featured heavily, particularly hexathiophene and alkyl–substituted polythiophene, illustrating their importance. Deposition methods have been demonstrated to play a pivotal role in increasing FEMs, with vacuum sublimation proving the most reliable, if prohibitively expensive for large scale production. [58] As research into the application of oligomers and polymers of thiophene continues, devices are being developed incorporating thiophene in its various forms; such as TFTs, LCDs and chemosensors. [64–69]

Conversion of thiophene derivatives from p–type to n–type semiconductors

The ease of functionalisation of thiophene and the stability of its derivatives have led to the development of methods that give products n–type semiconducting properties. In an attempt to control the band–gap of thiophene oligomers and polymers and therefore, potentially, their properties, Ho *et al.* [70] developed molecules substituted with cyano groups, following work reported by Friend *et al.* [71]

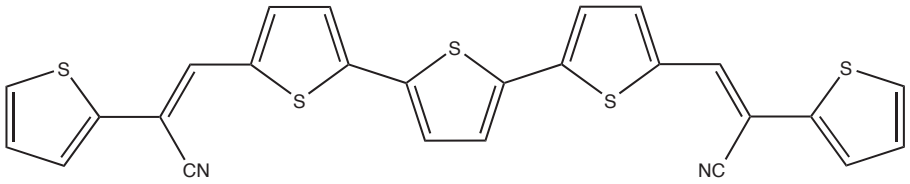

Figure 3.2: The low band gap oligomeric species reported by Ho *et al.*, designed with cyano groups to afford band–gap control. [70]

The result was oligomers with an increased electron affinity (see Figure 3.2), which, as Barbarella *et al.* indicated, is one of the ways to create an n–type semiconducting polymer. [72]

Barbarella suggested another method which was the oxidation of thiophene. Oxidation of thiophene generates the sulphone thiophene-1,1-dioxide. Oxidation has been shown to cause dearomatization of the ring and an increased electron affinity. [72] Due to this molecule's ability to act as an electron–deficient diene, the early

literature reported its usage in various organic syntheses including cycloaddition reactions, [73] and nucleophilic ring–opening reactions. [74, 75] More recently it has been recognised for its potential as an n–type semiconductor (see section 3.1.2 and Figure 3.3).

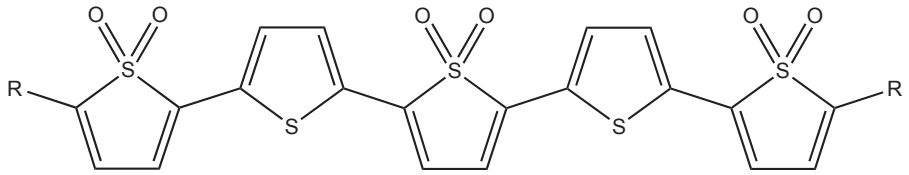

Figure 3.3: Compound prepared by Barbarella *et al.* incorporating thiophene-1,1-dioxide to generate an n–type semiconducting thiophene oligomer. [72]

3.1.2 Thiophene-1,1-dioxide

The sulfone derivative of thiophene, thiophene-1,1-dioxide, has attracted attention concerning its aromaticity since the 1950's, where knowledge of this property was necessary to answer questions regarding sulfur's valency and aromatic resonance. [76] Sulfur's ability to form bonds to six atoms, affording double bonds to two oxygen atoms in the case of thiophene, means that, in the oxidised state sulfur's lone pairs are no longer contributing to the aromatic ring's π–electron cloud. The effect of this is dearomatization of the ring, increased electron delocalisation over the oligomer, as well as an increased propensity for the aromatic ring to react as a diene.

The potential of thiophene-1,1-dioxide to act as an n–type semiconductor was realised by Barbarella *et al.* in 1998 when it was incorporated in an oligothiophene (see Figure 3.3). [72, 77] Thiophene groups substituted with bromine and alkylsilyl groups were oxidised using *meta*–chloroperoxybenzoic acid (*m*-CPBA), allowing for further coupling *via* Stille reactions.

Barbarella reported that two otherwise identical quaterthiophene oligomers (termed TTTT and OTTT, with T denoting thiophene units and O denoting a thiophene-1,1-dioxide unit) showed absorption maxima differing by a red shift of 58 nm on inclusion of the oxidised thienyl ring. This was indicative of the oxidation causing dearomatisation of the ring, with concomitant delocalization of electronic charge. The effect was substantiated by the inclusion of several thiophene-1,1-dioxide groups

in larger oligomers *e.g.* pentameter OTOTO c.f. TTTTT displays a 122 nm red–shift. The research also included the first electrochemical investigation into thiophene-1,1-dioxides. Upon inclusion of the sulfone the oxidation potential showed only a slight increase (0.09 V), but the reduction potential was significantly increased (shifted towards less negative values by 0.84 V), indicating the sulfone containing oligomers were much more easily reduced than the parent oligothiophenes. These results demonstrated that the sulfone containing analogues had significantly altered π—π^* molecular orbital energy levels, explaining the reduced energy gap (and red–shift in the absorption band), and that inclusion of alternating thiophene/thiophene-1,1-dioxide moieties, along with alteration of oligomer length, allowed tuning of the band–gap of the materials.

Control over the position of frontier energy levels of oligothiophenes affords control of the electron affinity and the ionisation potential, both important factors pertaining to the intended application for these molecules. Thus, it is clear that an understanding of the properties of these systems, and how to tune them, is desirable.

The heavy atom effect (in thiophene's case, sulfur) can lead to deactivation of emissive excited states by intersystem crossing, affording non–radiative decay of the triplet. Also, aggregation of smaller oligomers quenches luminescence as exciton interactions can lead to non–emissive states. Hence polythiophene fluorescence quantum efficiencies have typically struggled to reach 2 %, disfavouring them for use as the active material within OLEDs. In 1998 Granlund *et al.* [78] reported a thiophene polymer heavily substituted with dioctyl-phenyl groups acting as the emissive layer in a laser. The polymer was reported to achieve a PL efficiency of 24 %.

Using similar means to increase PL efficiency, Gigli *et al.* reported the addition of long alkyl substituents to several oligothiophenes containing oxidised units. [79] Relative to the unsubstituted pentathiophene, pentathiophene-3,3',4"',3""-tetramethyl-3",4"-dihexyl-2,2':5',2":5",2"':5"',2""-quinquethiophene-1",1"-dioxide (T5OME, Figure 3.4a) achieved a 20–fold increase in PL efficiency – 37 % in the solid state *i.e.* spin-cast film and powder – suggesting the long alkyl substituents were inhibiting aggregation and reducing non–radiative decays.

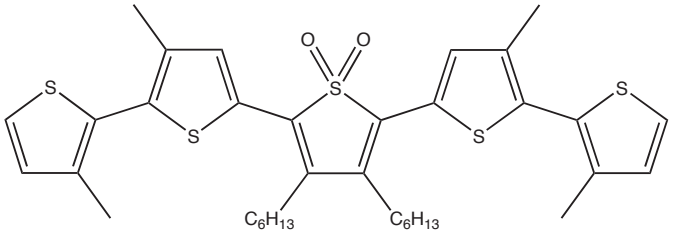

(a) T5OMe reported by Gigli *et al.*

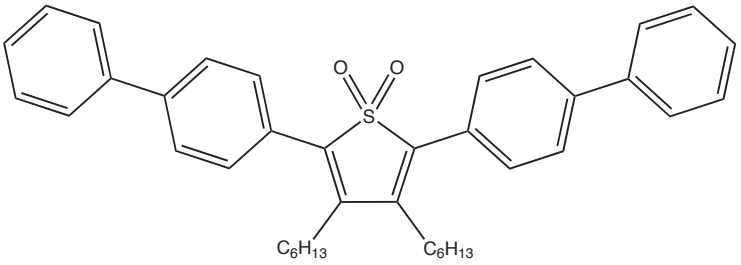

(b) Compound capable of PL efficiency of 70 %.

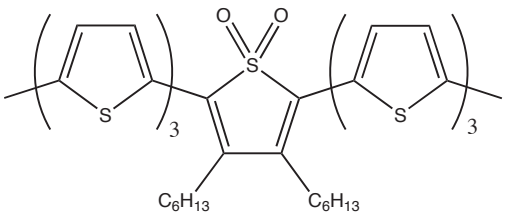

(c) Compound with PL efficiency of 2 % with emission in near–IR.

Figure 3.4: Compounds developed by Barbarella *et al.*. [80]

To further understand and tune the properties of these oligothiophene–based systems, a systematic analysis of the effects of each type of functionalisation was performed:

- unsubstituted pentathiophene (PL efficiency = 2 %);
- pentathiophene with the central thiophene disubstituted with hexyl chains (2–3 %);
- the central core substituted *and* oxidised (11–13 %);
- T5OMe (see Figure 3.4a) (37 %).

It was concluded that the 5–fold increase in efficiency could arise from disrupted molecular packing, occurring with the oxidised species because the oxygen atoms sit above and below the plane of the oligomer, preventing close packing.

Further work by Barbarella and collaborators [80] on these compounds and other derivatives has seen the tuning of their EL emission from green to near-IR, and PL efficiencies as high as 70 % (see Figures 3.4b and 3.4c). Inclusion of these compounds and several derivatives in blended PV devices, in which they were designed to act as electron-acceptor materials, was reported later. [81, 82]

3.1.3 3,4-Ethylenedioxythiophene derivatives

Capping of the *3* and *4* positions of the thiophene ring with an ethylenedioxy (EDO) bridge forms 3,4-ethylenedioxythiophene, EDOT. In 1988 Bayer AG filed a patent for poly(3,4-ethylenedioxythiophene) (Figure 3.5), a polymer they had developed when trying to circumvent the insolubility of thiophene oligomers and polymers, caused by unwanted couplings along the backbone of the polymer *via* the *3* and *4* sites.

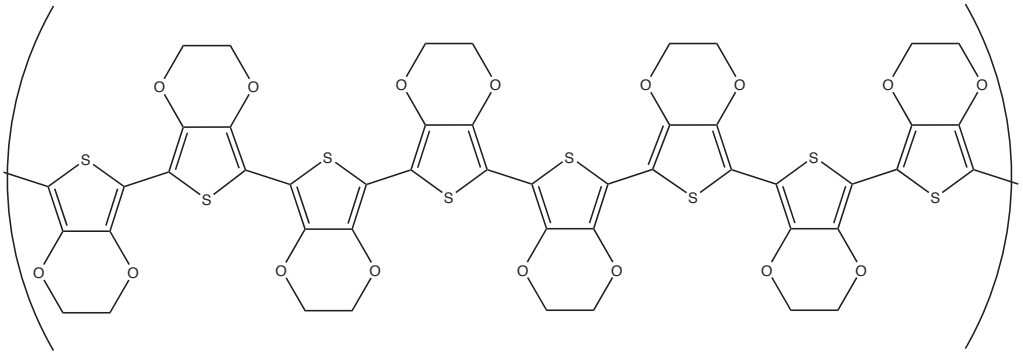

Figure 3.5: Poly(3,4-ethylenedioxythiophene).

The EDO bridging unit also increases electron density in the thiophene ring, thereby increasing the electron–rich character of the unit. Prepared by either oxidative chemical or electrochemical polymerisation techniques PEDOT was, ironically, found to be insoluble. Means to negate this problem were found in the form of the water soluble electrolyte poly(styrene sulfonic acid) (PSS) which acted as a charge balancing dopant. The polymer (PEDOT) exhibited very interesting properties, notably high conductivities (~ 300 Scm^{-1}) and transparency upon oxidation as a thin film. Furthermore, it was largely stable in this oxidised state. Consequently a film of PEDOT/PSS provided a robust and useful conductive material with good optical properties that led to its application as an antistatic coating on photographic film

for AGFA. [83] It has also been developed for use as a layer in OLEDs to aid charge injection, and in photovoltaic devices. [84, 85]

Films of PEDOT are transparent and light blue in the oxidised, conducting, form whereas, in the neutral form, the PEDOT film is dark blue (λ_{max} = 610 nm). It has a low oxidation potential, and as such can oxidise in air, so handling requires an inert atmosphere. Alkylated derivatives have been prepared which are stable enough to afford characterisation.

Bayer AG produce 3,4-ethylenedioxythiophene on an industrial scale and sell it commercially as BAYTRON–M (where M stands for monomer). It can be prepared *via* the route described by Groenendaal *et al.*, [83] however the first four steps were described in 1967 by Gogte *et al.* [86] Decarboxylation is achieved with a copper salt, leaving unsubstituted 3,4-ethylenedioxythiophene (see Figure 3.6).

Due to its impressive conduction, film–forming and optical properties, as well as its ready availability as BAYTRON–M and BAYTRON–P (commercially available polymer blend of PEDOT/PSS by Bayer AG), the EDOT group has been incorporated into a wide range of molecules for a myriad of applications.

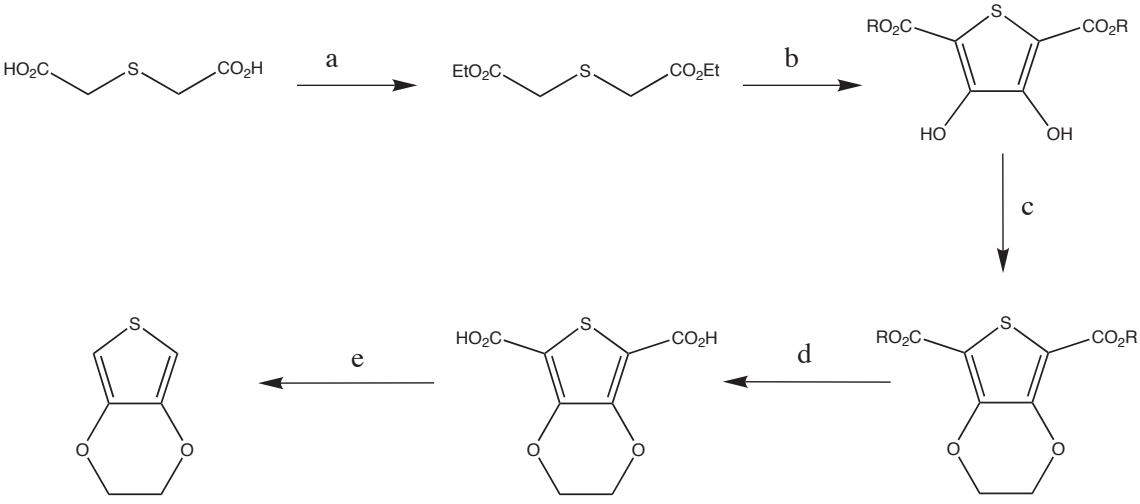

Figure 3.6: Route to 3,4-ethylenedioxythiophene as reported by Groenendaal *et al.*. [83] a) EtOH; b) ethyl oxalate/NaOMe; c) dichloroethane; d) i/NaOH, ii/ HCl; e) CuO.

Reynolds *et al.* have reported the preparation and subsequent electrochemical study of several compounds which display electrochromism. [87] Control over the electronic band–gap for a polymer system can be obtained by adjusting the π–

overlap along the polymer's backbone, as well as by altering the π–system with substitution of electron donating or withdrawing groups. Reynolds has shown this to be possible with EDOT–based polymers. Several EDOT containing oligomers were prepared, with the EDOT groups separated by various bridging moieties, including ethene, benzene, tolan and other heterocycles. The group reported colours ranging from deep purple through deep blue to red and orange, corresponding to band–gaps ranging from 1.4 eV to 2.3 eV. The polymeric system of bis(ethylenedioxythiophene) pyridine was shown to be capable of undergoing n– and p–type doping to display electrochromism; red when neutral, pale blue when reduced, and dark blue/purple when oxidised (Figure 3.7). [88] The protonated species was also reported as being coloured dark blue/indigo, suggesting potential applications as a pH sensor or switch.

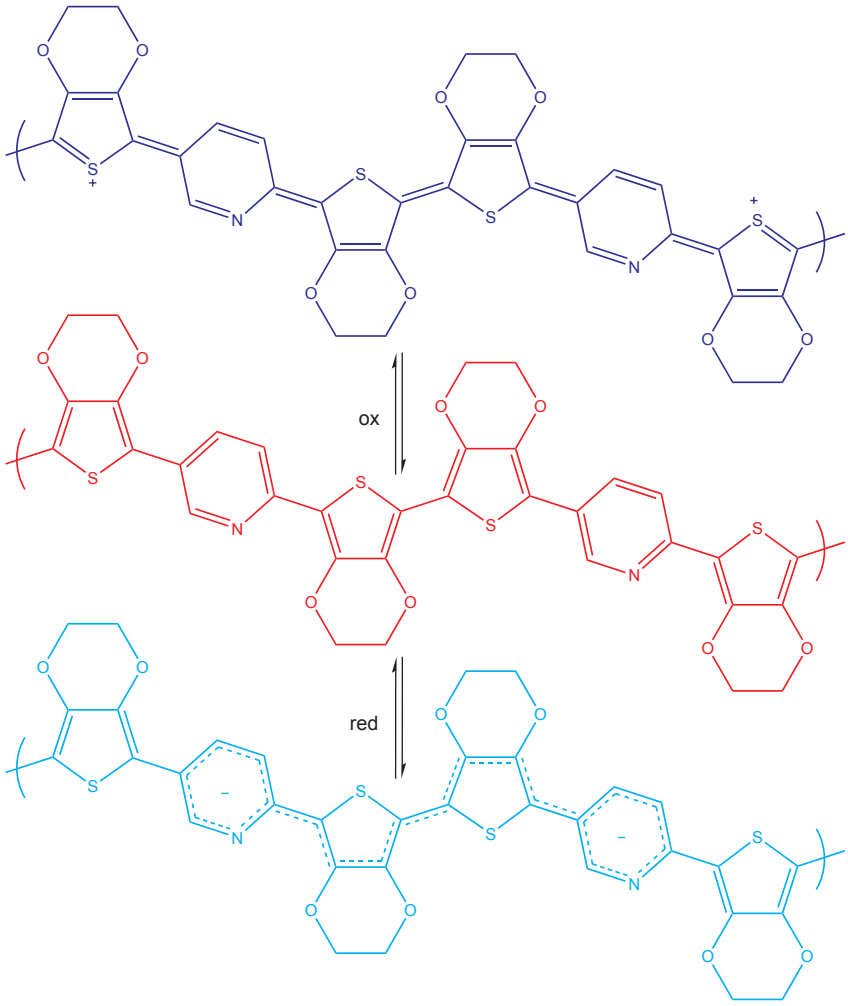

Figure 3.7: The neutral and electrochemically oxidised and reduced compound reported by Reynolds *et al.* [88]

3.1.4 3,4-Ethylenedioxythiophene-1,1-dioxide derivatives

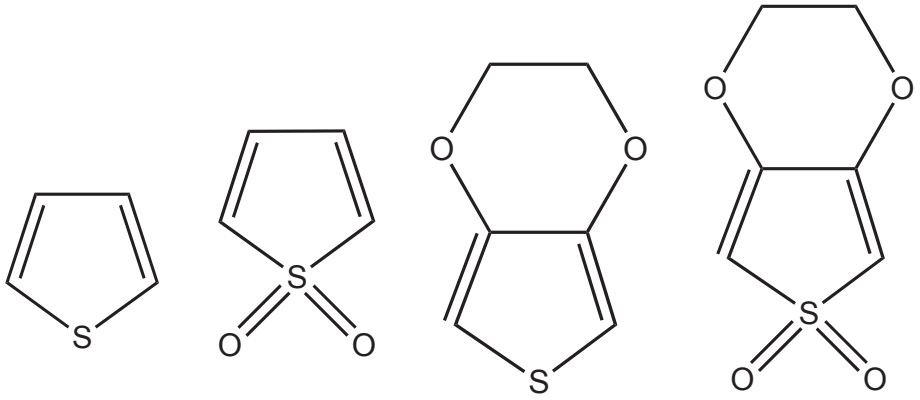

(a) Thiophene. (b) Thiophene-1,1-dioxide. (c) 3,4-Ethylenedioxythiophene. (d) 3,4-Ethylenedioxythiophene-1,1-dioxide.

Figure 3.8: Chemical modifications of thiophene that have been discussed.

The combination of an electron donating ethylenedioxy (EDO) bridge and the electron withdrawing S,S–dioxide as a singly thienyl moiety was discussed by Zotti and co-workers (see Figure 3.8d). [89, 90] 3,4-Ethylenedioxythiophene-1,1-dioxide ($EDOTO_2$) was coupled with thiophene and EDOT to form oligomers. In the paper the attempted analysis of the effect of the different groups on the oligomers' overall properties, including magnetism, conductivity and luminescence, was carried out by systematically pairing different thiophene derivatives together. The inclusion of the sulfone character was expected to improve photoluminescence efficiencies, with the EDO bridge lowering the oxidation potential (and improving charge injection properties) whilst also reducing the possibility of oxidative defects during polymerisation. The alternation of electron–rich and electron–deficient units to create finite windows of conductivity was described and built on findings from their earlier work involving alternating pyrroles, phenyl and thiophene rings.

Using anodic electropolymerisation of the monomers Zotti prepared several polymer systems. Due to the insolubility of the polymers, Zotti only reported absorption properties of the monomers, observing various subtle effects attributed to the $EDOTO_2$ group.

A review of the peak reduction and oxidation potentials indicated that the oligomers containing thiophene-1,1-dioxide as the central core were more easily re-

	Compound	λ_{abs} / nm	E_p^{ox} / V	E_p^{red} / V
1	EDOT - TO_2 - EDOT	463	0.70	-1.60
2	T - TO_2 - T	415	1.25	-1.65
3	EDOT - $EDOTO_2$ - EDOT	452	0.47	-1.90
4	T - $EDOTO_2$ - T	439	0.78	-1.76

Table 3.1: The absorption maxima and peak potentials for the $EDOTO_2$–containing oligomers as reported by Zotti and co-workers, compared to TO_2–containing oligomers (T = thiophene).

duced, and compound 2 (T - TO_2 - T) exhibited the highest oxidation potential, attributed to it not containing any electron–rich EDO groups. The presence of the EDO bridge on the thiophene-1,1-dioxide ring appeared to impede reduction of both systems, whilst facilitating oxidation.

3.1.5 Fused thiophene systems

The last class of thiophene derivatives to be discussed in this chapter is fused thiophenes. A thorough review of the syntheses and reactions of thienothiophenes was written in 1976 by Litvinov and Gol'dfarb. [91] More recently new synthetic routes which are more elegant have been reported, and have facilitated development of a broad range of novel materials, with a myriad of potential applications for the polyheteroarene.

Interest in fused thiophenes for their potential application in conducting polymers began in the late 1980's, [92,93] perhaps predictably around the same time that conducting polymers of thiophene were making an impact on the scientific community, combined with interest in compounds such as pentacene for use in FETs. [94]

Fused thiophene systems afford greater π—π overlap and stacking, potentially improving the internal charge transfer and thus conduction properties of bulk polymers. Furthermore, the fusion affords greater ordering of the bulk material, which in itself has been shown to improve the conduction properties of polymers. Their planarity also aids in this respect. [66,94–96] The fused systems are superior to non–sulfur containing analogues due to their enhanced stability and robust nature, and exhibit face-to-face stacking *c.f.* 'herringbone' type packing (as seen with non–fused

oligothiophenes and pentacene), attributed to an S—S interaction. This stability affords advantages over the non–sulfur–containing analogues. For instance, whilst hole mobilities in pentacene (Figure 3.9a) are two orders of magnitude (5 $cm^2V^{-1}s^{-1}$) greater than pentathienoacene (Figure 3.9b), [93] pentacene is largely unstable in oxygen, and not at all under illumination.

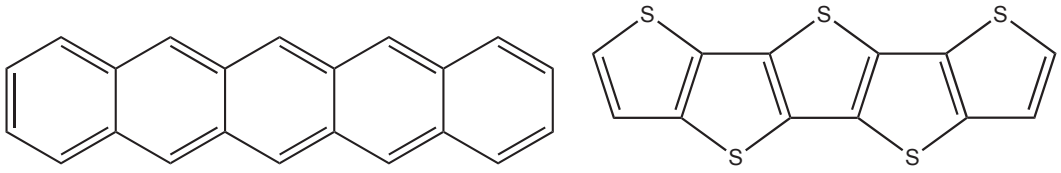

(a) Pentacene (b) Pentathienoacene

Figure 3.9: Fused arene systems.

Kim *et al.* incorporated fused thiophene systems as the relays between the donor and acceptor constituents of non–linear optical chromophores. The acceptor group's strength was altered, allowing the determination of the role of the relaying unit (dithienothiophene - DTT) in the solvatochromism and molecular non–linearity to be investigated. The fused system out–performed the bi– and terthiophene systems, as well as exhibiting improved thermal stability. [97]

McCulloch and co-workers have published several articles on polymers incorporating the thienothiophene group. [96, 98–100] In 2005 they published their work on a semiconducting polymer which contained thieno[2,3-*b*]thiophene in the backbone (see Figure 3.10a). This stable and readily prepared compound does not allow conjugation from its *2*– position to its *5*– position, blocking π–conjugation along the polymer backbone, ultimately allowing control over the HOMO level. Lowering the HOMO increases the ionisation potential hence improving polymer stability without the need for disrupting the packing and ordering of the bulk polymer, or hindering polymerisation techniques, which other means of control do. [98]

In 2006 McCulloch and co–workers published the preparation of the fully conjugated isomer (see Figure 3.10b). [99] This was also designed with the aim of controlling the ionisation potential; increased resonance stabilisation relative to single thiophene rings should reduce delocalisation of electrons from the fused system into the polymer backbone, hence lowering the HOMO level of the polymer. The

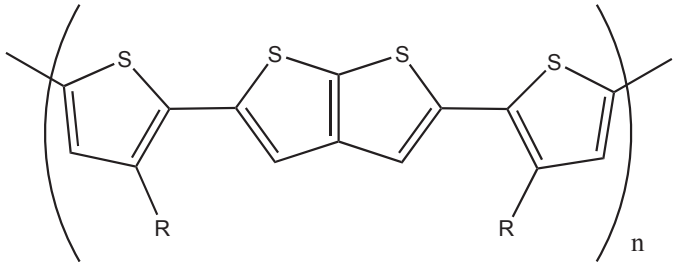

(a) Cross-conjugated poly(2,5-bis(3-alkylthiophen-2-yl)-thieno[2,3-*b*]thiophene, PBTCT.

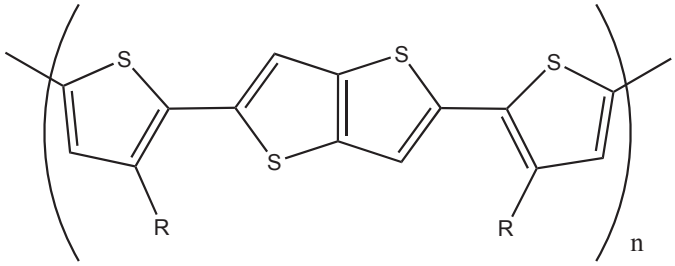

(b) Conjugated poly(2,5-bis(3-alkylthiophen-2-yl)-thieno[3,2-*b*]thiophene, PBTTT.

Figure 3.10: McCulloch's semiconducting thienothiophene-containing polymers.

measured ionisation potential of the polymer was 0.3 eV higher than that of the polymer P3HT, attributed to the reduced delocalisation. Further calculations on the systems in Figure 3.10, compared to data on P3HT systems, confirmed experimental data that the ionisation potential of PCTBT (incorporating the cross-conjugated thienothiophene) was the highest; the conjugation break induced by the [2,3-*b*]thiophene stabilised the HOMO. [100]

Research by Dong Hoon Choi published in 2007 showed incorporation of thiophene and fused thiophenes in "star-shaped" molecules, or cruciform structures, for application as organic semiconductors in FETs (see Figure 3.11). [101] Of the three systems reported the DTT derivative exhibited the highest mobilities (2.5×10^{-2} $cm^2V^{-1}s^{-1}$), 10 × greater than that for the thiophene derivative, and 100 × greater than the thieno[3,2-*b*]thiophene derivative. Furthermore its film–forming ability out–performed the others, with high degrees of homogeneity. It was suggested that it was these superior film–forming properties that could be responsible for the improved charge transporting properties. Photophysical analysis of the cruciforms taken in solution and as films was also presented. Solution measurements

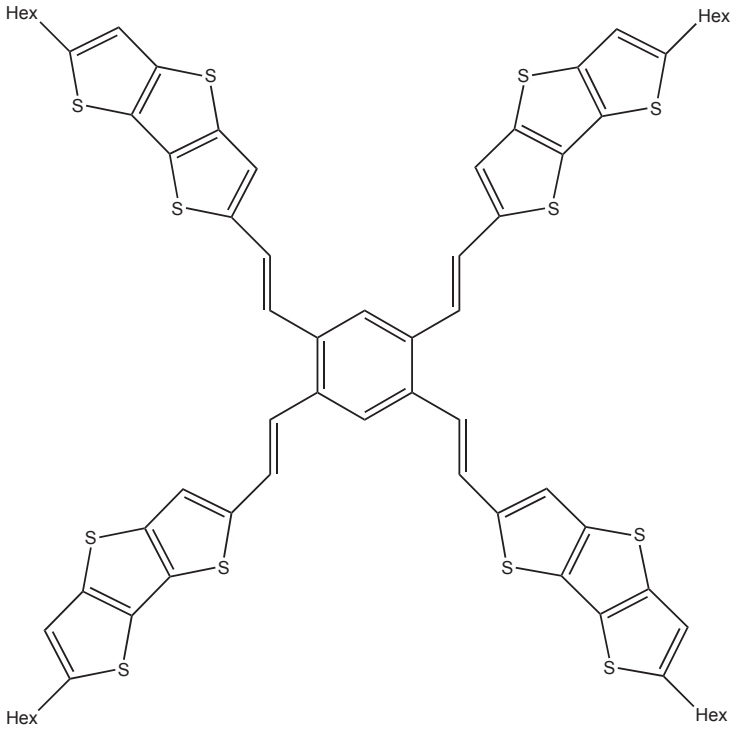

Figure 3.11: Choi's cruciform, featuring DTT as the spacer group. Cruciforms featuring thiophene and thieno[3,2-*b*]thiophene as the spacer group were also prepared.

demonstrated that the intramolecular conjugation affected the absorption λ_{max} substantially, and the thieno[3,2-*b*]thiophene derivative exhibited the highest energy absorption, at 395 nm, attributed to it having the shortest conjugation length. In the solid state, notable changes in the spectral profile were observed, dependent on the thermal annealing process for the thiophene and DTT–containing analogues. This was assigned to high degrees of molecular interaction; essentially the compounds which afforded greater packing and homogeneity exhibited greater vibronic fine structure, due to π–stacking. Emission spectra were typical, with maxima subject to a red–shift with increasing conjugation length. Furthermore, the Stoke's shifts for the fused thiophene systems were lower than that of the thiophene analogue. This is attributed to an enforced planarity in the ground state of the fused systems requiring less structural reorganisation upon excitation (see the Franck Condon principle, section 1.4.1).

Recent work has seen thienothiophenes incorporated in photo–switching molecules. [102] Ko *et al.* coupled methyl–substituted thienylboronic acids with brominated thieno[3,2-*b*]thiophene and DTT cores, under Suzuki-Miyaura conditions, to cre-

ate a series of thienothiophene oligomers which display photochromism, as well as photo–switchable luminescence (see Figure 3.12).

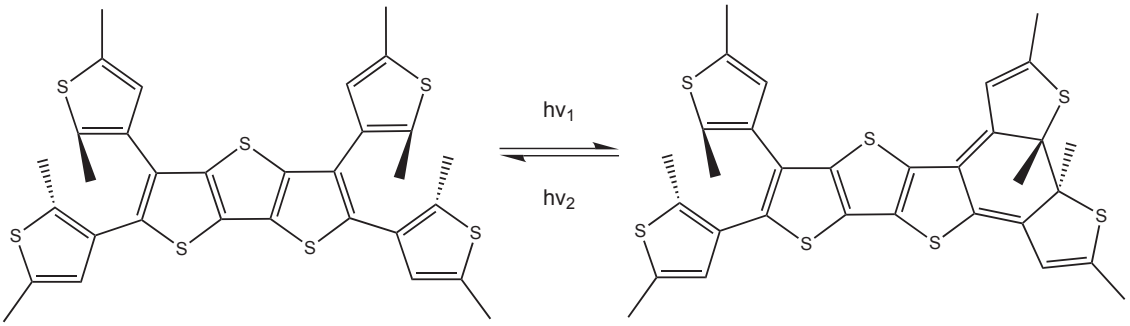

Figure 3.12: Photo–switchable thienothiophene group by Ko *et al.*

Perepichka *et al.* have developed rings of fused thiophenes. [103] In an effort to improve organic semiconductor mobilities, and to avoid using benzene rings, Perepichka's group took the novel approach of increasing conjugation by fusing thiophene into a macrocycle; a circulene. An 8–ring circulene, octathio[8]circulene, was synthesised and proved capable of p–type semiconduction, with a hole mobility of 9 $\times$ 10^{-3} $cm^2V^{-1}s^{-1}$. It is thought that the π–stacked columns engendered a largely one–dimensional charge transfer *along* the columns, but little *inter* column charge transport.

The virtues and properties of general arylethynylene–based systems were briefly discussed earlier (see section 1.3.1, from page 10). The inclusion of heterocycles in these systems has been less widely studied. Of these heterocycles thiophene derivatives are among the most studied and as such a selection of the myriad papers published on thienylethynylene systems are discussed in the next section. [5, 9, 22, 104–115]

3.1.6 Arylethynylenes incorporating thiophene derivatives

Typical of both the thiophene derivatives and phenylethynyl systems examined so far, the highly conjugated and linear structure of thienylethynylenes gives rise to high conduction and luminescence, whilst the bent nature of some oligomeric species highlights their potential in the field of liquid crystals. [109]

In the early 1990s poly(phenylenevinylene) (PPV) polymers were exhaustively studied and their properties reported, but poly(aryleneethynylenes) (PAEs) were largely ignored. This was most likely due to their poor solubility in normal solvents. [9, 104] This issue was circumvented in 1993 when Yamamoto and co-workers reported the synthesis of PAE's incorporating an alkyl–substituted thiophene. [105, 106] Yamamoto cross–coupled hexyl–substituted 2,5-diiodothiophene with 1,4-bis-(ethynylene) benzene and 2,5-bis(ethynylene)pyridine in a palladium catalyzed polycondensation reaction (using Sonogashira conditions), forming polymeric compounds that were soluble in chloroform, THF and acetonitrile. This allowed simple electrochemical and photophysical analyses to be performed, which indicated that the pyridine–containing polymer was readily reduced (attributed to the electron–withdrawing pyridine and acetylene bonds). The following year Yamamoto published further work, [107] with PAEs consisting entirely of thiophenes linked through acetylene bridges. Cyclic voltammetry revealed that reversible reduction (n–doping) was possible on the PAE consisting of thiophene and pyridine rings but, curiously, oxidation (p–doping) was not (see section 3.1.1).

Tour discussed the synthesis of organic electronic devices based primarily on thienyl oligomers following advice from Ari Aviram. [22, 116] Aviram suggested that molecules with certain physical properties could be connected as molecular scale electronic devices. The physical properties cited were that the molecule should be over 50 Å in length and contain orthogonally and non–conjugatedly bound chains. To this end, Tour's group prepared several compounds comprising thiophene oligomers orthogonally bound through a silicon–centered spiro–core moiety. After several unsuccessful attempts to achieve the desired chain length using polythiophene (poor solubility and low yields), an alternative approach was taken. The inclusion of ethynylene bridging units, and thus the use of an iterative divergent/convergent

synthetic route, afforded preparation of the 59 Å long molecule in Figure 3.13.

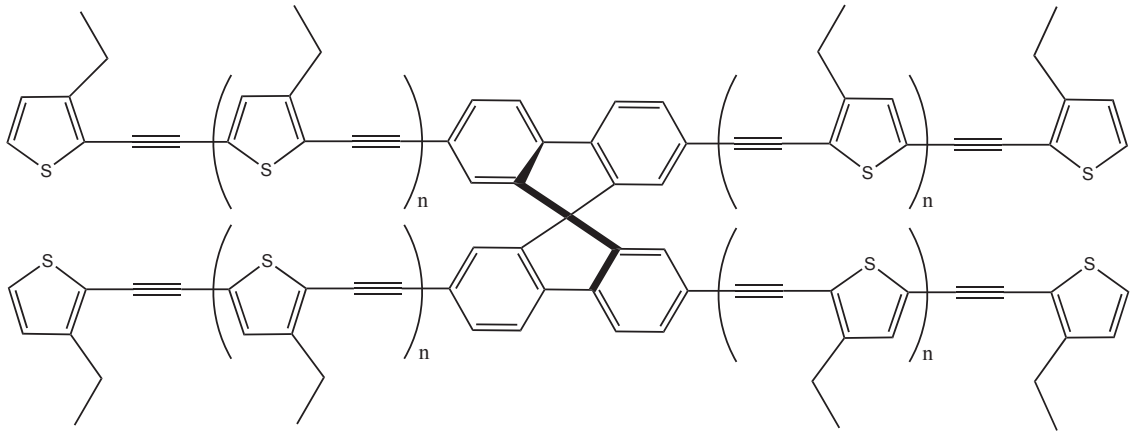

Figure 3.13: Potential molecular switch as devised and prepared by Tour *et al.* [116]

The basic nature of the coupling methods (Sonogashira conditions) was causing decomposition of the central silicon spiro–core, which was replaced by a spirobifluorene. The iterative divergent/convergent coupling sequence initially required a single iodinated thiophene ring that was coupled with TMSA (see Figure 3.14). The

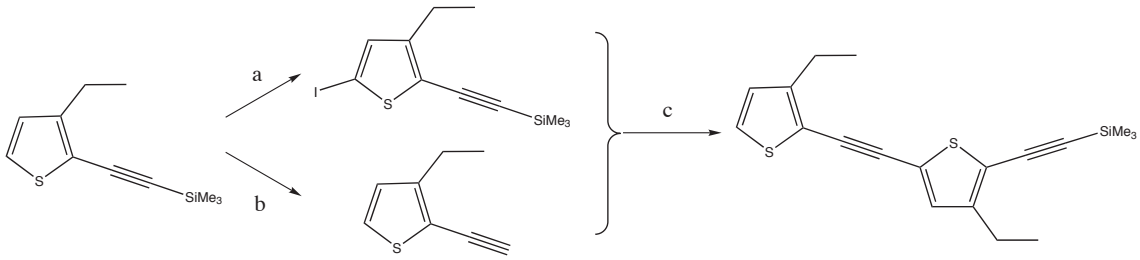

Figure 3.14: Iterative divergent/convergent coupling sequence devised by Tour *et al.* to prepare oligo(thiophene ethynylene)s. [22] a) i/LDA, Et_2O, -78 °C – 0 °C, ii/ I_2, -78 °C; b) K_2CO_3, MeOH; c) Sonogashira using $PdCl_2(PPh_3)_2$, CuI, *i*–Pr_2NH/THF.

product from this was then deprotected and halogenated, so the sequence continued. Quick chain growth was possible with chain propagation at a rate of 2^n (where n is the iteration number), and any potential solubility problems were negated by inclusion of ethyl–substituted thiophene.

In 1998 Zotti *et al.* reported the synthesis of several monomers consisting of thiophene and EDOT linked by acetylenes. The monomers were anodic coupled to form polymeric systems whose solubility was enhanced by substitution with octyl chains. [117] The electrochemical data led to the conclusion that the electron accepting acetylene moiety greatly hindered oxidative–defect–free polymerisation, but

this could be improved with substitution of electron–donating groups such as alkoxy and alkyl chains. The polymerisation of the EDOT–ethynylene monomer allowed formation of hexamers *i.e.* 12 thiophene units (as determined by IR spectroscopy), however these were insoluble in chloroform.

Yamamoto reported the first synthesis of an phenylethynylene-alternating thiophene-1,1-dioxide polymer in 1999 [118] (see Figure 3.15), by palladium catalysed cross coupling. Due to its insolubility, solution state photophysical and electrochemical spectroscopy was not performed, therefore CP–MAS solid state ^{13}C NMR and IR–spectroscopy provided the only means of characterisation.

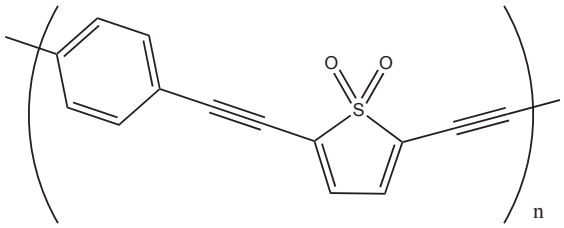

Figure 3.15: Yamamoto's alternating phenylethynylene thiophene-1,1-dioxide polymer.

As mentioned in section 3.1.1, Bäuerle reported that oligomers can act as models for polymers. [43] Citing thermal stability, ease of functionalisation, and potentially interesting optical properties, Rodriguez *et al.* [110,113] prepared several short BPEB–type oligomers featuring thiophene as the central ring (see Figure 3.16). The oligomers were synthesised using the Sonogashira cross–coupling method and varied in length from three (n = 0) to seven (n = 2) rings. Different terminal moieties were appended, including TMSA and N,N-dimethylamino groups, which had an effect on the fluorescence spectra. The five ring (n = 1) system featuring the N,N-dimethylamino capped terminus displayed a higher fluorescent quantum yield than the shorter chain, and each featured a single broad band in the emission spectra. This contrasted with the TMSA–terminated systems, which featured two bands in the emission spectra, although their fluorescent quantum yields also increased with chain length (see Table 3.2 for data).

Tanifuji *et al.* demonstrated use of an oligomeric species based on 2,5-bis(arylethynyl)-thiophene as a photoswitching device (see Figure 3.17). [111] The arylethynylene terminal units were substituted with nitronyl nitroxide radicals at the *meta*

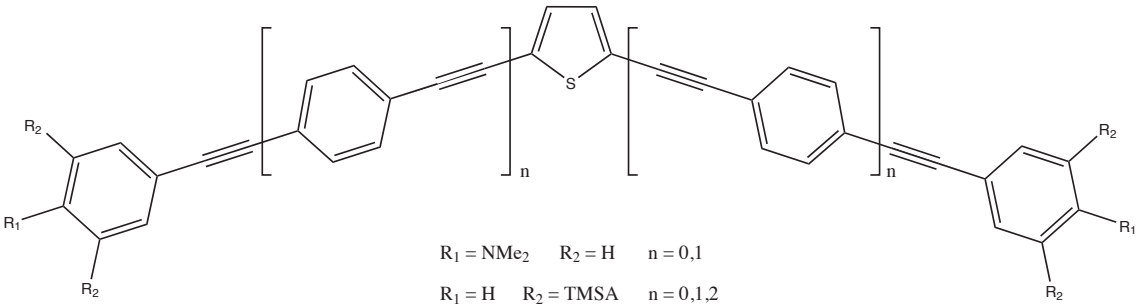

Figure 3.16: Molecules prepared by Rodriguez *et al.*

Compound	Photophysical Properties			
	absorption λ_{max}/nm	emission λ_{max}/nm	ε $M^{-1}cm^{-1}$	ϕ_f
n = 0, NMe_2	385	456	57 500	0.23
n = 1, NMe_2	393	512	104 320	0.30
n = 0, TMSA	355	391, 410	46 900	0.20
n = 1, TMSA	379	421, 447	78 900	0.42
n = 2, TMSA	377	429, 454	113 000	0.54

Measurements obtained in DCM. Data from literature. [113]

Table 3.2: Photophysical properties of compounds reported by Rodriguez *et al.* in DCM.

positions to the ethynylene bridges. The thiophene ring was substituted with a moiety which could undergo cyclization to the 2–position on the thiophene, where the carbon switches from sp^2 hybridisation to sp^3. This switched the conjugation along the main chain of the oligomer up the substitent 'arm' on thiophene, altering the magnetic interaction of the two radicals at the terminus of the arylethynylene chain.

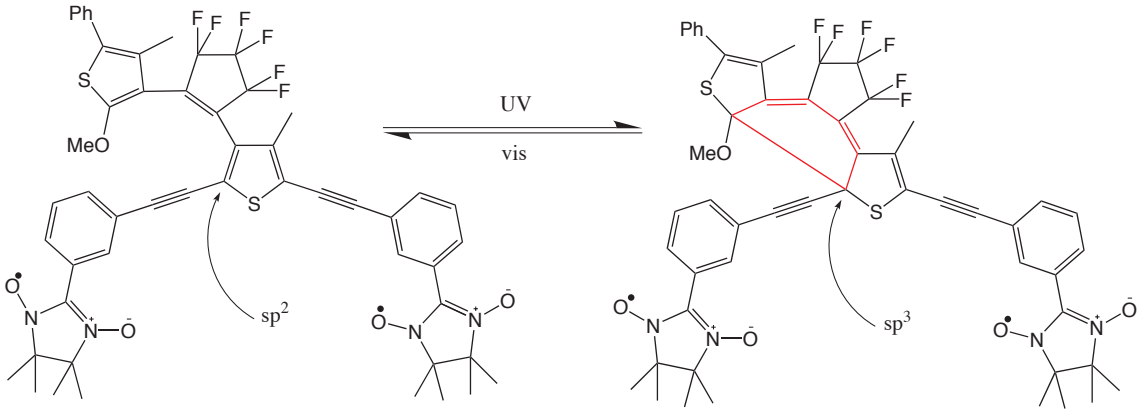

Figure 3.17: Photoswitching molecule reported by Tanifuji *et al.* [111]

In an effort to continue and expand work focused on the photophysical properties of several 1,4-bis(phenylethynyl) arylene systems [26, 119, 120], groups within the University of Durham's Chemistry Department started to investigate thiophene analogues. The photophysical properties of 2,5-bis(phenylethynyl)thiophene were examined by Siddle *et al.* [114] where an appreciation of the electronic structure of several derivatives was probed by the appendage of different groups at the para positions on the terminal phenyl rings; namely electron donating groups NMe_2, OMe, Me and H, and electron withdrawing groups NO_2, CN, CO_2Me and CF_3. Using Sonogashira conditions, two equivalents of the relevant *para*–substituted alkyne were cross–coupled with 2,5-diiodothiophene, to form the various BPET compounds in fair yields (26–60%). The photophysical analyses revealed that appendage of both electron–withdrawing and electron–donating groups resulted in a red–shift of the absorption, suggesting that the $S_1 \leftarrow S_0$ energy gap was decreased by electron–donating groups destabilising the HOMO more than the LUMO, whilst electron–withdrawing moieties stabilised the LUMO more than the HOMO. The spectroscopic observations were rationalised with the aid of DFT calculations. The quantum yields for

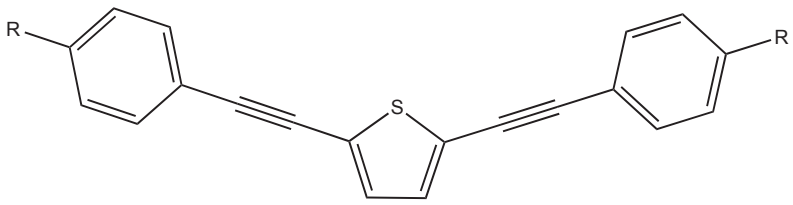

Figure 3.18: 2,5-bis(Arylethynyl)thiophene derivatives as studied by Siddle *et al.* R = H, Me, OMe, NMe_2, NO_2, CN, CO_2Me, CF_3.

the bis(arylethynyl)thiophenes ranged from 19–33 % in toluene. The excited state of the nitro–derivative was subject to non–radiative decay in toluene solutions, as nitro groups have the propensity to undergo facile quenching by electron transfer. In DCM, however, this compound exhibited a quantum yield of 17 %. The reported quantum yields of the **BPET.R** were generally lower than those of the analogous benzene–based **BPEB** systems from which, Marder indicated, they took inspiration. [26, 121] This is attributed to the presence of the moderately heavy sulfur atom, which increases spin–orbit coupling and thus the propensity of the excited

singlet state to undergo ISC to the triplet state, resulting in lower emissive decay.

3.2 Synthesis of the di-halogenated thiophene derivatives

The arylethynylenes prepared for this work were all the product of a cross–coupling reaction of a di-halogenated thiophene derivative with an arylacetylene. In this section various literature methods for the synthesis of the di-bromo and di-iodo thiophene derivatives will be discussed. This will be followed by a discussion of the syntheses undertaken, including the isolation and characterisation of the di-halogenated species.

3.2.1 Preparation of 2,5-dibromothiophene-1,1-dioxide

In order to prepare 2,5-bis(arylethynylene) thiophene-1,1-dioxides, the dibrominated sulfone precursor is required which can then be coupled with the appropriate arylacetylene under Sonogashira conditions to afford the desired product. However, preparation of the sulfone is non-trivial, as oxidation of substituted thiophene is significantly hindered by deactivating substituents (e.g. bromine). Several routes have been described in the literature.

In 1990 Miyahara *et al.* reported a 93 % yield of S,S-dioxide produced by oxidizing 2,5-dimethyl thiophene with the highly selective oxidizing agent dimethyldioxirane, DMD. The yield for 2,5-dibromothiophene was considerably reduced, at 31 %, [122] even with a concomitant stoichiometric increase of DMD. This method was also chosen by Nakayama *et al.*, the first group to report the synthesis of unsubstituted thiophene-1,1-dioxide [123, 124]. Until this publication the existence of the pure thiophene sulfone was only inferred from chemical trapping experiments. [76]

A second method uses peroxy trifluoroacetic acid, generated from TFAA and concentrated hydrogen peroxide or high test peroxide, as the oxidizing agent. [125–127] Nenajdenko *et al.* reported a solvent–dependent yield of up to 82 % for the oxidation of 2,5-dibromothiophene, illustrating the capability of this system even

with a deactivated thiophene. This method is generally not applicable due to a lack of commercially available high test peroxide.

A third common oxidizing agent is *meta*-chloroperoxybenzoic acid (*m*-CPBA). Literature has shown it to be a weaker oxidizing agent, producing poor yields and impure products [122] when compared to DMD, especially for the deactivated thiophenes. In 1992 Furukawa *et al.* described a very simple three step route (see Figure 3.19), each with yields of > 72 %, converting thiophene through to the desired product, via 2,5-bis(trimethylsilyl)thiophene-1,1-dioxide. [127] This approach

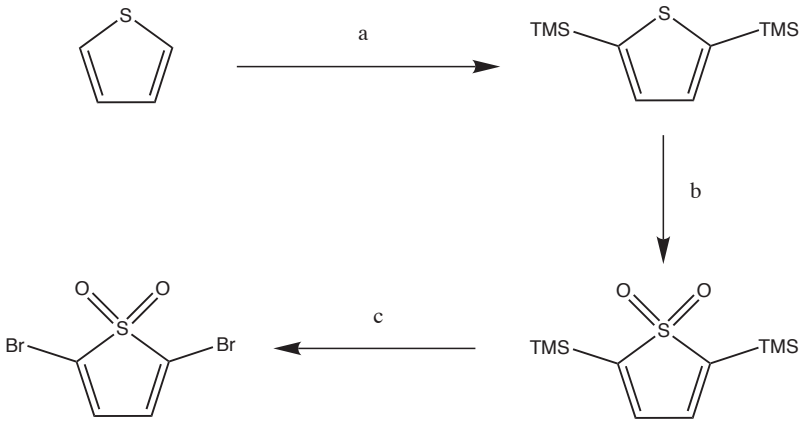

Figure 3.19: Furukawa's [127] route to 2,5-dibromothiophene-1,1-dioxide. a) i/*n*–BuLi/THF/-20 °C, ii/ TMSCl; b) *m*–CPBA/DCM; c) $Br_2/AgBF_4$/DCM.

circumvents the problem of oxidising a deactivated thiophene whilst providing steric stabilization. According to Furukawa *et al.* the trimethylsilyl groups can be converted to the more useful bromine substituent by treatment with elemental bromine in the presence of an excess of silver tetrafluoroborate ($AgBF_4$). Without this reagent this halogenation step carried a significantly lower yield, especially when iodine was the halogen (0 % yield reported).

A fourth route uses the acetonitrile complex of hypofluorous acid, $HOF.CH_3CN$, as the oxygen–transfer agent. [128] The complex is made by bubbling fluorine through acetonitrile and Rozen and Bareket demonstrated its ability to oxidise thiophenes which were not possible to oxidise by other methods, specifically 2,5-dibromothiophene. They reported a 95 % yield after 20 mins at room temperature. More recently this method has been shown to oxidise various other sulfur–containing compounds, [129] including bis(thiophene) in 10 seconds, with excellent yields (85

%). [130]

Discussion of the synthesis of 2,5-dibromothiophene-1,1-dioxide

The third synthetic route to 2,5-dibromothiophene-1,1-dioxide was chosen. This was due to the mild conditions required, the cost and availability of the starting materials and reagents, and the relative convenience of the route. Coupling of thiophene with chlorotrimethylsilane (TMSCl) was possible by reaction of *n*-butyllithium with thiophene in anhydrous THF, at -78 °C. With the heteroatom activating the ring towards ortholithiation and coordinating with the lithium, removal of the *2*-H proton by the butyl group forms the dilithiothiophene. Treatment of the organolithium reagent *in situ* with the electrophile TMSCl afforded the product as a yellow oil (75 %).

The 2,5-bis(trimethylsilyl)thiophene was oxidised in DCM solution by treatment with m-CPBA for 24 h. The yield for this reaction was not as high as the 91 % reported in the literature (achieved 56 %), however, the desired product was readily isolated from the mixture with good purity and large crystals were obtained on recrystallization from hot hexane.

The bromination step was performed under a nitrogen atmosphere and in darkness (equipment covered with Al-foil) due to the propensity of the silver salts to photooxidize and deactivate. Bromine was added dropwise to the stirred mixture, held at 0 °C in an ice bath, and stirring continued for 3 hours. Copious quantities of fumes were produced during this stage and a silver salt precipitate formed. The desired product, 2,5-dibromothiophene-1,1-dioxide, was readily isolated as a very light beige powder (60 %), as confirmed by ^{1}H and ^{13}C NMR spectroscopy and GC MS.

Colleagues within the department from Professor Graham Sandford's group provided us with approximately 1 g of 2,5-dibromothiophene-1,1-dioxide, prepared using the fourth method discussed here. Interestingly, subsequent couplings under Sonogashira conditions were unsuccessful. This route is being continued separately.

3.2.2 Preparation of the dihalogenated-3,4-ethylenedioxy thiophene derivatives

The preparation of the EDOT derivatives was a continuation of work started by Dr S R Rutter who prepared 2,5-bis(phenylethynyl)-3,4-ethylenedioxy thiophene during the course of his work. [42] The dominant route to di-halogenated EDOTs involves the reaction of either N-iodo or N-bromosuccinimide with the commercially available EDOT. As discussed in section 1.6.4 the reactivity of an iodinated-aryl group in a Sonogashira cross coupling reaction is considerably greater than that of an equivalent bromoarene group. Thus, the synthesis of 2,5-iodo-3,4-ethylenedioxythiophene was undertaken, following an adaptation of the method described by Zotti *et al.* (see Figure 3.20). [117]

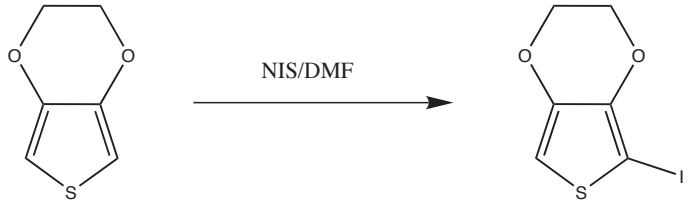

Figure 3.20: Zotti's preparation of 3,4-ethylenedioxy-2-iodothiophene. [117]

Discussion of the synthesis of 2,5-diiodo-3,4-ethylenedioxythiophene

For dihalogenation of 3,4-ethylenedixoythiophene 2.5 equivalents of N–iodosuccinimide (NIS) were used. The synthesis proceeded successfully. The desired product, 2,5-diiodo-3,4-ethylenedioxythiophene, was isolated as a light cream solid (70 %) after purification through a silica-gel plug, eluting with chloroform. ^{1}H NMR spectroscopy and GC MS confirmed the identity of the product.

Oxidation of 2,5-diiodo-3,4-ethylenedioxythiophene was attempted, following the method described by Berlin *et al.* (see Figure 3.21). [89] Possibly due to the increased lability of iodine *c.f.* bromine, isolation of the desired product after oxidation failed. The forcing conditions of the oxidation reaction may have caused cleavage of the C—I bond; certainly oxidation of the sulfur will have removed electron density from the C—I, potentially labilising iodine even more so. As such, preparation of 2,5-dibromo-3,4-ethylenedioxythiophene-1,1-dioxide was required.

Discussion of the synthesis of 2,5-dibromo-3,4-ethylenedioxythiophene-1,1-dioxide

The brominated analogue, 2,5-dibromo-3,4-ethylene-dioxythiophene, was prepared following a known literature method [89, 131, 132], almost identical to that of the iodo-analogue. However, the dibromoethylenedioxythiophene displayed an increased instability with respect to decomposition relative to the iodo–analogue – as Perepichka has shown, it has a propensity to self polymerise, necessitating its storage under nitrogen at low temperature. [133]

Chevrot and co-workers reported the bromination of EDOT using N-bromo-succinimide in chloroform and acetic acid (1:1 v/v), by stirring at room temperature for $\sim$ 3 hours. [131]

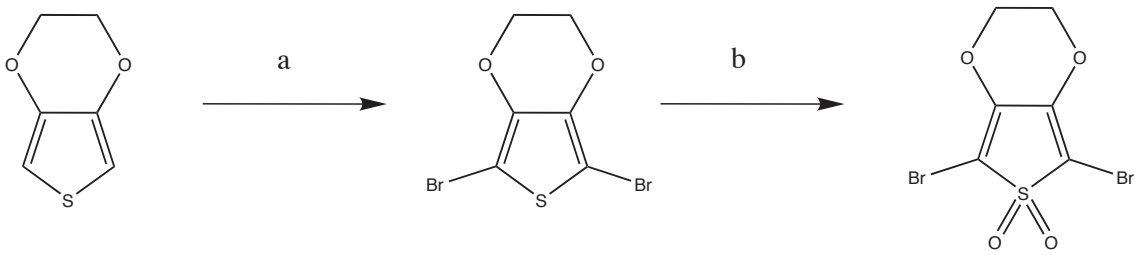

Figure 3.21: Synthetic route to 2,5-dibromo-3,4-ethylenedioxythiophene-1,1-dioxide. a) NBS/$CHCl_3$/AcOH; b) *m*–CPBA/DCM.

During the extraction and isolation of 2,5-dibromo-3,4-ethylene-dioxythiophene (see section 6.1.11, page 212) sodium bicarbonate was used for neutralisation. On one occasion improper neutralisation caused the product to degrade at an accelerated rate, even with containment in an inert atmosphere. Apart from this one occasion, this reaction is robust and efficient and the product was isolated as an off-white powder in 70 % yields. It should be noted that even with sufficient neutralisation *and* storage under an inert atmosphere, the product decomposed over a period of approximately one week, and thus a clean–up using a short silica-gel plug with chloroform or DCM eluent was necessary prior to further use.

Oxidation to the sulfone was carried out using *m*–CPBA, similar to the oxidation of 2,5-bis(trimethylsilyl)thiophene (section 3.2.1, page 67). The brown crude product isolated in this step required purification *via* column chromatography, which yielded a yellow powder in 40 % yield, and was confirmed as the desired product by

^{1}H NMR spectroscopy and GC MS.

3.2.3 Preparation of 2,5-dibromothieno[3,2-*b*]thiophene

In the interests of solubility, ease of preparation, and perceived usefulness of potential data, only thienothiophenes containing two fused thiophene rings were prepared. Larger fused thiophene systems were not attempted. Two routes were attempted for the synthesis of 2,5-dibromothieno[3,2-*b*]thiophene with the first attempt being that used by Frère *et al.* (see Figure 3.22). [134]

Discussion of the synthesis of 2,5-dibromothieno[3,2-*b*]thiophene

Starting from the commercially available 3-bromothiophene, thiophene was lithiated using *n*-BuLi, to which sulfur was added, to generate the anion (Thienyl–S^-) which was reacted without isolation with a separately prepared aqueous solution of potassium bromoacetate. The acetate underwent nucleophilic substitution to create the thiophene–thioacetic acid. A Friedel–Crafts reaction closed the second thiophene ring to produce the dihydrothiophene which was reduced using sodium borohydride to form thienothiophene. Bromination at the *2* and *5* positions was achieved by reaction with 2 equivalents of N-bromosuccinimide.

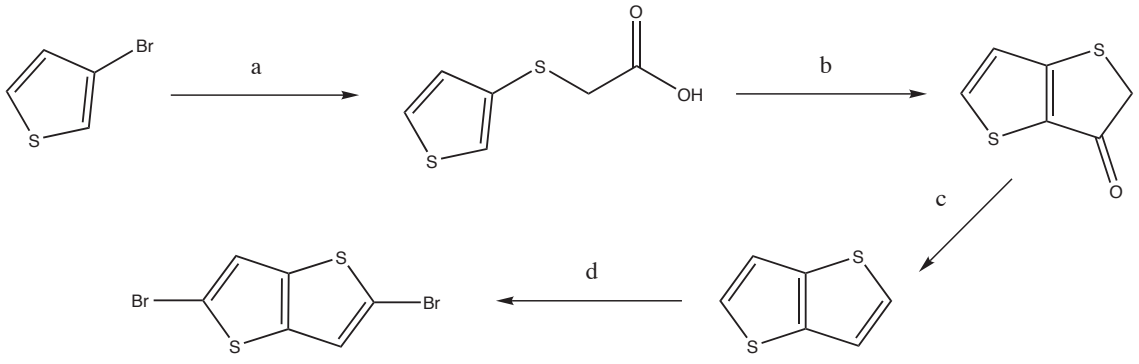

Figure 3.22: First attempted synthetic route to 2,5-dibromothieno[3,2-*b*]thiophene described by Frère *et al.*. [134] a) i/ *n*–BuLi/EtO_2, ii/ sulfur/EtO_2, iii/ potassium bromoacetate/H_2O/THF, iii/ HCl; b) i/$SOCl_2$/EtO_2, ii/ $AlCl_3$/DCE, iii/ 0 °C/HCl; c) $NaBH_4$/DCM/MeOH, ii/ 1M HCl; d) NBS/DMF at 0 °C.

The first step (Figure 3.22 (a)) of this reaction proceeded well, achieving almost quantitative yields of 3-(carboxymethylsulfanyl)thiophene as a light brown oil (puri-

fied by Kugelrohr vacuum distillation). The subsequent ring–closing Friedel–Crafts reaction performed inconsistently between attempts but, when successful, the crude product was obtained as a brown solid (41 % yield). Further purification of this product was deemed unnecessary on inspection of the ^{1}H NMR spectrum and GC MS. As such, the reduction of the carbonyl was performed, affording thieno[3,2-*b*]thiophene as a white solid (75 % yield). Bromination was carried out using NBS, allowing isolation of 2,5-dibromothieno[3,2-*b*]thiophene as a cream solid (96 %), with the GC MS spectrum showing splitting characteristic of the isotopic abundances attributable to a dibrominated species.

As the second step of the synthesis outlined above (Figure 3.22) was relatively slow and low yielding, a large amount of starting material was required to prepare a useful amount of the dibrominated core (overall yield of 29 %). After at least two attempts where the second step achieved a yield substantially lower than that reported above, this route was abandoned in favour of the alternative method, described below.

The second route attempted was an adapted version of that reported by Iddon *et al.* [135] and more recently by Kim [136] and Shim [137] (see Figure 3.23). The same starting material as the first route was used. This was deprotonated at the *2*–position by lithium diisopropylamide (LDA), which was reacted with N-formylpiperidine to generate 2-formyl-3-bromothiophene. Reaction of 2-formyl-3-bromothiophene with ethylglycolate under basic conditions brought about nucleophilic substitution followed by a condensation to form an ester–functionalised thieno[3,2-*b*]thiophene. The ester was then base–hydrolysed to yield the carboxylic acid. Literature methods suggest treatment of the acid with copper powder in quinoline, with heating to 260 °C to remove the acid moiety, and then brominating using NBS in DMF. However, treatment with NBS resulted in simultaneous decarboxylation and bromination and second bromination in a one–pot reaction (see Figure 3.23). This method proceeded well, achieving a global yield of 48 % (*c.f.* 29 % for the first route). 3-Bromothiophene-2-carbaldehyde was isolated as a dark yellow oil (76 %) after purification of the crude brown oil product by vacuum distillation. The second step proceeded similarly well, requiring a vacuum distilla-

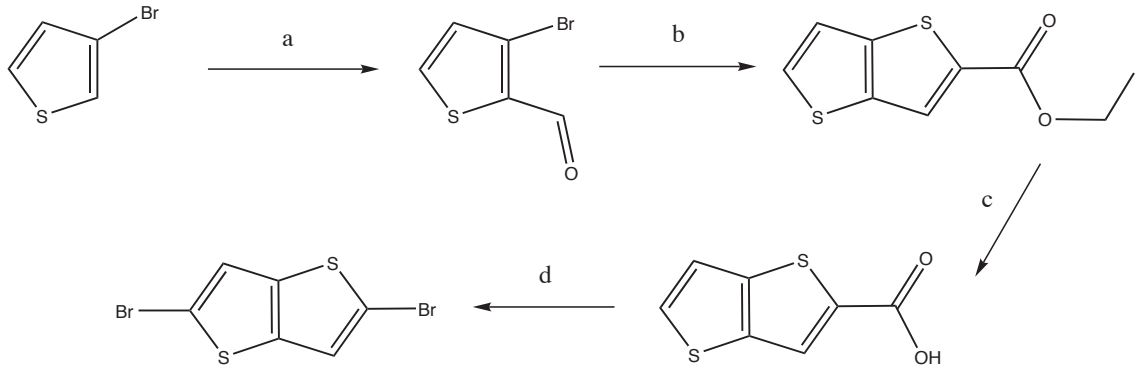

Figure 3.23: Iddon's reported synthesis of 2,5-dibromothieno[3,2-*b*]thiophene. [135] a) i/LDA/THF at 0 °C, ii/ N-formylpiperidine, iii/NH_4Cl; b) Ethylthioglycolate/K_2CO_3/DMF/H_2O; c) i/ LiOH/THF, ii/ 5M HCl; d) NBS/NMP.

tion of the crude product to isolate ethyl thieno[3,2-*b*]thiophene-5-carboxylate as a light orange oil (85 %). Atmospheric Solids Analysis Probes (ASAP) mass spectrometry was performed, confirming the presence of the desired product, corroborating the ^{1}H NMR spectroscopy characterisation. The ester was then hydrolysed to afford thieno[3,2-*b*]thiophene-5-carboxylic acid as a white solid (90 %). The bromination step performed was an adapted method of that reported by Campbell *et al.* for the decarboxylation-dibromination of 3,4-dimethylthieno[2,3-*b*]thiophene-2,5-dicarboxylic acid. [138] The acid was dissolved in N-methylpyrrolidone and 2.3 equivalents of NBS in a minimum amount of water were added slowly over one hour followed by stirring over night. On addition of further water a solid precipitated, which was isolated and dried. Characterisation confirmed the isolated solid as being the desired product, 2,5-dibromothieno[3,2-*b*]thiophene, a white solid with no need for further purification (83 % yield).

3.2.4 Preparation of 3,6-dibromothieno[3,2-*b*]thiophene

3,6-Dibromothieno[3,2-*b*]thiophene can be prepared *via* two different reaction routes. A route was reported by Matzger *et al.* only recently, [139] and employs lithiation to deprotonate at the *3* and *6* positions of 2,5-dibromothieno[3,2-*b*]thiophene (see Figure 3.24). Using kinetic–controlled conditions the bromines swap positions and the *2* and *5* positions accept protons.

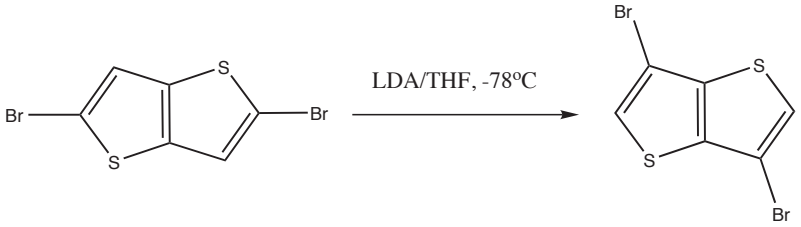

Figure 3.24: Matzger's route to 3,6-dibromothieno[3,2-*b*]thiophene.

The route reported by Iddon *et al.* [135] was slightly modified for use in the preparation of the compound presented in this work.

Discussion of the synthesis of 3,6-dibromothieno[3,2-*b*]thiophene

Iddon's route has been reported numerous times in the literature [96, 140, 141] and requires, as its starting material, thieno[3,2-*b*]thiophene-2-carboxylic acid. The synthesis of the acid was by addition of elemental bromine in acetic acid with bromination of the rings favoured over bromo-decarboxylation. After the initial aliquot of bromine, water was added to the acetic acid and precipitation of the mono–brominated acid occurred. The precipitate was then refluxed in acid, and a second aliquot (1.5 equivalents) of bromine was added. A final excess of bromine (4 equivalents) ensured each proton was displaced by a bromine atom. The removal of the bromine atoms at the *2* and *5* position with zinc in acetic acid at reflux afforded isolation of the desired product in 75 % yield.

The modified procedure used to generate 3,6-dibromothieno[3,2-*b*]thiophene for preparation of **BPEantXTT.tBu** is depicted in Figure 3.25. The starting material, 2,5-dibromothieno[3,2-*b*]thiophene, was prepared as described in section 3.2.3, page 72. Isolation of the tetrabrominated thienothiophene proceeded easily, following the methodology described by Iddon. A pink solid was precipitated initially, but recrystallisation out of hot THF yielded white needles (75 %), confirmed as the product by ^{1}H NMR spectroscopy (only residual solvent peak), GC MS (molecular ion peak included the splitting characteristic of isotopic abundances of a tetrabrominated species), and elemental analysis. Debromination proceeded as per the literature method, with an excess of zinc added after the GC MS indicated the presence of the tribrominated species. The desired product, 3,6-dibromothieno[3,2-*b*]thiophene,

was isolated pure as a grey/white solid in 60 % yield.

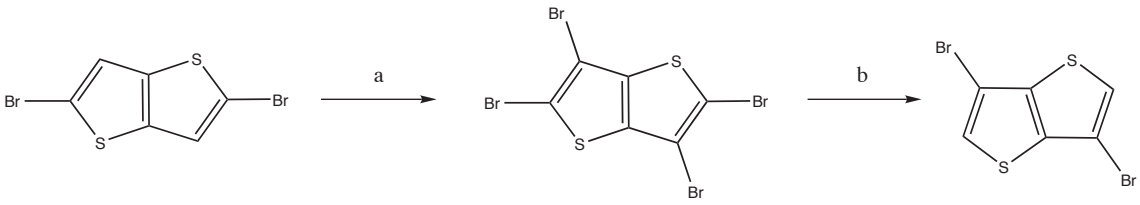

Figure 3.25: An adapted version of Iddon's reported route to 3,6-dibromothieno[3,2-*b*]thiophene. a) i/ AcOH/Br_2, ii/ Br_2, iii/ excess Br_2; b) AcOH/Zn dust.

A comparison of the ^{1}H NMR spectra of 2,5– and 3,6-dibromothieno[3,2-*b*]thiophene shows the difference in chemical shift of the two thienyl protons (see Figure 3.26). The effect of the electron-withdrawing sulfur is evident, with the protons on 3,6-dibromothieno[3,2-*b*]thiophene being deshielded by 0.17 ppm relative to the protons at the *3* and *6* position on 2,5-dibromothieno[3,2-*b*]thiophene.

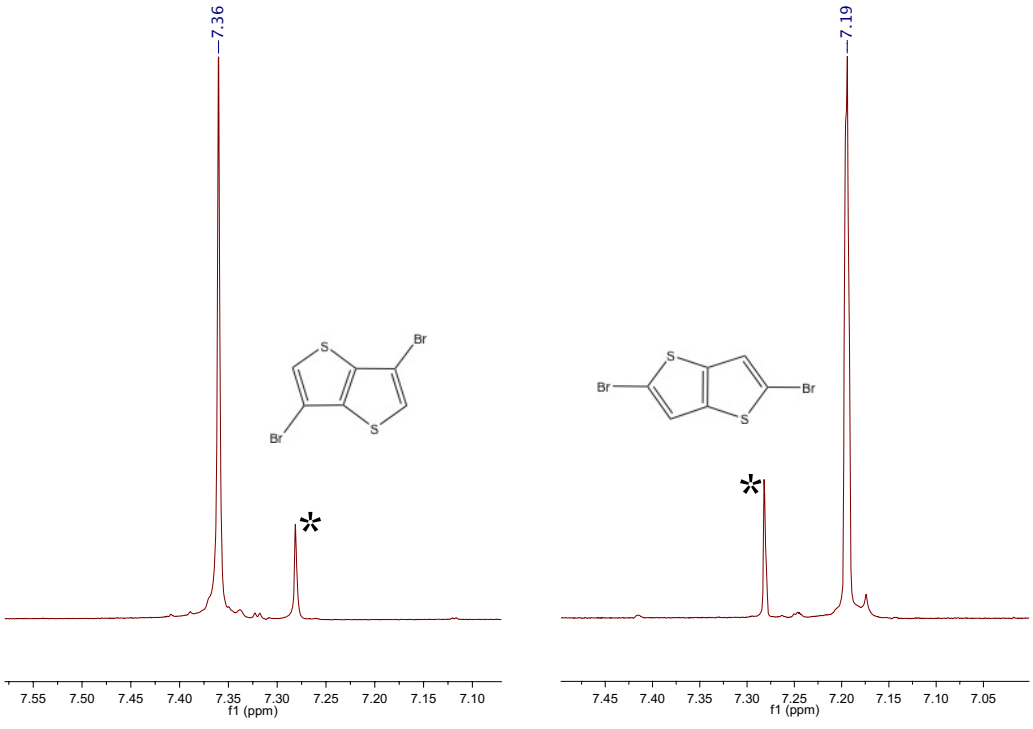

Figure 3.26: Expanded section of 400 MHz ^{1}H NMR spectra of the 2,5- and 3,6-dibromothieno[3,2-*b*]thiophene, recorded in $CDCl_3$. * denotes residual solvent peak.

3.2.5 Preparation of 2,5-dibromothieno[2,3-*b*]thiophene

Several synthetic routes exist for the preparation of thieno[2,3-*b*]thiophene, [96,142–145] with the methodology reported by Kirsch and Comel [145] followed for preparation of the compound presented herein. Kirsch and Comel's paper also provided a good source of literature on the *syn*-thienothiophene group and its synthesis.

Gronowitz and Persson reported one of the earliest routes, [142] but the methodology reported by Brandsma and de Jong [143] is far more elegant. It also provides the basis for the route described by Kirsch.

Brandsma reasoned that information known about thiophene ring opening reactions and, conversely, preparations of thiophene, could be applied to thienothiophenes. 1,3-diynes were known to react with H_2S to form thiophenes, and Brandsma considered this methodology, if applied to the correct diiyne, a potential synthetic route to thienothiophenes. The scheme in Figure 3.27 illustrates Brandsma's route.[2]

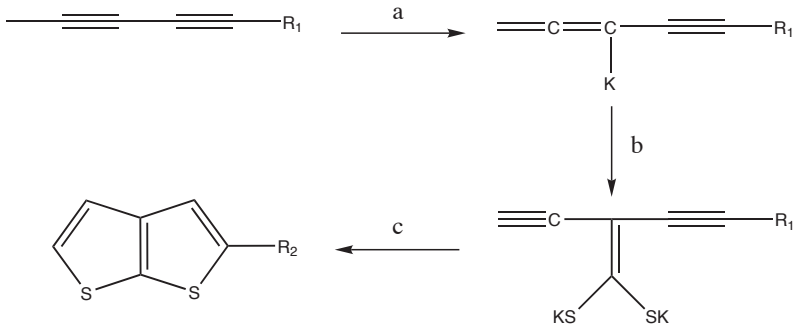

Figure 3.27: Brandsma's synthetic scheme to thieno[2,3-*b*]thiophene. [143] a) i/ BuLi/THF, ii/ *t*–BuOK/THF/hexane; b) CS_2/-100 °C; c) *t*–BuOH/HMPT.

A second route, described by McCulloch *et al.*, [96] starts with alkylation of 2-thiophenethiol by bromoacetaldehyde dimethylacetal to give the protected aldehyde. This can then be deprotected and the ring closed in one reaction by refluxing in chlorobenzene with polyphosphoric acid (PPA).

[2]When R_1 was initially a trimethylsilyl group, it was believed to be cleaved by a *tert*–butoxide group during the reaction, leaving R_2 as H.

Discussion of the synthesis of thieno[2,3-*b*]thiophene

Kirsch's route (Figure 3.28) involved the symmetrical ring closure alluded to by Brandsma. Pentan-2,4-dione was reacted with carbon disulfide under basic conditions, which formed a ketene dithioacetal dipotassium salt. This was immediately reacted with ethylbromoacetate, which is thought to undergo a Dieckmann type cyclisation. This generated diethyl 3,4-dimethylthieno[3,2-*b*]thiophene-2,5-carboxylate as a white powdery solid in 93 % yield. The ester was hydrolysed in ethanol and water with an excess of potassium hydroxide for 12 hours. The acid was isolated as a tacky white solid in 85 % yield, and was characterised by ^{1}H NMR spectroscopy and mass spectrometry (ASAP+). Decarboxylation/bromination was readily achieved by the same method employed for decarboxylation/bromination of *anti*thienothiophene, described earlier (see page 74). A white solid was isolated in 90 % yield after stirring over night.

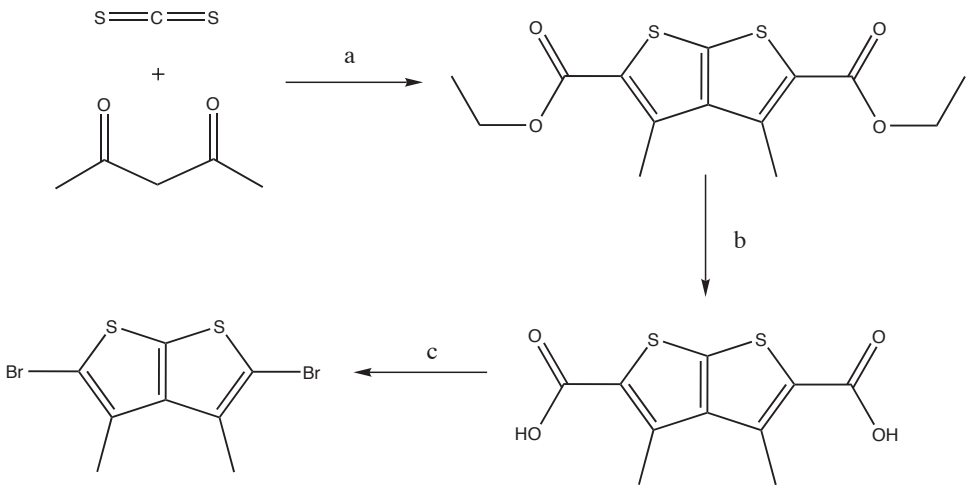

Figure 3.28: Route to 2,5-dibromothieno[2,3-*b*]thiophene, adapted from methods described by Kirsch and Campbell. [138, 145] a) i/ K_2CO_3/DMF, ii/ ethylbromoacetate/DMF, iii/ H_2O; b) i/ NaOH/EtOH, ii/ 5M HCl; c) NBS/NMP.

3.3 Novel arylethynylene-substituted thiophene derivatives

In the following section is a discussion of the synthesis of the novel thienyl arylethynylenes which have been prepared for this work. All of these compounds have been prepared by the Sonogashira cross–coupling of various arylacetylenes with the relevant dibromo– or diiodohetercycle. For a complete list of the aryleneethynylenes prepared in this chapter see Appendix A.

3.3.1 2,5-bis(Arylethynyl)thiophene-1,1-dioxide

Coupling of 2,5-dibromothiophene-1,1-dioxide with phenylacetylene was successful on the first attempt using palladium dichloride bis(triphenylphosphine) as the coupling catalyst. Separation of the diiyne and desired product was trivial. The reaction was complete within one hour, although precipitate could be seen in the reaction vessel almost immediately, indicative of success. The crude product was chromatographed on silica gel and the light brown solid taken into warmed ether and crystallised overnight with the addition of hexane. **BPETO$_2$** crystallised as short orange/brown needles, affording the crystal structure in Figure 3.29.

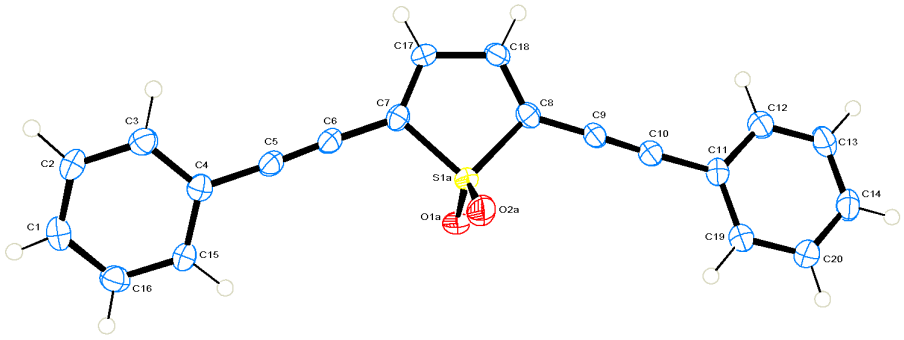

(a) **BPETO$_2$**; face–view.

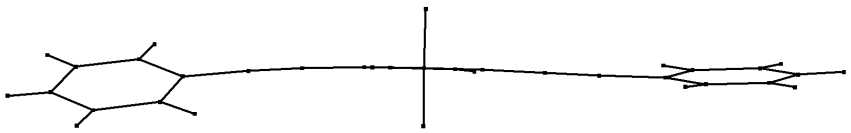

(b) **BPETO$_2$**; in plane.

Figure 3.29: **BPETO$_2$** molecular structure as determined by X–ray crystallographic analysis.

Coupling of 2,5-dibromothiophene-1,1-dioxide with 4-ethynylanisole was performed with the same catalyst, and proceeded similarly. Initial column chromatography could not provide adequate separation of the product from impurities, and as such use of a Harris–Curan Chromatotron (4 mm gypsum plates, hexane/DCM 1:1) was required. This allowed isolation of a red fraction which was reduced *in vacuo* to yield a red powder, **BPETO$_2$.OMe**. This was recrystallised from diethylether over night, yielding orange diamond–shaped crystals which afforded the structure in Figure 3.30. Characterisation for **BPETO$_2$** and **BPETO$_2$.OMe** by typical methods (^{1}H and ^{13}C NMR, accurate MS and CHN elemental analysis where possible) was also performed, as well as Raman spectroscopy (see section 3.4.4).

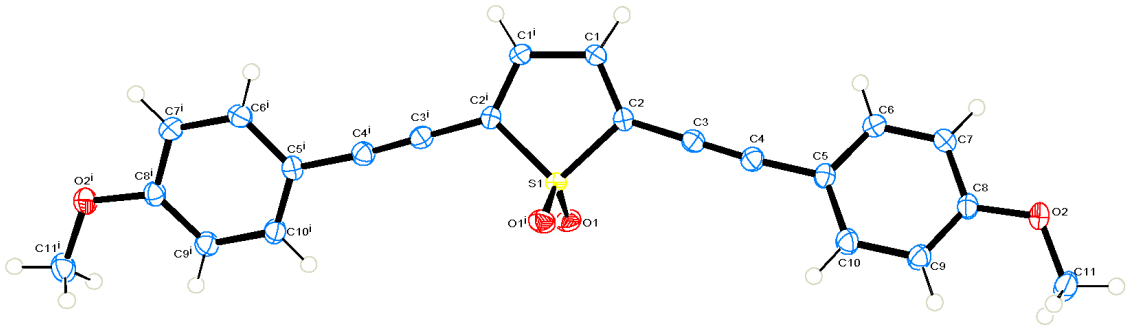

(a) **BPETO$_2$.OMe**; face–view.

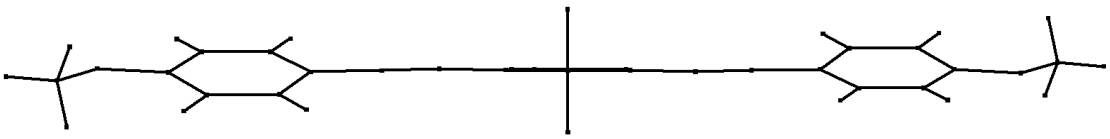

(b) **BPETO$_2$.OMe**; in plane.

Figure 3.30: **BPETO$_2$.OMe** molecular structure as determined by X–ray crystallographic analysis.

Attempts at preparing the cyano-substituted derivative were made on several occasions. ^{1}H NMR spectroscopic analysis of one of the attempts suggested the product was formed, and MALDI mass spectrometry revealed masses equivalent to the desired end product with a sodium ion *i.e.* $[M + Na]^+$, and without a cyano group *i.e.* $[M - CN]^+$. However, the product was impure by CHN and attempts to purify the very small quantity of compound were unsuccessful.

An ester derivative was similarly attempted, providing an ^{1}H NMR spectrum indicative of success (see section 6.1.6, page 207), but mass spectrometry was not

performed. The low yield and lack of starting materials meant that the work was not repeated and was abandoned.

3.3.2 2,5-bis(Arylethynyl)-3,4-ethylenedioxy-thiophenes

The parent product, 2,5-bis(phenylethynyl)-3,4-ethylenedioxythiophene, **BPEEDOT**, was prepared by an earlier group member, Dr Simon Rutter. [42] The effect of electron–withdrawing and electron–donating substitution was not considered at that time so only now has preparation of compounds appended with substituted arylethynylene groups been undertaken.

Both coupling reactions were carried out using palladium tetrakis triphenylphosphine, and both achieved fair yields (**BPEEDOT.OMe** 43 %; **BPEEDOT.CN** 55 %). Due to the problems faced previously with the preparation of cyano–containing derivatives, this coupling was carried out with heating for 60 h, even though the diiodo-EDOT was used in the reaction.

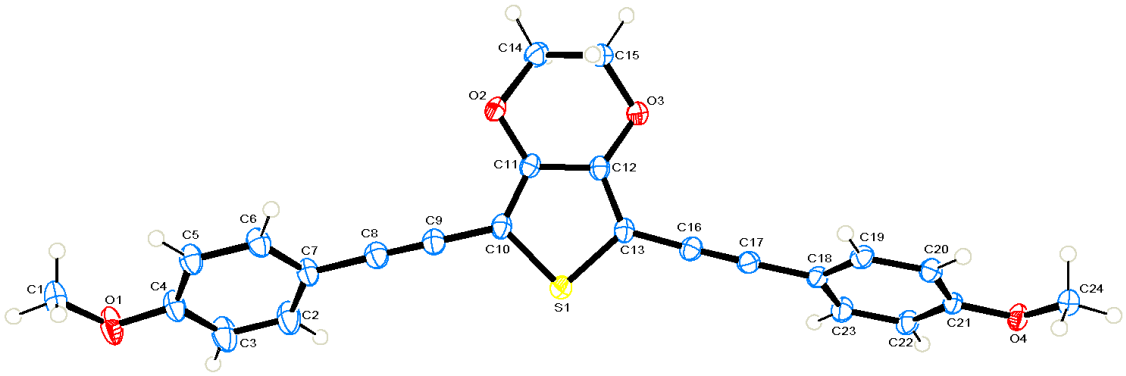

(a) **BPEEDOT.OMe**; face–view.

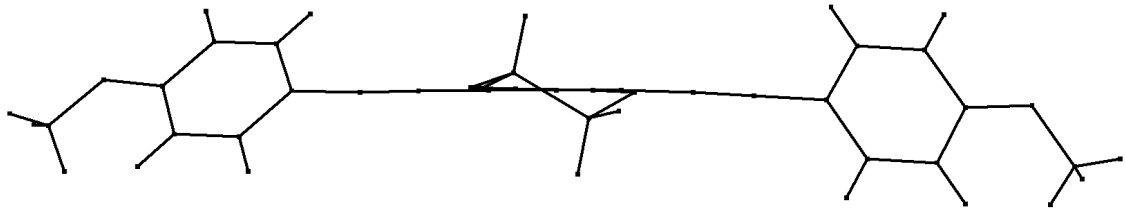

(b) **BPEEDOT.OMe**; in plane.

Figure 3.31: **BPEEDOT.OMe** molecular structure as determined by X–ray crystallographic analysis.

Each compound was isolated by column chromatography, and recrystallised out of solvents; **BPEEDOT.OMe**, after some time, as red plates (Figure 3.31);

BPEEDOT.CN out of warm hexane, allowed to cool over night, as light green/yellow shards (Figure 3.32).

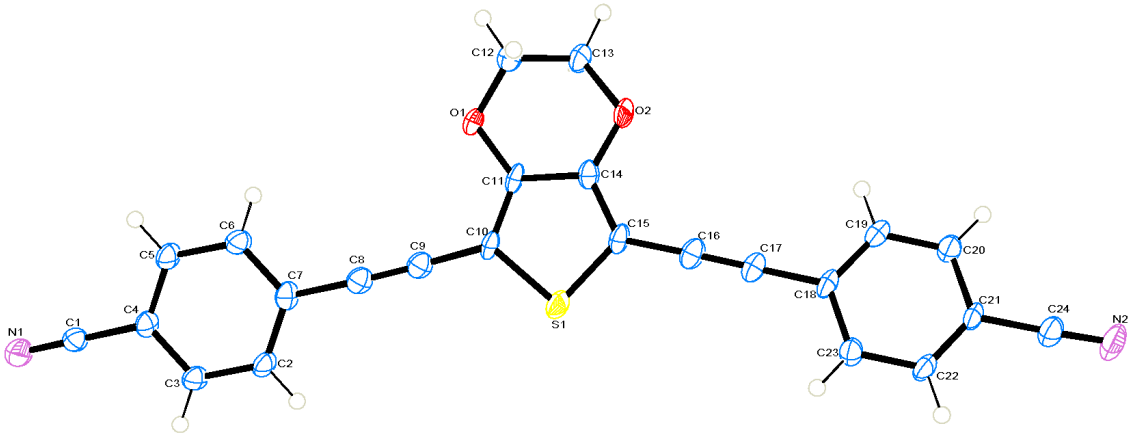

(a) **BPEEDOT.CN**; face–view.

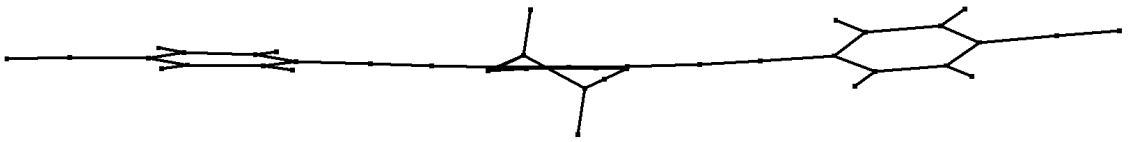

(b) **BPEEDOT.CN**; in plane.

Figure 3.32: **BPEEDOT.CN** molecular structure as determined by X–ray crystallographic analysis.

Full characterisation was also performed on the pure samples (^{1}H and ^{13}C NMR spectroscopy, and accurate mass spectrometry).

3.3.3 2,5-bis(4-*tert*-Butylphenylethynyl)-3,4-ethylenedioxy thiophene-1,1-dioxide

There is no literature precedent for the preparation of an acetylene–coupled 3,4-ethylenedioxy thiophene-1,1-dioxide. Only small quantities of the dibromo-EDOT core were available, hence only cross–coupling reactions with *tert*-butylphenylacetylene and phenylacetylene were performed. Of these, only that with *tert*-butylphenylacetylene yielded an isolated and characterised product.

Palladium tetrakis(triphenylphosphine) was used as the catalyst, to reduce the possibilities of diiyne impurities being formed. The reaction was heated at 70 °C for 24 h, after which the reaction mixture had formed a deep red suspension. An

ether silica gel plug removed any salts, and the crude product from this was chromatographed on a silica gel column with gradient elution. A bright yellow fraction collected at 3:2 ether/hexane (v/v) was reduced *in vacuo* to yield a bright yellow/orange fine powder, **BPEEDOTO$_2$.tBu**, in 11 % yield. ^{1}H NMR spectroscopy and accurate mass spectrometry confirmed the successful isolation of pure product; unfortunately after photophysical analysis there was not enough sample left for CHN elemental analysis. ^{13}C NMR revealed only 10 carbon environments under typical conditions. In order to separate potentially coincidental shifts of carbon species, a longer relaxation decay was allowed (10 s *c.f.* 2 s) and data collected over a 30 h period.

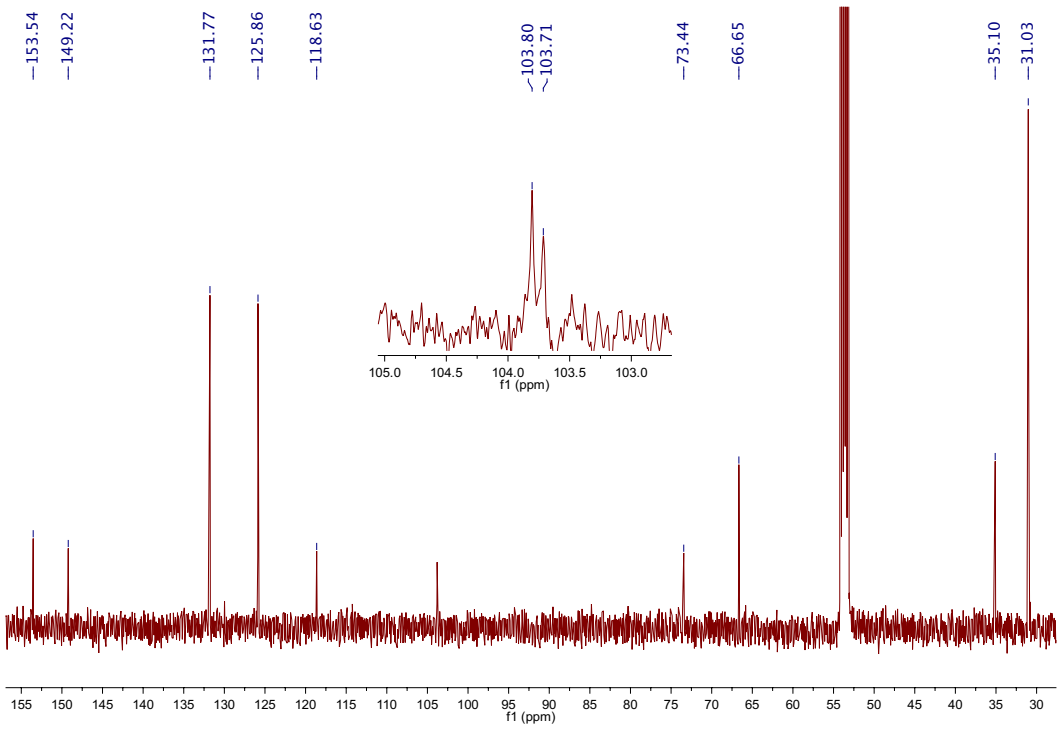

Figure 3.33: 700 MHz ^{13}C NMR spectrum of **BPEEDOTO$_2$.tBu**, in CD_2Cl_2.

As can be seen by the expanded section in Figure 3.33 (inset), there are two peaks that are almost coincident at $\sim$ 103.8 ppm. Several crystals were obtained out of a minimal amount of DCM with cyclohexane layered on top, with glass shards added to act as nucleation sites. X–ray crystallographic structure determination afforded the structure shown in Figure 3.34.

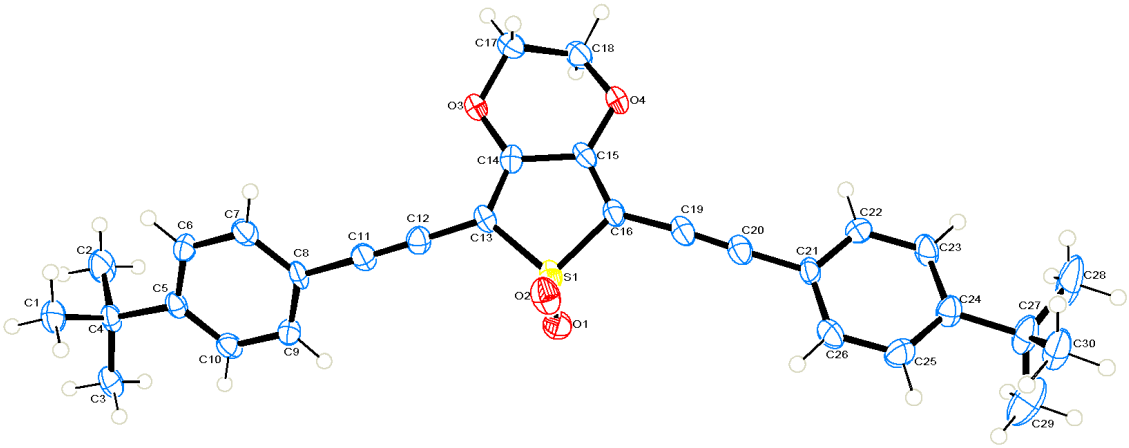

(a) **BPEEDOTO$_2$.tBu**; face–view.

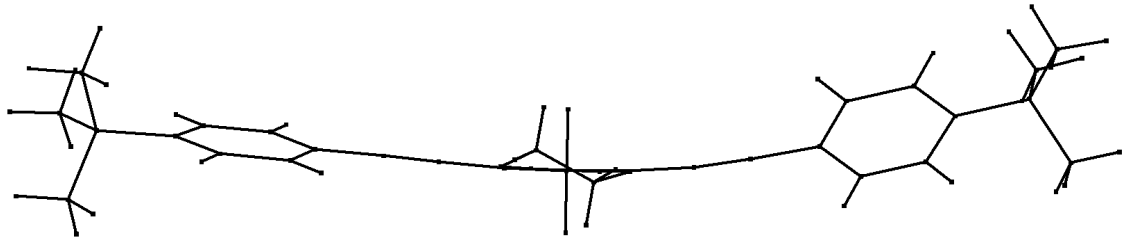

(b) **BPEEDOTO$_2$.tBu**; in–plane.

Figure 3.34: **BPEEDOTO$_2$.tBu** molecular structure as determined by X–ray crystallographic analysis.

3.3.4 2,5-bis(Arylethynyl)thieno[3,2-*b*]thiophenes

Preparation of the *tert*-butylphenylacetylene–derivative was trivial and used standard conditions (Et_3N, $Pd(PPh_3)_4$, CuI). The reaction vessel was heated due to the nature of the halogen (bromine *c.f.* iodine), and stirred over night. Analysis by TLC indicated presence of no starting material after 18 h, but was continued for a further 6 h anyway. The end product was isolated as fluffy yellow solid **BPEantTT.tBu** in 60 % yield, from a silica gel column, eluted with toluene. The solid was subjected to a high–vacuum to remove any trace of toluene, and a small amount was taken into warmed DCM, with cold hexane added to help precipitation. Crystals of sufficient quality were obtained, allowing X–ray crystallographic structure determination (see Figure 3.35). ^{1}H and ^{13}C NMR spectroscopy and accurate mass spectrometry confirmed characterisation and identity of the product, and CHN elemental analysis confirmed the purity of the bulk solid.

The preparation of the anisole–derivative was significantly less successful. Prod-

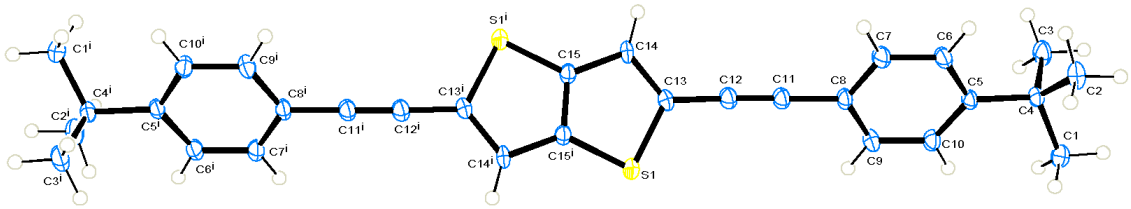

(a) **BPEantTT.tBu**; face–view.

(b) **BPEantTT.tBu**; plane of thienothiophene.

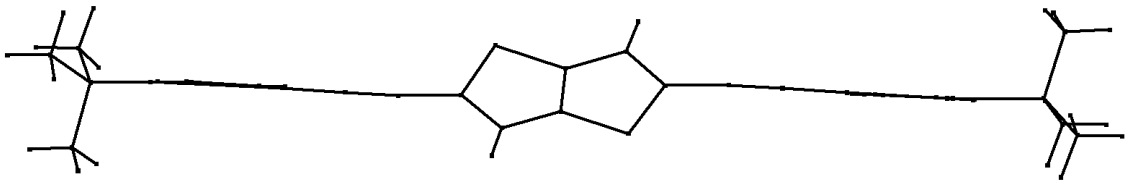

(c) **BPEantTT.tBu**; plane of phenyl rings.

Figure 3.35: **BPEantTT.tBu** molecular structure as determined by X-ray crystallographic analysis.

uct **BPEantTT.OMe** was isolated as a flaky yellow solid, but only in 14 % yield, possibly due to the electron donating effect of the methoxy group hindering removal of the acetylenic proton. The reaction had been monitored by TLC analysis after 15 h, and it appeared to have finished. It was allowed to stir (at room temperature, lower than previously) for the rest of the day, and TLC analysis indicated the reaction was unchanged. Salts were removed from the reaction by means of silica gel plug, with ether eluent. Further column chromatography was performed, with the product isolated at 1:3 (v/v) hexane/ether. Characterisation by ^{1}H and ^{13}C NMR spectroscopy and accurate mass spectrometry confirmed isolation of the desired product. Attempts to recrystallise this compound failed to give crystals of adequate quality for analysis.

3.3.5 3,6-bis(4-*tert*-Butyl-phenylethynyl)thieno[3,2-*b*]thiophene

To examine the effect of the conjugation–break in thieno[3,2-*b*]thiophene across the oligomer system, cross–coupling of arylacetylenes to 3,6-dibromothieno[3,2-*b*]thiophene was limited to *tert*-butylphenylacetylene, which had the advantage of enhancing the solubility of the product. The cross–coupling proceeded similarly to the isomeric thienyl core 2,5-dibromothieno[3,2-*b*]thiophene, with the dark brown/black reaction mixture showing a precipitate of $[Et_3NH]Br$ after 24 h. TLC analysis was employed to monitor the reaction, and after 40 h at reflux the solution was cooled, and the product isolated and purified. **BPEantXTT.tBu** was isolated as a lustrous light brown solid. A sample was dissolved in DCM and cyclohexane layered on top, affording crystals from which the structure was determined by X–ray crystallography (see Figure 3.36a–c). Typical characterisation methods were also used to confirm isolation of the product..

3.3.6 2,5-bis(Arylethynyl)thieno[2,3-*b*]thiophene

The *syn*–fused thienothiophene system was cross coupled with phenylacetylene, affording the disubstituted derivative. The coupling was carried out using palladium tetrakis(triphenylphosphine) as the catalyst, in triethylamine solution. The reaction mixture was heated at reflux for 12 h, after which time TLC analysis indicated no starting material was present. After cooling the mixture was eluted through a silica-gel plug with ether, and chromatographed further on a silica-gel column, with toluene eluant. An orange fraction was evaporated under reduced pressure to yield a yellow flaky solid. This was dissolved in a minimum amount of hot cyclohexane, from which yellow plate-like crystals, pure **BPEsynTT**, formed over night (35 %). Characterisation by ^{1}H and ^{13}C NMR spectroscopy, accurate mass spectrometry and CHN elemental analysis confirmed the identity of the desired product. A crystal structure was also obtained, although the structure showed whole molecule disorder (see Figure 3.36d).

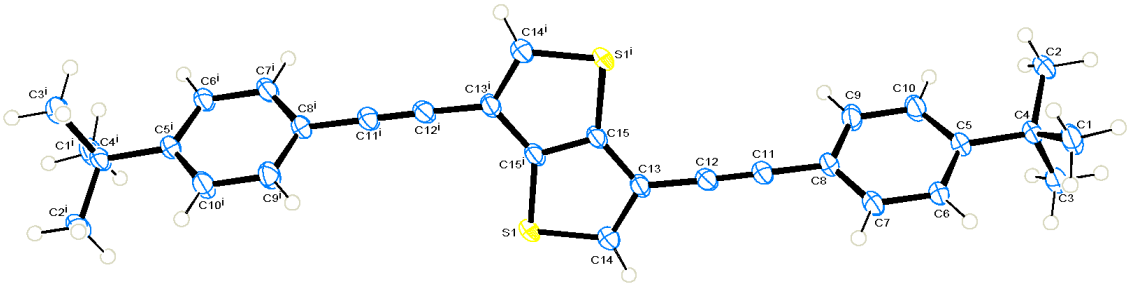

(a) **BPEantXTT.tBu**; face–view.

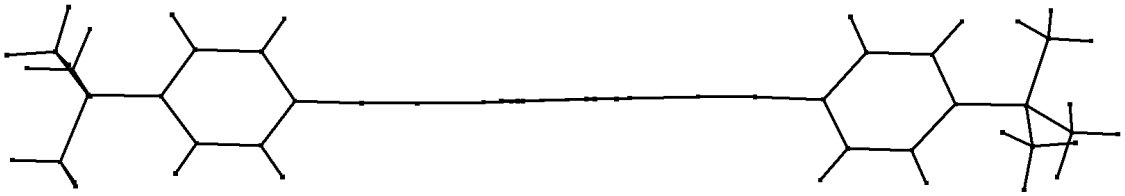

(b) **BPEantXTT.tBu**; plane of thienothiophene.

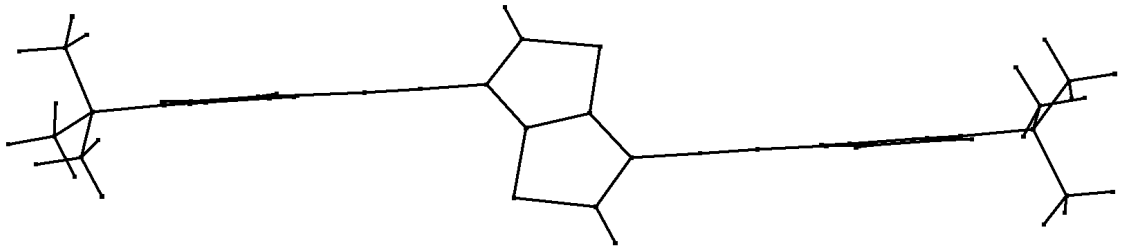

(c) **BPEantXTT.tBu**; plane of phenyl rings.

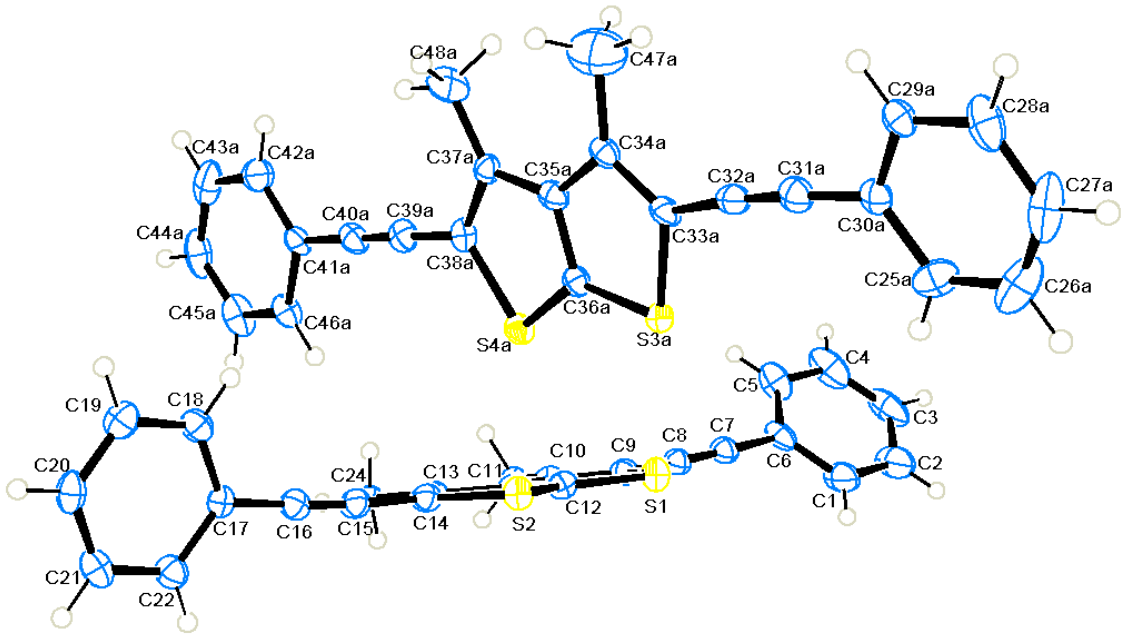

(d) **BPEsynTT** molecular structure. The crystal exhibited whole–molecule disorder

Figure 3.36: Molecular structures of **BPEantXTT.tBu** (a – c) and **BPEsynTT** (d) as determined by X-ray crystallographic analysis.

3.4 Analysis of molecular structures of thiophene–based arylethynylenes

In the following section the crystallographically determined bond lengths and angles are compared to the optimised geometries predicted by DFT methods (B3LYP functional and 6–31G(d) basis set) in the gas–phase.

3.4.1 The effects of oxidation on the structure of the thiophene moiety

By considering the data obtained through crystallographic analysis and comparing pertinent bond lengths within a family of homologues, the effects of the functionalisation of thiophene, *e.g.* oxidation, have been monitored and compared to calculated bond lengths.

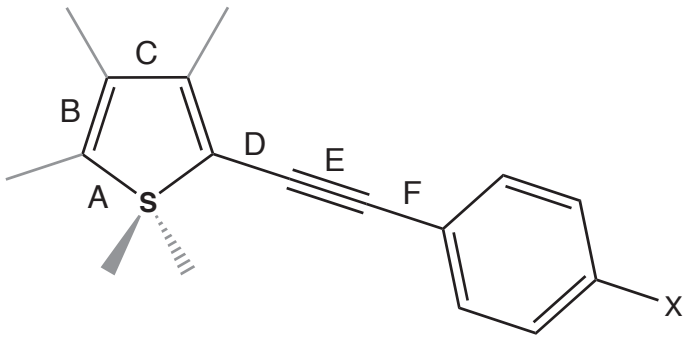

Figure 3.37: Selected bonds in thiophene derivatives which are altered by functionalisation of 2,5-bis(arylethynyl)thiophene.

From the data in Table 3.3 it can be seen that oxidation to the sulfone causes an overall reduction in the aromaticity of the thiophene ring; there is an increase in **A** and **C**, and a shortening of the double bonds (**B**). For **BPETO$_2$**, the change in bond length upon oxidation extends to bonds **D** and **E** which are shorter and longer, respectively, than in the other three systems *i.e.* the loss of aromaticity felt in the sulfone ring extends to its substituents. This effect is not seen in **BPEEDOTO$_2$.tBu**.

BPETO$_2$ is not a planar molecule. However, it exhibits an approximate C_{2V} symmetry (Figure 3.29). The oxygen atoms sit out of the plane of the ring, at an angle of 90 ° (to 2 s.f.) in agreement with Barbarella *et al.* [79] In **BPEEDOTO$_2$.tBu**

	Mean bond lengths / Å Observed (ESD)/Calculated					
	A	**B**	**C**	**D**	**E**	**F**
BPET	1.732(3) 1.757	1.378(3) 1.388	1.411(4) 1.412	1.424(4) 1.405	1.197(4) 1.220	1.444(4) 1.424
BPEEDOT	1.737(1) 1.763	1.372(2) 1.385	1.418(2) 1.422	1.417(2) 1.399	1.199(2) 1.219	1.435(2) 1.421
BPEEDOT.OMe	1.739(1) 1.764	1.371(2) 1.384	1.416(2) 1.422	1.412(2) 1.399	1.196(2) 1.219	1.437(2) 1.420
BPEEDOT.CN	1.733(3) 1.762	1.367(5) 1.386	1.422(4) 1.421	1.407(5) 1.397	1.198(4) 1.219	1.432(5) 1.418
BPETO$_2$	1.790(3) 1.836	1.339(4) 1.358	1.459(4) 1.452	1.404(4) 1.391	1.202(4) 1.220	1.432(4) 1.420
BPETO$_2$.OMe	1.784(1) 1.836	1.347(2) 1.359	1.463(2) 1.451	1.411(2) 1.390	1.198(2) 1.221	1.432(2) 1.417
BPEEDOTO$_2$.tBu	1.773(3) 1.824	1.340(3) 1.362	1.475(3) 1.466	1.415(4) 1.389	1.193(3) 1.220	1.437(4) 1.419

Table 3.3: Mean bond lengths (Å) of selected thiophene–derivatives (see Figure 3.37) from X–ray structure determination, and DFT structure optimisation calculations.

the plane of the oxygens is similarly perpendicular (87 ° to 2 s.f.).

Selected bond lengths from the X–ray diffraction data analysis have been compared with bond lengths obtained from DFT calculations of the optimised structures (red values), using the B3LYP functional and 6-31G(d) basis set. Siddle *et al.* reported excellent agreement ($\leq$ 1.5 %) between the theoretical and observed bond lengths for the parent system **BPET**. [114] A similar comparison of **BPEEDOT**, **BPETO$_2$** and **BPEEDOTO$_2$.tBu** reveals a slightly larger difference for the sulfone systems; the C—S bond in both **BPETO$_2$** and **BPEEDOTO$_2$.tBu** is over estimated by 2.5–3 %.

3.4.2 Structural similarities and differences between 2,5- and 3,6–disubstituted thienothiophene

As the images in Figures 3.35 and 3.36 show, the thienothiophene ring systems are planar, as expected, and the phenyl rings are co-planar with each other. Phenyl

rings in **BPEantTT.tBu** exhibit a dihedral angle with the thienyl system of approximately 44 °. In **BPEantXTT.tBu** this has increased up to 57 °. Packing in the crystal (see Figure 3.38) shows that the thienyl rings are aligned parallel to each other, as are the phenyl rings, parallel with phenyl rings in adjacent molecules. These compounds pack similarly to other thienothiophene derivatives, exhibiting face–to–face stacking *c.f.* herringbone packing typically seen in thiophene–containing oligomers (see section 3.1.5, page 57). [94, 114]

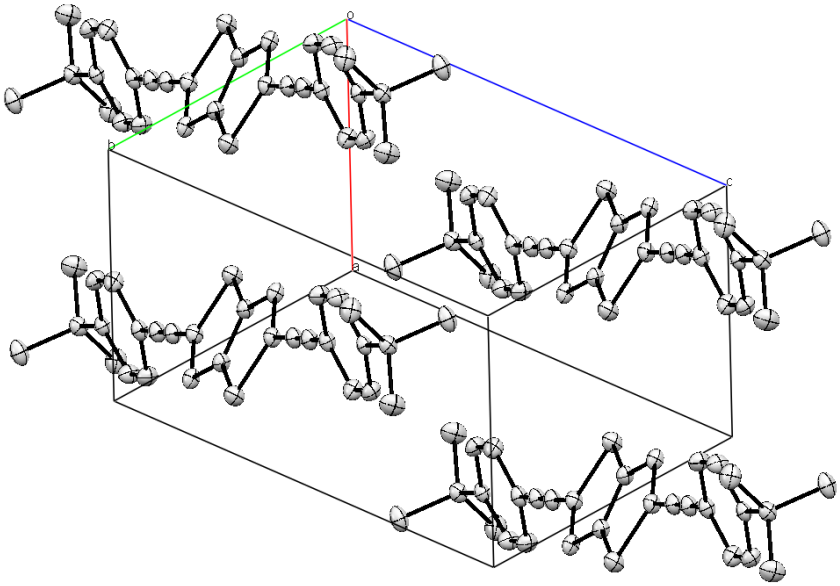

(a) **BPEantTT.tBu**

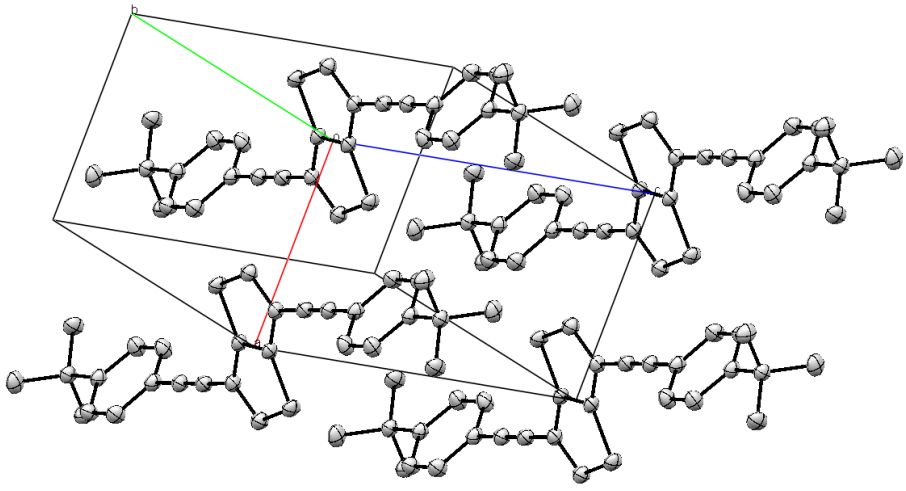

(b) **BPEantXTT.tBu**

Figure 3.38: Crystal packing of **BPEantTT.tBu** and **BPEantXTT.tBu**.

X–ray diffraction data indicates the bond lengths of **D** and **E** are significantly

different in length, being approximately 0.03 Å longer in the fully conjugated system *i.e.* in the non-conjugated system the double bond displays enhanced double bond character. The calculated bond lengths show good agreement ($\leq$ 2 %) with the observed bond lengths.

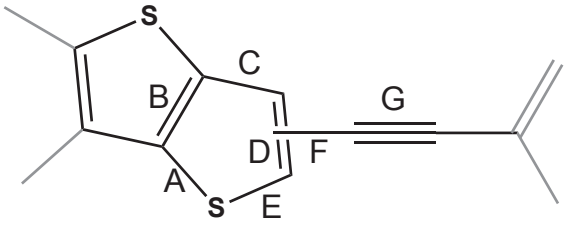

Figure 3.39: Selected bonds in disubstituted thieno[3,2-*b*]thiophene, labelled to help examine bond length changes upon substitution at either the *2* and *5* or *3* and *6* positions.

	Mean bond lengths / Å Observed (ESD)/Calculated						
	A	**B**	**C**	**D**	**E**	**F**	**G**
2,5–	1.716(1) 1.744	1.387(3) 1.398	1.436(2) 1.414	1.403(2) 1.384	1.749(1) 1.779	1.415(2) 1.402	1.203(2) 1.219
3,6–	1.723(2) 1.742	1.385(4) 1.382	1.427(3) 1.439	1.377(3) 1.381	1.718(2) 1.742	1.428(3) 1.416	1.200(3) 1.217

Table 3.4: Mean bond lengths (Å) of 2,5– and 3,6– disubstituted thieno[3,2-*b*]thiophene, see Figure 3.39.

3.4.3 Effects of electron–withdrawing and electron–donating substituents on thienyl bond lengths

Substitution with electron–donating and withdrawing groups on these thiophene systems was performed in order to examine the effect on their excited state properties by monitoring the effects on their electrochemistry and photophysics. Effects of substitution on molecular structure have also been examined, as bond lengths can sometimes be affected by electronic effects, as shown above (Table 3.3).

As noted earlier, **BPETO$_2$** has a non–planar conformation and only approximate C_{2V} symmetry. Similarly, **BPETO$_2$.OMe** does not adopt a planar conformation, but exhibits an almost perfect C_2 axis (Figure 3.30), which could be a packing effect

attributable to the methoxy groups interacting with neighbouring phenyl rings (see Figure 3.40).

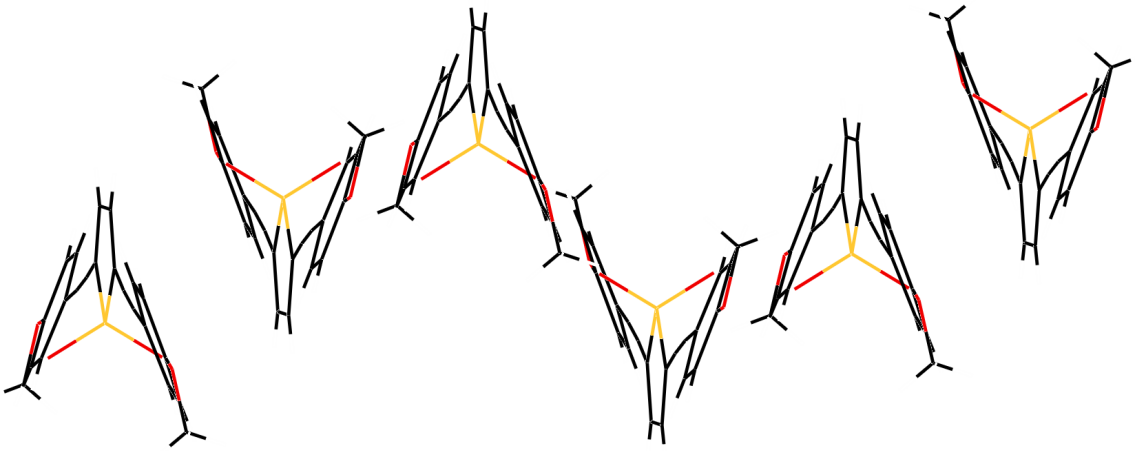

Figure 3.40: Crystal packing of **BPETO$_2$.OMe**.

Comparison of the observed bond lengths for **BPETO$_2$** and **BPETO$_2$.OMe** indicate a slight lengthening of the thiophene bond lengths **B**, **C** and **D** in the methoxy– substituted derivative. The EDOT– series displays largely similar bond lengths, although the **A** bond increases in length with electron input (**BPEEDOT.-OMe**) and shortens with it electron withdrawal (**BPEEDOT.CN**), relative to the parent **BPEEDOT**.

Furthermore, the parent **BPEEDOT** is not planar, with no symmetry evident. This is also the case for the methoxy– and cyano– substituted derivatives. The whole molecule bend, inherently caused by bonding through thiophene, is observed on each EDOT derivative, but there is also a bend along the long axis of the molecule, in the plane of thiophene. The bend in **BPEEDOT** serves to push the terminal phenyl rings away from each other, whereas in **BPEEDOT.CN**, **BPEEDOT.OMe** and **BPEEDOTO$_2$.tBu** the bend causes a bowing in the whole molecule, pulling the terminal R groups in the same direction (see Figures 3.31 and 3.32).

3.4.4 Observed and predicted Raman spectra of the novel thienyl arylethynylenes

In many of the examples described previously it was possible to compare the observed bond lengths/angles with those predicted by *ab initio* theoretical calculations. However, when no crystal structure was available, this was not possible. Instead, observed Raman spectra of the materials were compared with that calculated using DFT methods.

Raman spectroscopy is a useful analytical technique for probing and identifying acetylene–containing compounds due to the reliable C≡C stretch at 2100–2200 cm^{-1}. It can thus be used to rapidly identify whether even a very small quantity of compound contains an acetylene moiety. Unfortunately the common impurity in Sonogashira cross coupling reactions is the diiyne, itself containing two acetylene groups. DFT frequency calculations have been performed on optimised structures of several of the compounds prepared and the generated Raman spectra have been compared to the experimentally obtained spectra as a further means of characterisation (see Figure 3.41).

There is excellent agreement between calculated and observed spectra, after application of a correction factor of 0.96 to the wavenumber on the calculated spectra (typical for this level of DFT calculation [114]). Due to the magnitude of several peaks, most notably the acetylene stretch, several of the smaller peaks were not represented, hence normalisation is not always to the most intense vibration.

The symmetrical acetylene vibration at ~ 2200 cm^{-1} is prominent in all spectra, although it is consistently predicted to be at a slightly higher energy. Likewise, although the vibration frequencies are predicted with a good degree of accuracy, their relative intensities are often inaccurate. The DFT method used here assumes no solvent interactions, and it applies a harmonic oscillator model, providing a source of discrepancy with the observed spectra.

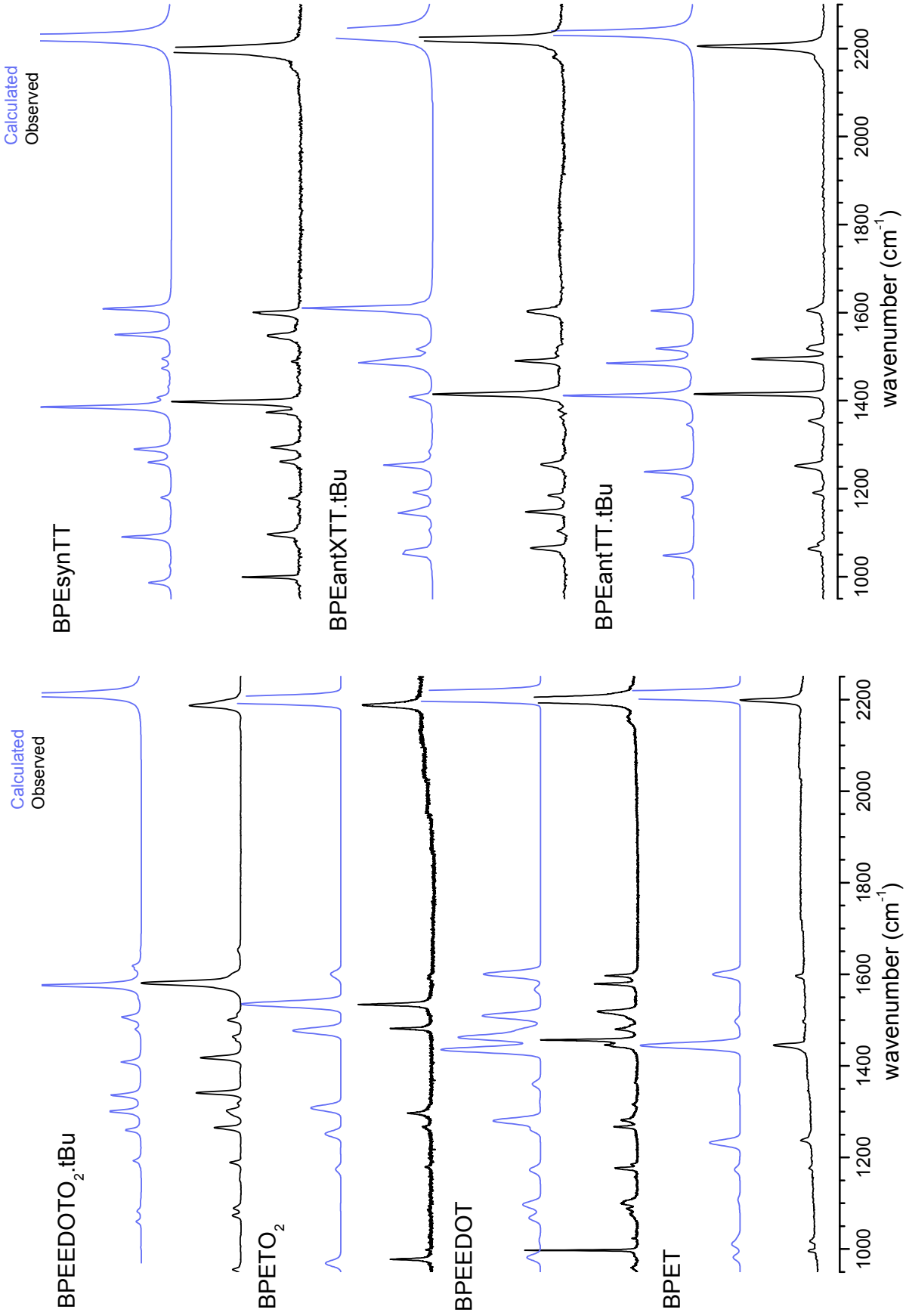

Figure 3.41: Theoretical and observed Raman spectra for the thienyl arylethynylenes.

3.5 Excited state properties of the novel thienyl arylethynylenes

Photophysical data on the prepared compounds has been obtained using UV–vis absorption and fluorescence spectroscopy, allowing the determination of room and low temperature (using the solvent EPA, see sections 1.4.6 and 2.4) absorption, excitation and emission maxima, as well as molar extinction coefficients. Photoluminescent quantum yields and fluorescent lifetimes have been determined for all compounds, where possible. All photophysical data (unless otherwise stated) were obtained in toluene at room temperature (293–298 K).

These data, in conjunction with theoretical modelling data, are used to explain the photophysical properties of these thienyl arylethynylenes upon derivatisation of thiophene and upon substitution with electron donor and acceptor substituents. Electrochemical data has also been obtained to show the effect of oxidation and reduction on these compounds.

3.5.1 Photophysical analysis of the novel thienyl arylethynylenes

The absorption, excitation and emission spectra of the unsubstituted arylethynylenes are presented in Figure 3.42. Spectra maxima and other pertinent information are presented in Table 3.5.

The spectra are arranged with respect to the parent compound (**BPET**; GREEN) so that those with blue–shifted maxima are above **BPET** and those with red–shifted maxima are below. The spectra are also colour coded to reflect this distinction.

As the noise present in the emission profile indicates, **BPEsynTT** is only weakly emissive. Furthermore it exhibits an absorption spectrum that is different to the excitation spectrum, suggesting the absorbing species is different to the species responsible for emission, possibly due to a trace of fluorescent impurity. For all other compounds the absorption and excitation spectral profiles are almost identical, indicating purity of samples. All of the fully conjugated systems display a bathochromic

	R–group	λ_{max} abs/nm	ε/ $M^{-1}cm^{-1}$	λ_{max} ex/nm	λ_{max} em/nm	Stokes' shift/cm^{-1}	PLQY ϕ_f (± 10 %)	lifetime τ_f / ns (± 0.1 ns)	Calculated k_f / ns^{-1} (± 14 %)
BPET♠	H	350	33 000	n/a	382	2390	0.20	0.24	0.83
	OMe	345	39 000	n/a	394	3600	0.22	0.27	0.81
	CN	365	49 000	n/a	401	2670	0.31	0.32	0.97
BPEEDOT	H♣	361	45 200	362	395	2380	0.12	0.13	0.92
	OMe	367	38 600	366	402	2370	0.14	0.14	1
	CN	381	59 100	380	421	2490	0.24	0.28	0.86
BPETO$_2$	H	415	21 000	409	519	4830	0.24	1.1	0.22
	OMe	444	19 700	443	553	4440	0.15	1.1	0.14
BPEEDOTO$_2$	tBu	433	24 300	427	553	5010	0.02	n/a♡	n/a
BPEantTT	tBu	371	62 300	371	402	2080	0.43	0.38	1.13
	OMe	377	58 200	370	407	1960	0.39	0.39	1
BPEantXTT	tBu	320	37 900	320	341	1920	0.08	n/a♡♢	n/a
BPEsynTT	H	322	42 300	325*	366	3730	0.03	n/a♡	n/a

Measurements recorded in toluene unless otherwise stated.
♠ = data taken from work published by Marder and co-workers. [114]
♣ = compound prepared by Dr S R Rutter, previous group member.
♡ = fluorescence lifetime could not be measured accurately.
♢ = phosphorescence lifetime obtained at 77 K.

Table 3.5: Thienyl arylethynylenes' photophysical properties.

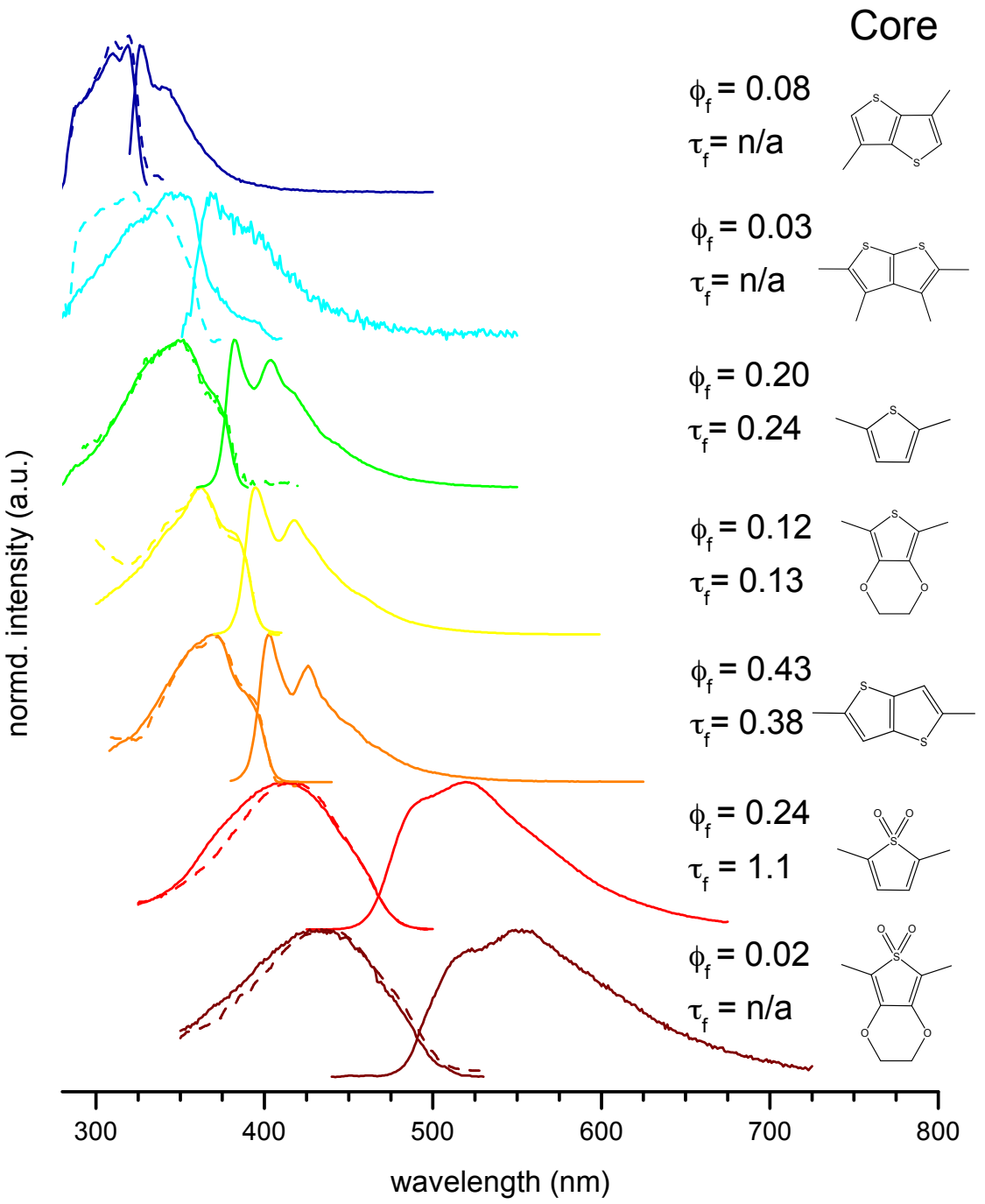

Figure 3.42: Absorption (dashed), excitation and emission spectra for the seven thiophene–based arylethynylene compounds. Lifetimes given in ns.

shift of both the absorption and emission maxima, relative to **BPET**.

TD-DFT calculations have been performed on each system (Gaussian 03W, B3LYP/6-31G(d) [47]), and throughout this discussion comparisons will be made between empirical observations and the properties predicted by theory. Figure 3.43

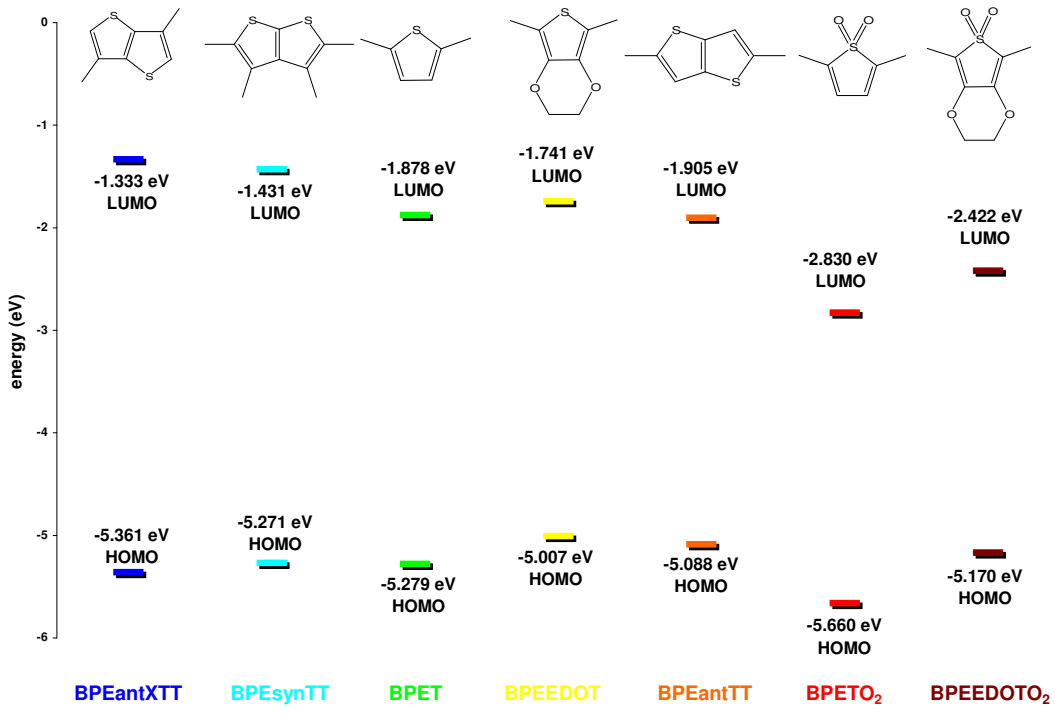

Figure 3.43: HOMO—LUMO gaps from *ab initio* calculations, using TD-DFT methods with the B3LYP functional and 6-31G(d) basis set, performed on previously optimised structures.

represents the amalgamated HOMO—LUMO energy levels for each of the unsubstituted compounds, and is also colour coded to match the UV–vis absorption and fluorescence spectra in Figure 3.42. The trend of decreasing $S_1 \leftarrow S_0$ transition energy is corroborated by the calculations, and the rise and fall of the HOMO and LUMO levels give an indication as to the effect of the substitution and modification of the thiophene core.

Unless specifically addressing the issue of substituent effects, all TD-DFT calculations have been performed on unsubstituted systems, *i.e.* phenylethynyl only, to facilitate computation.

Analyses of the photophysical properties of BPET, BPEEDOT and BPEantTT.tBu

These compounds all exhibit very similar spectral profiles, with red and blue–shifted shoulders on the excitation λ_{max} and a second emission band $\sim$ 20–30 nm red–shifted to the emission λ_{max}. In each case the emission spectrum features more vibrational structure than the absorption/excitation spectra which, in parent compound 1,4-bis(phenylethynyl)benzene, **BPEB**, is attributed to Frank Condon rearrangements. **BPEEDOT** shows a red–shift in the emission λ_{max} of 13 nm, whilst **BPEantTT.tBu** is shifted by a further 7 nm, λ_{max} = 402 nm. This implies that the effect of the electron–rich ethylenedioxy bridge decreases the $S_1 \leftarrow S_0$ transition energy due to the raising of the energy of the HOMO to a greater extent to which the LUMO is raised. The increased conjugation of the fused thiophene system has a similar effect. The TD–DFT calculations predict that **BPEEDOT**'s HOMO and LUMO are both subject to an increase in energy relative to **BPET**, but the HOMO to a greater extent. **BPEantTT.tBu** actually experiences a lowered LUMO and slight increase in HOMO relative to **BPET**.

Measurement of the excitation and emission spectra of these compounds at 77 K in a transparent glass matrix shows increased vibrational structure, as explained in section 1.4.6, attributed to the preferential formation of the rotational conformation in which the three aromatic rings are coplanar. This has indeed resulted in an increased red edge of the absorption spectra. Furthermore, there is now a greater degree of 'mirror–image' symmetry between the excitation and emission spectra, due to the rigid organic glass enforcing planarity in the ground state of the species (see Figure 3.44 and accompanying data in Table 3.6).

For each of these systems molecular modelling (DFT, B3LYP/6-31G(d)) has predicted the lowest excited singlet state energy $S_1 \leftarrow S_0$ UV-vis absorption to be assigned to the LUMO←HOMO transition. It has also permitted visualisation of the HOMO and LUMO for each species (see Table 3.7).[3] From these MO representations

[3]The photophysical properties and molecular orbitals of **BPET** and **BPEEDOT** were studied in depth by Dr S. R. Rutter, but owing to the nature of this work they are being discussed here to provide background and to act as parent compounds for comparisons.

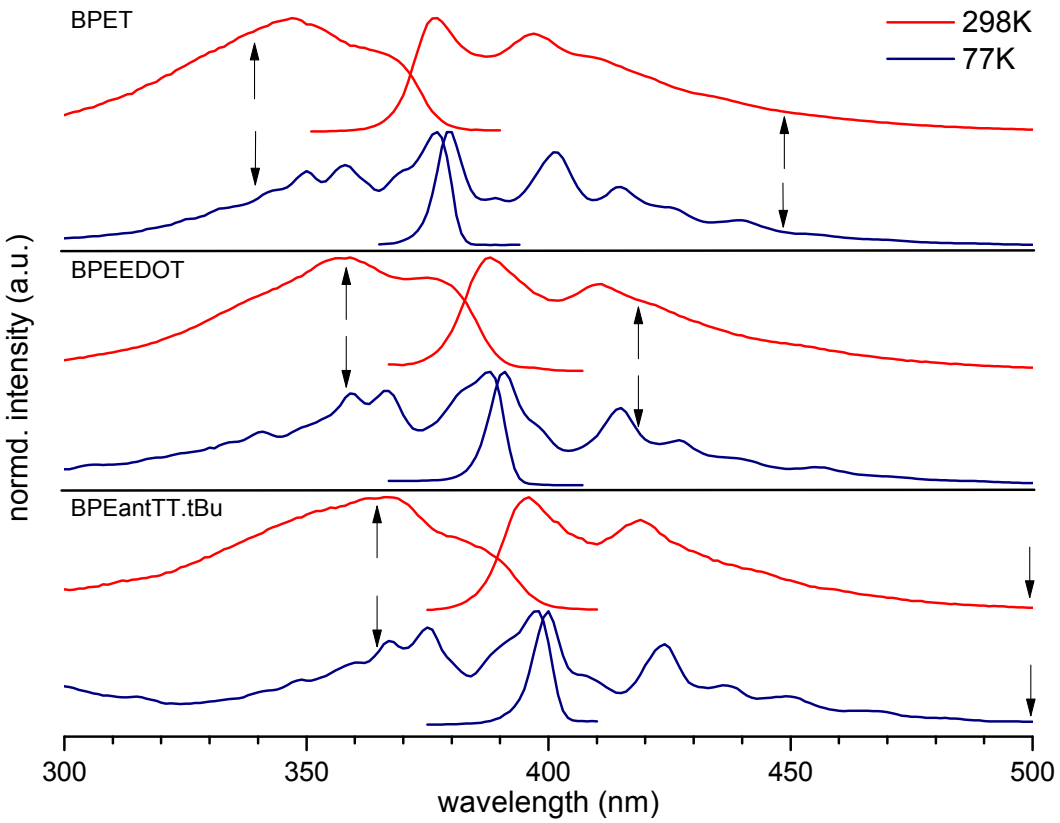

Figure 3.44: UV–vis fluorescence spectra of **BPET**, **BPEEDOT** (spectra by Dr S. R. Rutter) and **BPEantTT.tBu**, at 298 K and 77 K in EPA. Arrows indicate wavelengths of excitation and emission.

it is clear that electron density within these two orbitals is extensively delocalised over the whole molecule. Predicted oscillator strengths for these transitions are all large (f = 1.5–2.3), in agreement with the measured extinction coefficients (see Table 3.5).

Fluorescence quantum yields were measured in toluene allowing comparisons to that reported by Marder, with **BPEEDOT** exhibiting $\phi_f = 0.12$ and **BPEantTT-.tBu** giving $\phi_f = 0.43$. These valules straddle that of **BPET** ($\phi_f = 0.20$).

Fluorescence lifetimes were recorded using TCSPC methods, detecting at the emission λ_{max} of the relevant sample. The EDOT derivative features the shortest lifetime, $\tau_f = 130$ ps, whilst the thienothiophene system displays a lifetime of $\tau_f = 380$ ps. These two parameters allow calculation of the rate of fluorescent decay, k_f, using Equation 1.10 from section 1.4.4. As the end column in Table 3.5 shows, these values are all similar in magnitude, ~ 1 ns^{-1}, indicating their radiative decay is by

Compound	Temp. / K	Excitation features / nm	Emission features / nm
BPET	298	347*, 366	377*, 397, 409
	77	350, 358, 377*	380*, 401, 415
BPEEDOT	298	359*, 376	388*, 410
	77	359, 368, 388*	391*, 415, 429
BPEantTT.tBu	298	367*, 386	396*, 419
	77	367, 375, 398*	400*, 424, 437

Table 3.6: Spectral features from Figure 3.44

a similar process. Using this knowledge and Equation 1.9, it can be shown that the rate of non–radiative decay (k_{nr}) for **BPEantTT.tBu** is lower than in the other compounds, hence its increased quantum yield.

Analyses of the photophysical properties of $BPETO_2$ and $BPEEDOTO_2$.tBu

The oxidised compounds exhibit much broader spectral profiles (see Figure 3.42), indicative of a charge transfer process. The excitation spectra feature no shoulders, but the emission profiles both show a shoulder approximately 25 nm blue-shifted relative to the maxima. The effect of oxidation of thiophene to the sulfone thiophene-1,1-dioxide has been consistently shown to reduce aromaticity from the ring. [72] The highly electron–withdrawing SO_2 group reduces the electron density from the thienyl ring, making thiophene-1,1-dioxide electron–deficient. Both **$BPETO_2$** and **$BPEEDOTO_2$.tBu** exhibit large red–shifts relative to **BPET** (> 6910 cm^{-1}).

TD-DFT calculations on **$BPETO_2$** have predicted that the first excited state can be attributed to a LUMO←HOMO transition, with a smaller contribution from the LUMO+5←HOMO-2 transition (see Table 3.8). It has been calculated to have a large oscillator strength (f = 1.05), corresponding to the large extinction coefficient, $\varepsilon = 21\ 000$ M^{-1}cm^{-1}.

The electron density in the HOMO and LUMO of **BPET** is largely delocalised over the whole molecule. This is not the case in **$BPETO_2$** where the large electron withdrawing effect of the SO_2 moiety can be seen to attract a lot of the density in the LUMO. This is in contrast to the HOMO, where it features none. The calculated electron density for the HOMO-2 and LUMO+5 levels suggests a more centralised

	BPET	**BPEEDOT**	**BPEantTT**
LUMO			
HOMO			

Table 3.7: Molecular orbital visualisation of the HOMO and LUMOs of **BPET**, **BPEEDOT** and **BPEantTT**, using GaussView 4.1.

BPETO$_2$	**BPEEDOTO$_2$**
LUMO+5 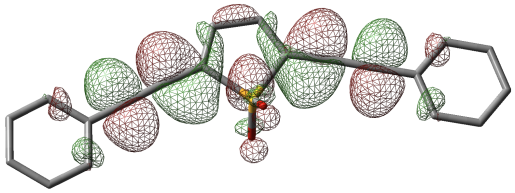	**LUMO+5** 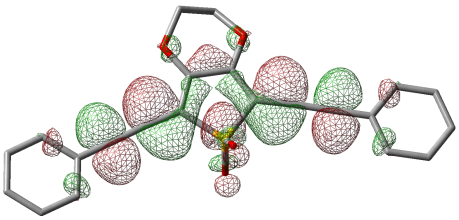
LUMO 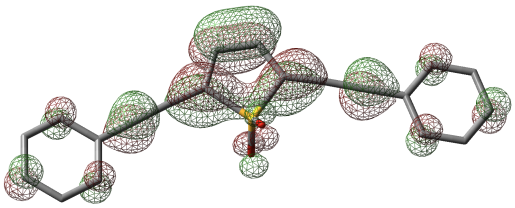	**LUMO** 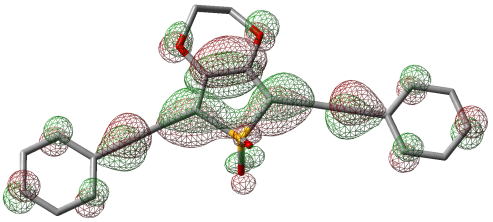
HOMO 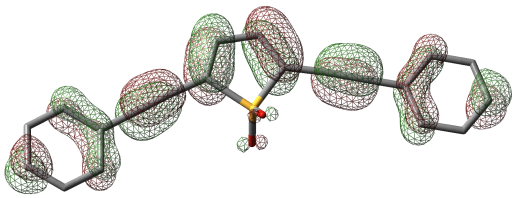	**HOMO** 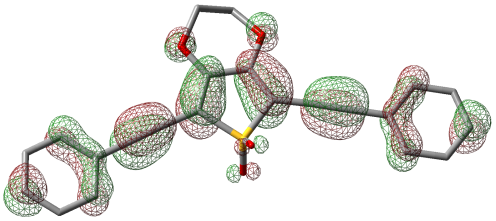
HOMO-2 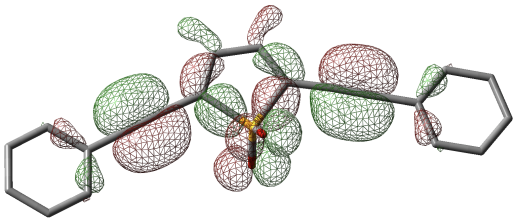	**HOMO-4** 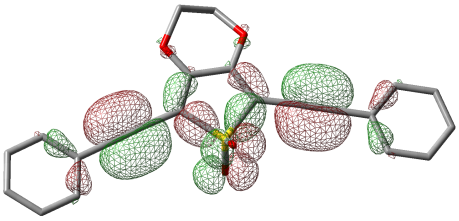

Table 3.8: Visualisation of the MOs for the transitions predicted to contribute to the first excited state of **BPETO$_2$** and **BPEEDOTO$_2$** using GaussView 4.1.

electron density, with hardly any contribution from the peripheral phenyl rings, and closer inspection of LUMO+5 shows segmentation of the electron density over the diene backbone of thiophene. There appears to be a nodal plane on the C—S bonds, separating the electron density on SO_2 from that on the diene. The first excited state of **BPEEDOTO$_2$.tBu** is similarly attributed to the LUMO←HOMO transition, along with contribution from the LUMO+5←HOMO-4 transition. A large oscillator strength (f = 1.14) is predicted, concomitant with the measured

extinction coefficient ($\varepsilon = 24\ 300\ M^{-1}cm^{-1}$). Distribution of electron density on the orbitals is calculated to be similar to that of **BPETO$_2$**, albeit with some localisation on to the oxygens of the ethylenedioxy bridge. In this respect the HOMO and LUMO resemble those on the non–oxidised analogue **BPEEDOT**.

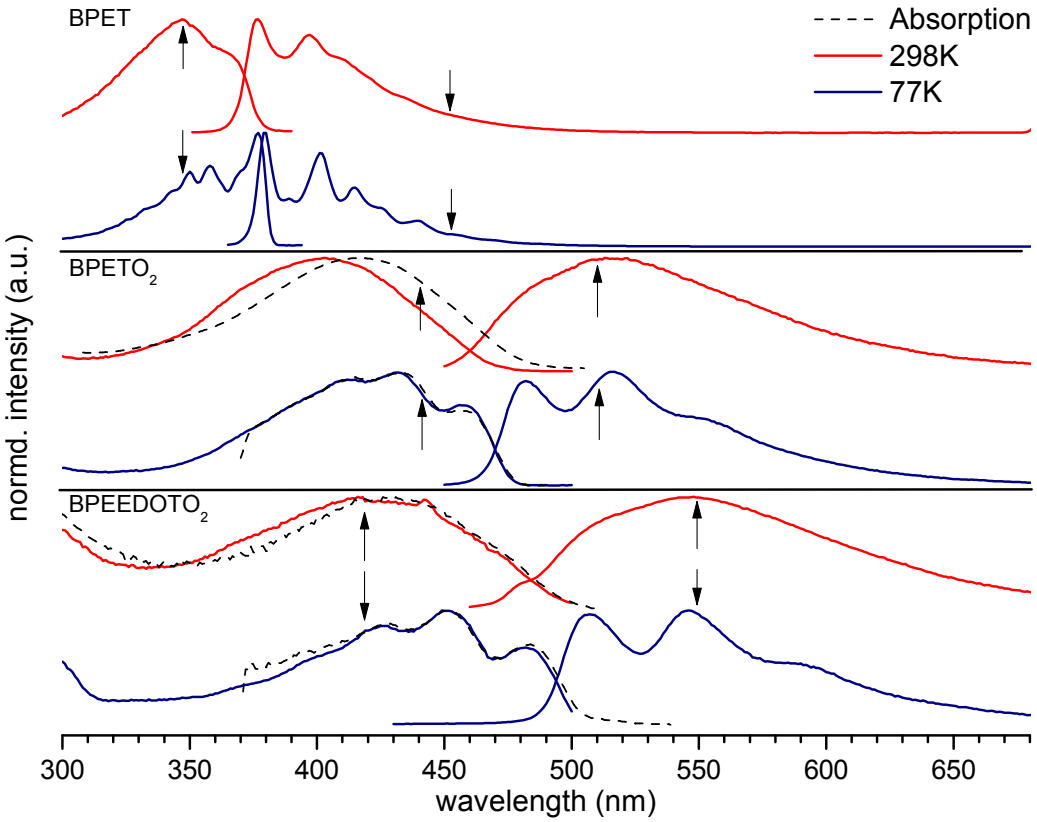

Figure 3.45: UV-vis and fluorescence spectra of **BPETO$_2$** and **BPEEDOTO$_2$.tBu** at 298 K and 77 K in EPA. **BPET** is included for comparison. Arrows indicate excitation and emission wavelengths.

The low temperature excitation and emission spectra (Figure 3.45) showed increased vibrational structure, with similar spectral profiles for the two compounds. The dramatic rise in the red edge of the absorption spectra upon cooling to 77 K is not observed for these compounds, most likely attributable yet again to the charge transfer nature of the compounds. The absorption spectra are included in this figure due to a discrepancy between the absorption and excitation maxima of **BPETO$_2$**. There is a 14 nm red shift in the absorption maximum relative to the excitation maximum, although at low temperature the absorption and excitation maxima coincide within 2 nm. There is also a $\sim$ 8 nm difference between the absorption and

excitation maxima of **BPEEDOTO$_2$.tBu**, although this is most likely due to poor intensity of the excitation spectrum. Table 3.9 lists the spectra maxima.

The room temperature and low temperature excitation and emission spectra for **BPET** are included as a basis for comparison, showing the loss of vibrational fine structure upon oxidation, as well as the accompanying large bathochromic shift.

Compound	Temp / K	Absorption features / nm	Excitation features / nm	Emission features / nm
BPETO$_2$	298	417	403	513
	77	415(sh), 433*, 457	412(sh), 431*, 457	482, 515*, 551(sh)
BPEEDOTO$_2$.tBu	298	426	418	548
	77	427(sh), 452*, 483	426(sh), 449*, 482	507, 546* 592(sh)

(sh) = shoulder
* denotes peak of maximum intensity

Table 3.9: Spectral features from Figure 3.45

A solvent effect was observed whilst obtaining photoluminescent quantum yields for **BPETO$_2$** using an integrating sphere. The value for ϕ_f obtained first was recorded in DCM. It was determined to be 2.5 ± 0.2 % (based on standard deviation). The value obtained in cyclohexane averaged to 30 ± 1.9 %. Consequently a series of measurements were taken to calculate quantum yields in a total of five solvents of increasing polarity. As Table 3.10 illustrates, the increase in solvent polarity causes a decrease in fluorescence quantum yields by an order of magnitude. Similar findings were made for the methoxy–substituted derivative. Lifetimes were also measured for these compounds in the various solvents. These also exhibit a decrease as solvent polarity is increased.

Due to this apparent quenching of the fluorescent singlet state in more polar solvents, emission spectra were obtained for **BPETO$_2$** and **BPETO$_2$.OMe** in five different solvents of increasing polarity, shown in Figure 3.46. As can be seen, particularly for the methoxy–derivative, there is a large red-shift observed upon increasing the solvent polarity. The effect is greater in the methoxy derivative due to the enhanced charge-transfer nature of this compound, inducing a larger dipole

Solvent	n	ε	**BPETO$_2$**			**BPETO$_2$.OMe**		
			ϕ_f / %	τ_f / ns	k$_f$ / ns^{-1}	ϕ_f / %	τ_f / ns	k$_f$ / ns^{-1}
C_6H_{12}	1.426	2.02	30	2.1	0.15	38	2.2	0.17
Toluene	1.486	2.20	24	1.1	0.22	15	1.1	0.14
Ether	1.353	4.34	8.8	0.64	0.14	11	0.59	0.19
DCM	1.424	9.08	2.5	n/a	-	3.0	n/a	-
MeCN	1.344	36.6	2.0	n/a	-	1.9	n/a	-

n = refractive index of solvent.
ε = dielectric constant of solvent.
n/a = lifetime could not be measured accurately.

Table 3.10: Variation of quantum yield and lifetime with solvent for **BPETO$_2$** derivatives.

moment in the ground and excited states.

Application of the Lippert equation (see Equation 1.11, page 25) with the absorption and emission maxima for the **BPETO$_2$.R** compounds is presented in Figure 3.47. A linear relationship between the Stokes' shifts of **BPETO$_2$**, $\bar{\nu}_{abs} - \bar{\nu}_{fl}$, and the solvents' orientation polarizability, Δf, is observed, which indicates the change in dipole moment, $\Delta\mu$, is constant between these solvents.

Compound	Gradient / cm^{-1}	Intercept / cm^{-1}	a / Å	μ_G / D	μ_E / D	$\Delta\mu$ / D
BPETO$_2$	-517	4853	8.83	3.11	9.05	5.94
BPETO$_2$.OMe	4581	3194	10.18	4.64	26.51	21.87

Table 3.11: Data from the Lippert Plots in Figure 3.47 with calculated change in dipole moments ($\Delta\mu$ / D) and excited state dipole moments (μ_E / D) determined from the gradient. Approximate radii for determination of spherical cavities (a / Å) and ground state dipole moments (μ_G / D) were estimated from optimised geometries calculated using Gaussian 03 [47] with the B3LYP functional and 6-31G(d) basis set.

From the gradient of the graphs in Figure 3.47 it has been determined (see Table 3.11) that the excited state dipole of the unsubstituted **BPETO$_2$** is substantially lower than that for **BPETO$_2$.OMe**. This is attributed to the enhanced charge transfer the substituted species experiences due to the electron–donating methoxy group.

Closer inspection of the different emission profiles for **BPETO$_2$.OMe** reveals a

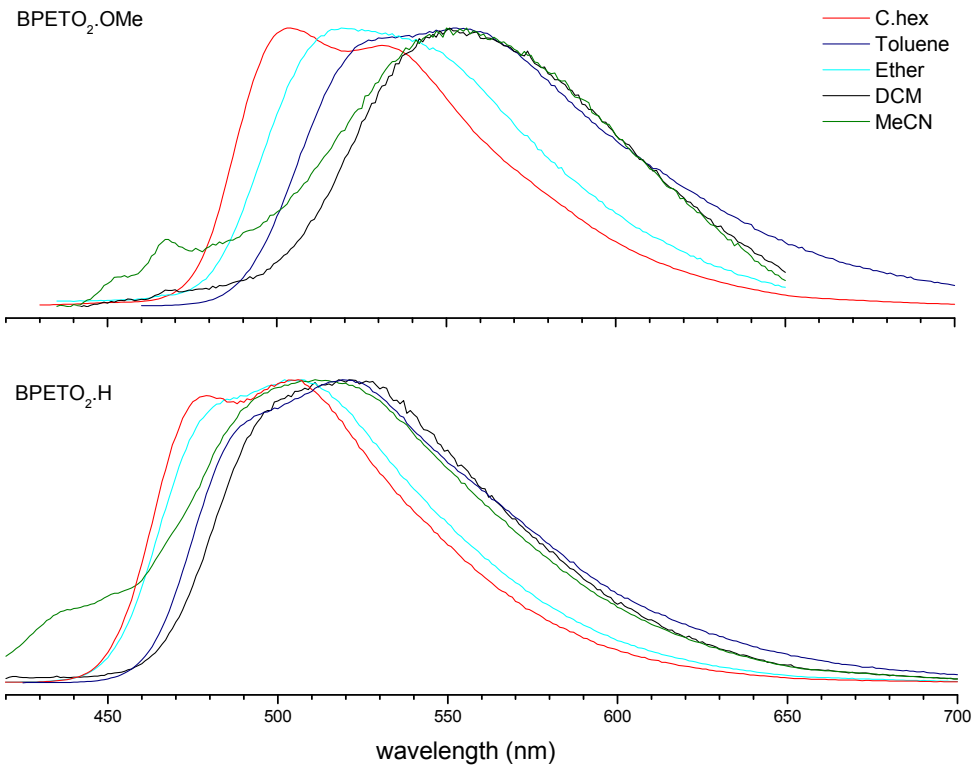

Figure 3.46: Emission spectra of **BPETO$_2$.R** in various solvents.

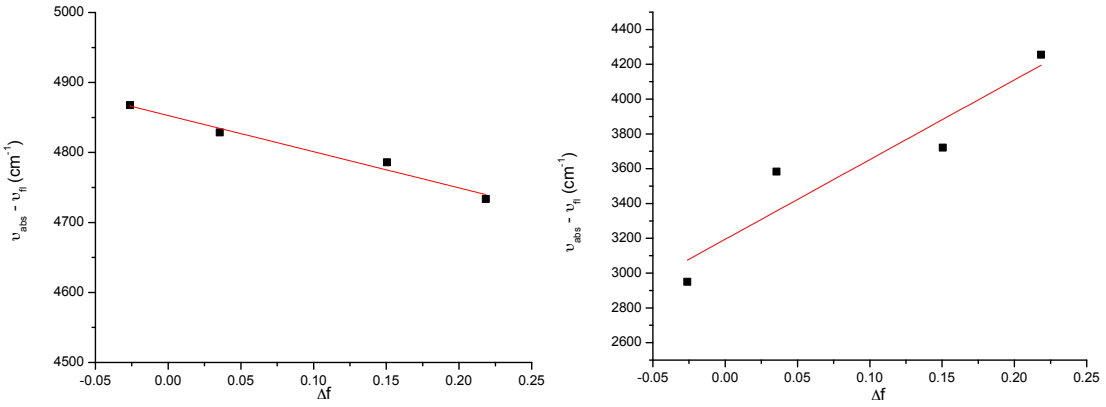

Figure 3.47: Lippert plots of **BPETO$_2$** (LEFT), and **BPETO$_2$.OMe** (RIGHT).

switch in the most intense band with an increase in solvent polarity (Figure 3.46, TOP). In cyclohexane the emission λ_{max} is 503 nm, with a prominent red–shifted shoulder at 531 nm. In ether and toluene there are still two peaks, although their intensities vary, effectively shifting the emission λ_{max}. In DCM and acetonitrile the emission spectra are broad and unstructured.

Although there are shoulders in the lower polarity solvents, the profiles for these systems all exhibit ICT, characterised by their broad emission profiles and large Stokes' shifts. It is also suggested that the radiative decay from the excited states of **BPETO$_2$.R** is effectively quenched by this internal charge transfer pathway made accessible by dissolution in more polar solvents, hence the decrease in fluorescence quantum yield. The concomitant decrease in fluorescence lifetime with increasing solvent polarity results in consistent values for k_f for these systems, ~ 0.14–0.22 ns^{-1}. This rate is substantially lower than those determined for **BPET**, **BPEEDOT** and **BPEantTT.tBu** (0.83 ns^{-1}, 0.92 ns^{-1} and 1.13 ns^{-1} respectively) suggesting a different mechanism is responsible for the fluorescent decay in the charge–transfer based thiophene-1,1-dioxide compounds.

The quantum yield of **BPEEDOTO$_2$.tBu** was measured in toluene, $\phi_f = 0.02$. There was insufficient material to investigate the solvent–dependent quantum yield behaviour. Equally, due to the low quantum yield the fluorescent lifetime, τ_f, could not be measured accurately, although it is noted that the observed decay was short, displaying a similar decay profile to that of the scatter, suggesting $\tau_f < 100$ ps.

Analyses of the photophysical properties of BPEsynTT and BPEantXTT.tBu

These two compounds both feature a break in conjugation across the arylethynylene system. They exhibit blue shifted absorption, excitation and emission relative to the parent compound **BPET**. During measurement of their excitation and emission spectra a narrow peak of moderate intensity relative to the fluorescence was observed, whose wavelength was dependent on excitation wavelength (see Figure 3.48). This was attributed to a Raman vibrational frequency arising from the solvent, with an energy of 2950 cm^{-1} in both toluene and cyclohexane. To remove this peak identical experimental parameters were applied to a sample of pure solvent, and these spectra subtracted from that of the compound, producing the emission spectra of the compound. The emission is so weak from these compounds that the solvent–borne Raman transition is of comparable intensity. The break in conjugation across the thienothiophene group in these compounds is likely to be the cause

for their increased energies and low fluorescence intensities (see Figures 3.42 and 3.43). TD–DFT calculations have indicated that the lowest energy excited state for

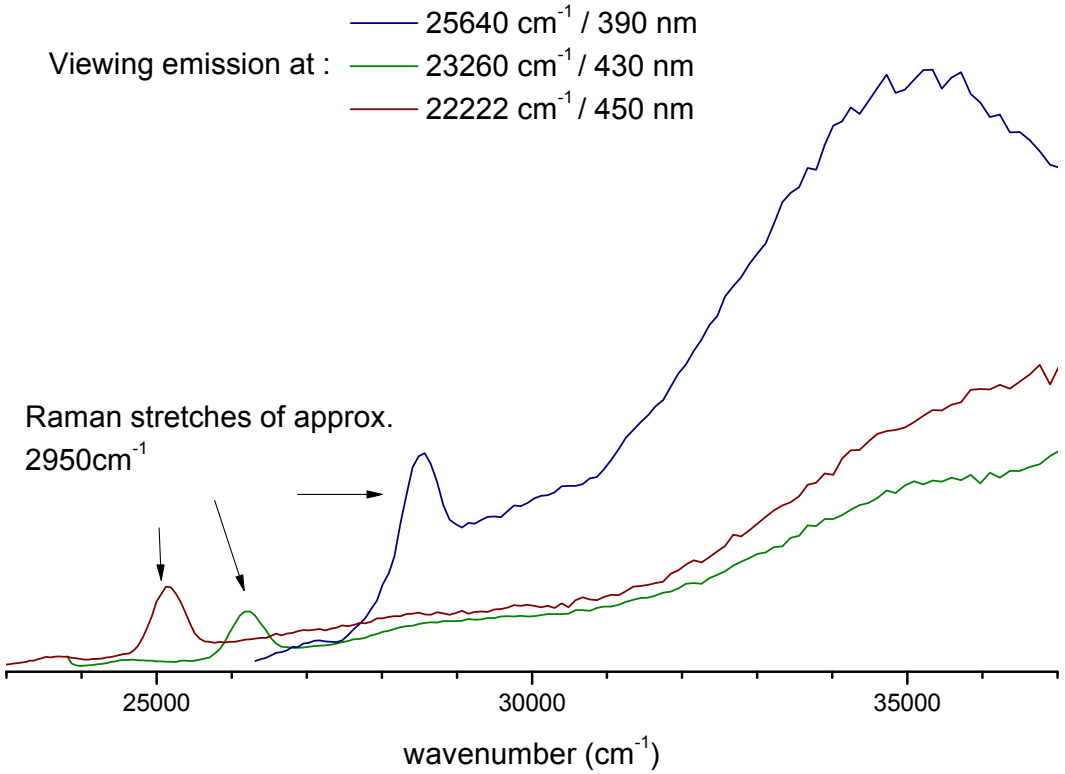

Figure 3.48: **BPEsynTT** excitation spectra recorded in toluene, viewing emission at different excitation wavelengths.

these systems can be assigned to the LUMO←HOMO transition. However, each compound features contributions from other transitions in its lowest excited state and, more notably, larger oscillator strengths are assigned to higher energy excited states (f values are reported in Table 3.12). As Equation 1.3 (section 1.4) indicates, this lowered oscillator strength reduces k_f.

As Table 3.12 shows, the lowest energy excited state of **BPEantXTT.tBu** features the LUMO←HOMO transition, but also the LUMO←HOMO-2 and the LUMO+1←HOMO-1 transitions. It predicts the wavelength of this S_1←S_0 transition to be 329 nm. The fourth excited state has a much stronger oscillator strength than the first excited state, with a wavelength of 294 nm. It also arises from the LUMO←HOMO-2 and the LUMO+1←HOMO-1 transitions, as well as the LUMO+2←HOMO transition.

A similar case is predicted for **BPEsynTT**, with the first excited state assigned

to a combination of the LUMO←HOMO transition and the LUMO+1←HOMO-1 transition. The higher energy excited state has a larger oscillator strength, assigned as the LUMO←HOMO-1 transition. Their MOs are illustrated in Table 3.13.

Excited state	**BPEantXTT** Transition (oscillator strength)	**BPEsynTT** Transition (oscillator strength)
1st	LUMO←HOMO LUMO←HOMO-2 LUMO+1←HOMO-1 (f = 0.50)	LUMO←HOMO LUMO+1←HOMO-1 (f = 1.12)
2nd	(f = 0.00)	(f = 0.02)
3rd	(f = 0.00)	LUMO←HOMO-1 (f = 1.16)
4th	LUMO←HOMO-2 LUMO+1←HOMO-1 LUMO+2←HOMO (f = 1.48)	(f = 0.00)

Table 3.12: Predicted transitions contributing to the excited states of **BPEantXTT** and **BPEsynTT**.

The room and low temperature (77 K) UV–vis absorption and fluorescence spectra of **BPEsynTT** are presented in Figure 3.49. The room temperature spectra features a shift of 3070 nm between the maxima of the excitation and absorption spectra, similar to that observed in toluene. The Raman band (denoted X in Figure 3.49 and ✠ in Table 3.14) is present in the excitation and emission spectra at room temperature, due to the low intensity of emission, however at low temperature it is virtually undetectable due to the increased fluorescence quantum yield. At room temperature the emission bands are relatively broad and unstructured. At low temperature there is enhanced vibrational structure, with a dramatic rise in the red–edge of the excitation spectrum attributed to the planarisation of the compound, as is commonly observed in arylethynylenes. The excitation and emission profiles also exhibit a degree of symmetry, due to enforced planarity in the ground state, and a Stoke's shift of just 235 cm^{-1}. The room and low temperature excitation display a similar high energy band at $\sim$ 280 nm, although the lower energy bands in the 77 K rigid glass spectrum are absent in solution state. The TD–DFT calculated

BPEantXTT	BPEsynTT
LUMO+2 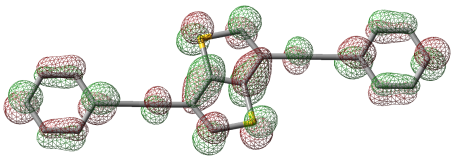	
LUMO+1 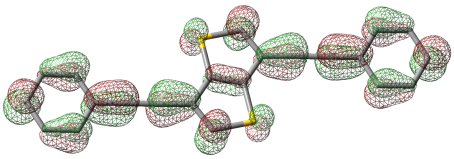	**LUMO+1** 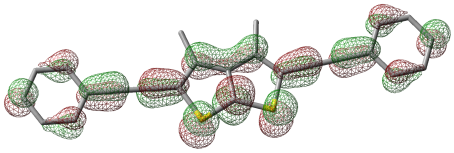
LUMO 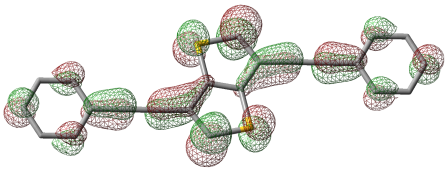	**LUMO** 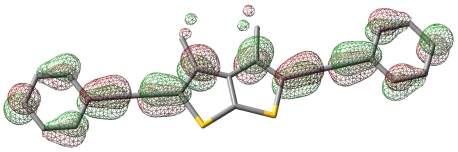
HOMOs 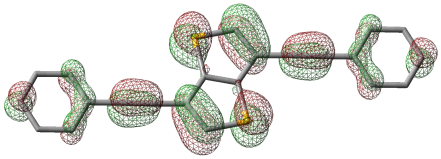	**HOMO** 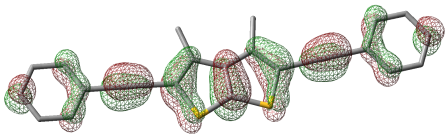
HOMO-1 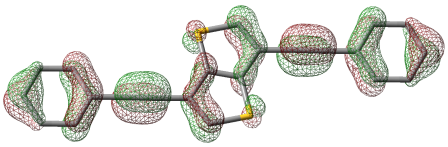	**HOMO-1** 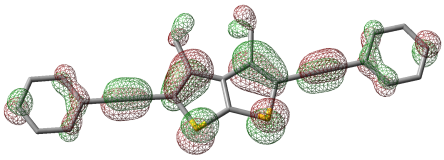
HOMO-2 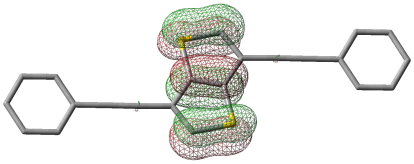	

Table 3.13: Visualisation of the MOs for the transitions predicted to contribute to the first excited state of **BPEsynTT** and **BPEantXTT** using GaussView 4.1.

absorptions and the observed UV-vis absorption bands at low temperature show excellent agreement, with the $S_1 \leftarrow S_0$ predicted to be 361 nm (measured λ = 356 nm) and the second excited state predicted as 326 nm (measured absorption λ_{max} = 320 nm). Spectral features for Figure 3.49 are listed in Table 3.14.

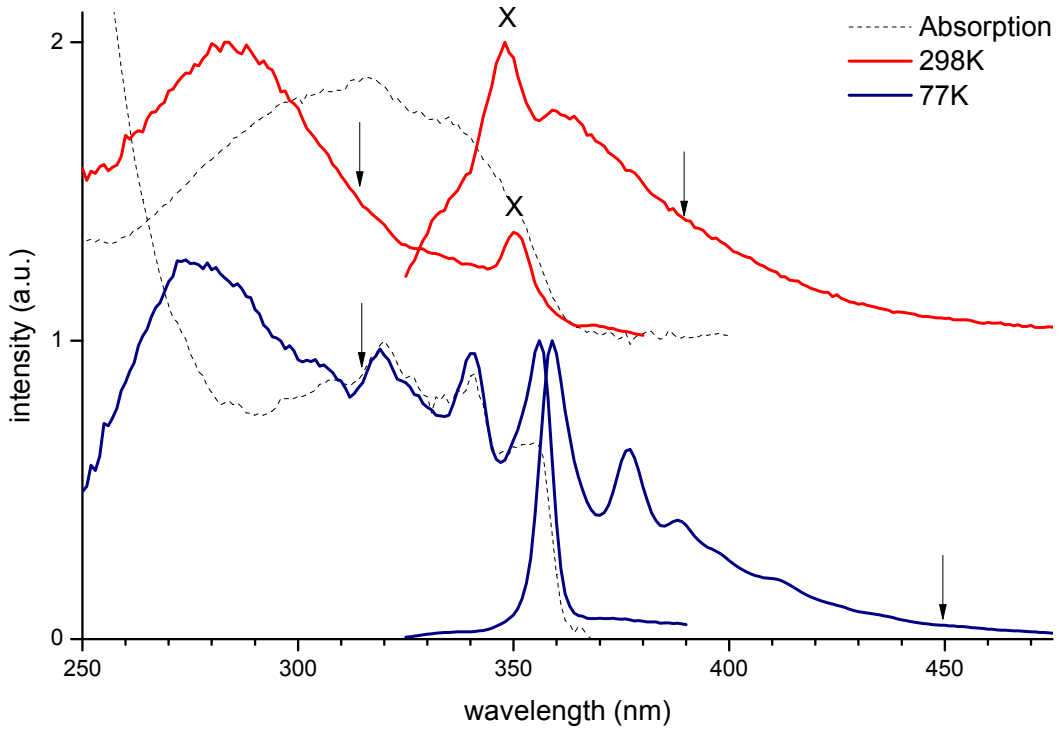

Figure 3.49: UV-vis and fluorescence spectra of 2,5-bis(phenylethynyl)-3,4-dimethylthieno[2,3-*b*]thiophene [**BPEsynTT**] at 298 K and 77 K in EPA. X denotes Raman bands.

	Absorption features / nm	Excitation features / nm	Emission features / nm
298 K	316	283, 350✠	348✠, 360
77 K	320*, 341, 355	273*, 319, 340, 356	359*, 377, 388

* denotes maximum peak.
✠ denotes Raman excitation band.

Table 3.14: Spectral features from Figure 3.49.

The 298 K absorption and excitation spectra of **BPEantXTT.tBu** (Figure 3.50) feature similar profiles, both displaying bands at 306 nm and 316 nm. There is also a more intense and broader band at higher energy, $\sim$ 262 nm and 272 nm.

The emission spectrum at room temperature features a main band at 323 nm, with a red–shifted shoulder at 337 nm. As expected, the lower energy absorption bands mirror the high energy emission bands although there are discrepancies between the low temperature absorption and excitation profiles, likely due to artefacts and scatter from the glass at low temperature.

From TD–DFT calculations this is assigned as absorption to the fourth excited state, $S_4 \leftarrow S_0$, featuring a higher oscillator strength, but which is not attributed to the LUMO←HOMO transition (see Table 3.12).

The UV–vis absorption and fluorescence spectra measured in a 77 K rigid organic glass also features the high energy absorption band at $\sim$ 270 nm, although in the excitation spectrum the lower energy band at 321 nm is more intense, indicating the $S_1 \leftarrow S_0$ transitions is the primary absorption even at low temperature, when planar conformations are favoured. The emission spectrum features increased vibrational structure in the low temperature glass. It also features a second series of emission bands at lower energy, approximately 9050 cm^{-1} red–shifted to the fluorescence emission. These are attributed to phosphorescence emission, with several bands visible (see Table 3.15). The sample was irradiated using the Fluorolog at λ_{ex} = 300 nm and emission monitored with time–drive. The shutter was closed and decay in emission intensity was measured. The lifetime for this phosphorescent decay has been measured as 0.13 s.

	Absorption features / nm	Excitation features / nm	Emission features / nm
298 K	262*, 307, 316	272*, 306, 316	323*, 337
77 K	268*, 309, 321	275, 309, 321*	323*, 338, 487

Table 3.15: Spectral features from Figure 3.50.

Although intensities of emission are low, quantum yields have been measured for both **BPEsynTT** and **BPEantXTT.tBu**. Due to these low values (see Table 3.5 on page 96) the accurate measurement of fluorescent lifetime has not been possible, therefore the rate of fluorescent decay of both species is undetermined.

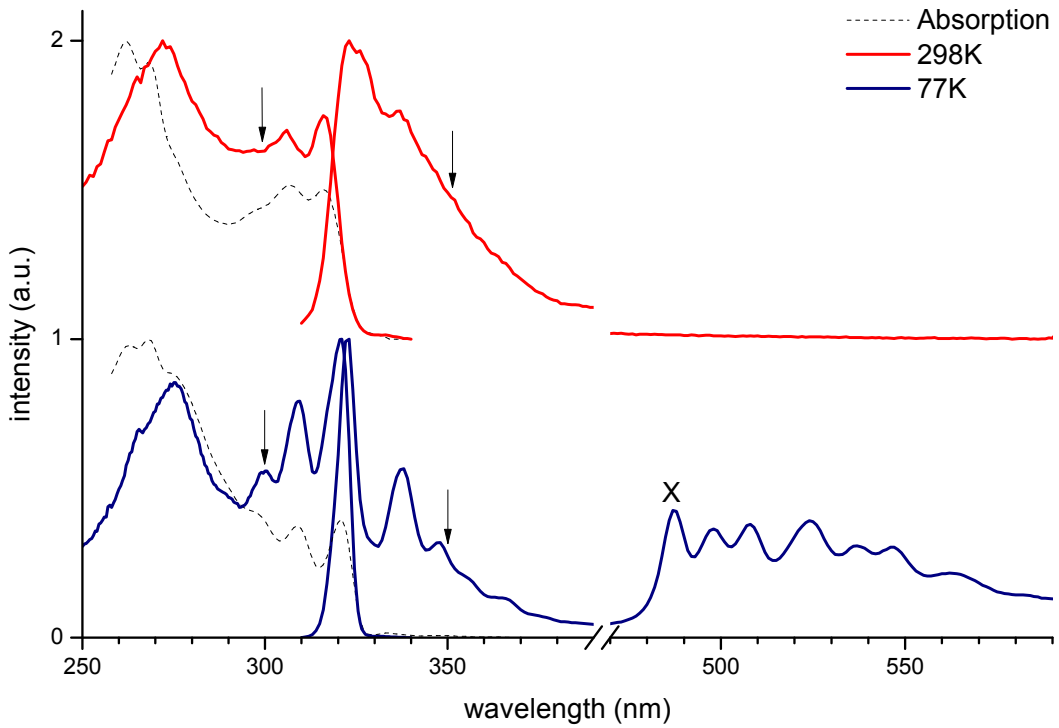

Figure 3.50: UV-vis and fluorescence spectra of 3,6-bis(4-*tert*-butylphenylethynyl)-thieno[3,2-*b*]thiophene **BPEantXTT.tBu** at 298 K and 77 K in EPA. X denotes triplet emission.

Effects of electon–donating and electron–withdrawing substitutents on the photophysical properties of various thienyl arylethynylenes

Chemical modification of the central arene has been discussed with respect to the effect on the photophysical properties. Several of these compounds derivatives have been prepared with electron donor and acceptor groups as substituents. The effect of these different groups, *e.g.* methoxy and cyano, on the electronic structure and excited states of **BPET** has already been reported [114]. The effect of peripheral electron–donating and withdrawing groups on the emission spectra of these novel arylethynylene systems is presented here.

Figure 3.51 shows the emission spectra of the substituted thienyl arylethynylenes. As can be seen both types of substitution induce a bathochromic shift in the EDOT–containing compounds, corroborating observations by Siddle *et al.* [114] who concluded that electron donors raise the HOMO more than the LUMO, and electron accepting substituents stabilise the LUMO relative to the HOMO. The emission spec-

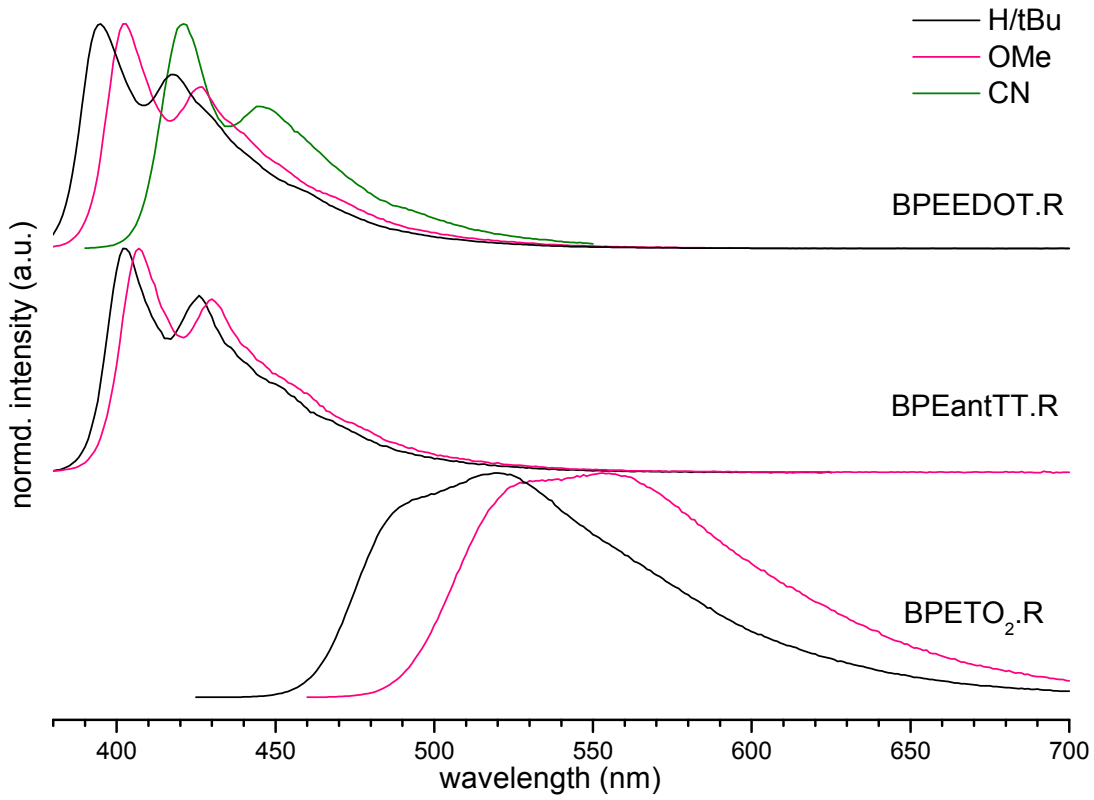

Figure 3.51: Effect of electron–donating and withdrawing substituents on three thiophene–derivative arylethynylenes.

tra obtained here, coupled with results of the TD–DFT calculations indicates this is also the case for the EDOT and thienothiophene based systems. Although only the methoxy–substituted analogue of **BPEantTT.R** was prepared for comparison, TD–DFT calculations indicate the cyano–containing derivative would have exhibited a lower energy emission maximum, similar to that observed with the **BPET.R** and **BPEEDOT.R** systems.

Conversely TD-DFT calculations predicted that **BPETO$_2$.CN** would have featured a higher energy emission than the methoxy–substituted derivative, although it is still expected that the LUMO would be stabilised relative to the HOMO. The compound was not successfully purified and isolated so its photophysical properties are unavailable for analysis.

R Group	**BPEEDOT**	**BPEantTT**	**$BPETO_2$**
	Emission maximum / nm		
H/tBu	395	402	519
OMe	402	407	553
CN	421	-	-

Table 3.16: Spectral features from Figure 3.51.

3.5.2 Electrochemical analysis of the novel thienyl arylethynylenes

Cyclic voltammetry (CV) studies have been performed on selected thiophene–arylethynylenes, with 0.1 M Bu_4NPF_6 in DCM as supporting electrolyte. See Figure 3.52.

Compound	E^{ox} / V	E^{red} / V
BPET	1.11	-
BPEEDOT.H	0.84	-
BPEEDOT.OMe	0.70	-
BPEEDOT.CN	1.00	-2.10
$BPETO_2$	-	-1.22
BPEantTT.tBu	0.85	-
BPEsynTT	0.93	-
BPEantXTT	1.01	-

Table 3.17: Cyclic voltammetry data for thiophene-containing arylethynylenes. See Figure 3.52. Voltages referenced to $FcH/FcH^+ = 0.00$ V.

Irreversible oxidations were observed for all of the systems except **$BPETO_2$**. **$BPETO_2$** was only observed to undergo reduction, which is attributed to the electron–deficient nature of the thiophene-1,1-dioxide group.

The CV for the systems containing the fused thiophene core all exhibited irreversible oxidations, with increasing oxidation potential for **BPEantTT.tBu** < **BPEsynTT** < **BPEantXTT.tBu**.

BPEEDOT.CN underwent irreversible reductions and irreversible oxidation, at 1.00 V. This can be attributed to this species containing both the electron–donating EDO–bridge as well as the electron–withdrawing cyano substitution. The other EDOT–derivatives only exhibited an irreversible oxidation.

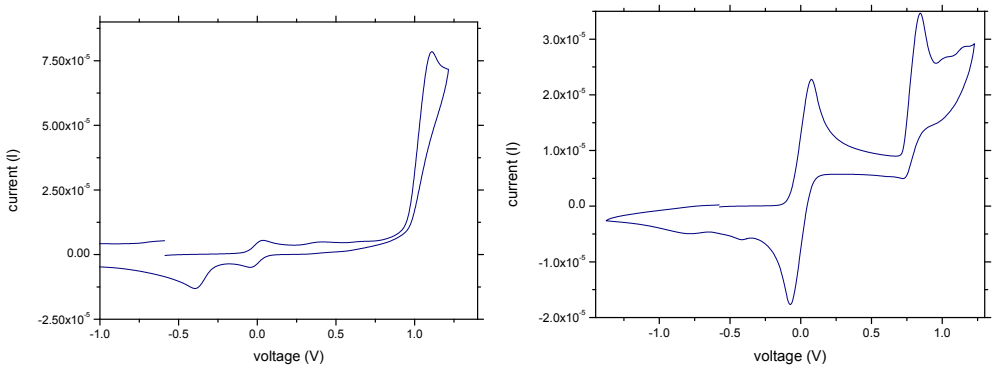

(a) **BPET** (b) **BPEEDOT**

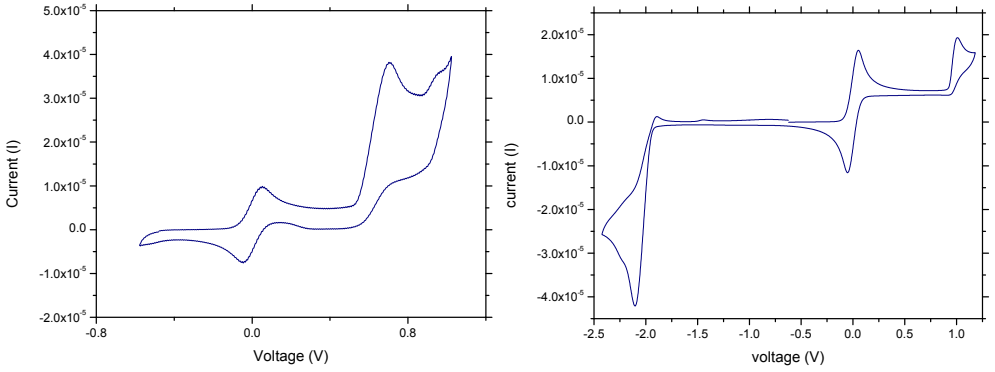

(c) **BPEEDOT.OMe** (d) **BPEEDOT.CN**

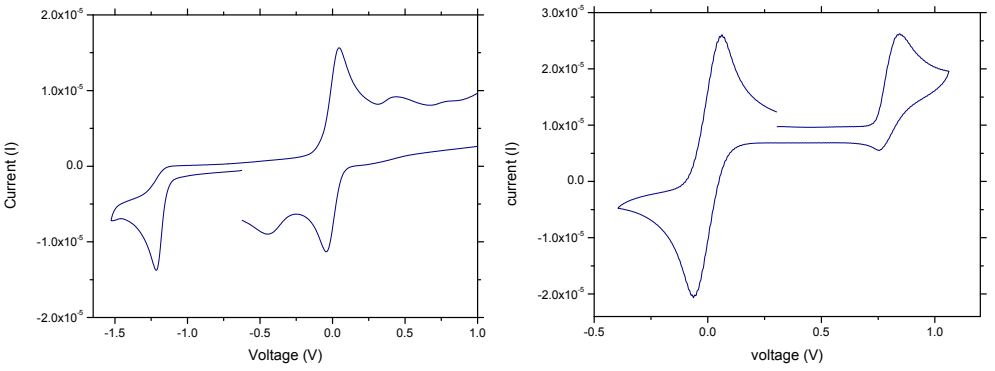

(e) **BPETO$_2$** (f) **BPEantTT.tBu**

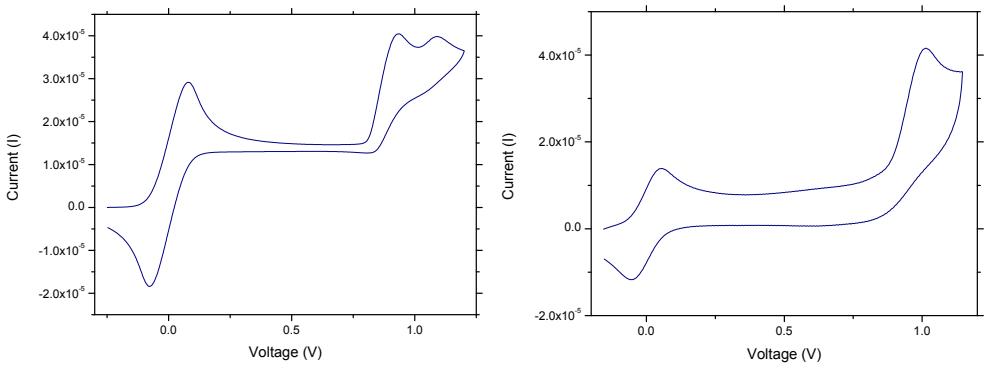

(g) **BPEsynTT** (h) **BPEantXTT.tBu**

Figure 3.52: Cyclic voltammograms of thiophene-containing arylethynylenes in DCM, 0.1 M Bu_4NPF_6 at 100 mV s^{-1}. Potentials are referenced to FcH/FcH^+ = 0 V.

3.6 Conclusions for the novel thienyl arylethynylenes

A series of halogenated–thiophene derivatives have been prepared and these have been subsequently cross–coupled with various arylacetylenes to form nine novel bis(arylethynylene)thienyl derivatives. The electronic properties of the thiophene central core have been modified, and electron–donating and withdrawing groups have been appended to investigate their effects on the overall compounds' structure and properties.

X–ray crystallographic analysis has shown that thiophene-1,1-dioxide has a significantly altered bonding structure compared to thiophene and ethylene-3,4-dioxythiophene, indicative of a loss of aromaticity in favour of diene character. This effect is also evident in the ethylene-3,4-dioxythiophene-1,1-dioxide, although to a lesser extent. Their appears to be no substantive effect attributable to electron–donating/withdrawing appendages on the structure. Equally, the substitution across the thienothiophene as to remove a conjugative pathway appears to have little structural effect.

Calculations have afforded optimised structures of the novel thienyl arylethynylenes, allowing comparisons with observed bond lengths obtained using X–ray crystallography. On the systems which feature a charge–transfer system, such as **BPETO$_2$**, the calculated bond lengths are less accurate, but overall there is excellent agreement. The calculated Raman spectra also show excellent agreement with the observed spectra.

Photophysical analyses have demonstrated that a change in the central heterocycle has a dramatic effect on the photophysical properties, causing shifts in absorption λ_{max} from 320 nm to 433 nm (8160 cm^{-1}). Furthermore, emission maxima have demonstrated a total shift of 11240 cm^{-1} with variation of the heterocycle. The fully conjugated species exhibit high quantum yields, $0.12 \leq \phi_f \leq 0.43$, with the exception of **BPEEDOTO$_2$.tBu**, $\phi_f = 0.02$. This value is similar to those exhibited by the cross–conjugated systems **BPEsynTT** and **BPEantXTT.tBu**. Fluorescent lifetimes could not be obtained for these three systems; their decay pro-

files resembled that of the scattering source, indicating a lifetime, $\tau_f < 100$ ps. This contradicts their predicted oscillator strengths, which for $S_1 \leftarrow S_0$ are all $f > 0.5$.

Electrochemical analysis has shown that the electron–deficient **BPETO$_2$** is not oxidised, and exhibits an irreversible reduction at E = -1.22 V. **BPEEDOT.CN** was the only compound studied to undergo both reduction and oxidation, attributed to the presence of the electron–rich EDO bridge and electron–withdrawing cyano groups.

4

Aryleneethynylenes Containing Oxadiazole, Benzofurazan and Benzothiadiazole

4.1 Introduction to oxadiazoles and thiadiazole derivatives

The other class of heterocycle investigated in this work are arylethynyl–substituted diazoles, specifically oxadiazole (Figure 4.1a), benzofurazan (Figure 4.1b) and benzothiadiazole (Figure 4.1d). Oxadiazole-containing compounds have attracted considerable interest in the field of organic electronics due to their electron–deficiency, which affords them great potential as electron–conducting, hole–blocking (ECHB) layers in OLEDs. They are also electrochemically active with well documented reversible reduction potentials. [85, 146] The sulfur-containing analogue of 1,3,4-oxadiazole is 1,3,4-thiadiazole (Figure 4.1c), which has not been as thoroughly investigated. Furthermore, there are very few examples of oxadiazole and thiadiazole substituted with ethynylenes reported in the literature. Similarly, there have been relatively few benzofurazan and benzothiadiazole derivatives reported. Although the fluorescent properties of 7-substituted-4-nitrobenzofurazan (NBD) compounds have been studied for many years (see section 4.3.2) there is very little research into arylethynylene substituted benzofurazans, whereas a relatively large amount of work into the excited state properties of arylethynylene–substituted benzothiadiazole oligomers has been reported (see section 4.3.3).

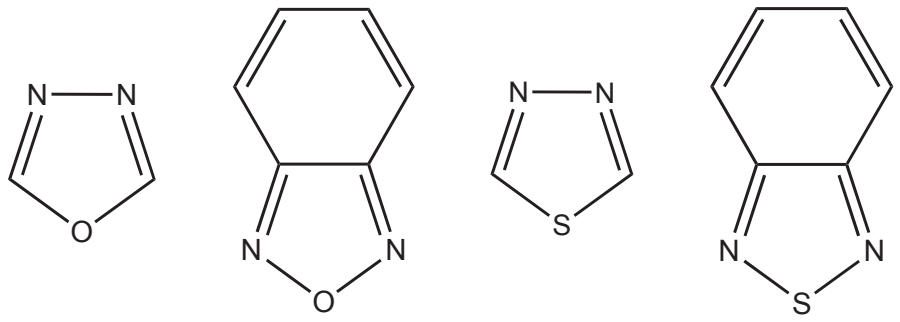

(a) (b) (c) (d)

Figure 4.1: Heterocycles investigated in this chapter: (a) 1,3,4-oxadiazole; (b) benzofurazan; (c) 1,3,4-thiadiazole; (d) benzothiadiazole.

4.2 Oxadiazole and thiadiazole

Oxadiazole is available in several isomeric forms. It is a five–membered ring, containing two carbons, two nitrogens and an oxygen. 1,2,4-oxadiazole has been investigated and experimented with for use in applications as diverse as liquid crystals and immunosuppressants. [147] For the purpose of presenting literature relevant to this work the isomer of interest is 1,3,4-oxadiazole as it is in this form that oxadiazole has been used for application in OLEDs and other organic electronic and optoelectronic devices.

What follows is a brief examination of some of the work in recent literature on compounds containing 1,3,4-oxadiazole. It is not meant to be exhaustive as interest in oxadiazole for this work is primarily on its properties and electronic nature when substituted with acetylenes. The following literature should provide a useful introduction into its properties and explain its potential.

4.2.1 Oxadiazole as a component in electron-conducting hole-blocking species

Van Slyke and Tang [148] reported in the late 1980s the improvement of electroluminescence of an organic LED upon inclusion of a second layer which could only transport one type of charge carrier. This was taken further by Adachi *et al.* who included two extra layers, each only capable of transporting one type of charge. [149]

Due to its highly electon–deficient nature it is a poor hole–acceptor, and as such 1,3,4-oxadiazole derivatives have been incorporated into compounds enabling them to act as an electron–conducting, hole–blocking layer for application in OLEDs (see section 1.3.1, page 8).

Oxadiazole was realised as a good candidate for the role of electron–conducting hole–blocking (ECHB) layer by Saito *et al.* [150] who went on to produce a blue emitting OLED which incorporated both a hole–transporting and hole–blocking layer. This afforded it a very high luminance (700 cd/m^2). [151] The ECHB layer used was 2-(4'-biphenylyl)-5-(4"-*tert*-butylphenyl)-1,3,4-oxadiazole (PBD). Brown *et al.* later quantified the improvement the inclusion of this ECHB layer generated,

and suggested that the electron transport layer confined the holes to the emissive layer. They showed that PBD improved efficiencies at lower voltages by 10–fold, and at high voltages by 8–fold. [12]

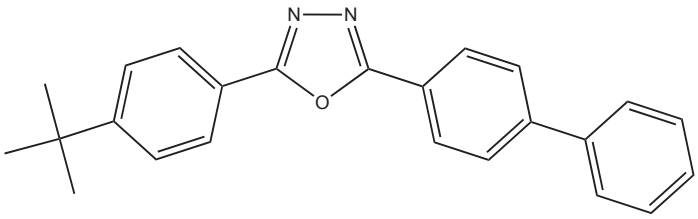

Figure 4.2: PBD, commonly used as an additive, dispersed in PPV, to act as an electron–transporting layer.

Heeger and co-workers incorporated 2-(4'-biphenylyl)-5-(4"-*tert*-butylphenyl)-1,3,4-oxadiazole (PBD) in the preparation of yellow and green OLEDs. The incorporation differed in preparation of the devices. In the yellow–emitting devices PBD was dispersed in poly(methyl methacrylate) (PMMA) and layered between the semiconducting emissive polymer and the metal electrode. In the green emitting device, PBD was dispersed *within* the semiconducting polymer itself. In each case the emissive polymer was a substituted PPV derivative. It was reported that inclusion of the ECHB layer resulted in improvements in quantum efficiencies of two and 16–fold, for the yellow and green devices, respectively. [152, 153]

Similar work was reported by Yoshida *et al.* who dispersed PBD within films of poly(3-hexylthiophene) (P3HT), resulting in improved EL efficiency and varied colours being observed. [154]

Oxadiazole containing materials have predominantly been used as an ECHB layer in organic LEDs, but Heeger has also demonstrated its potential as combined emitter–ECHB material, when conjugated within the polymer. In 1998 he reported the preparation of a polymer containing oxadiazole, P3HT and phenyl rings, alternating in a polymer, affording blue emission with a photoluminscence efficiency of 79 % and potential as an emissive layer in PLEDs. [155]

Synthesis of a large range of oxadiazole containing compounds has been carried out at the University of Durham over the past decade, in a collaboration between the departments of Chemistry and Engineering. [84, 85, 146, 156–158] Their work was initially interested in four oxadiazole–containing oligomers, one of which also

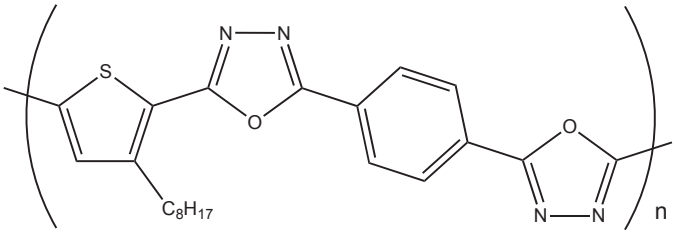

Figure 4.3: Polymer POTOBz developed by Heeger *et al.*, containing oxadiazole.

incorporated pyridine. Each were investigated as hole–blocking materials. The UV–vis absorption and PL characteristics were investigated, as were EL studies by incorporation into bilayer LEDs. It was determined that the pyridine containing oligomer caused a 40–fold increase in the external quantum efficiency over the single layer OLED, from 6×10^{-3} % to 0.24 %.

This work was continued with the central core changed from 2,5– to 2,6– 3,5– , and 2,4-disubstituted pyridine and 2,5-disubstituted pyrimidine (see Figure 4.4), although no improvement on performance of LEDs constructed with these was observed. It was also noted that calculations performed on the LUMO of the compounds prepared could not predict external quantum efficiencies (EQE). It is clear that the EQE is not just related to the electronic configuration of the compound, but also structure, packing effects and film formation, as well as other constituents within the device.

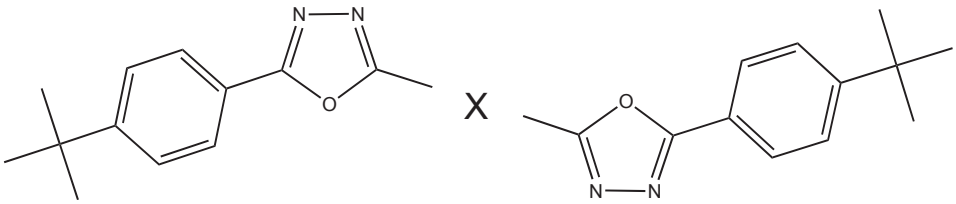

Figure 4.4: ECHB compounds prepared by Bryce and co-workers., featuring different cores 2,5– to 2,6– 3,5–, and 2,4-disubstituted pyridine and 2,5-disubstituted pyrimidine.

Due to fluorene's propensity to emit in the blue region Bryce's group have incorporated it in several oxadiazole and pyridine–containing oligomers in attempts to synthesize a blended–layer OLED capable of blue emission. Through experimentation and analysis it was found that EQEs could be improved by inclusion of an ECHB-type blend, *or* by use of a lower work function electrode *i.e.* calcium in-

stead of aluminium. Unfortunately calcium electrodes are not ideal for application in OLEDs as they tend to decompose. Consequently, blended polymers are believed to hold more potential.

4.2.2 Aryleneethynylenes containing thiadiazole

Whilst the lack of a successful synthetic method for 2,5-dibromo-1,3,4-oxadiazole has hindered the preparation of 2,5-bis(phenylethynylene)-1,3,4-oxadiazole, the sulfur containing analogue 2,5-bis(phenylethynylene)-1,3,4-thiadiazole has been prepared from the isolated 2,5-dibromo-1,3,4-thiadiazole, and its basic photophysical properties have been investigated. Like oxadiazole it is a strong electron acceptor and should display similar properties to that of its oxadiazole analogue, including being electrochemically active.

In 2005 Yamamoto published two papers. The first article reported the synthesis of 2,5-dibromo-1,3,4-thiadiazole and the second discussed its cross–coupling with phenylacetylene and the resulting compound's (see Figure 4.5) basic photophysical properties. [112, 159]

Synthesis of the dibrominated core was achieved by bromination of 2-amino-1,3,4-thiadiazole with bromine, in acetic acid. This allowed isolation of 2-amino-5-bromo-1,3,4-oxadiazole, which was brominated *via* a Sandmeyer reaction, using $CuBr_2$ and t-$BuNO_2$ in dry acetonitrile, affording 2,5-dibromo-1,3,4-thiadiazole, in good yields ($\sim$ 80 %).

Selected photophysical properties were reported for this compound (absorption λ_{max} = 334 nm, log ε = 4.56, emission λ_{max} = 396 nm, ϕ_f = 15 % in chloroform). The electronic structure of this compound as deduced by DFT calculations was also reported, with the HOMO and LUMO being delocalised over the whole of the molecule. The paper also reported the preparation of polymer systems incorportating thiadiazole. The electrochemistry of these was investigated, and found to be largely similar to other electron-transporting materials *i.e.* oxadiazole derivatives. Electrochemical analysis of the oligomeric species was not discussed.

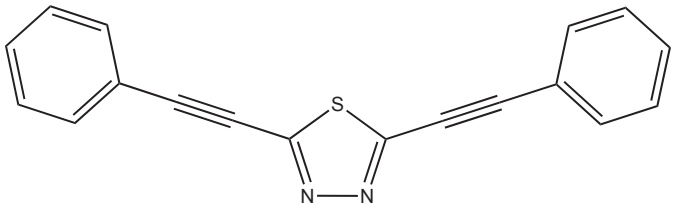

Figure 4.5: 2,5-bis(Phenylethynyl)-1,3,4-thiadiazole, **BPETd**.

4.3 Benzofurazan and benzothiadiazole systems

As mentioned earlier, there is a wealth of research into arylethynylene–substituted benzothiadiazoles, but only limited coverage of benzofurazans. Consequently, what follows will introduce benzofurazan through its original and most commonly used application, as a fluorescent probe for biological systems. After that will be a review of some of the work done on 4,7-disubstituted benzothiadiazoles, focusing on recent work developing arylethynylene–type systems.

4.3.1 Benzofurazan systems

Benzofurazan is a derivative of oxadiazole; it also referred to as 2,1,3-benzoxadiazole. It features a five–membered ring containing an oxygen and two nitrogen atoms, fused through two carbon atoms to a six–membered ring (see Figure 4.1).

Benzofurazan derivatives have long been associated with luminescence. Whilst researching derivatisation of 4-nitrobenzofurazan (NBD) for pharmacological application and thiol-blocking abilities, Whitehouse and Ghosh [160] reported high fluorescence of products from reactions of 7-chloro-NBD with various aliphatic amines. Chloro-NBD is a yellow, non-fluorescent compound, prepared from nitration of chlorobenzofurazan, itself prepared from dichloroaniline (see section 4.4.2, Scheme 4.18). When substituted with an amine however, Whitehouse and Ghosh observed strong fluorescence ($\lambda_{em} \sim 510 - 520$ nm), particularly in non–polar solvents.

Due to its strong fluorescence, there have been a significant number of publications on the use of NBD and derivatives as biological probes and sensors. [161–163] NBD derivatisation of lipids has enabled membrane studies. [161] Mazarguil and Dufau have synthesized a fluorescent amino acid, Nα-Fmoc, Nβ-NBD, L-diamino propionic acid, enabling the fluorescent tagging of peptides. [162] Ammonium-7-fluoro

benzo-2-oxa-1,3-diazole-4-sulfonic acid (SBD-F) has been used to help measure the homocysteine content in various food stuffs. [164] Haselberg *et al.* used the fluorescence of 4-(*N*-methylamino)-7-nitro-2,1,3-benzooxadiazole (MNBDA) to quantitatively monitor the activity of microperoxidases, a catalyst for the oxidation of non–fluorescent hydrazino– substituted benzofurazan with hydrogen peroxide. [165]

The success of this "fluorescent handle" as a probe for amines and thiols [166] and as a biosensor in peptides, has led to the development of sensors for various metal ions, exploiting the phenomenon of quenching by photo–induced electron transfer (PET[1]).

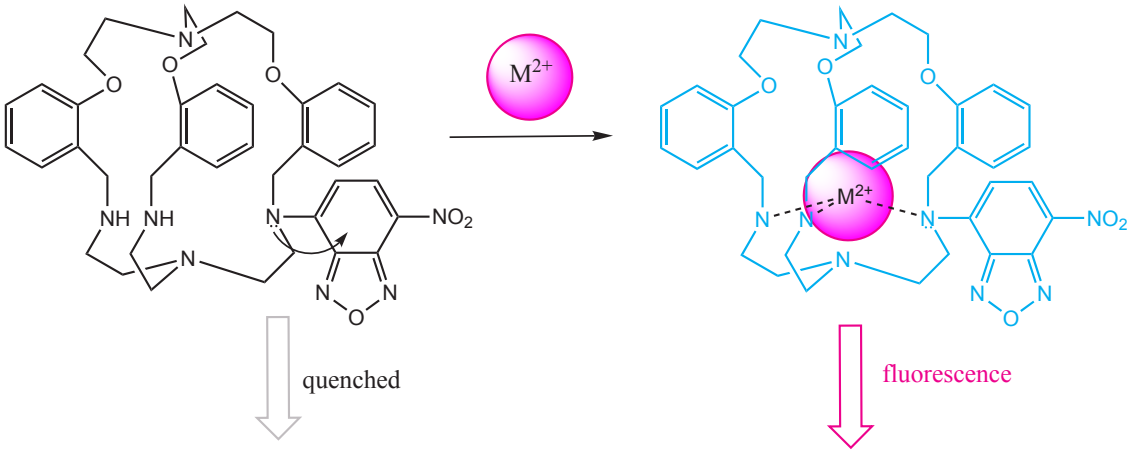

Figure 4.6: Demonstration of PET. LEFT: Binding site (*e.g.* cryptand) without cation means electron transfer of free lone pair on nitrogen into excited state of fluorophore, resulting in non–radiative decay. RIGHT: Cation bound, lone pair no longer available, so fluorescent decay from excited state is allowed. [167]

Bharadwaj's group have reported the development of cryptands coupled to NBD. [167,168] In 2004 they showed modulated fluorescence from a cryptand–NBD species by the binding and translocation of cadmium(II). Without any metal ion bound within the cavity of the cryptand, the lone pair on the nitrogen of the cryptand, through which NBD is connected, was donated to the excited state of the fluorophore by PET. This quenched any fluorescence. On binding of Cd(II) within the cryptand, the lone pair could not donate to the excited state of the fluorophore, resulting in no

[1]Photoinduced electron transfer is a quenching mechanism whereby a complex is formed by a donor and acceptor moiety in a species. The charge-transfer complex can decay non-radiatively, and the electron is returned from the acceptor to the donor. [33] This is the case for the benzofurazan-containing sensors discussed here.

quenching mechanism; hence fluorescence was observed. In this case emission was 240–fold that without the metal ion present. Bharadwaj took the study further, noting that the electron–withdrawing nature of NBD allowed for certain counteranions to pull the metal cation out of the cryptand, allowing PET to quench any emission. This was illustrated by addition of potassium thiocyanate (NCS^-), which lowered the emission to that of the unbound–cryptand ($\phi_f = 0.006$). This was then reversed by addition of silver tetrafluoroborate, which preferentially bound the anion, allowing the Cd(II) to re–enter the cage and prevent PET quenching. Bharadwaj continued this work with the addition of a second type of fluorophore onto the cryptand unit. [167] The cryptand was substituted with both NBD and anthracene to generate fluorescence resonance energy transfer (FRET[2]) which could be activated when the cryptand hosted a metal ion.

A range of other cation detection systems based on NBD have been published, using macrocycles as opposed to cryptands. Boiocchi *et al.* prepared a cyclam–like macrocycle appended with NBD (see Figure 4.7). Upon addition of Cu(II) to a solution of the compound, they noted a colour change from orange/red to yellow, with concomitant quenching of its fluorescence upon excitation at 470 nm. [169] A similar system containing two fluorophores was prepared and studied by Kim *et al.* in 2006. [170] This compound featured NBD and pyrene, substituted on opposite nitrogens of the binding cyclam. They observed that Hg(II) caused a 10–fold increase in the fluorescence at 538 nm, the region of fluorescence attributed to the NBD moiety. As with Fabbrizzi's work, introduction of the paramagetic Cu(II) ions resulted in a quenching of any fluorescence in the same region.

A recent communication reported the substitution of NBD with a macrocycle which could accept four protons, meaning pH–dependent fluorescence experiments could also be performed. [171] When fully protonated the compound was emissive (pH = 2; $\lambda_{em} = 532$ nm; $\phi_f = 0.22$). When the pH was raised, fluorescence was quenched (pH = 11; $\lambda_{em} = 562$ nm; $\phi_f < 0.001$), which is typical behaviour of a photo–induced electron transfer quenching mechanism. This paper also reported

[2]Fluorescence resonance energy transfer requires two fluorophores, essentially a donor and acceptor. The emission of the donor needs to be high in energy, to overlap the absorption profile of the acceptor.

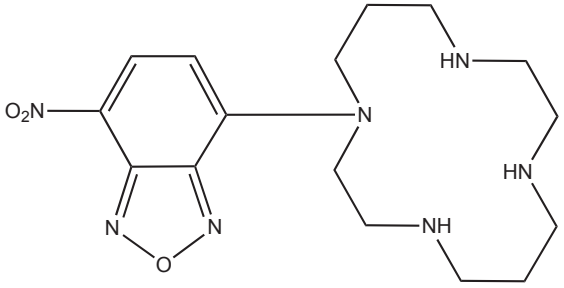

Figure 4.7: Cyclam with fluorescent handle NBD by Boiocchi *et al.*.

metal–ion–dependent fluorescence.

Last year Wanichacheva *et al.* published work on a highly selective mercury sensor. The NBD–derivative was able to discriminate between many cations including Cu(II) and Pb(II), important due to their chemical similarity to Hg(II). [172]

4.3.2 Materials incorporating benzofurazan and benzothiadiazole

Considering the prolific research into benzofurazan derivatives as fluorescent markers, the low level of interest in π–conjugated derivatives for material applications is strange, given its potential applicability. The sulfur containing derivative, benzothiadiazole, has been investigated more thoroughly. It has been incorporated into fluorescent polymers for use in OLEDs, fluorescent dyes for application in LCDs, two–photon absorbing compounds, as a component in solar cells, and in DNA detection fluorophores. [17, 173–178]

Structural modification by Kitamura *et al.* of one of the most prolifically researched semiconductors, polythiophene, to benzo[c]thiophene, achieved a decrease in band–gap of 1 eV, revealing the potential in the derivatisation of heterocycles [179] for use in BHJ devices (see section 1.3.2, from page 10). Attempts at prediction of band–gap energies from the structure of polymers led co–workers to copolymerise electron–rich with electron–deficient units, affording raised HOMOs and lowered LUMOs, and therefore facilitating intramolecular charge transfer. Mühlbacher *et al.* developed a BHJ–based device with the polymer poly[2,6-(4,4-bis-(2-ethylhexyl)-4*H*-cyclopenta[2,1-b;3,4-b']-dithiophene)-*alt*-4,7-(2,1,3-benzothiadiazole)]. Mühlbacher's

material featured cyclopentadithiophene as the electron–donating unit and benzothiadiazole as the electron–deficient unit. Fluorescence spectroscopy indicated the polymer had a band-gap in the IR-region, with a solid state absorption peak at $\sim$ 775 nm and emission at $\sim$ 890 nm. It was also subject to an almost complete quenching of fluorescence on addition of the accepting fullerene. This implied fast photoinduced charge transfer, essential in PV cells.

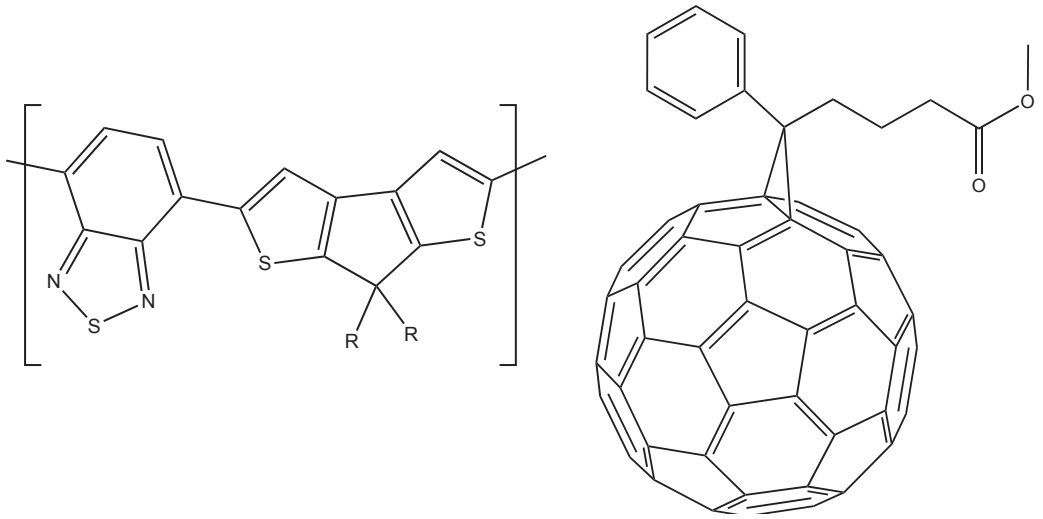

(a) (b)

Figure 4.8: Mühlbacher's PV polymer system. (a) Poly[2,6-(4,4-bis-(2-ethylhexyl)-4*H*-cyclopenta[2,1-b;3,4-b']-dithiophene)-*alt*-4,7-(2,1,3-benzothiadiazole)]. (b) PCBM.

Work by Leclerc and co-workers on polymers for use in solar cells led to the development of several copolymers. Using DFT calculations (B3LYP/6-31G(d)) they estimated the band–gap for a range of heterocycles'. Knowing desirable band–gap energies led to the development of several polymers incorporating benzothiadiazole and benzofurazan, amongst others, as the electron–deficient units. As an electron–rich component they incorporated poly(2,7-carbazole) units, a compound they knew from earlier work would afford good efficiencies and carrier mobilities. [177] Solution-state UV–vis absorption data were obtained at 135 °C in trichlorobenzene, after observing a red–shift of $\sim$ 20 nm due to aggregation at room temperature. Similarly, a high degree of structural organisation was presumed to be the cause of the significant ($\sim$ 35 nm) bathochromic shift in the solid state absorption spectra. The band–gap

estimated from optical spectroscopic methods was shown to be largely dependent upon the electron-deficient heterocycle. From electrochemical data they concluded that the HOMO was not altered by the electron-deficient heterocycles, which suggested the carbazole moiety was responsible for this level. Conversely the LUMO appeared to be dependent upon the nature of the electron-deficient heterocycle. From this data, and some further measurements of field mobility and PV solar cell development, they concluded that the benzothiadiazole-containing polymer showed the greatest potential out of the heterocycles tested. Benzofurazan suffered from poor solubility, but with adequate substitution it was anticipated that this problem could be circumvented.

Further work on alternating copolymers incorporating benzothiadiazole and benzofurazan has been published by Swager and Bouffard, [180] who commented on the surprising lack of research involving materials composed of π–conjugated benzofurazan. Their work featured substitution of the heterocycles with ethynylene bridges forming arylethynylene–type polymers, linking the heterocycles through extended π–conjugation to three specific moieties; alkoxy–substituted phenyl groups, alkyl–substituted fluorene, and pentiptycene. Solubility problems necessitated alkoxy–substitution on benzofurazan, although this undoubtedly increased the electron–density on the system. The insolubility of one of the polymers in hot THF also prohibited the determination of its molecular weight by gel permeation chromatography (GPC). UV–vis absorption and fluorescence spectra of these systems exhibited a red–shift relative to arylethynylene polymers lacking the heterocycles. The shift appeared to be relative to the strength of the electron–deficient heterocycle, with the unsubstituted, oxygen–containing benzofurazan exhibiting the greatest effect when coupled to the electron rich fluorene derivative. High fluorescent quantum yields were reported, similar to those of the non–heterocycle–containing pure polymers, and due to the reported emission wavelengths ($\sim$ 520–550 nm), Swager suggested their potential use in green polymers, for application in OLED manufacture.

Swager's paper represents one of the only instances of compounds featuring the benzofurazan in a π–conjugated arylethynylene system. There are, however, several examples of benzothiadiazole–containing arylethynylenes to review. These should

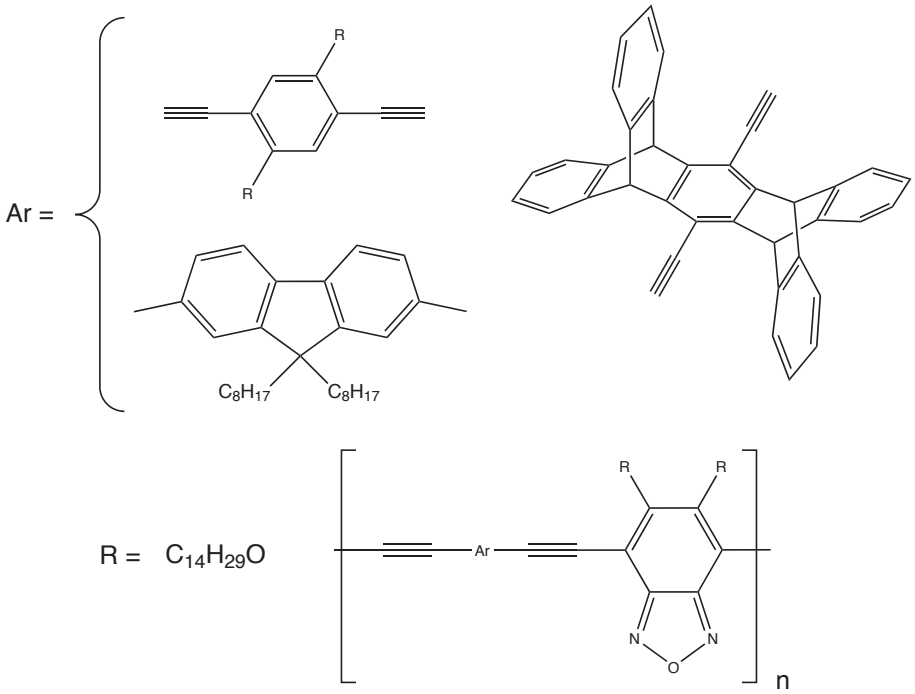

Figure 4.9: Polymers prepared by Swager and Bouffard featuring ethynyl–bridged units of benzofurazan and alkyoxy–substituted benzene, fluorene, and pentiptycene. [180]

have similar basic properties to the oxygen containing analogues. [17, 177, 178, 180–186]

4.3.3 Arylene-ethynylene benzothiadiazole systems

The preparation of bis(arylethynyl)–functionalised benzothiadiazole oligomer species has been reported by several groups. However, studies of their photoluminescent and electrochemical properties were, until recently, relatively limited. Bunz reported the preparation of a polymer of just 18 repeating units, along with the absorption and emission spectra (solution state absorption λ_{max} = 498 nm, emission λ_{max} = 562 nm). He also presented data from PM3 (semi–empirical) calculations and CV studies, confirming the polymer as a low band–gap n–dopable species, with the HOMO delocalised and the LUMO localised on the heteroaromatic groups. [181]

Studies on the oligomer conforming to the bis(phenylethynyl)heteroarene motif were first published in 2002, when Yamashita incorporated benzothiadiazole as a spacer group between 2–, 3– and 4-pyridylethynyl groups. [182] These compounds

were synthesised by palladium cross–coupling of the various pyridylacetylenes with 4,7-dibromobenzothiadiazole, under Sonogashira conditions. Yields were moderate and both mono and di–coupled products were isolated. UV–vis absorption and fluorescene spectroscopy indicated that the benzothiadiazole induced a large red–shift relative to the analogous benzene derivative (emission λ_{max} 464 nm *c.f.* 344 nm for the bis-3-pyridylethynyl derivative and λ_{max} 479 nm *c.f.* 342 nm for the bis-4-pyridylethynyl derivative). Absorption spectra exhibited a solvent–dependency, which indicated a more polar ground state. Quantum yields were high, and also solvent dependent. A quantum yield of 100 % ($\phi_f = 1.0$), in dioxane, was reported for the derivative substituted with 4-ethynylpyridine.

A further study on these systems was published in 2005 when Dupont and co-workers reported the preparation of several 4,7-bis(arylethynyl)-benzothiadiazole compounds [184], in conjunction with the preparation of their non–ethynylene–containing analogues. The article presented an improved synthesis of the acetylene–bridged systems. Dupont first prepared the bis-ethynylene-benzothiadiazole compounds, and appended these with various arylbromides. The photophysical and electrochemical properties of several compounds were presented as was a discussion on the effect of the compounds' overall properties attributable to substitution on the appended phenyl rings (see Figure 4.10).

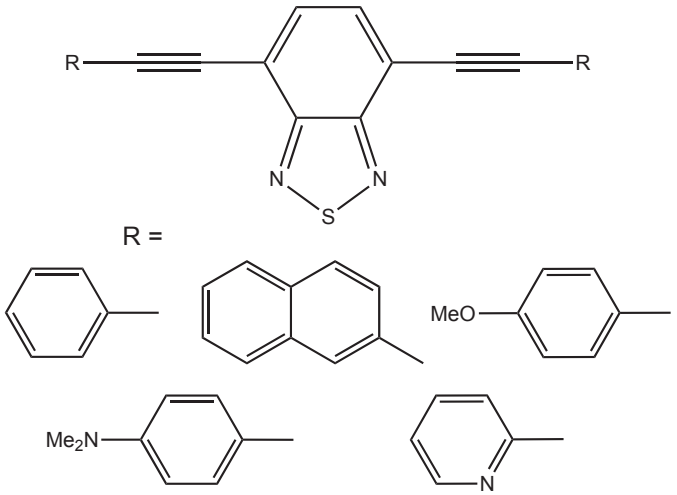

Figure 4.10: Various arylethynylene–benzothiadiazoles reported by Dupont and co-workers.

Photophysical properties of selected compounds from Dupont's paper are pre-

Compound	R-group	Log ε	λ_{max} abs/nm	λ_{max} ems/nm	ϕ_f	τ_f /ns	E_{red}^{onset} /V
BPEBtd	H✠	4.99	403	497	0.37	5.53	–1.57
	OMe	4.40	393	542	0.29	6.42	–0.95
	NMe_2	4.11	407	438	0.15	8.18	–1.37
BPyEBtd	—	4.40	394	469	0.86	4.52	–0.68

✠ = also prepared separately in this work.

Table 4.1: Photophysical data on arylethynyl–substituted benzothiadiazole compounds obtained in acetonitrile by Dupont and co-workers.

sented in Table 4.1. As the data shows, all compounds exhibited a range of quantum yields, with the 2-ethynyl pyridyl– substituted derivative achieving $\phi_f = 86$ %. The reported fluorescence lifetimes (τ_f) were good for organic systems. The dimethylamino– substituted derivative achieved $\tau_f = 8.18$ ns. A large Stoke's shift of 6995 cm^{-1} was observed for the methoxy– substituted derivative which was attributed to efficient intramolecular charge transfer between the electron–rich terminal methoxy groups and the central electron–deficient benzothiadiazole core. It does not, however, explain the relatively small Stoke's shift for the dimethylamino-substituted derivative (1740 cm^{-1}).

A brief analysis of the cyclic voltamogramms for both the ethynyl–bridged and the directly coupled systems was provided. Of the arylethylenes, only the unsubstituted BPEBtd (Table 4.1, top line) exhibited an oxidation process. Furthermore, two reduction events occurred for the arylethynylenes, whereas only one was observed for the directly coupled species. The first reduction of the arylethynylene species was attributed to the quasi–reversible reduction of the benzothiadiazole ring, as it was also present in the non–acetylene–containing compounds' cyclic–voltammogram. The second reduction was assigned as an irreversible reduction of the acetylene bond. From comparison of E_{red}^{onset} values for the arylethynylene– derivatives it was also evident that inclusion of electron–withdrawing groups increased the reduction potential *i.e.* they facilitated reduction

To follow up, Dupont published a second paper [178] which illustrated arylethynyl-substituted benzothiadiazole compounds as fluorophores for 'light-up' DNA inter-

calating probes *i.e.* their absorption and emission intensities significantly increased upon detection of analyte. It was concluded from the results that the acetylene spacer provided necessary π–extended conjugation, facilitating intercalation with the DNA. Detection of DNA showed sensitivities on the 1 ppm levels, and resulted in red–shifts in absorption of up to 19 nm and fluorescence emission of 5 nm upon binding of the compound with DNA, with a significant increase in intensity for one particular derivative (see Figure 4.11). It was also evident that an electron donating moiety was required to provide intramolecular charge transfer to the benzothiadiazole group, affording appreciable detection of DNA by means of increased luminescence.

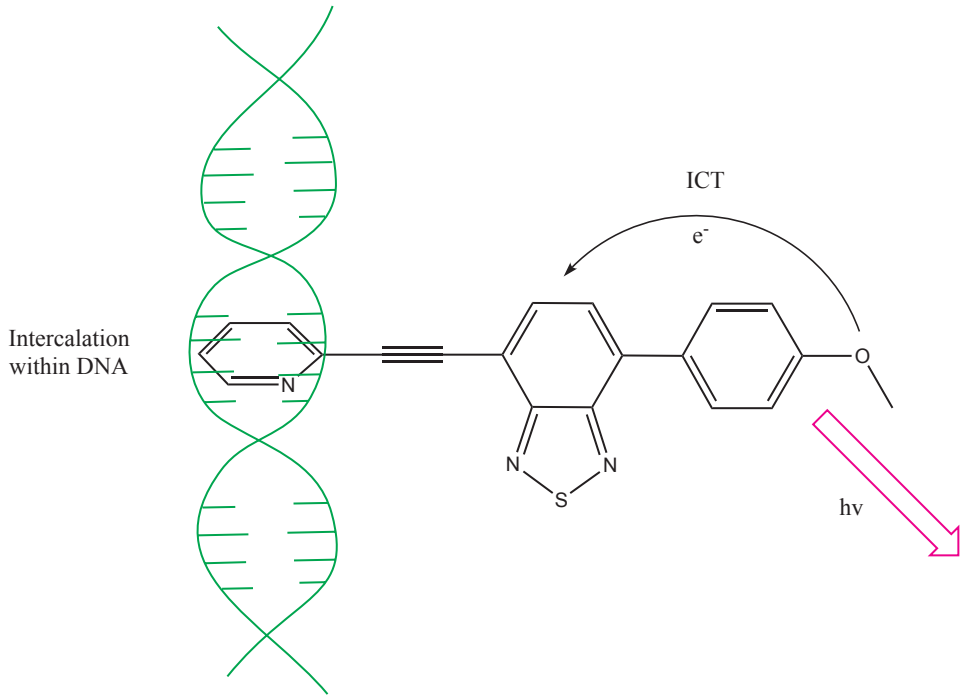

Figure 4.11: Dupont's DNA 'light-up' probe.

4.4 Synthesis of the arylethynyl diazoles discussed in this chapter

In this, and the following sections, the synthesis of the novel oxadiazole, benzofurazan and benzothiadiazole derivatives will be discussed. For a complete list of the arylethynylene materials prepared in this chapter, see Appendix A (on the included laminate).

4.4.1 Literature preparations of 1,3,4-oxadiazole containing compounds

The synthesis of oxadiazole–containing arylethynylenes is not possible by the standard cross coupling of arylacetylenes onto a dihalogenated oxadiazole core as there is no known literature preparation for 2,5-dibromo-1,3,4-oxadiazole. Oxadiazole–based compounds are prepared by two main synthetic strategies. These methods are oulined below and are exemplified by work by Schulz and Bryce. [84, 157, 187]

Silane–containing polymers have exhibited improved electrochemical properties due to σ—π conjugation of the phenyl rings with the silicon atom in the main chain, aiding electron transport. Schulz has described two methods of preparation of silicon-containing polyoxadiazole polymers. Their structure was designed to increase processability of the normally insoluble polyoxadiazole. Schulz's first method involved direct coupling of two dicarboxylic acids and hydrazine hydrate. These were heated together at 80 °C for 24 h in a mixture of methanesulphonic acid and P_2O_5, as illustrated in Figure 4.12. Schulz's second method involved the mixing of a di–acylchloride with a di–acylhydrazide in NMP and pyridine at 0 °C. This formed a polyhydrazide, which was subjected to chemical cyclodehydration, either perfomed by heating with polyphosphoric acid at 190 °C, or by stirring the polymer at 285 °C for 5 h, to yield the polyoxadiazole. Thermal cyclodehydration was also attempted, but yielded a brown polymer only soluble in concentrated sulfuric acid. The chemical cyclodehydration technique yielded a black polymer, soluble in NMP and DMF, with blue fluorescence observed in solution.

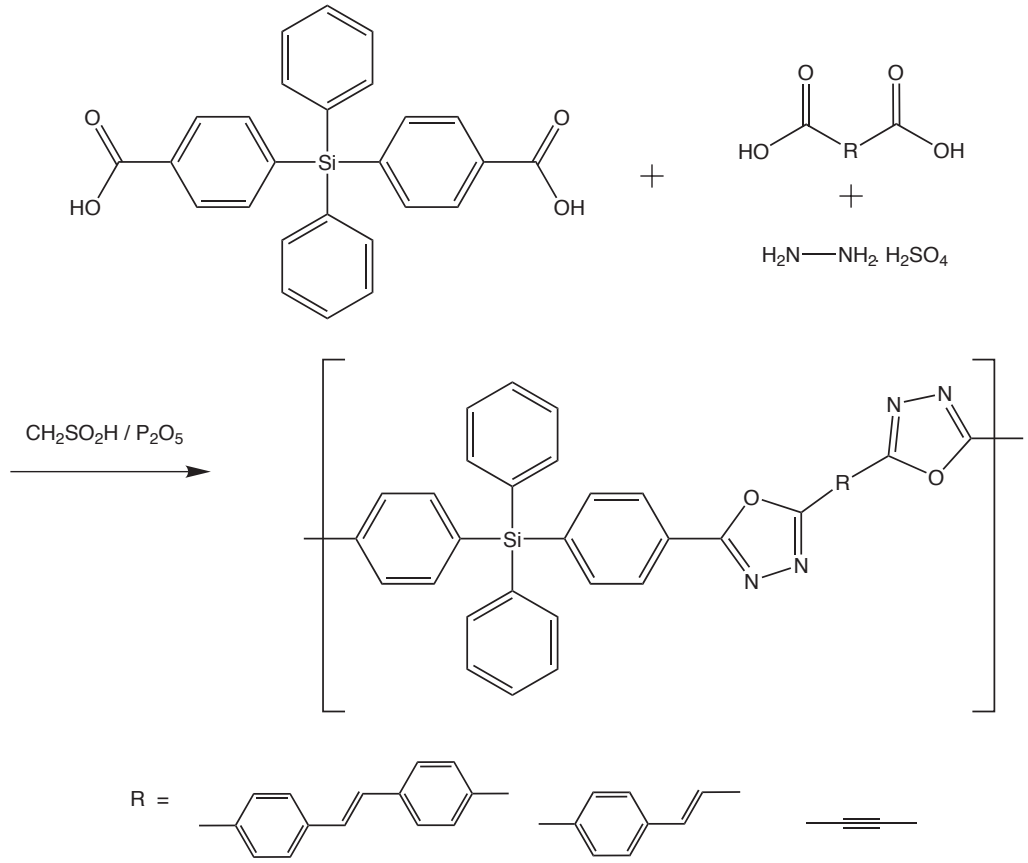

Figure 4.12: Polymer prepared by Schulz's first method. [187]

Bryce's synthetic route also involved the dehydration/cyclisation of the di–acylhydrazide. To synthesize 2-phenyl-5-pyridyl-1,3,4-oxadiazole (Figure 4.13), [84] a carboxylic acid was reacted with thionyl chloride to generate the acyl chloride. This was reacted with the *para*–substituted benzoic acid hydrazide, to form a dihydrazide intermediate. This was then immediately subjected to a dehydration/cyclisation in phosphorous oxychloride at reflux, and the oxadiazole ring was formed.

Bryce used the same method and reagents (the relevant di–acylhydrazide in $POCl_3$ at reflux) for the dehydration/cyclisation step to form the oxadiazole–containing compounds in recent publications, [85, 146] the latter of which involved incorporation of an acetylene moiety substituted *para* on the phenyl ring directly bonded to the oxadiazole. Acetylene–derivatization has been shown to be possible with oxadiazoles by Schulz (Figure 4.12), and Bryce and co-workers have demonstrated Sonogashira cross–couplings with oxadiazole–containing molecules.

As discussed earlier, preparation of 2,5-bis(phenylethynyl)-1,3,4-thiadiazole (**BP-**

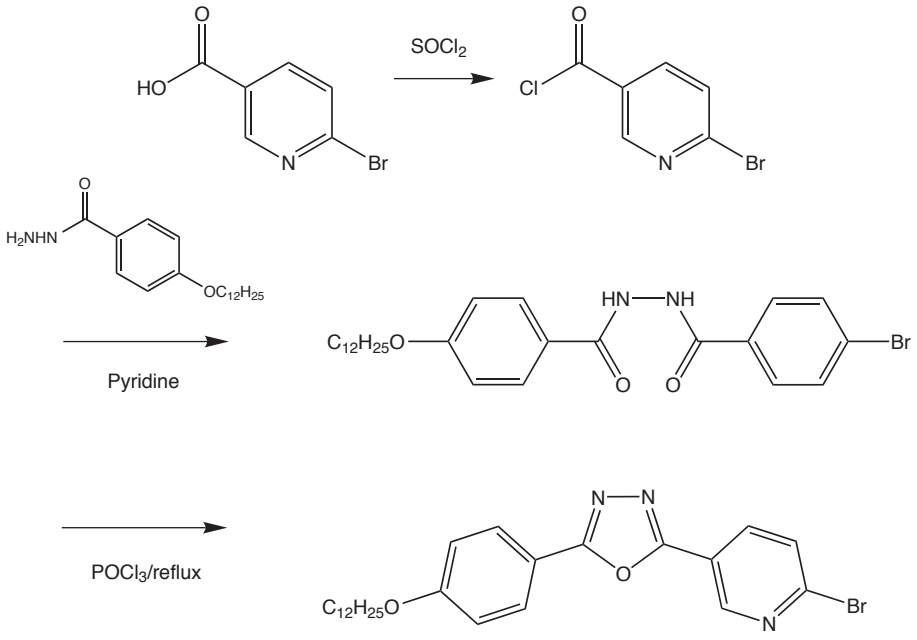

Figure 4.13: Synthetic route to 2-phenyl-5-pyridyl-1,3,4-oxadiazole reported by Bryce and co-workers. [84]

ETd) has been reported by Yasuda *et al.* [112] They isolated 2,5-dibromo-1,3,4-thiadiazole [159] and cross coupled it with phenylacetylene under Sonogashira conditions, forming **BPETd**. This route is not available to the oxygen-containing analogue.

Katritzky *et al.* have published the relatively facile preparation of several 2,5-disubstituted 1,3,4-oxadiazoles, achieving yields in excess of 60 %. [188] In the article it is stated that high yields are hard to achieve when oxadiazoles are prepared from carboxylic acids in which the carbonyl is conjugated with π–functionality to a substituent, or is appended with a nucleophilic group. Calling on some of their earlier work, [189] the advantage of converting the carboxylic acid to an activated derivative, N-acylbenzotriazole, is demonstrated. The substituted acylbenzotriazole was reacted with the appropriate hydrazide, forming the target oxadiazole in high yields. As illustrated in Figure 4.14 they have prepared 2-phenyl-5-phenylethynyl-1,3,4-oxadiazole using this method, achieving a 73 % yield. This involved use of a compound from their earlier paper, 1-benzotriazol-1-yl-3-phenylpropynone, which afforded inclusion of the acetylene moiety.

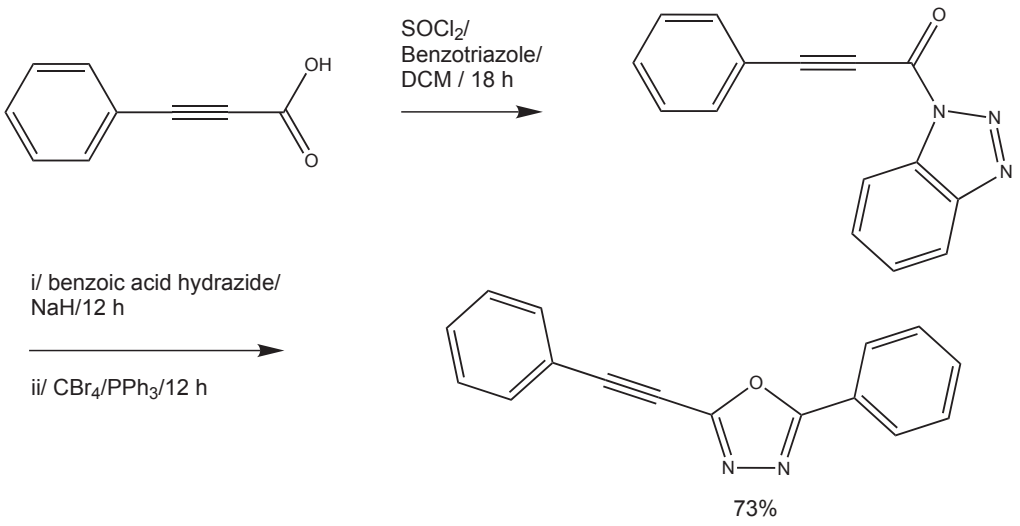

Figure 4.14: Katritzky's route to 2-phenyl-5-phenylethynyl-1,3,4-oxadiazole. [188, 189]

Discussion of the synthesis of 2,5-bis(phenylethynyl)-1,3,4-oxadiazole

In the work presented here, Katritzky's method has been adapted for preparation of the desired product 2,5-bis(phenylethynyl)-1,3,4-oxadiazole, **BPEOx**. The bis–acetylene nature of **BPEOx** necessitated synthesis of phenyl propynoic hydrazide. This was prepared by reaction of phenylpropynoic acid ethyl ester with hydrazine. The ester was prepared from the commercially available phenylpropynoic acid by acid–catalysed esterification, heating phenylpropynoic acid in ethanol at reflux for 3 h, with a catalytic quantity of concentrated hydrochloric acid. An oil was isolated in 90 % yield, confirmed as the desired product (^{1}H NMR spectrometry and GC MS) and subsequently reacted with hydrazine in solution at 0 °C. The low temperature was essential for this step to prevent the hydrazide from cyclising to form a pyralozone. [190] Precautions were taken during the work–up, ensuring minimal heating during the solvent removal. Phenylethynyl acylhydrazide was isolated as a cream solid (77 %), and its identity confirmed by ^{1}H NMR spectroscopy and mass spectrometry. The benzotriazole derivative was prepared in accordance with Katritzky's method, in good yields. Complete assignment of the ^{1}H and ^{13}C NMR spectra obtained for this product confirmed its identity, along with mass spectrometry analysis. The subsequent reaction with the hydrazide, generated earlier, was

also performed following Katritzky's method. The target compound **BPEOx** was isolated as a white solid in very low yield (4 % yield, Figure 4.15), and its identity confirmed by ^{1}H and ^{13}C NMR and accurate mass spectrometry. There was insufficient sample for CHN analysis, and the product did not form crystals of sufficiently high quality to afford X-ray crystallographic structure analysis. The low yield is disappointing considering the yields achieved by Katritzky for related compounds. Analysis by TLC indicated a large quantity of hydrazide went unreacted, suggesting that the alkynyl group has reduced the reactivity of the hydrazide.

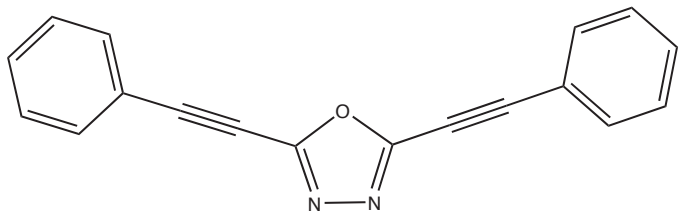

Figure 4.15: 2,5-bis(Phenylethynyl)-1,3,4-oxadiazole, **BPEOx**.

4.4.2 Synthesis of brominated benzofurazan and benzothiadiazole

Literature preparations of bromobenzofurazan

Retrosynthetic analysis (Figure 4.16) on the desired [**BPEBf.R**] products, where R represents substitution on the phenyl ring *para* to the ethynyl bridge, shows that the simplest route involves the reaction of arylacetylenes with 4,7-dibromobenzofurazan. Recent literature by Leclerc has provided a simple synthetic strategy to this compound, [177] made even simpler by the commercial availability of benzofurazan.

Swager and Bouffard reported another route which allowed preparation of substituted derivatives such as 5,6-dialkoxy-4,7-dibromobenzofurazan, starting from 1,2-dialkoxy-4,5-dinitrobenzene. After boiling in toluene with sodium azide in the presence of n-Bu_4NBr, the intermediate was cyclised by the subsequent addition of triphenylphosphine. Bromination by elemental bromine in DCM and acetic acid generated the desired product.

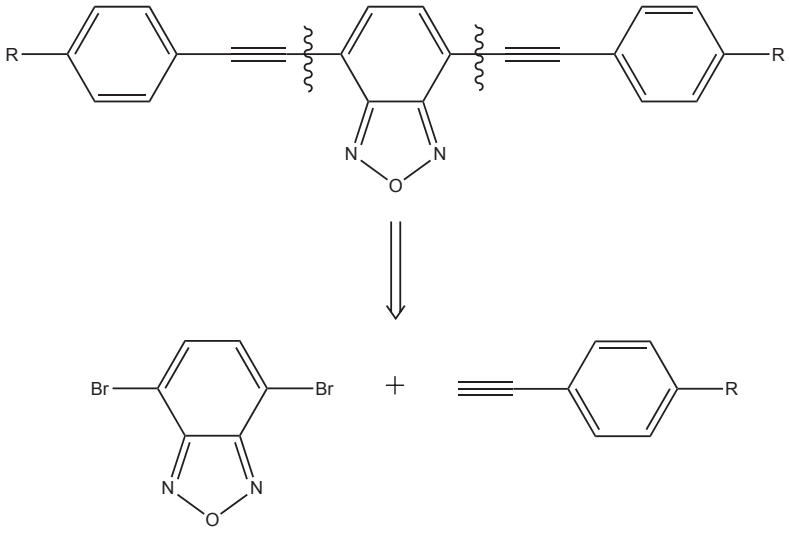

Figure 4.16: Retrosynthesis of 4,7-bis(arylethynyl)benzofurazan.

Discussion of the synthesis of 4,7-dibromobenzofurazan

4,7-Dibromobenzofurazan was prepared following Leclerc's method, which required heating of benzofurazan with iron powder, followed by the slow addition of elemental bromine at 90 °C (see Figure 4.17). This allowed isolation of 4,7-dibromobenzofurazan as a cream solid, in good yield (78 %).

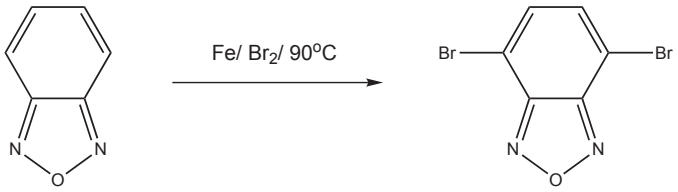

Figure 4.17: Synthesis of 4,7-bis(phenylethynyl)benzofurazan from commercially available starting materials.

Discussion of the synthesis of 4-bromobenzofurazan

Formation of several novel, singularly substituted, products (**PEBf**, **PEBf.NH$_2$** and **BBfEB**) required preparation of 4-bromobenzofurazan. The synthetic route followed for this was based on the original preparation of NBD as described by Ghosh *et al.*, [160, 191] but the actual procedure is adapted from the method of Salvati *et al.* [192]

Commercially available 2,6-dibromoaniline was oxidised by treatment with an excess of *m*-CPBA, to form 1,3-dibromo-2-nitrobenzene. This was reacted without isolation with a slight excess of sodium azide in DMSO, affording closure of the ring and formation of 4-bromobenzofurazan, as a brown solid, obtained in good yield (87 %).

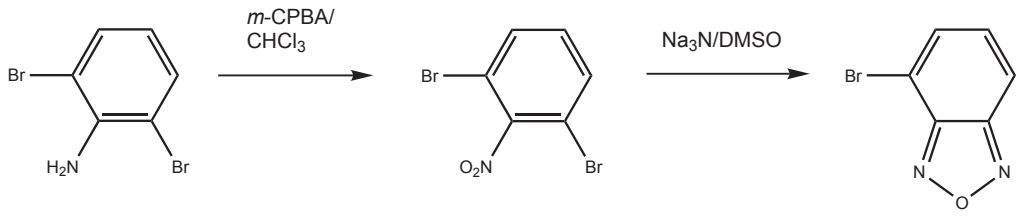

Figure 4.18: Synthetic route to 4-bromobenzofurazan from Salvati *et al.* [192]

Preparation of benzothiadiazole

To allow for a thorough and fair comparison to be made of the photophysical and electrochemical properties of arylethynyl–substituted benzofurazans and benzothiadiazoles, under electron withdrawing and donating conditions, a series of bis–arylethynyl substituted benzothiadiazoles have been prepared, which necessitated the synthesis of 4,7-dibromobenzothiadiazole.

Swager and Bouffard reported a method for the synthesis of this moiety, allowing substitution with alkyoxy groups at the *5* and *6* positions. They treated 1,2-dialkoxy-4,5-dinitrobenzene with tin(II) chloride in refluxing ethanol and hydrochloric acid to reduced the nitro groups, and then closed the ring with *N*-thionylaniline. Bromination of the alkyl–substituted benzothiadiazole was achieved using the same method employed for the benzofurazan analogue (see above).

Discussion of the synthesis of 4,7-dibromobenzothiadiazole

A different route to Swager's, described by Dupont and co-workers in recent literature (see Figure 4.19), was followed for the synthesis of 4,7-dibromobenzofurazan. [184, 193, 194] Commercially available *o*-phenylenediamine was treated with thionyl chloride and heated at reflux for three hours in DCM and triethylamine. Benzoth-

iadiazole was isolated as an orange solid and immediately taken into 48 % hydrobromic acid and heated at reflux, with the slow addition of elemental bromine. 4,7-Dibromobenzothiadiazole was isolated as a light brown solid in good yield (90 %). Product identity was confirmed by ^{1}H NMR spectroscopy and GC MS, which showed isotopic abundances indicative of a dibrominated species.

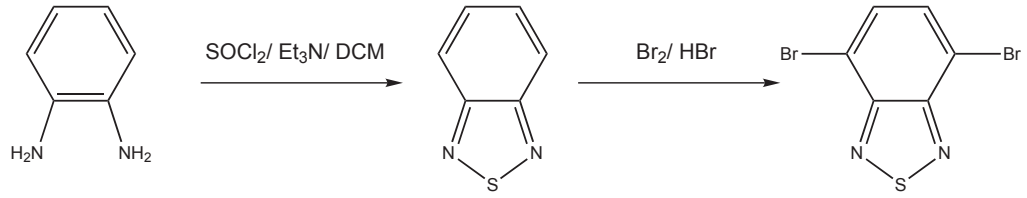

Figure 4.19: Route to various 4,7-bis(arylethynyl)-benzothiadiazole derivatives, as described by Dupont and co-workers. [184, 193]

4.4.3 Discussion of the synthesis of the novel 4,7-bis(arylethynyl)benzofurazans

Palladium catalysed cross–coupling of the bromoheteroarenes with various arylacetylenes under Sonogashira conditions readily yielded the desired end products. The electron–deficient nature of the heteroarenes ensured that these reactions were relatively facile and fast.

Cross couplings of 4,7-dibromobenzofurazan with phenylacetylene yielded **BPEBf**, with *tert*-butylphenylacetylene yielded **BPEBf.tBu**, with 4-ethynylanisole yielded **BPEBf.OMe**, with 4-ethynylaniline yielded **BPEBf.NH$_2$**, with 4-ethynylmethylbenzoate yielded **BPEBf.CO$_2$Me**, with 4-ethynylbenzonitrile yielded **BPEBf.CN**, and with 4-nitrophenylacetylene yielded **BPEBf.NO$_2$**. They were all prepared following the same method, and yields varied from 12 % to 67 % after purification.

The Sonogashira couplings were carried out using a mixture of THF/Et$_3$N as the solvent to ensure solubility, and employed tetrakis palladium triphenylphosphine and copper iodide at five mol% quantities. Typically the reactions were stirred at 65 °C for 48 h, and monitored by TLC analysis. In every case apart from the cyano– and nitro–containing derivatives, a large quantity of precipitate (Et$_3$N.HBr) was

observed after 6–12 h, and the suspension was highly fluorescent when viewed under illumination with a long–wave (365 nm) UV lamp.

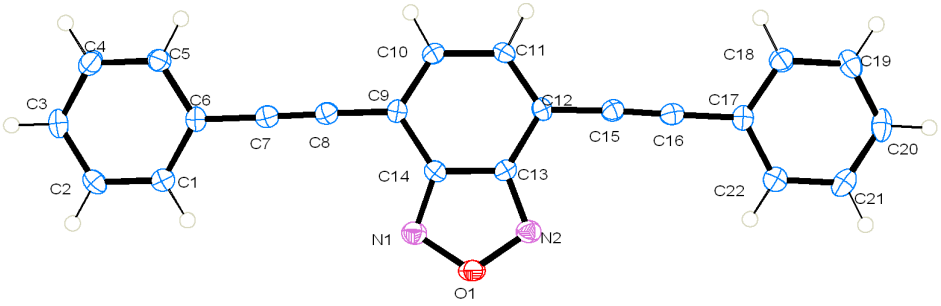

(a) **BPEBf**; face–view

(b) **BPEBf**; in plane

(c) **BPEBf**; out of plane

Figure 4.20: **BPEBf** molecular structure as determined by X–ray crystallographic analysis.

Initial purification of the crude suspension was by eluting through a silica gel plug with ether or DCM. Further purification was achieved by column chromatography with gradient elution and dry–loaded compound. This method proved adequate for separation and was used in isolation of pure samples of **BPEBf** and **BPEBf.NH$_2$**. The yellow solid isolated as product **BPEBf** was recrystallised from hot ethanol, allowing structure determination by X–ray crystallography (see Figure 4.20). **BPEBf.NH$_2$** could not be recrystallised and remained as a very dark red powder.

Excluding the cyano– and nitro–containing derivatives, the other **BPEBf.R** compounds were isolated by crystallisation from a solvent; **BPEBf.tBu** and **BPEBf.OMe** precipitated out of hot ether over night, as yellow plate-like crystals and an orange solid respectively. A sample of the orange solid **BPEBf.OMe** was recrystallised out of warmed DCM/cyclohexane, forming crystals of sufficient quality to afford X-ray crystallographic structure determination (see Figure 4.21). **BPEBf.CO$_2$Me** was isolated in a similar fashion to **BPEBf.tBu**, although as a luminous yellow/green solid and with DCM instead of ether.

The ^{1}H NMR spectra of **BPEBf**, **BPEBf.OMe** and **BPEBf.CO$_2$Me** are pre-

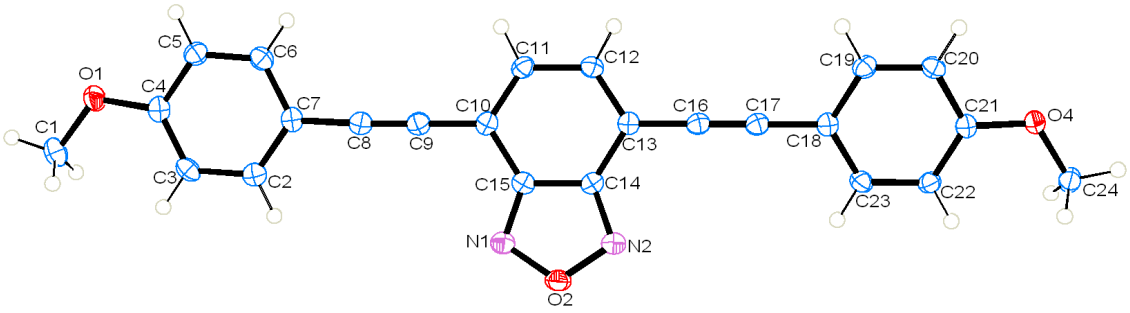

(a) **BPEBf.OMe**; face–view.

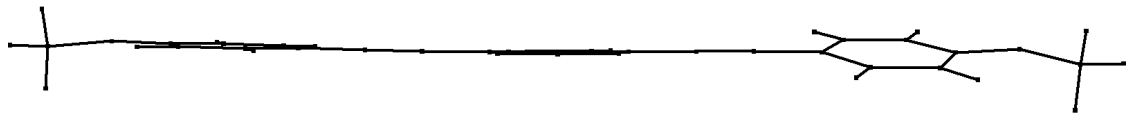

(b) **BPEBf.OMe**; in plane.

Figure 4.21: **BPEBf.OMe** molecular structure as determined by X–ray crystallographic analysis.

sented in Figure 4.22. The aromatic region shows the effect of the phenyl–group substituent on the aromatic protons. The electron withdrawing ester clearly acts to deshield the aromatic rings and the effect is still evident on the benzofurazan moiety. Likewise, the electron–donating methoxy groups shield the phenyl protons, shifting the pair closest to the *2*-H $\sim$ 1.16 ppm, relative to the equivalent protons on the ester derivative. The shifts for the protons of **BPEBf** are central relative to their equivalents.

The cyano– and nitro–containing derivatives, **BPEBf.CN** and **BPEBf.NO$_2$**, only produced a very small quantity of precipitate during the cross coupling reaction. During preparation of the cyano–derivative, analysis of the reaction mixture by TLC indicated that all the starting material had reacted after 48 h, but attempts to extract and purify the product yielded only 12 % of **BPEBf.CN** as a yellow powder, which was insoluble in all common solvents. ^{1}H NMR spectroscopy was attempted on a saturated solution of the compound in hot DMSO although there were no discernible peaks to aid characterisation. Accurate mass spectrometry (ASAP+) confirmed the presence of the desired product, although purity could not be confirmed. Determination of its photophysics in the solution state was impossible due to questionable purity and insolubility in available solvents. The nitro–derivative was similarly elusive. Its solubility could not be ascertained as it was never successfully

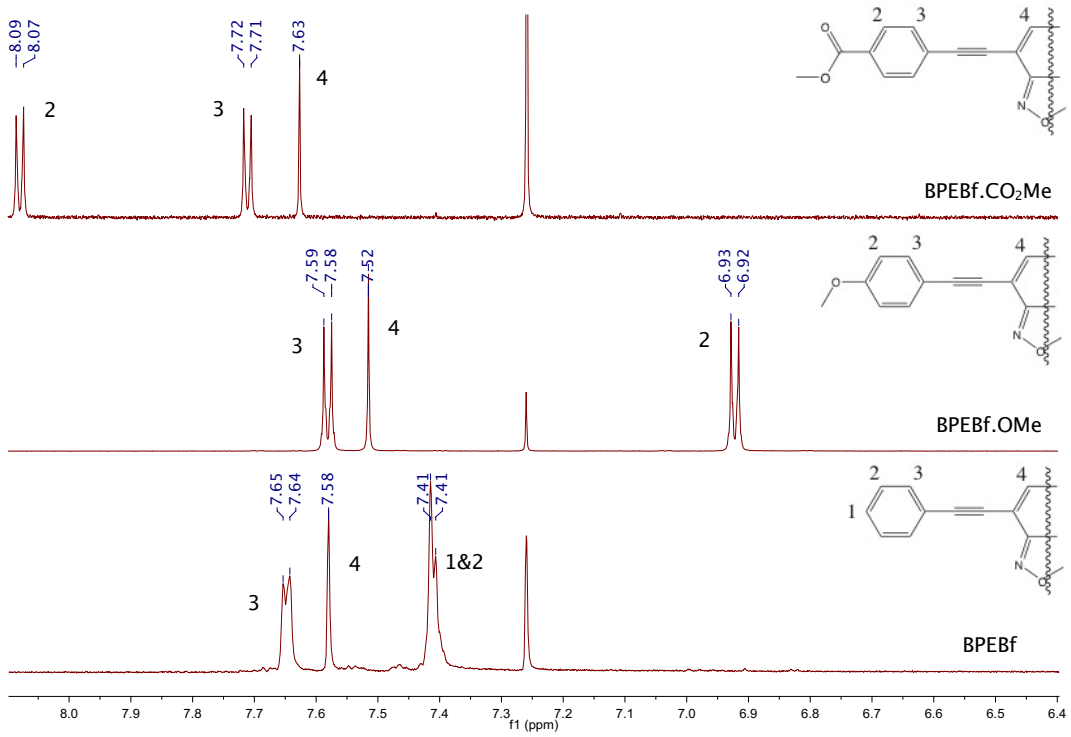

Figure 4.22: 700 MHz ^{1}H NMR spectra in $CDCl_3$ of **BPEBf.R**, illustrating the effect of the electron withdrawing–groups and electron–donating groups on the shift of the aromatic protons.

purified, although nitro-derivatives of compounds of this nature are usually highly insoluble. A crude sample was analysed by accurate mass spectrometry (ASAP+), revealing the desired product had been synthesised. It can be argued that the highly electron–withdrawing nature of these arylacetylenes necessitates use of a stronger catalyst *e.g.* $PdCl_2(PPh_3)_2$, heating, or longer reaction times.

Sonogashira cross–coupling of the monobrominated benzofurazan with various acetylenes afforded three novel compounds: 4-(phenylethynyl)-benzofurazan, **PEBf**, 4-(4-ethynylaniline)-benzofurazan, **PEBf.NH$_2$**, and 1,4-bis(4-ethynylbenzofurazan)-benzene, **BBfEB**.

These compounds were prepared using the same methods as for the di-substituted systems discussed above, although yields were generally lower. Precipitation of a luminescent solid during the reaction was observed for all of the reactions. During the work–up of **PEBf**, a faintly orange solid was obtained after column chromatography, but analysis by ^{1}H NMR spectroscopy revealed that the sample was impure.

The sample was analysed by accurate mass spectrometry (ASAP+) which confirmed presence of the desired product. Further purification of the sample was performed, affording **PEBf** as a yellow solid, confirmed by ^{1}H and ^{13}C NMR.

Synthesis of **PEBf.NH$_2$** produced a brown solid, after purification through a silica gel plug (ether eluent). This was taken into hot cyclohexane and hot–filtration performed. The filtrate was allowed to cool and dark red solid precipitated, along with some long, needle-like, crystals (total yield $\sim$ 30 %). A crystal was selected allowing X–ray crystallographic structure determination (Figure 4.23). ^{1}H and ^{13}C NMR spectroscopy and accurate mass spectrometry (ASAP+) confirmed isolation of the desired product.

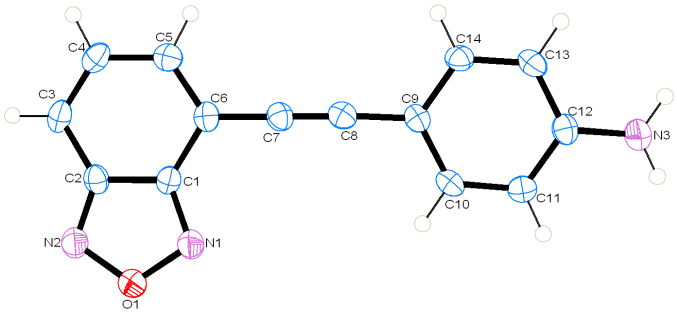

(a) **PEBf.NH$_2$**; face–view.

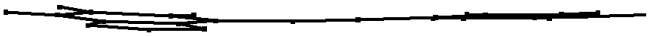

(b) **PEBf.NH$_2$**; in plane.

Figure 4.23: **PEBf.NH$_2$** molecular structure as determined by X-ray crystallographic analysis.

BBfEB was isolated in a similar manner to that of **PEBf.NH$_2$**, although on dissolving in hot cyclohexane, only a very fine yellow powder precipitated in fair yields (55 %). Additional attempts at recrystallising from ether and DCM yielded very fine yellow crystals, but these were ultimately unsuitable for X–ray crystallography.

4.4.4 Discussion of the synthesis of novel 4,7-bis(arylethynyl)-benzothiadiazoles

Several analogous arylethynylene systems containing benzothiadiazole as the central heteroarene have been prepared in good yields. This was achieved by cross–

coupling of 4,7-dibromobenzothiadiazole with phenylacetylene yielding **BPEBtd** (previously reported in the literature [184]), with *tert*-butylphenylacetylene yielding **BPEBtd.tBu**, with 4-ethynylaniline yielding **BPEBtd.NH$_2$** and with 4-ethynylmethylbenzoate yielding **BPEBtd.CO$_2$Me**. These Sonogashira couplings were carried out using a similiar method to that described above for the benzofurazan systems (see section 4.4.3, page 143). Work–up and purification procedures were also similar to those described above for the benzofurazan systems.

Column chromatography was performed on **BPEBtd** using gradient elution (ether/DCM), affording the product as a dark orange powder (62 %). This was recrystallised from hot ethanol, producing very short, needle–like, crystals. Structure determination by X–ray crystallography was not attempted as this has already been reported by Vieira *et al.* [185]

BPEBtd.tBu was isolated similarly, from column chromatography performed with gradient elution. The product was isolated as a bright orange solid (70 %).

BPEBtd.NH$_2$ was isolated as a bright red, fluffy/light solid (31 %) by precipitation from hot ether with the slow addition of cold hexane.

The ester derivative **BPEBtd.CO$_2$Me** was chromatographed on silica gel, with a gradient elution of hexane and ether. As the polarity was increased to 3:2 ether/hexane a highly luminescent orange solution was observed, and upon reduction *in vacuo* yielded the product as a light orange solid (47 %).

All systems have been characterised using ^{1}H and ^{13}C NMR spectroscopy, melting point determination and accurate mass spectrometry.

Several systems featuring this motif have been reported in the literature previously, including BPEBtd (also prepared for this work), BPEBtd.NMe$_2$, BPEBtd.OMe and a pyridine–substituted system, BPyEBtd. [182, 184, 185]

4.5 Structural observations and comparisons

4.5.1 Calculated and observed structural comparisons of the novel benzofurazan arylethynylenes

From the data in Table 4.2 it can be seen that the N—S bond in benzothiadiazole is significantly longer ($\sim$ 0.2 Å) than the N—O bonds in the benzofurazan derivatives. This is attributed to the increased size of sulfur, and this increase in bond length is also observed for the C—N (B) and C—C (C) bonds.

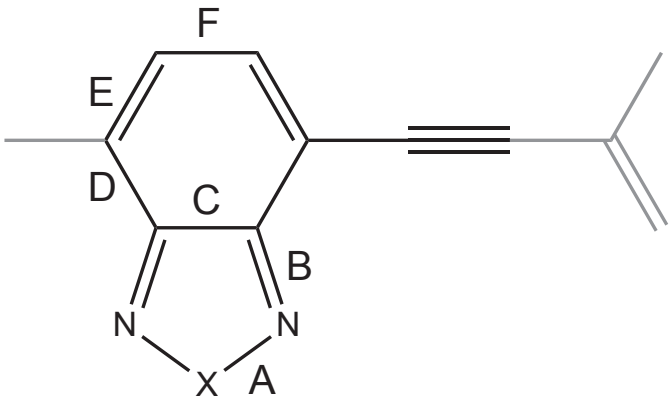

Figure 4.24: Selected bonds in benzofurazan and benzothiadiazole derivatives.

	Mean bond lengths / Å Observed (ESD) Å/Calculated					
	A	**B**	**C**	**D**	**E**	**F**
BPEBf	1.387(1) 1.368	1.316(2) 1.320	1.411(2) 1.435	1.438(2) 1.440	1.372(2) 1.388	1.424(2) 1.421
BPEBtd*	1.609(2) 1.645	1.345(3) 1.355	1.430(3) 1.451	1.429(4) 1.441	1.374(3) 1.390	1.411(3) 1.415
BPEBf.OMe	1.382(1) 1.369	1.311(2) 1.320	1.425(2) 1.435	1.440(2) 1.441	1.374(2) 1.389	1.424(2) 1.420
PEBf.NH$_2$	1.386(2) 1.370	1.315(2) 1.323	1.430(2) 1.437	1.424(3)/ 1.438(2)♣ 1.425	1.354(3)/ 1.370(2)♣ 1.371	1.423(2) 1.431

* = from Vieira *et al.* [185]

Table 4.2: Mean bond lengths (Å) of selected benzofurazan and benzothiadiazole derivatives (see Figure 4.24) from X–ray structure determination, and DFT structure optimisation calculations (B3LYP functional and 6-31G(d) basis set).

All of the observed lengths are quoted as the average of the two equivalent bonds for a system (*e.g.* the label **B** applies to *both* C—N bonds), due to the error associated with the measured bond length. In the unsymmetrical system **PEBf.NH$_2$** the difference between the two C—C bonds at **D** and double C—C bonds at position **E** can not be ignored (see ♣ in Table 4.2), as it is greater than the error. On the side of benzofurazan substituted with the ethynlene moiety, **D** and **E** are longer than on the unsubstituted side (see Figure 4.25). This attributed to the electron–donating amine.

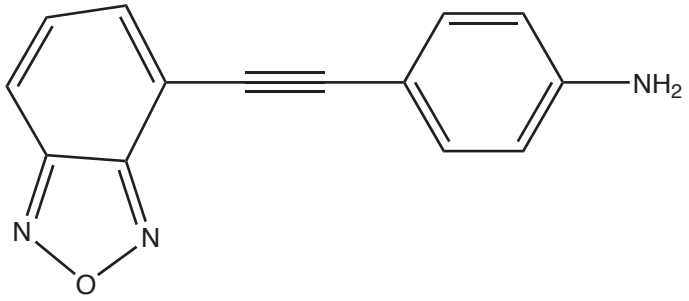

Figure 4.25: The observed distortion of **PEBf.NH$_2$**.

As the molecular structure images in the previous section illustrated, the ring systems in the benzofurazan systems are coplanar. **BPEBf** has torsional angles between the rings of ~ 2 °. In **BPEBf.OMe** the angle between the plane of the right hand phenyl ring and the central group is 13 °. The left side ring is twisted by only 2 ° to the benzofurazan group. The angle between the phenyl ring and benzofurazan moiety in **PEBf.NH$_2$** is just 3 °.

Packing in the crystals of **BPEBf** (shown in Figure 4.26a) (and **BPEBf.OMe**, not shown) show an inversion between layers in the same orientation, as well as layers perpendicular (86 °) to each other. This is different to that in **PEBf.NH$_2$** (Figure 4.26b), which indicates that all layers are coplanar, but there is an almost perpendicular rotation of the molecule between adjacent layers. In each case there appears to be a high-degree of π—π stacking, suggested by the positioning of the aromatic groups.

Comparison of these bond lengths of these crystal structures with those of optimised structures obtained from DFT calculations (6-31G(d)/B3LYP level of theory) show excellent ($\pm$ 1.1 %) agreement with actual bond lengths and co–planar systems

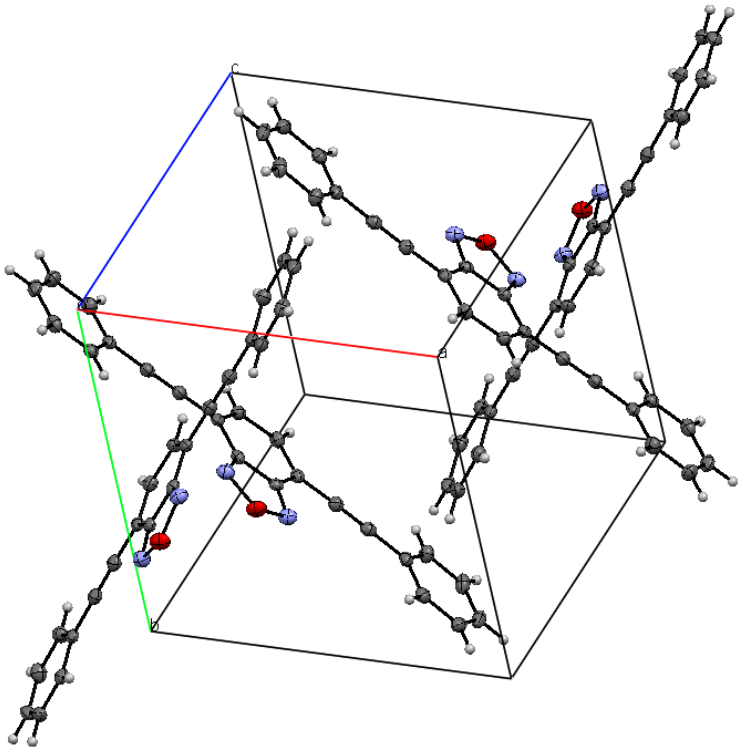

(a) **BPEBf**

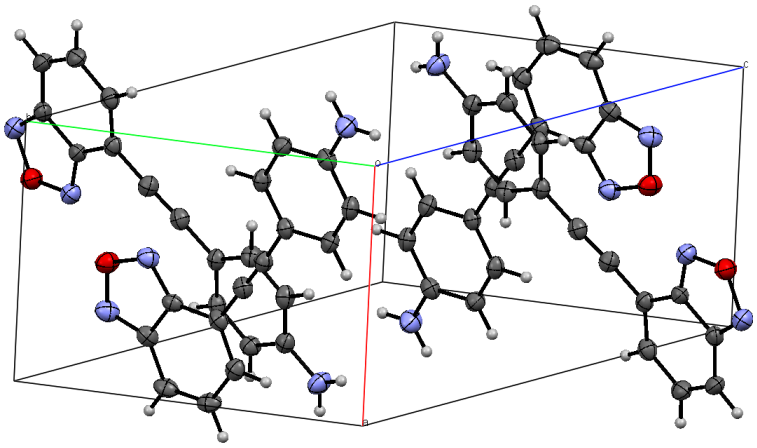

(b) **PEBf.NH$_2$**

Figure 4.26: Crystal packing of the benzofurazan arylethynylenes.

were predicted as the lowest energy conformation. Distortions from planarity are most likely to be packing effects in the crystal.

4.5.2 Observed and predicted Raman spectra of the arylethynylene diazoles

As discussed earlier (see section 3.4.4, page 93) theoretical Raman spectra have been obtained by performing DFT frequency calculations on the optimised structures of the compounds discussed in this chapter. These have been compared with observed Raman spectra for stretching frequency analysis, aiding characterisation.

The observed and calculated Raman spectra show excellent agreement (see Figure 4.27) after applying a correction factor of 0.96 (typical for DFT calculations at this level of theory [114]). This has allowed assignment of several bands (see Table 4.3). For the asymmetrical system **PEBf.NH$_2$** the prediction is less accurate, which is attributed to the use of the B3LYP functional on a system which will experience enhanced charge transfer effects.

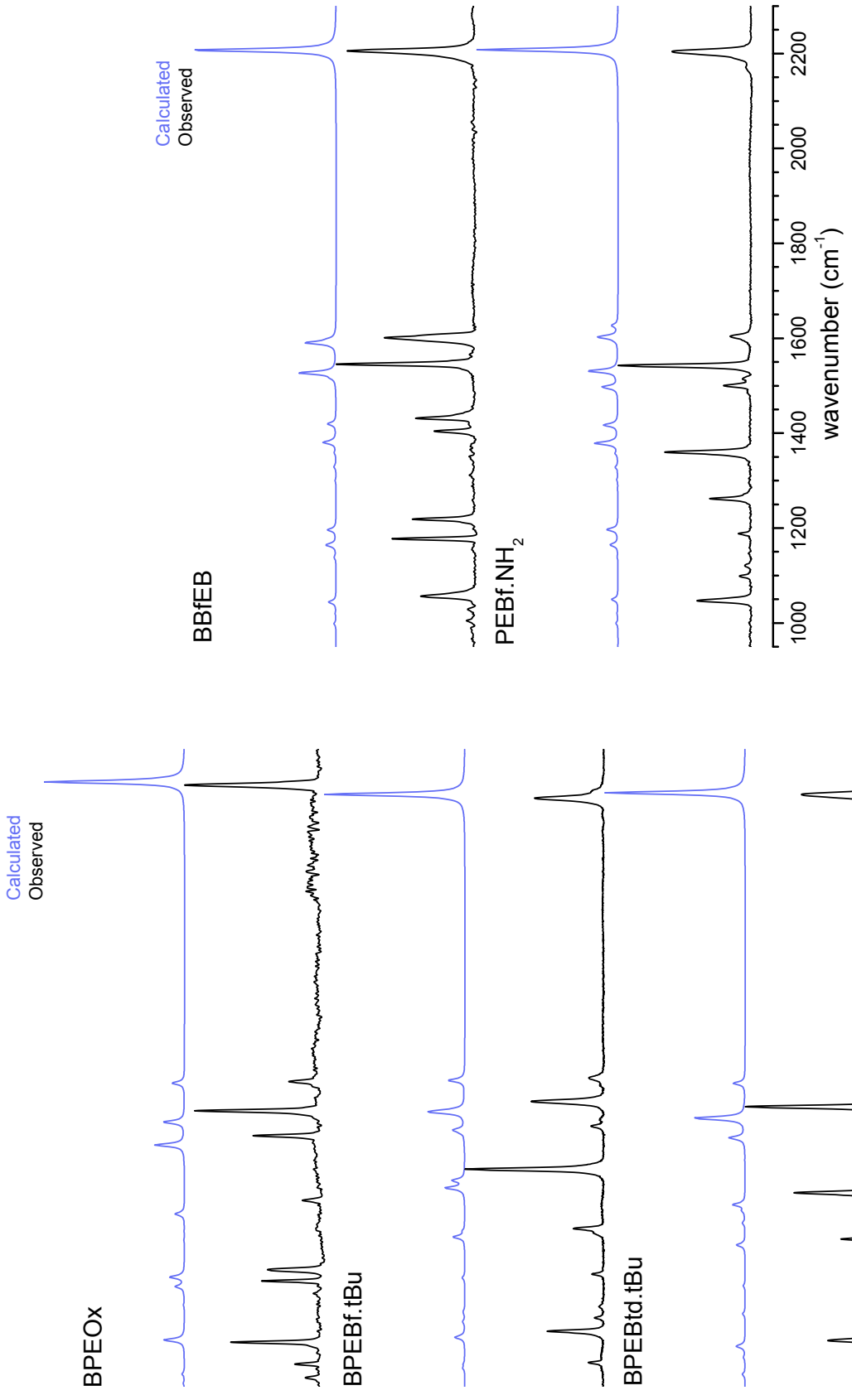

Figure 4.27: Observed and calculated Raman spectra for selected compounds.

Compound	Stretch/cm^{-1} (description)									
BPEOx	**1043** 1048 *N—N* stretch	**1173** 1162 *Ph C—H* *wag*	**1197** 1181 *C—C* *stretch*	**1481** 1461 *C—N* *stretch*	**1534** 1571 *C—N/C=C* *stretch*	**1596** 1592 *Ph C—C* *stretch*	**2224** 2231 *acetylene* *stretch*			
BPEBf.R	**1066** 1065 *Bf* C—H *wag*	**1284** 1278 *Ph* C—H *wag*	- 1385 *benzofurazan* *stretches*	**1410** 1400	**1501** 1507	**1554** 1548 *phenyl* *stretches*	**1603** 1614	**2197** 2229 *acetylene* *stretch*		
BPEBtd.R	**1047** 1044 *Btd* C—H *wag*	**1262** 1265 *Ph* C—H *wag*	**1360** 1348 *Btd* *stretch*	**1501** 1505	**1542** 1536 *phenyl* *stretches*	**1603** 1614	**2204** 2229 *acetylene* *stretch*			
PEBf.NH$_2$	**1059** 1093 *Bf* C—H *wag*	**1180** 1178 *Ph* C—H *wag*	**1216** 1209 C—H *wag*	**1404** 1393	**1432** 1432 *benzofurazan stretch* * *phenyl* C—H *wag*	**1514*** 1513*	**1550** 1546	**1606** 1620 *aniline* *wag*	- 1643 NH_2 *wag*	**2198** 2231 *acetylene* *stretch*
BBfEB	**1056** 1055 *whole molecule* *stretch*	**1178** 1177 *Ph* C—H *wag*	**1218** 1209 *Bf* C—H *wag*	**1404** 1395	**1431** 1435 *benzofurazan* *stretches*	**1545** 1543	**1601** 1607 *phenyl* *stretch*	**2206** 2239 *acetylene* *stretch*		

Bold = observed stretching frequency
Normal font = theoretical stretching frequency according to DFT frequency calculation (B3LYP/6-31G*)
Italicised = stretching description

Table 4.3: Observed and calculated Raman stretches for the arylethynylenes containing oxadiazole, benzofurazan and benzothiadiazole.

4.6 Excited state properties of the arylethynylene diazoles

4.6.1 Introduction

Photophysical measurements have been made on the various oxadiazole, benzofurazan and benzothiadiazole–containing compounds, both at room temperature and in 77 K rigid organic glasses. These data have afforded the determination of absorption, excitation and emission maxima, molar extinction coefficients, fluorescence quantum yields and fluorescence lifetimes. As discussed previously the use of the solvent EPA, which forms a transparent glass at 77 K, has allowed determination of the absorption and fluorescence spectra at low temperature. This is particularly useful for these compounds as it allows the quenching of rotational iosomers to the the lowest energy form. Thus samples at room temperature exhibit a broadening of lines due to an averaging of all rotamers present in solution. All room temperature photophysical measurements were obtained in toluene, unless stated otherwise.

Due to the potential electrochemically–active nature of oxadiazole and its derivatives, electrochemical measurements have been performed on several of the systems prepared here. This has allowed the investigation of many of the benzofurazan derivatives' oxidation and reduction potentials, and selected benzofurazan–containing arylethynylenes have been studied further using spectroelectrochemical methods.

Together with TD-DFT calculations (B3LYP functional and 6-31G(d) basis set [47]), photophysical and electrochemical observations have been rationalised and used to understand the excited state properties of the prepared systems.

4.6.2 Photophysical analysis of the novel unsubstituted phenylethynyldiazoles

Figure 4.28 shows the combined absorption, excitation and emission spectra for **BPEOx**, **BPEBf**, **BBfEB**, **PEBf** and **BPEBtd**, taken in toluene. They are arranged in decreasing energy, from top to bottom, and coloured to affect this distinc-

tion. There is excellent agreement between the absorption and excitation spectral profile of all compounds, indicating the purity of the sample, *i.e.* that the absorption species is that responsible for emission. The most notable observation in the absorption and excitation spectra of the benzofurazan and benzothiadiazole–containing materials is the presence of two distinct bands separated by $\sim$ 100 nm. In several cases the high energy band is the most intense, although, as expected from Kasha's rule, the emission profile only features one main band, mirroring the lower energy absorption band. When the higher energy band is excited internal conversion leads to the lower emissive excited state being populated, from which fluorescence is observed. Only the emission spectrum of **BPEOx** features any vibronic fine structure, although the emission spectrum of **BBfEB** features a shoulder red-shifted of the emission maximum. Table 4.4 details pertinent photophysical properties of these systems.

2,5-bis(Phenylethynyl)-1,3,4-oxadiazole, BPEOx

The excitation and emission profiles of **BPEOx** feature the λ_{max} at 303 nm and 357 nm respectively. The absorption and excitation profiles show evidence of shoulders which are attributed to vibrational fine–structure. The emission profile also features some resolved vibronic structure. At low temperature both the absorption and emission spectra exhibit enhanced vibronic fine structure (see Figure 4.29 and Table 4.5).

The low temperature excitation spectrum displays the increase in absorbance at the red–edge of the band due to increased population of the lower energy, planar conformations. The spectral features have sharpened relative to the room temperature spectra, revealing shoulders as pronounced bands. In the absorption spectrum these correspond to energies of approximately 1060 cm^{-1}, which are consistent with the vibrational wavenumber of the symmetrical N—N stretch of oxadiazole. The observed Raman spectrum of **BPEOx** (Figure 4.27, page 153) shows a strong band at 1044 cm^{-1} which equates to this A_1 symmetrical stretching mode.

TD-DFT calculations indicate that the $S_1 \leftarrow S_0$ electronic absorption is dominated by a LUMO←HOMO transition. The transition is predicted to have a large

	R–group	λ_{max} abs/nm	ε/ $M^{-1}cm^{-1}$	λ_{max} ex/nm	λ_{max} em/nm	Stokes' shift/cm^{-1}	PLQY ϕ_f (± 10 %)	lifetime τ_f / ns (± 0.1 ns)	Calculated k_f / ns^{-1} (± 14 %)
BPEOx	H	304	31 900	303	357	4990	0.57♠	0.81♠	0.71
BPETd♡	H	334	36 300	n/a	396	4690	0.15	n/a	n/a
BPEBf	H	410	27 800	407	470	3290	0.80	3.1	0.26
	tBu	418	33 500	419	480	3030	0.96	3.0	0.32
	OMe	434	32 200	431	501	3240	0.63	3.1	0.20
	NH_2	309/464	29 700	310/461	560	3830	0.86	3.7	0.23
	CO_2Me	411	37 200	406	459	2840	0.85	2.4	0.21
BBfEB	H	383	35 800	378	428	3090	0.67	2.1	0.32
PEBf	H♣	283/359	12 600	288/362	431	4420	0.31	2.8	0.11
	NH_2	286/405	14 500	289/402	527	5900	0.67	5.8	0.12
BPEBtd	H	303/413	44 900	302/411	483	3630	0.85	4.1	0.21
	tBu	306/421	36 400	305/418	493	3640	0.84	4.0	0.21
	NH_2	319/461	31 900	318/462	567	4010	0.81	4.7	0.17
	CO_2Me	315/412	24 800	315/409	473	3310	0.77	3.7	0.21

Measurements recorded in toluene unless otherwise stated
♠ = measurements taken in DCM
♡ = from work by Yasuda *et al.* [112]
♣ = photophysics recorded by group member

Table 4.4: Oxadiazole, thiadiazole, benzofurazan and benzothiadiazole-containing arylethynylenes' photophysical properties.

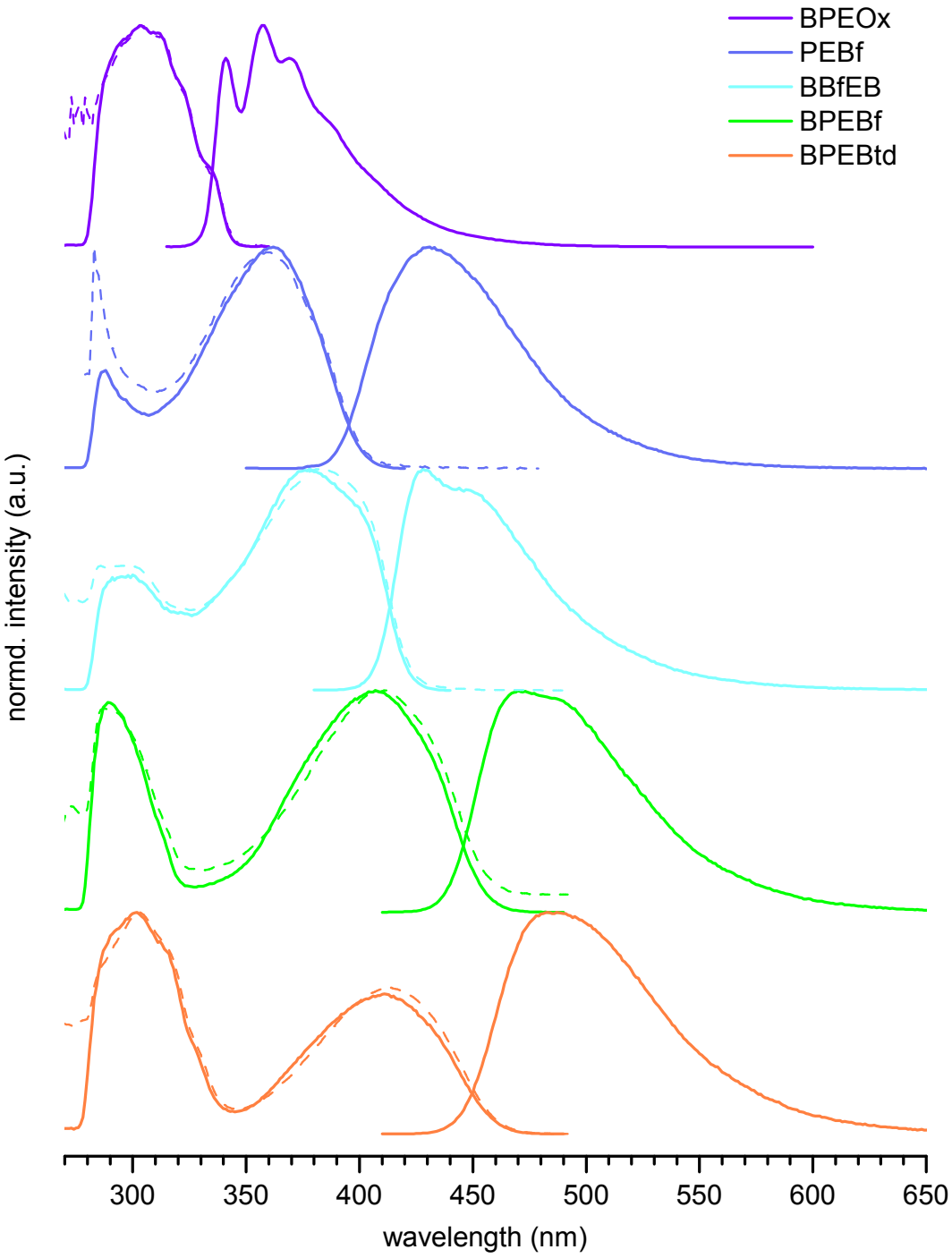

Figure 4.28: Absorption (dashed), excitation and emission spectra for the oxadiazole, benzofurazan and benzothiadiazole-containing phenylethynylene compounds.

oscillator strength (f = 1.45), which correlated to the high extinction coefficient observed for this compound in toluene (ε = 31 900 $M^{-1}cm^{-1}$). Use of the program GaussView has afforded visual representation of the HOMO and LUMO (Figure

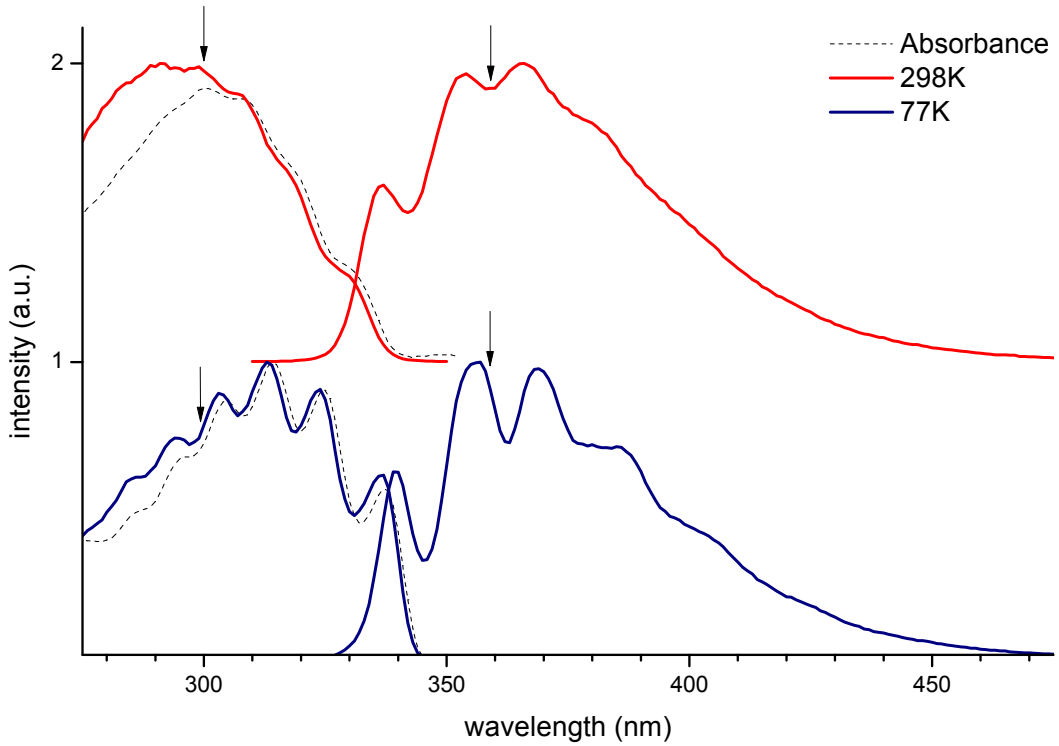

Figure 4.29: UV-vis and fluorescence spectra of **BPEOx** at 298 K and 77 K in EPA.

Temp / K	Absorption features /nm	Excitation features /nm	Emission features /nm
298	301*, 308, 331(sh)	291*, 299, 308(sh), 330	337, 354, 366*, 380(sh)
77	286, 295, 305, 314*, 325, 337	285, 294, 303, 313*, 324, 336	339, 357*, 369 386(sh), 404(sh)

* = maximum and (sh) = shoulder

Table 4.5: Spectral features of absorption, excitation and emission spectra for **BPEOx** at room and low temperature, see Figure 4.29, in EPA.

4.6), which shows that in both the electron density is delocalised over the whole molecule, with a slight decrease on the terminal phenyl rings on the LUMO. The energy gap for the LUMO←HOMO transition is predicted to be 3.56 eV. This correlates very well (0.04 eV difference) with the observed gap estimated from the onset of UV–vis absorption at 77 K, at $\sim$ 345 nm.

A fluorescence quantum yield of 57 % and lifetime of 0.81 ns were recorded for this compound in DCM. This has allowed determination of the rate of fluorescence, k_f, as 0.71 ns^{-1} (see Table 4.4).

	Molecular Orbital
LUMO	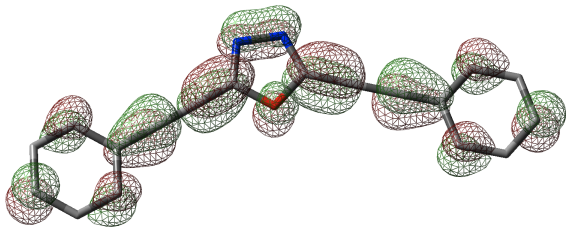
HOMO	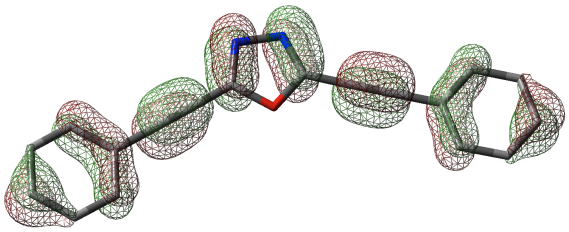

Table 4.6: Visualisation of the HOMO and LUMO of **BPEOx**, using GaussView 4.1. ΔE = 3.56 eV.

BPEOx displays higher energy absorption and emission maxima than the thiadiazole derivative, **BPETd**, prepared and studied by Yasuda *et al.* [112] **BPETd** also features a much lower quantum yield, $\phi_f = 0.15$, measured in chloroform. A lifetime is not reported however, so further analysis is not possible. The report included HOMO and LUMO energies calculated at the same level of theory as those reported in this work, and found the predictions to be approximately 0.3 – 0.5 eV higher. Qualitative analysis of the HOMO and LUMOs indicates that the electron density is expanded over the whole molecule similarly to that calculated for **BPEOx**.

Only small quantities of **BPEOx** were available and hence the quantum yield and lifetime measurements were not repeated in toluene, although UV–vis absorption and emission showed no significant spectral changes.

The asymmetrical systems PEBf and PEBf.NH$_2$

Of all the benzofurazan– and benzothiadiazole–containing systems, **PEBf** exhibits the highest energy absorption and emission maxima. There is good agreement between the absorption and excitation profiles, both featuring distinct lower and higher energy bands. However, there is some difference observed between the relative in-

tensities of the two bands. The origin of this difference is not clear, but may arise due to poor correction of the excitation spectra in the region < 300 nm. As the plot in Figure 4.30 shows, there is no evidence of vibronic structure in the spectra, and no spectra were obtained at low temperature for this compound.

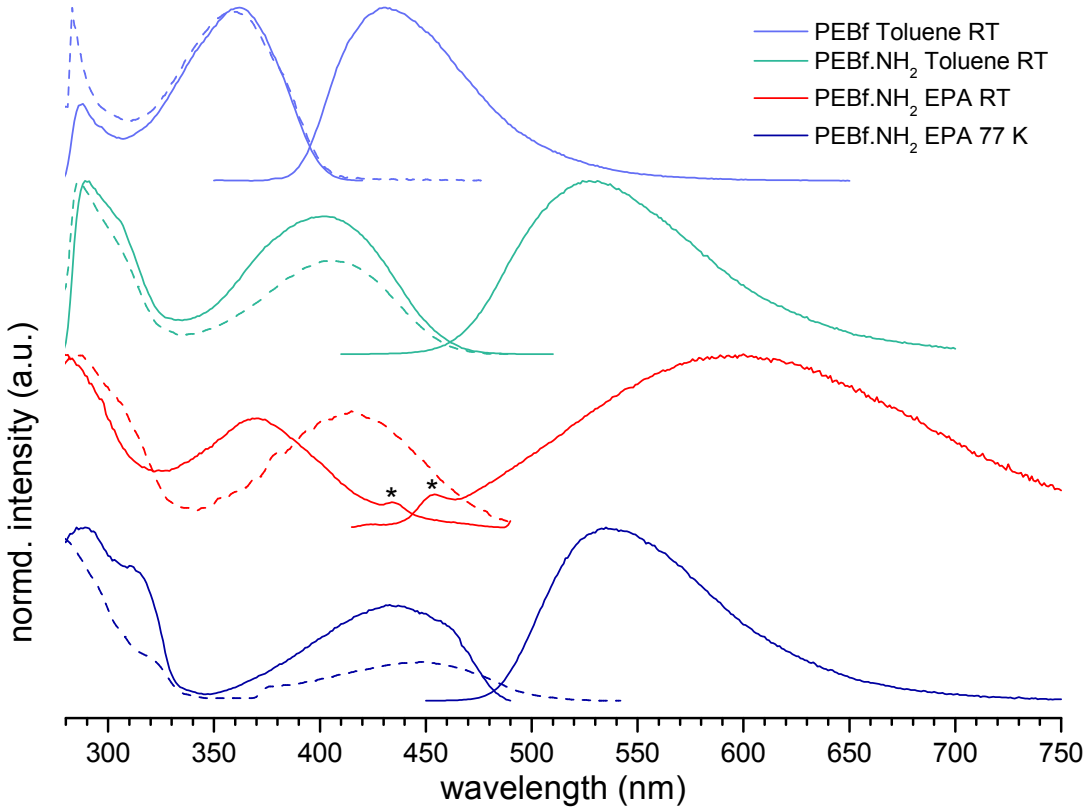

Figure 4.30: Absorption (dashed), excitation and emission spectra of **PEBf.NH$_2$** at room temperature and low temperature (* indicates Raman bands).

The aniline derivative, **PEBf.NH$_2$** has also been prepared and similarly studied, and low temperature spectra have been obtained (see Figure 4.30). The spectra obtained at room temperature in toluene show that addition of the electron donating amine group on the unsymmetrical system induces a large ($\sim$ 100 nm) bathochromic shift relative to **PEBf** and substantial broadening of the emission profile, as well as a marked increase in both the fluorescence quantum yield and lifetime (see Table 4.4).

In EPA at room temperature there is a large shift between the low energy absorption and excitation bands. Furthermore, both the excitation and emission profiles

feature small bands at approximately 440 nm and 460 nm, attributed to Raman bands, indicating that, in this solvent, **PEBf.NH$_2$** exhibits a low quantum yield. At room temperature in EPA the emission profile is broad and devoid of vibrational structure. At low temperature however, the emission profile is subject to a hypsochromic shift, and considerably narrowed.

A poor correlation is observed between the absorption and excitation spectra for the amino–substituted derivative **PEBf.NH$_2$** at room temperature in EPA, yet not at low temperature, nor in toluene. A similar observation is made for **BPEBf.NH$_2$** and is explained later (see section 4.6.3, page 172).

Excited state	**PEBf**	**PEBf.NH$_2$**
	Transition	
1st	LUMO←HOMO (f = 0.4)	LUMO←HOMO LUMO+1←HOMO (f = 0.41)
2nd	(f = 0.00)	(f = 0.07)
3rd	(f = 0.00)	(f = 0.00)
4th	(f = 0.13)	(f = 0.00)
5th	LUMO←HOMO-4 LUMO+5←HOMO-3 LUMO+2←HOMO-2 LUMO+1←HOMO (f = 0.37)	LUMO←HOMO-4 LUMO+5←HOMO LUMO+2←HOMO (f = 0.63)

Predicted oscillator strengths shown in parentheses

Table 4.7: Predicted transitions contributing to the excited states of **PEBf** and **PEBf.NH$_2$**

TD-DFT calculations performed on the optimised structures of both of these unsymmetrical systems indicate (see Table 4.7, page 162) that the first excited state of **PEBf.H**, S_1←S_0, can be attributed to the LUMO←HOMO transition, whereas the first excited state of **PEBf.NH$_2$** features both LUMO←HOMO and LUMO+1←HOMO character. The predicted oscillator strengths, f, for both transitions are ~ 0.4, in agreement with the relatively low extinction coefficients measured for these systems ($\varepsilon \sim 12000$ – 14000 $M^{-1}cm^{-1}$) . As shown in Table 4.7, the next state with a non–zero oscillator strength is the fifth excited state of both **PEBf.R**

compounds, suggesting this transition be associated to the higher energy band in the absorption profile. For both systems the relative magnitudes of the different states' predicted oscillator strengths match those observed experimentally. The calculated HOMO—LUMO gaps for **PEBf** and **PEBf.NH$_2$** are presented in Figure 4.31, demonstrating the observed red–shift upon substitution with the electron–rich amino group. The gaps correspond to a wavelength of 450 nm and 511 nm for **PEBf** and **PEBf.NH$_2$** respectively, which are at a significantly lower energy than those observed (estimated from the onset of absorption).

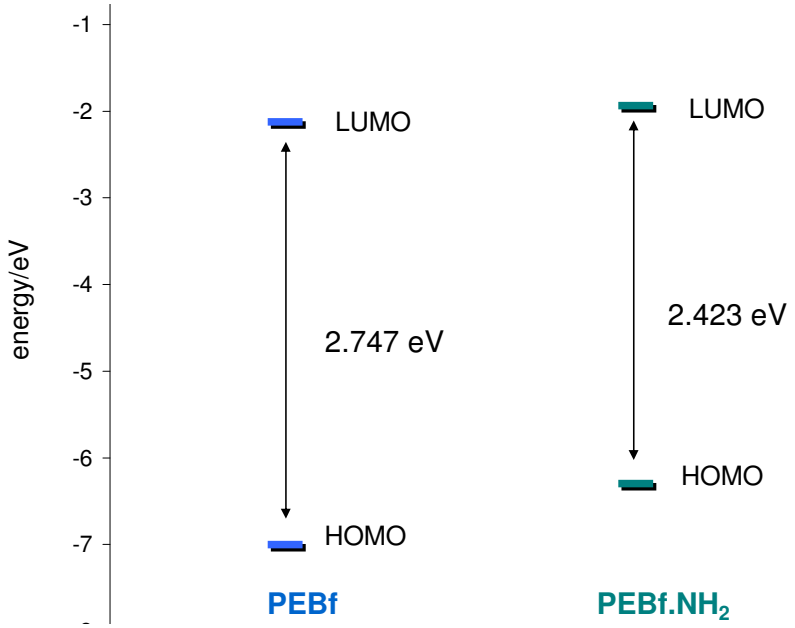

Figure 4.31: Predicted HOMO–LUMO gap for **PEBf** and **PEBf.NH$_2$**.

Table 4.8 shows the HOMO and LUMO of these two unsymmetrical systems, which succinctly demonstrate the 'push – pull' nature of the system. The differing degrees of electron density on the HOMO and LUMO of the aniline derivative suggests greater ICT character, with the electron density being localised on the benzofurazan group in the LUMO, and on the aniline moiety in the HOMO. The 'push – pull' molecule features the lone pair of electrons on the nitrogen of the amine pushing into the phenyl ring, and the electron–deficient benzofurazan moiety pulling electrons out from the acetylene bridge. This charge transfer is also present in the unsubstituted **PEBf**, albeit to a lesser extent; this is highlighted by examination of the solvatochromism of each compound in solvents of increasing polarity (see Figure

4.32). Here it is demonstrated that the aniline–substituted system experiences a greater solvatochromic effect than the unsubstituted **PEBf**.

	Molecular Orbitals	
	PEBf	**PEBf.NH$_2$**
LUMO	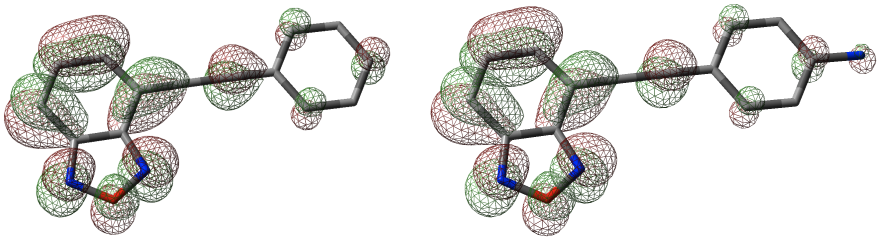	
HOMO	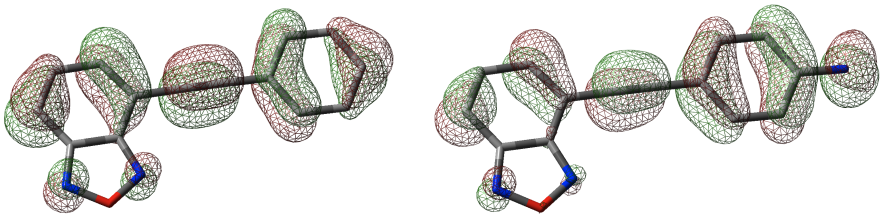	

Table 4.8: Visualisation of the HOMO and LUMO of **PEBf.R**, using GaussView 4.1.

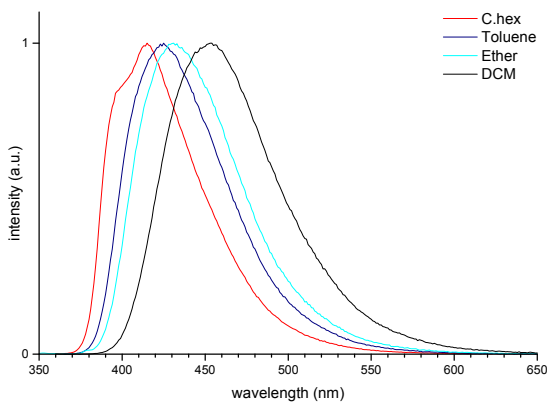

(a) Emission spectra of **PEBf**.

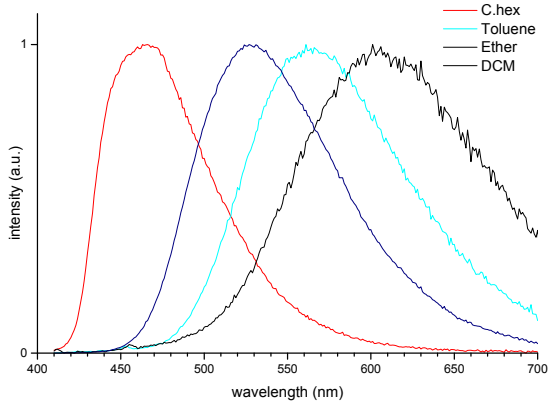

(b) Emission spectra **PEBf.NH$_2$**.

Figure 4.32: Emission spectra in different solvents, to illustrate their solvatochromic behaviour.

The symmetrical systems BPEBf, BBfEB and BPEBtd

BBfEB is different to the other symmetrical systems presented here because it features the electron–deficient benzofurazan groups as the outer groups of the system.

It is considered here first because this inversion, which implies charge transfer will occur symmetrically outward from the phenyl ring to the benzofurazan groups, has resulted in blue shifted absorption, excitation and emission maxima (Figure 4.28, 3rd from TOP) relative to that of **BPEBf.H** (Figure 4.28, 4th from TOP), where the charge can be said to be drawn centrally by the electron–deficient benzofurazan. The emission profile of **BBfEB** in toluene features a red–shifted shoulder, also evident in **BPEBf.H**. Again, there are two main absorption bands which show good agreement with the excitation spectrum, with the lower energy band of greater intensity (see Figure 4.28, page 158 for spectra).

Upon freezing in an organic glass these systems typically undergo a planarisation of the rings, as the lowest energy conformation is enforced, allowing enhanced vibrational structure to be observed. The emission profile of **BBfEB** in EPA at room temperature (Figure 4.33, TOP) displays a loss of the red–shifted shoulder observed in toluene due to the increased polarity of the solvent EPA. At low temperature however, the shoulder is redefined as a band. There is symmetry between the emission profile and the lower energy region of the excitation spectrum, which show evidence of vibrational structure with a maxima at 416 nm and a shoulder at 439 nm. The high energy region ($\sim$ 250–325 nm) also features enhanced vibrational structure. At low temperature, the emission profile is narrowed and two distinct peaks are present and the emission λ_{max} is shifted to higher energy.

BPEBf displays similar absorption and fluorescence spectra in toluene (Figure 4.28, GREEN) and EPA (Figure 4.33, MIDDLE), although the small red-shifted shoulder on the emission maximum in toluene is not present in the more polar EPA, similar to **BBfEB**. Furthermore, the high energy band's intensity is of greater intensity than the lower energy band in the excitation spectrum in EPA at room temperature, which effectively shifts the absorption λ_{max} by $\sim$ 100 nm, whereas in both toluene and at 77 K in EPA the lower energy band is of greater intensity. Enhanced vibrational structure at 77 K reveals symmetry between the emission spectrum and the lower energy bands of the excitation spectrum, with both featuring defined peaks compared to the broad, unstructured bands observed at room temperature.

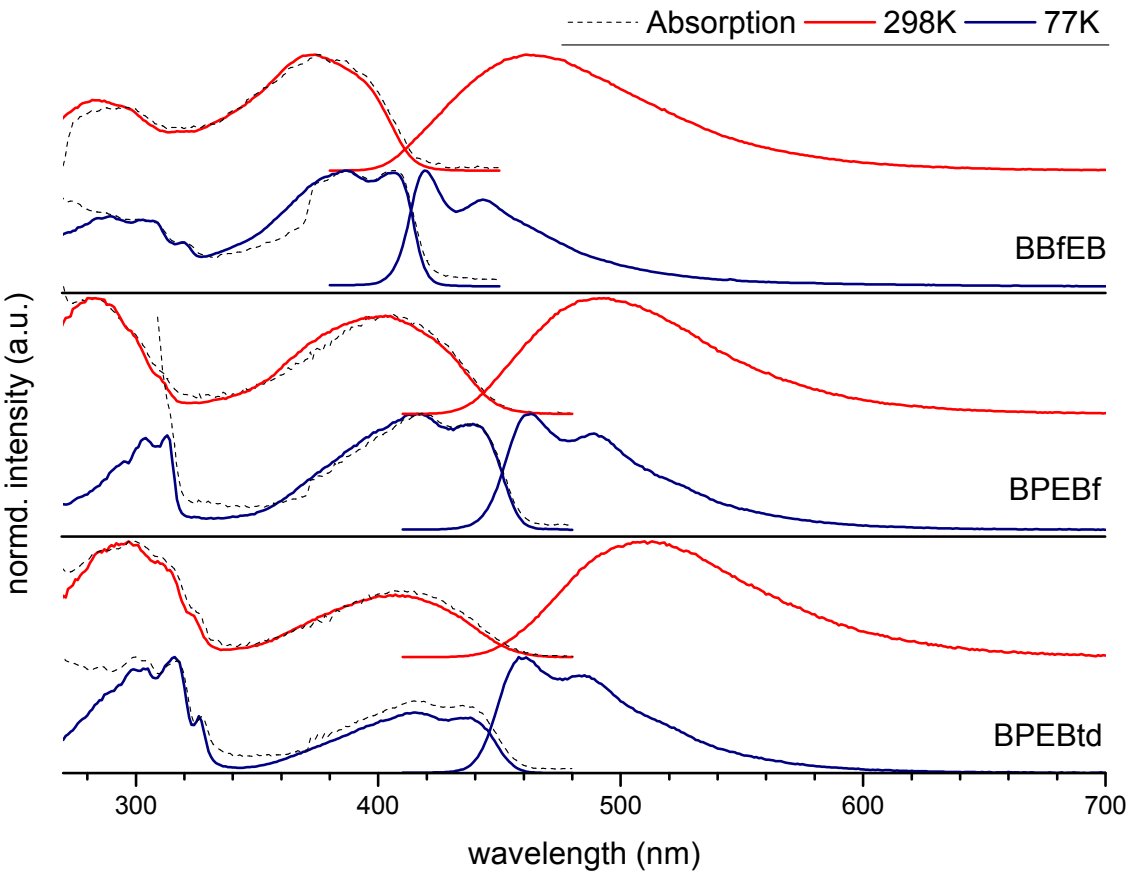

Figure 4.33: UV–vis and fluorescence spectra of **BBfEB**, **BPEBf** and **BPEBtd** at 298 K and 77 K in EPA. Values for λ_{max} and Stokes' shifts are given in Table 4.9. Absorption spectra are included to illustrate the close correlation they exhibit with the excitation spectra.

BPEBtd (Figure 4.33, BOTTOM) has been prepared in order to examine the effect of changing the oxygen to sulfur[3]. There is evidence of vibrational structure on the higher energy band, in the form of very faint shoulders, in both toluene and EPA at room temperature. These shoulders are more defined at 77 K.

TD-DFT calculations indicate that, for **BBfEB** and **BPEBf**, the first excited state, $S_1 \leftarrow S_0$, can be assigned as the LUMO←HOMO transition, and in the benzofurazan systems this is the dominant transition. The first excited state of **BPEBtd** is calculated to have some contribution from the LUMO+1←HOMO transition. It is also predicted a larger oscillator strength for its third excited state (f = 1.12

[3]The photophysical properties of **BPEBtd** have already been reported in the literature. [184] However, the low temperature UV-vis spectroscopy has not, to date, been reported. It is considered here for comparison, and to that end has been prepared independently and studied using the same procedures as the novel compounds.

Compound	Temp / K	Excitation features / nm	Emission features / nm	Stokes' shift / cm^{-1}
BBfEB	298	282, 374*	461	5000
	77	290, 306, 320 378, 386*, 406	419*, 443	700
BPEBf	298	283*, 403	493	4500
	77	295, 304, 313, 416*, 439	463*, 489	1200
BPEBtd	298	297*, 311, 326, 406	510	5000
	77	299, 304, 316* 326, 415, 438	458*, 485	1000

* denotes maxima

Table 4.9: Spectral features from Figure 4.33

c.f. 0.70). This higher energy excited state is expected to have some contribution from the LUMO+1←HOMO transition, which could explain the increased intensity of the higher energy absorption/excitation region. The benzofurazan–containing compounds also feature a large oscillator strength for a higher excited state, corresponding to the S_4←S_0 for **BPEBf** (LUMO←HOMO-4 and LUMO+1←HOMO) and the S_5←S_0 for **BBfEB** (LUMO←HOMO-3 and LUMO+2←HOMO) (see Table 4.10).

The HOMO and LUMO for **BBfEB**, **BPEBf** and **BPEBtd** are illustrated in Figure 4.11. Also shown are the other molecular orbitals predicted to contribute to the transitions responsible for the higher energy excited states. As can be seen the HOMOs feature electron delocalisation across the whole molecule, whereas the LUMO shows the effect of the highly electron-withdrawing benzofurazan and benzothiadiazole groups. The higher energy LUMO+n are even more localised on the heterocycle.

Fluorescent quantum yields and lifetimes have been measured, and rates of fluorescence decay subsequently calculated for these systems in toluene and are listed in Table 4.4 on page 157.

The systems featuring the centrally placed heterocycle exhibit very high quantum yields with fluorescence lifetimes of several nanoseconds; **BPEBf** displays $\phi_f = 0.8$

Excited state	**BPEBf**	**BBfEB** Transition	**BPEBtd**
1st	LUMO←HOMO (f = 1.00)	LUMO←HOMO (f = 1.22)	LUMO←HOMO LUMO+1←HOMO (f = 0.70)
2nd	(f = 0.00)	(f = 0.00)	(f = 0.00)
3rd	(f = 0.00)	(f = 0.00)	LUMO←HOMO-1 (f = 1.12)
4th	LUMO←HOMO-4 LUMO+1←HOMO (f = 0.78)	(f = 0.08)	(f = 0.00)
5th	(f = 0.00)	LUMO←HOMO-3 LUMO+2←HOMO (f = 0.55)	(f = 0.00)

Predicted oscillator strengths shown in parentheses

Table 4.10: Predicted transitions contributing to the excited states of **BPEBf**, **BBfEB** and **BPEBtd**.

and $\tau_f = 3.1$ ns. The sulfur–containing analogue **BPEBtd** exhibits a higher quantum yield and lifetime; $\phi_f = 0.85$ and $\tau_f = 4.1$ ns. Consequently, these two systems exhibit similar rates of fluorescence, $k_f = 0.26$ ns^{-1} and 0.21 ns^{-1} respectively. The peripherally–substituted derivatives of these systems display similar values, albeit with some discrepancies (see section 4.6.3, below).

BBfEB features a lower quantum yield and a shorter lifetime than the systems featuring the heterocycle positioned centrally ($\phi_f = 67\%$, $\tau_f = 2.1$ ns) which results in a slightly higher rate of fluorescence, $k_f = 0.32$ ns^{-1}.

Table 4.11: Molecular orbital visualisation of the HOMO and LUMOs of **BBfEB**, **BPEBf** and **BPEBtd**.

4.6.3 Effect of electron-donor and acceptor groups on the bis(arylethynylene)benzofurazan systems

A comparison of the emission profiles for the substituted benzofurazan systems, obtained in toluene, illustrates the effect of the electron-withdrawing and donating groups on the overall energy of the compound (Figure 4.34). Several substituted benzothiadiazoles have been reported in the literature [182, 184], but these studies are mainly based upon oligomers and lack a systematic approach to determining the effect of the various functional groups on the photophysics of the bis(arylethynyl)heteroarene motif. A similar study has been reported by Siddle *et al.* on 2,5-bis(arylethynyl)thiophenes. In the work presented here we will also consider the low temperature spectra, which reveal the effect of rotational conformation, brought about by the low barrier to rotation about the C≡C bond, on the optical spectra.

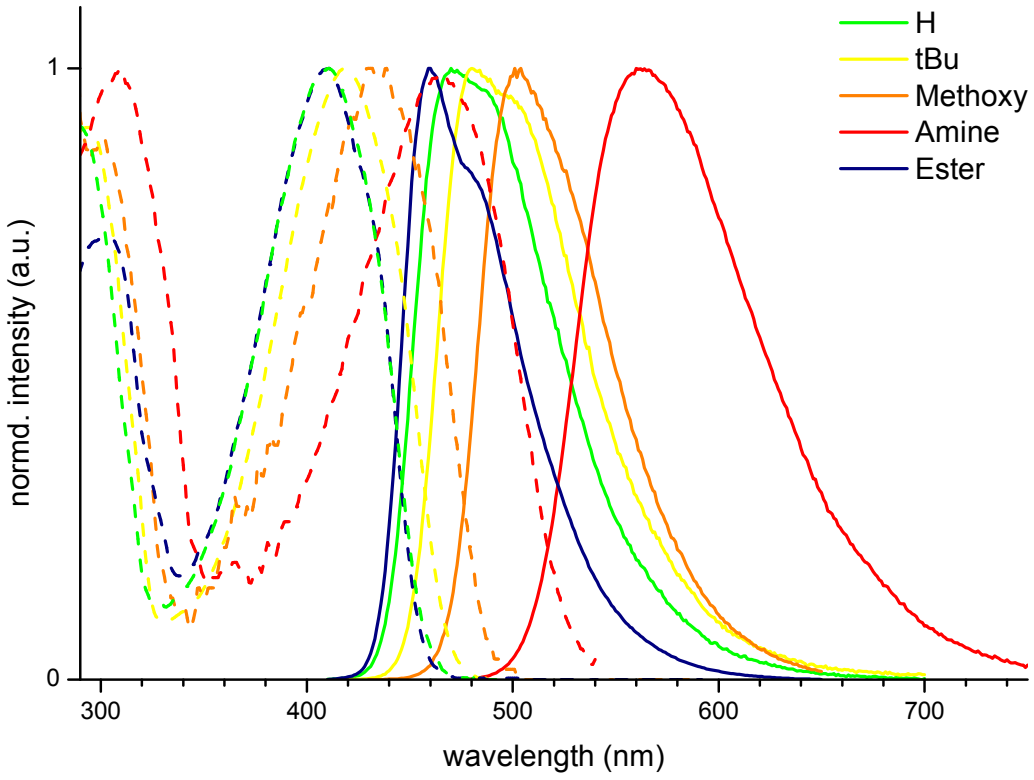

Figure 4.34: **BPEBf.R** absorption (dashed) and emission spectral profiles, recorded in toluene.

It is found that the electron withdrawing ester analogue (Figure 4.34, BLUE) features a hypsochromic shift in its emission maximum of just over 500 cm^{-1}, relative to the parent compound **BPEBf** (Figure 4.34, GREEN). The more electron donating derivatives are subject to increasing bathochromic shifts, with the amine derivative (RED) exhibiting a 3900 cm^{-1} red–shift relative to the ester, which equates to a 3400 cm^{-1} red–shift relative to the unsubstituted **BPEBf**. The emission profiles of **BPEBf**, **BPEBf.tBu** and **BPEBf.CO_2Me** show a red–edged shoulder to the maxima, whereas the compounds substituted with electron-donating substituents, **BPEBf.OMe** and **BPEBf.NH_2** do not. The emission of **BPEBf.NH_2** is the most broad. This can be attributed to a high degree of charge transfer in this system compared to the other derivatives.

From variations of the emission maximum it is evident that addition of the ester group has increased the LUMO←LUMO gap, either by lowering (stabilising) the HOMO relative to the LUMO, or raising (destabilising) the LUMO relative to the HOMO. Furthermore, electron–donating groups result in a red–shift, brought about by either raising the HOMO relative to the LUMO, or stabilising the LUMO relative to the HOMO. Gas–phase TD–DFT calculations have been performed on all systems to elucidate which is the case.

It is found that the addition of electron–donating and withdrawing substituents has the greatest effect upon the energy of the HOMO for all systems. The calculations correctly predict the ester's behaviour, as well as the red-shift for the order of the series H < tBu < OMe < NH_2, with the amine derivative's HOMO destabilised by 0.675 eV compared to the parent. The calculations also predict that there are two excited states with strong absorption bands that can be populated with $\lambda_{ex} >$ 200 nm. The first excited state, S_1←S_0, can be attributed to the LUMO←HOMO transition in all of the derivatives, and has a large oscillator strength (see Table 4.12). This is in agreement with the large extinction coefficients recorded for the lowest energy transition observed in the absorption spectra (see Table 4.4). A second higher energy excited state with a high oscillator strength is also predicted, which goes some way to explain the presence of two main bands in the absorption spectra of these systems. In the case of the aniline derivative this higher excited

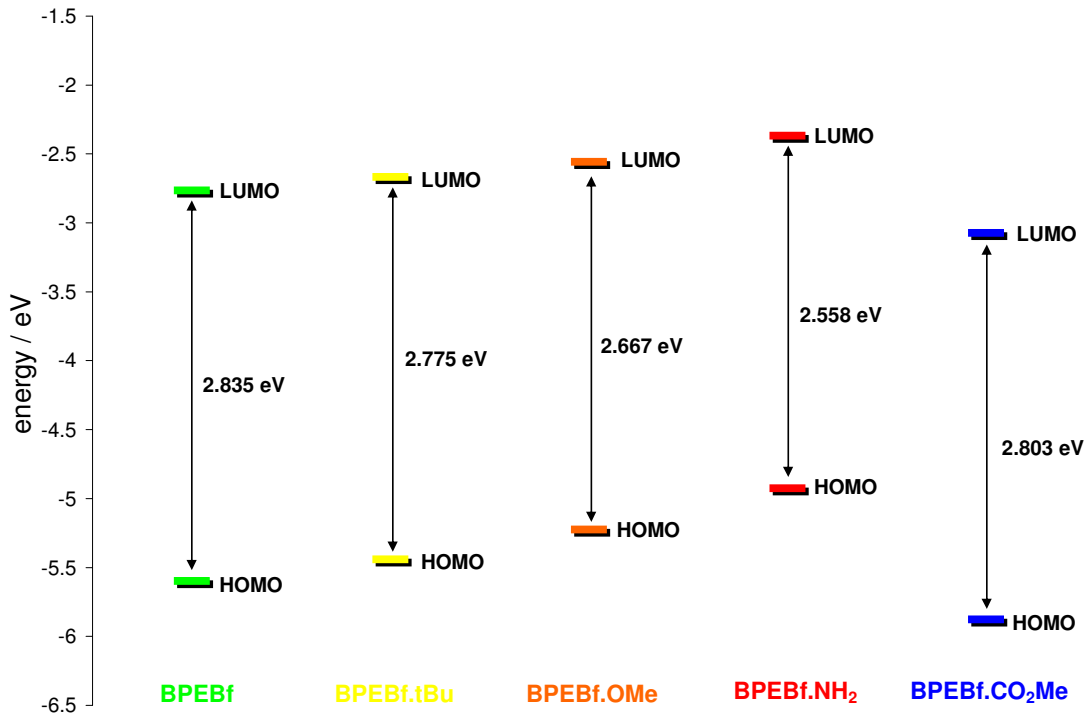

Figure 4.35: Calculated molecular orbital energies for the bis(arylethynyl)benzofurazan systems.

state, attributed to $S_3 \leftarrow S_0$, features a higher oscillator strength than for $S_1 \leftarrow S_0$, which is in agreement with the absorption spectrum (see Figure 4.34, RED). Table 4.12, page 173, lists the calculated transitions with highest oscillator strengths.

The low temperature spectra of these compounds have been measured in EPA and are presented in Figure 4.36. The upper portion displays the spectra for R = H, CO_2Me, tBu and OMe, in order of decreasing energy (top to bottom). At room temperature the emission profiles are broad and featureless, indicative of their charge transfer nature. Upon cooling there is an increase in vibrational structure across the series and the lower energy absorption/excitation region reveals some vibronic fine structure, as does the emission band. With the exception of **BPEBf.NH$_2$**, all of the absorption profiles resemble their counterpart excitation spectra, although all feature a step-like feature at $\sim$ 370 nm.

Presented in Figure 4.36 (lowest spectra) is the room and low temperature absorption, excitation and emission spectra for **BPEBf.NH$_2$**. The room temperature absorption and excitation profiles do not coincide; the maxima are separated by ap-

Excited state	**BPEBf**	**BPEBf.tBu**	**BPEBf.OMe**	**BPEBf.NH_2**	**BPEBf.CO_2Me**
			Transition		
1st	HOMO—LUMO (f = 0.78)	HOMO—LUMO (f = 1.20)	HOMO—LUMO (f = 1.11)	HOMO—LUMO (f = 1.07)	HOMO—LUMO (f = 1.43)
2nd	(f = 0.00)	(f = 0.00)	(f = 0.00)	(f = 0.00)	(f = 0.00)
3rd	(f = 0.00)	HOMO-4—LUMO HOMO—LUMO+1 (f = 0.99)	HOMO-2—LUMO HOMO—LUMO+1 (f = 1.03)	HOMO-2—LUMO HOMO—LUMO+1 (f = 1.08)	HOMO-6—LUMO HOMO—LUMO+1 HOMO—LUMO+2 (f = 0.67)
4th	HOMO-4—LUMO HOMO—LUMO+1 (f = 0.63)	(f = 0.01)	(f = 0.04)	(f = 0.05)	(f = 0.00)

Predicted oscillator strengths shown in parentheses

Table 4.12: Predicted transitions contributing to the excited states of **BPEBf.R**.

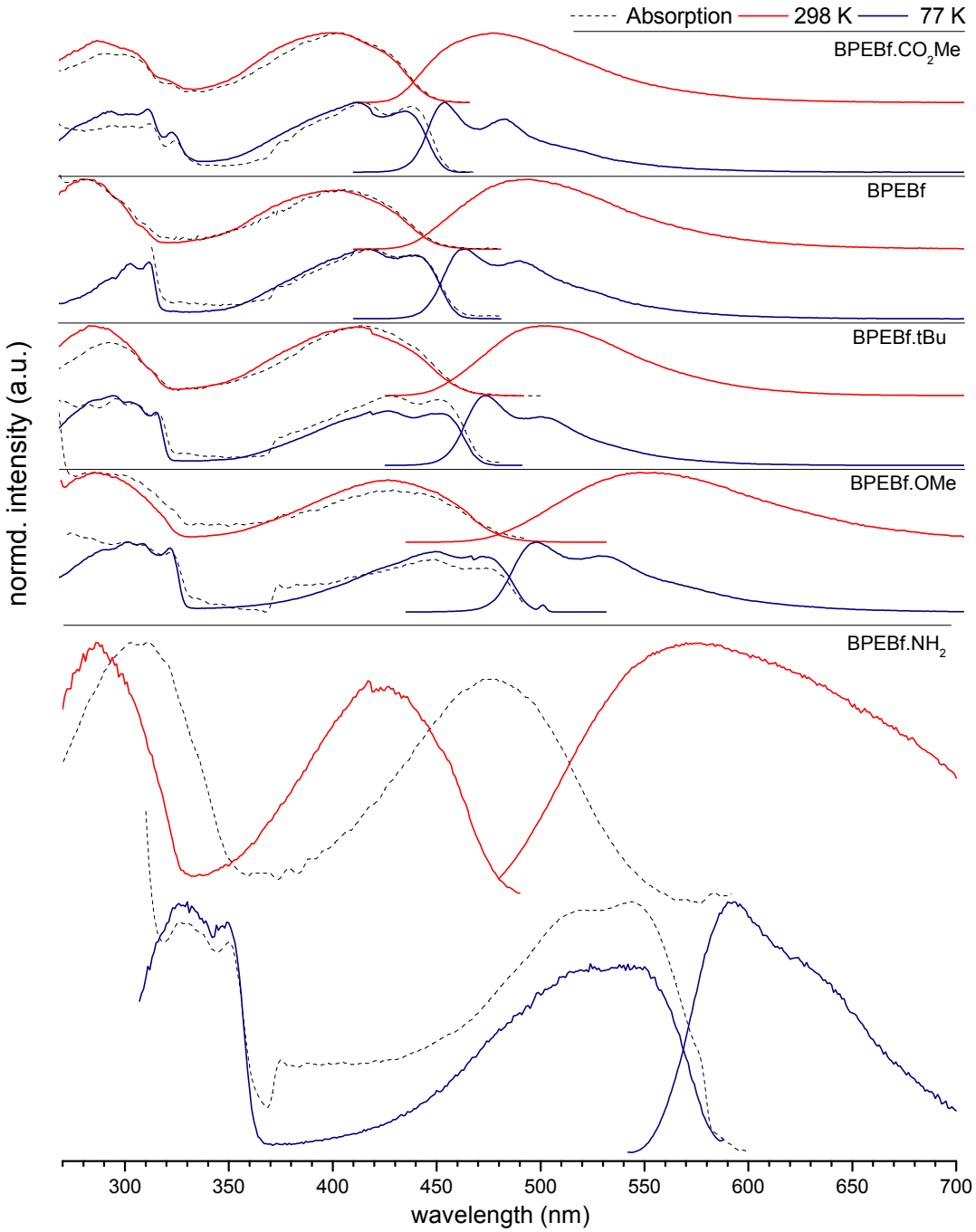

Figure 4.36: Room and low temperature absorption, excitation and emission spectra obtained in EPA of the various **BPEBf.R** compounds. Spectra for **BPEBf.NH$_2$** is enlarged (see text for discussion).

proximately 2500 cm^{-1}. This is similar to that observed for the asymmetrical amino derivative discussed earlier. This has been attributed to protonation of the amine group by the EPA solvent (containing ethanol). Presented in Figure 4.37a is an absorption profile of **BPEBf.NH$_2$** in toluene along with the absorption profile of the

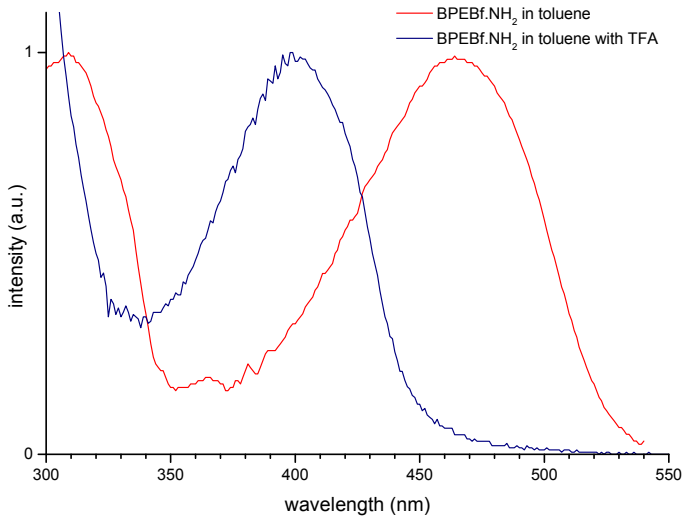

(a) Absorption profile of neutral and protonated **BPEBf.NH$_2$**.

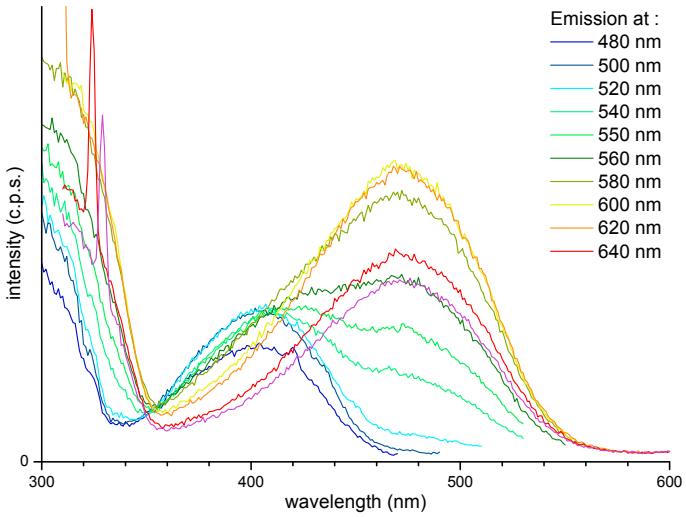

(b) **BPEBf.NH$_2$** in EPA viewing emission at different wavelengths.

Figure 4.37: Absorption profiles of **BPEBf.NH$_2$** in toluene and EPA to determine the nature of the discrepancy in the absorption and excitation spectral profiles shown in Figure 4.36.

same sample, but with trifluoroacetic acid in the solvent. Protonation has prohibited the lone pair on the amine's nitrogen donating into the oligomer, which has resulted in a blue shift of $\sim$ 3800 cm^{-1}. Figure 4.37b helps to explain the discrepancy between the absorption and excitation profiles in EPA for the amine–substituted oligomers. For both **PEBf.NH$_2$** (Figure 4.30) and **BPEBf.NH$_2$** (Figure 4.36) the room temperature excitation spectra were obtained by viewing emission at higher energy ($\sim$ 500 nm) *i.e.* from the protonated species, which was in an equilibrium

with the non–protonated form in the EPA solvent. As Figure 4.37b shows, had emission been viewed at a lower energy ($\sim$ 600 nm), the excitation spectra would have more closely resembled that of the absorption spectra for these systems.

Regardless of this protonation, there is a marked red–shift on the absorption maxima of **BPEBf.NH$_2$**, for both the high and low energy bands, at low temperature. Furthermore, the emission maximum has slightly red–shifted upon freezing, in contrast to all previously considered low temperature spectra, which have featured blue–shifted emission maxima. This has resulted in a dramatic change in the colour of the sample (see Figure 4.38). At room temperature in EPA the compound displays

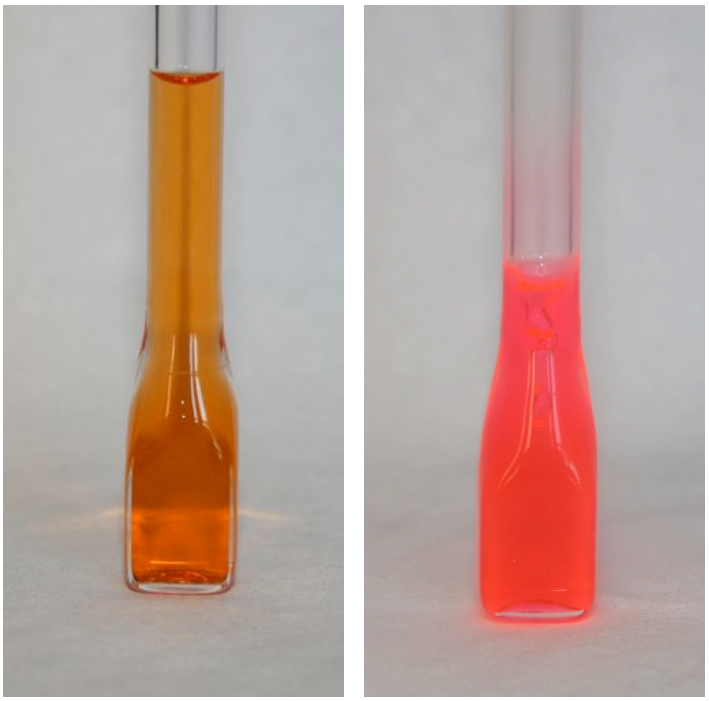

(a) 298 K (b) 77 K

Figure 4.38: **BPEBf.NH$_2$** at different temperatures, observed in room light.

negligible fluorescence, even under irradiation with the long-wavelength UV–lamp. Upon cooling to 77 K a pink luminescence is seen, with only room–light as a source of excitation. The low temperatures anneals the compound into its lowest energy planar conformation, in which state conjugation is increased and charge–migration between the amine and benzofurazan is thus improved.

The LUMO←HOMO energies calculated using Gaussian [47] have been compared to the observed LUMO←HOMO gap, estimated from the onset of the UV–vis

absorption spectra at low temperature. There is good agreement between these values, with the calculations generally over–estimating the energy gap by ~ 0.15 eV, except for the amino derivative which is overestimated by 0.47 eV. This is attributed to strong ICT character in this molecule, for which the B3LYP functional is known to be less accurate.

Due to their display of charge transfer the effect of increasing solvent polarity on the absorption and emission spectra of these compounds has been investigated. The Lippert plots in Figure 4.39 demonstrate that an approximate linear fit is observed for all species. This has allowed calculation of the change in dipole moment, $\Delta\mu$, determined from the gradient (using Equation 1.11, page 25), and thus the excited state dipole moment, μ_E, has been calculated (see Table 4.13).

Figure 4.39 shows that all compounds display an approximately linear increase in $\Delta\bar{\nu}$ with increasing solvent polarity. **BPEBf.CO$_2$Me** displays the largest change in dipole moment, experiencing a 36 Debyes increase in the dipole moment in the excited state relative to the ground state. The unsubstituted parent **BPEBf** displays the lowest change in dipole moment, as well as the lowest excited state dipole. The ester moieties cause greater electron delocalisation in the ground state. **BPEBf.OMe** features the largest excited state dipole moment. This is attributed to electron–donation from the methoxy groups in to the electron–deficient benzofurazan centre.

Compound	Gradient / cm^{-1}	Intercept / cm^{-1}	a / Å	μ_G / D	μ_E / D	$\Delta\mu$ / D
BPEBf	6298	2544	9.42	3.65	26.48	22.83
BPEBf.OMe	6395	2522	11.54	6.11	37.30	31.19
BPEBf.NH$_2$	8462	2757	10.23	3.35	33.30	29.95
BPEBf.CO$_2$Me	7479	2226	12.19	0.33	36.95	36.62

Table 4.13: Data from the Lippert Plots in Figure 4.39 with calculated change in dipole moments ($\Delta\mu$ / D) and excited state dipole moments (μ_E / D) determined from the gradient. Approximate radii for determination of spherical cavities (a / Å) and ground state dipole moments (μ_G / D) were estimated from optimised geometries calculated using Gaussian 03 [47] with the B3LYP functional and 6-31G(d) basis set.

Fluorescence quantum yields have been recorded for all of the benzofurazan–

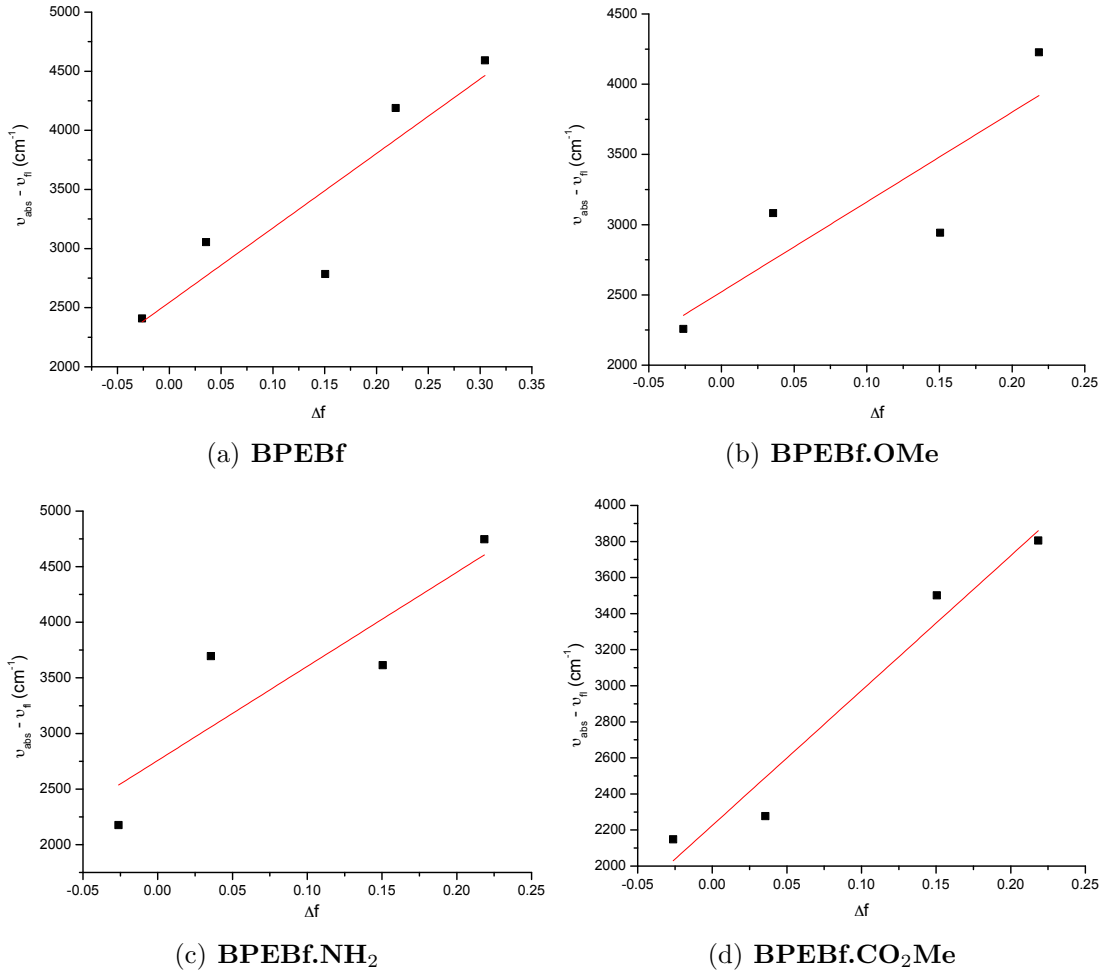

(a) **BPEBf** (b) **BPEBf.OMe**

(c) **BPEBf.NH$_2$** (d) **BPEBf.CO$_2$Me**

Figure 4.39: Lippert plots of selected bis(arylethynyl)benzofurazans. Solvents from left to right; cyclohexane, toluene, diethylether, DCM, acetonitrile (only **BPEBf** was soluble in acetonitrile).

containing systems in toluene, using both the absolute and comparative methods, which has allowed multiple readings to be obtained showing good agreement between the methods. Average values for ϕ_f are calculated and quoted in Table 4.4.

As shown in Table 4.4, all of the tricyclic systems display very high quantum yields, with **BPEBf.tBu** exhibiting $\phi_f = 0.96 \pm 0.09$. There is no discernible pattern to the quantum yield values measured, although the determination of PLQY is notoriously prone to errors, and an uncertainty of $\pm$ 10 % is given. As such the effect on quantum yield by the electron–donating and accepting substituents is unclear. Furthermore, quantum yields for the benzothiadiazole systems displayed no considerable change attributable to the presence of the heavy atom sulfur.

The fluorescence lifetimes for all the benzofurazan– and benzothiadiazole–contain-

ing systems are reported in Table 4.4. Several observations can be made from these data. Firstly, the bis(arylethynyl)benzofurazan systems have shorter lifetimes ($\sim$ 1 ns) than the equivalent benzothiadiazole systems. Secondly, the amine–substituted derivatives display the longest lifetimes, and the ester–containing analogue displays the shortest. This suggests that longer decay time is related to a charge–transfer process most likely due to a lower oscillator strength for the ICT transition.

These two properties allow determination of the rate of fluorescent decay, k_f (see Table 4.4). As mentioned earlier, the rates of fluorescence are similar across all of the tricyclic systems, including both the oxygen and sulfur analogues. **BPEBf.tBu** and **BBfEB** exhibit the highest rates, of 0.32 ($\pm$ 12 %) ns^{-1}, and the other systems are 0.17 – 0.26 ($\pm$ 12 %) ns^{-1}. This agreement implies that the radiative decay for these systems is by a similar process. The unsymmetrical systems both feature a lower radiative rate constant, and commensurately low extinction coefficients.

4.6.4 Preliminary electrochemical analysis of selected novel arylethynyldiazoles

BPEOx

Oxadiazole systems are renowned for their electron–deficient nature. As such, **BPEOx** was expected to exhibit interesting electrochemical behaviour; most likely a reversible reduction that could be further studied using spectroelectrochemistry to investigate the optical and vibrational spectra of the reduced spectra. As the cyclic voltamogramm in Figure 4.40 shows, there appears to be an irreversible oxidation at E_{pc} = 1.49 V and an irreversible reduction at E_{pa} = -2.24 V. The difference in the peak current of the oxidation and reduction events suggests that there is some process occurring at the electrode.

There was only a small amount of compound available so further study, under different conditions *e.g.* different solvent or counter electrolytes, could not be performed.

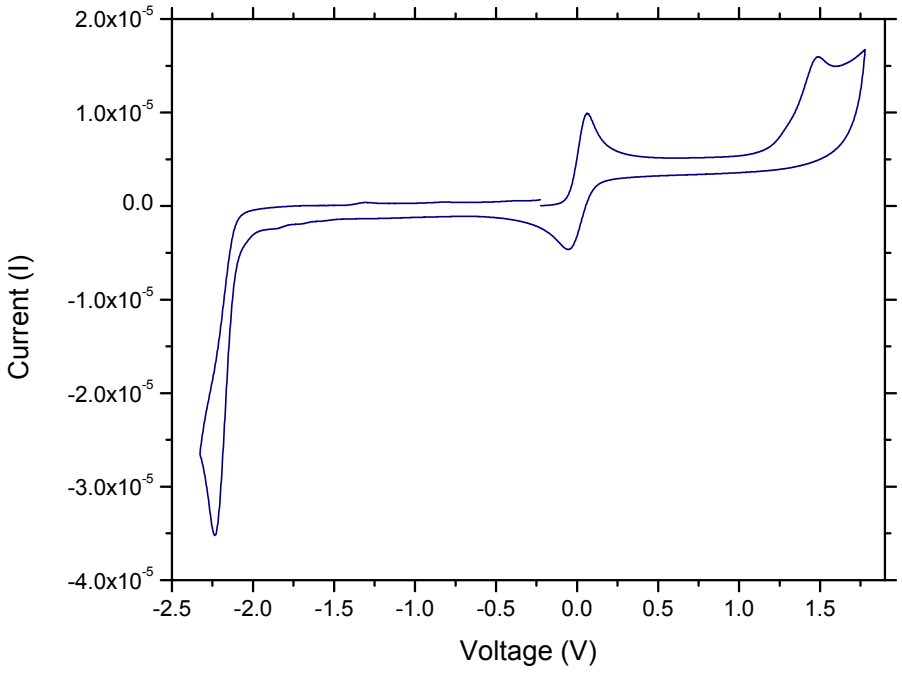

Figure 4.40: Cyclic voltammogram of **BPEOx** in 0.1 M Bu_4NPF_6 DCM solution, scanning at 100 mVs^{-1}, referenced to the FcH/FcH^+ couple (0.00 V).

Arylethynyl-benzofurazan compounds

Compound	$E^{red}_{1/2}$/V
BPEBf.CO_2Me	-1.370
BPEBf.tBu	-1.472
BPEBf.H	-1.496
BPEBf.OMe	-1.503
BPEBf.NH_2	-1.551

Table 4.14: Cyclic voltammetry data for benzofurazan-containing arylethynylenes presented in Figure 4.41. Data taken in DCM with 0.1 M Bu_4NPF_6. Potentials referenced to $FcH/FcH^+ = 0.00$ V.

Presented in Figure 4.41 are preliminary cyclic voltammograms for the prepared bis(arylethynyl)–benzofurazans. Each system exhibited reversible reductions between -1.37 – -1.77 V. The E^{red} increases in negativity across the series **BPEBf.-CO_2Me** < **BPEBf.tBu** < **BPEBf.H** < **BPEBf.OMe** < **BPEBf.NH_2**.

For this series of structurally similar compounds, the data largely supports the trend in the LUMO energy as determined by DFT calculations, which are corroborated by the photophysical data. However, there is a discrepancy for **BPEBf.tBu** and the parent **BPEBf.H**, which exhibit reduction potentials opposing this trend. The reason for this is unknown.

Cyclic voltammograms at increasing scan rates were obtained for each compound, affording plots as exemplified by Figure 4.42. Using the Randles-Sevcik equation [195]:

$$i_p = 0.4463nFAC\sqrt{\frac{nFvD}{RT}} \tag{4.1}$$

where all but i_p and v are constants, it can be shown that:

$$i_p \propto \sqrt{v} \tag{4.2}$$

This indicates that the peak current, i_p, should be proportional to the square root of the scan rate, v, for a reduction or oxidation process that is diffusion limited.

As Figure 4.42 demonstrates, there is a linear relationship between the peak current and the square root of the scan rate for each system, but only at lower scan

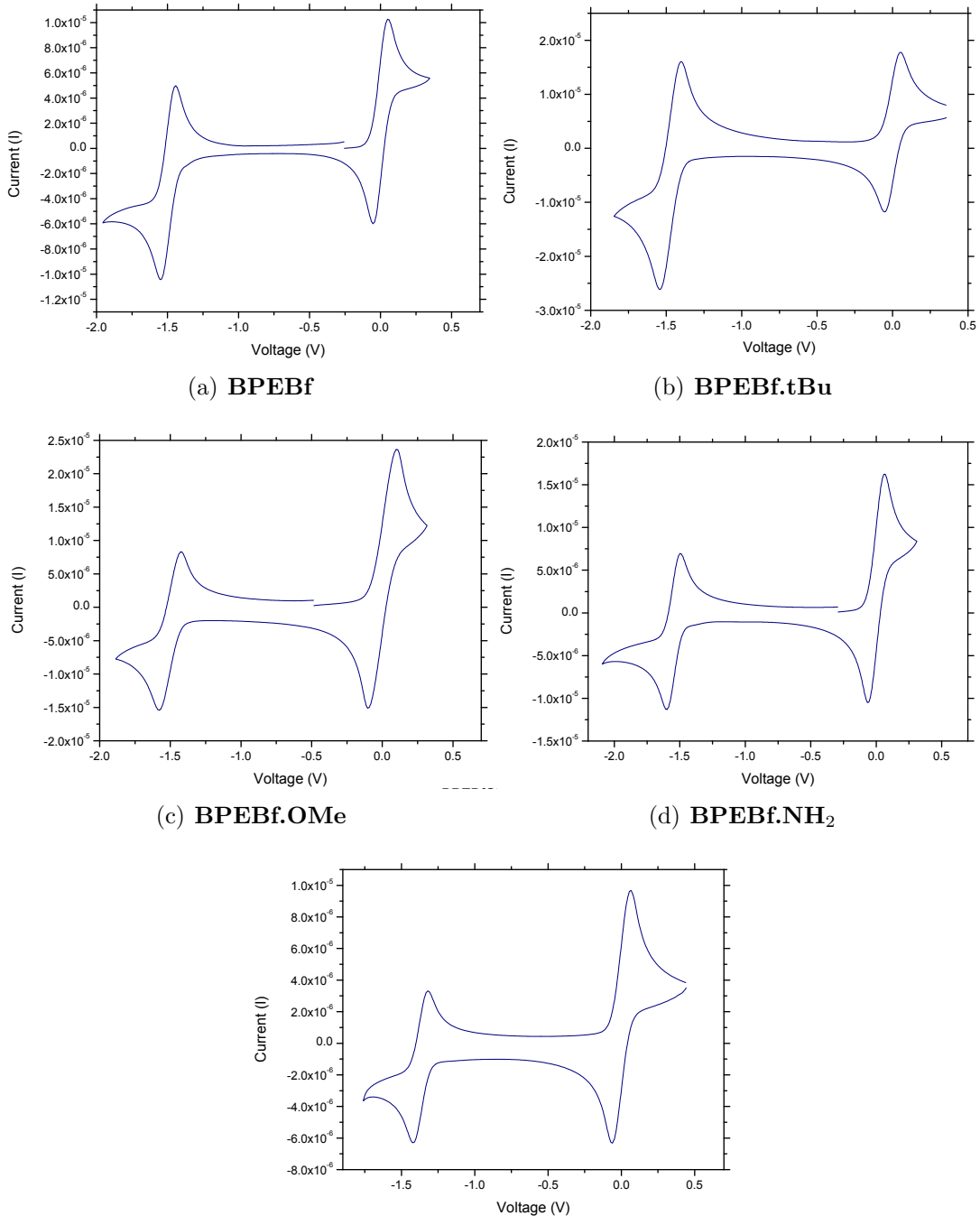

(a) **BPEBf** (b) **BPEBf.tBu**

(c) **BPEBf.OMe** (d) **BPEBf.NH$_2$**

(e) **BPEBf.CO$_2$Me**

Figure 4.41: Cyclic voltammograms of benzofurazan–containing arylethynylenes in DCM, 0.1 M Bu_4NPF_6 at 100 mV s^{-1}. Potentials are referenced to FcH/FcH^+ = 0.00 V.

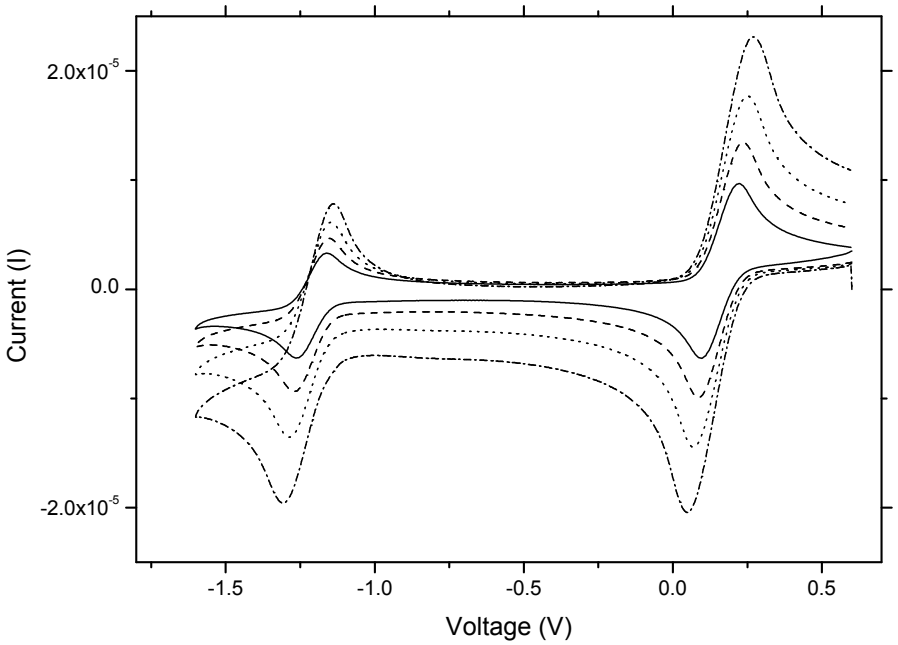

(a) **BPEBf.CO$_2$Me** CV with varied scan rates.

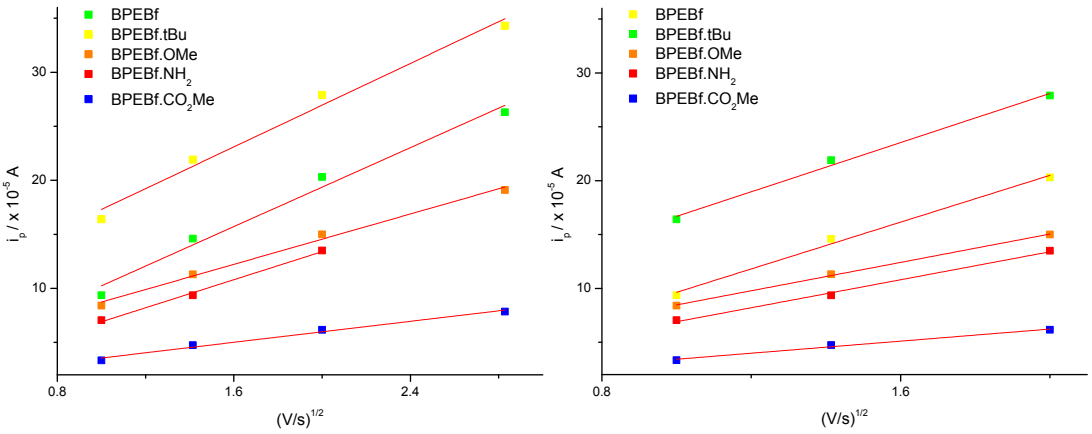

(b) 100 mV to 800 mV^{-1}. (c) 100 mV to 400 mVs^{-1}.

Figure 4.42: Cyclic voltammogram of **BPEBf.CO$_2$Me** at increasing scan rates (100, 200, 400 and 800 mVs^{-1}).

rates (Figure 4.42c). This implies that at the higher scan rate of 800 mVs^{-1} the reduction process is not diffusion limited.

Three selected compounds were further studied *via* spectroelectrochemical methods, using UV–vis absorption spectroscopy. **BPEBf.tBu**, **BPEBf.OMe** and **BPEBf.CO$_2$Me** were chosen to represent systems appended with substitutents of different electronic characteristics (*i.e.* donating/accepting).

Figure 4.43 shows the change in the UV–vis absorption spectra for **BPEBf.tBu**

with increased reduction potential. The main feature is a flattening of the two bands at 295 nm and 420 nm with concomitant emergence of bands at 255 nm and a series of bands of very low intensity between 490–800 nm (Figure 4.43, INSET). The low intensity of these low–energy bands is attributed to the reduced species being unstable and degrading over the time period required to study the species spectroelectrochemically. This may also account for this compounds irreversibility, as the neutral species spectrum was not observed upon oxidation.

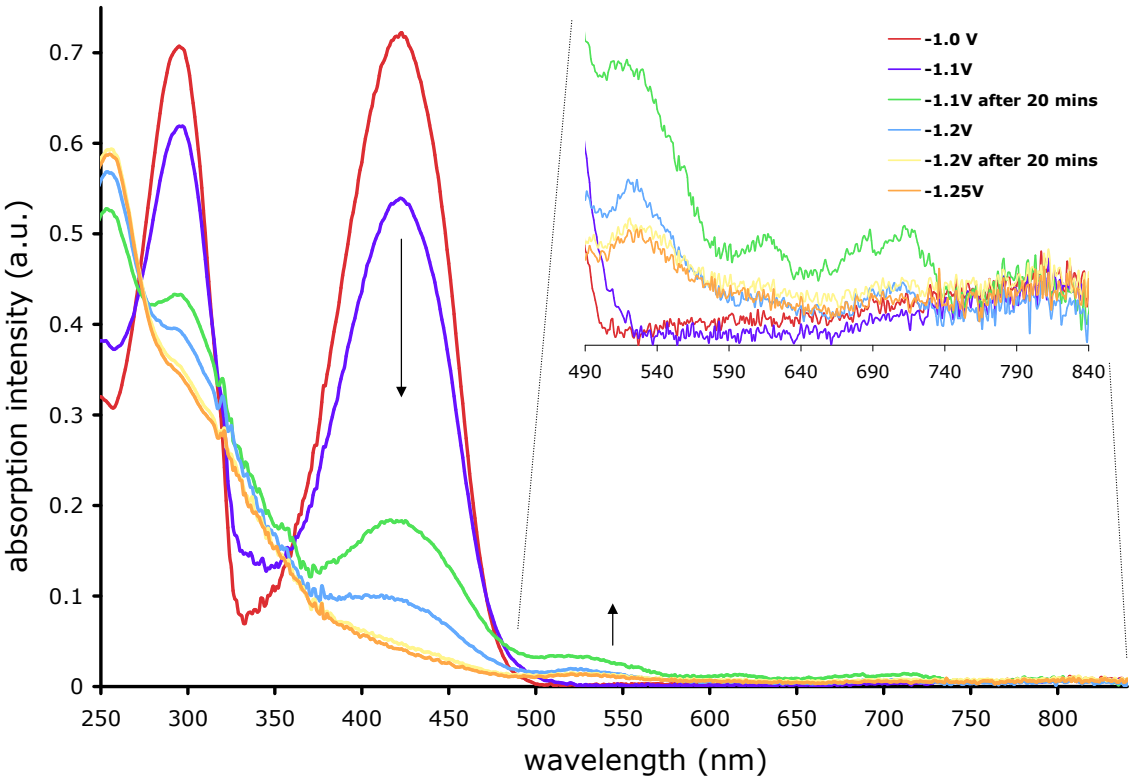

Figure 4.43: UV–vis spectroelectrochemistry of **BPEBf.tBu**.

The spectroelectrochemical study of **BPEBf.OMe** yielded the spectra in Figure 4.44. This shows a much more defined shift in absorption profile upon reduction. The two large bands at 297 and 436 nm (characteristic of the **BPEBf.R** series of compounds, see Figure 4.28), can be seen before reduction, E = 0.00 V.

As a reduction potential is applied to the cell, these bands lower in intensity, and a high energy peak forms at 261 nm. Furthermore, the band at $\sim$ 520 nm grows in, originally as a shoulder on the 436 nm band (not shown) but eventually as a separate band (RED; -1.02 V). It features several shoulders at lower energies,

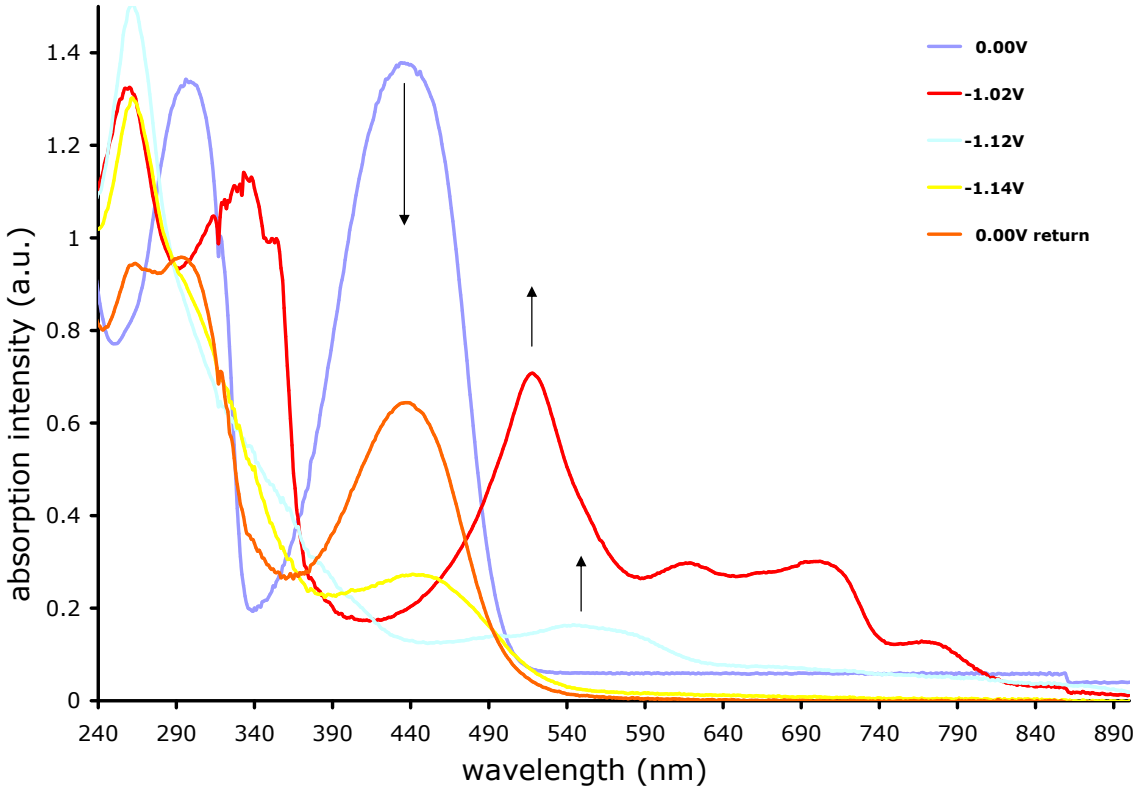

Figure 4.44: UV–vis spectroelectrochemistry of **BPEBf.OMe**.

and is attributed to the one electron reduction species. This series of bands is observed at the same energy range as those of substantially weaker intensity in the **BPEBf.tBu** spectroelectrochemical reduction (Figure 4.43). It is believed that in the methoxy–substituted system the reduced species is more stable, hence this increased band intensity. Again, however, the neutral species is not observed to recover upon reoxidation, indicating the reduced species is undergoing decomposition in the OTTLE cell, similarly to the *t*-butyl–substituted species.

Figure 4.45 shows the spectroelectrochemical analysis of **BPEBf.CO$_2$Me**. When the reduction potential reaches - 0.50 V the neutral species bands' intensities decrease and the reduced species bands grow in at 263 nm and 626 nm, around the isosbestic point at 452 nm. The lower energy band dominates as the reduction potential is increased, reaching a maximum at E = - 0.58 V. This band is attributed to the first electron reduction, as [**BPEBf.CO$_2$Me**]$^-$ is generated. TD-DFT calculations on the anions have shown that the LUMO features hardly any electron–density localised on the N—O—N group, in contrast to that of the non–reduced form.

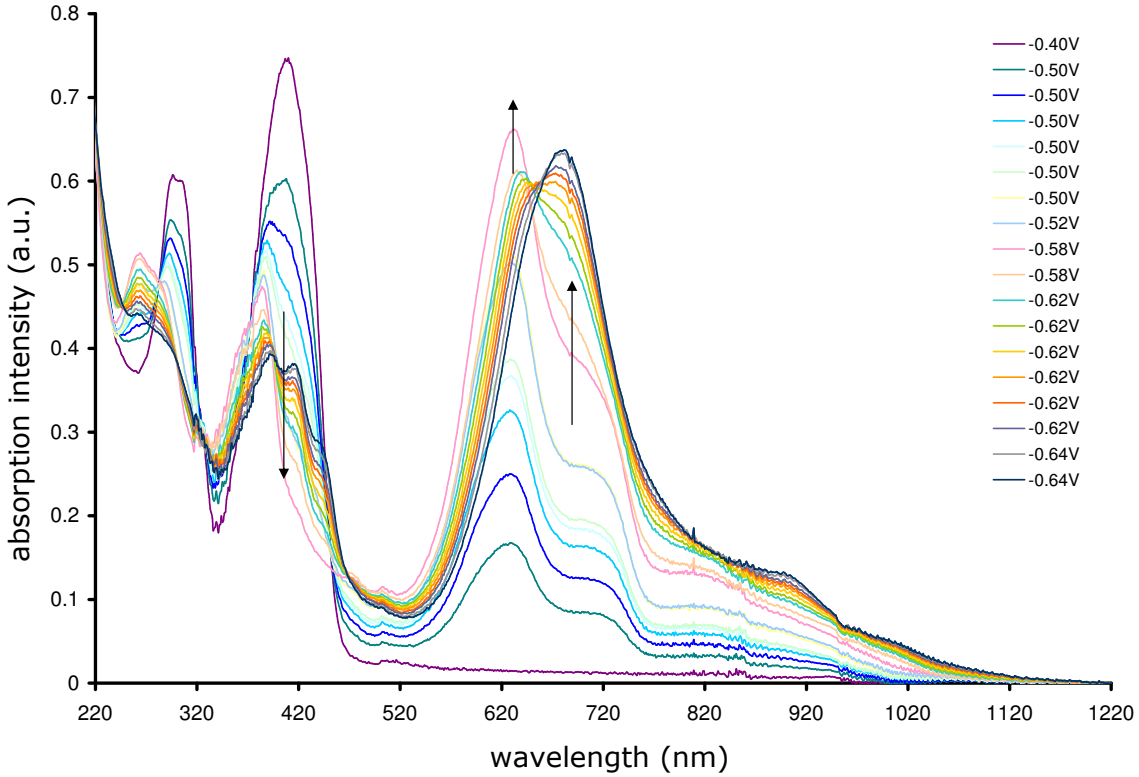

Figure 4.45: UV–vis spectroelectrochemistry of **BPEBf.CO$_2$Me**.

As the 626 nm band increases intensity it features a red-shifted shoulder at 710 nm. Eventually this shoulder, once the 626 nm band has reached a maximum, becomes a second, new, main band, with λ_{max} = 682 nm, suggesting generation of a doubly reduced anion. However, there is no second reduction event observed in the cyclic voltammogram. The lower energy series of bands exhibits a similar profile to that observed for **BPEBf.OMe**. This indicates that all three of these species undergo a single reduction process, although the reduced species is more stable in the methoxy– and ester–containing derivatives than in the *t*-butyl–substituted system. However, the reduced species is not stable for prolonged periods of time *i.e.* during the spectroelectrochemical study.

4.7 Summary and conclusions

A series benzofurazan– and benzothiadiazole–containing arylethynylenes have been prepared by Sonogashira cross-coupling various arylacetylenes with the relevant dibromo–heteroarene. This was seen as an opportunity to examine the effect of

switching the sulfur in the previously known arylethynyl–substituted benzothiadiazoles to oxygen. Furthermore, 2,5-bis(phenylethynyl)thiadiazole has been reported in the literature, whereas this thesis reports the first successful isolation and subsequent photophysical analysis of the oxygen analogue, 2,5-bis(phenylethynyl)-1,3,4-oxadiazole (**BPEOx**). **BPEOx** was isolated in low yields from the reaction of an acylhydrazide with an acylbenzotriazole. Furthermore, several compounds incorporating a mono–substituted benzofurazan moiety were prepared, allowing for the synthesis of two asymmetrical systems and the inverted analogue of the parent unsubstituted. Yields were generally good for the Sonogashira cross–coupled compounds.

Where possible, structures have been determined using X–ray crystallography on single crystals, and compared to calculated structures, optimised using DFT methods. There was shown to be excellent agreement between the observed and the calculated bond lengths (< 2.2 % discrepancy).

Of all the molecules in this chapter, **BPEOx** displayed the highest energy absorption and emission λ_{max}. It exhibits a much longer lifetime than the literature reported sulfur–containing analogue **BPETd**, whose absorption and emission are at slightly lower energies. Low temperature UV–vis absorption and fluorescence spectroscopy of **BPEOx** revealed well defined vibrational structure with a spacing corresponding to the A_1 symmetrical stretch of the N—N bond in oxadiazole.

In the benzofurazan systems the conformational restriction caused by the low temperature glass revealed some vibrational structure. However, all compounds display strong ICT character, characterised by broad emission spectra and large Stokes' shifts.

The benzofurazan and benzothiadiazole systems all exhibited high fluorescence quantum yields, $0.31 \leq \phi_f \leq 0.96$, and lifetimes of several nanoseconds, $2.1 \leq \tau_f \leq 5.8$ ns. Furthermore, they all exhibited two main bands in their room and low temperature absorption spectra. Using TD–DFT calculations, the first excited state, $S_1 \leftarrow S_0$, has been shown to correspond to the LUMO←HOMO transition for all the benzofurazan and benzothiadiazole derivatives, and all featured high oscillator strengths ($f < 0.70$). There is also a higher energy excited state predicted to have

a high oscillator strength; indeed in **BPEBtd** the oscillator strength for the third excited state, $S_3 \leftarrow S_0$, which corresponds to the LUMO←HOMO-1 transition, is larger than that calculated for the first excited state (f = 1.12 *c.f* 0.70 - see Table 4.10).

The addition of peripheral substituents (*t*-Bu, OMe, NH_2 and CO_2Me) on the benzofurazan– and benzothiadiazole–arylethynylenes was carried out in an attempt to elucidate the effect of electron–donating and electron–withdrawing substitutents on the molecules. The ester was observed to induce a hypsochromic shift in the emission spectrum, relative to **BPEBf**, and features an absorption maximum essentially the same as the parent. The electron–donating substituted systems feature a bathochromic shift relative to the parent, in the order *t*-Bu < OMe < NH_2. A dramatic increase in the quantum yield and lifetime was observed with substitution on the asymmetrical systems; appendage of a strongly electron–donating amine group raised the quantum yield 216 %, and the lifetime 207 %. This meant the radiative rate of decay remained comparable for the two systems (see Table 4.28). Furthermore, appendage of the amine group resulted in a solvatochromic shift of $\sim$ 5070 cm^{-1} relative to that observed for **PEBf**, which exhibits a solvatochromic shift of $\sim$ 2070 cm^{-1} (see Figure 4.32). The broad emission profiles and large Stokes' shifts are indicative of strong ICT character.

Quantum yields for the bis(arylethynyl)benzofurazan and benzothiadiazole derivatives were similar, whereas the benzothiadiazole derivatives displayed a slightly longer lifetime ($\sim$ 1 ns for each equivalent system). Otherwise, these two series of molecules exhibited very similar behaviour, and their radiative decay constants reflect this.

Preliminary electrochemical analysis revealed that **BPEOx** exhibited an irreversible oxidation and reduction, but further investigation is required to elucidate any more detail. The bis(arylethynyl)benzofurazan derivatives all exhibited a reversible reduction, expected for the electron–deficient benzofurazan ring, with the reduction potential following a similar trend to that observed by photophysical analysis with regards to the energy of the LUMO. Spectroelectrochemical analysis on three of the benzofurazan systems indicated that the reduced species was unstable

over prolonged periods of time, decomposing in the cell after reduction. All three systems displayed a similar profile upon reduction, but **BPEBf.CO_2Me** displayed the most stable reduced species, attributed to the electron–withdrawing ester.

5

Future Work and Conclusions

5.1 Future work

5.1.1 Thiophene derivatives

There are a several avenues that require exploring regarding the furthering of this work. So far, modification of the central ring species has shown that the photophysical properties of the molecule can be varied dramatically.

A complete set of derivatives incorporating the peripheral substitutents (R = *t*-Bu, OMe, NH_2, CO_2Me, CN and NO_2) for each set of systems *i.e.* **BPETO$_2$**, **BPEEDOT** and **BPEantTT**, would allow direct comparison to work done by Siddle *et al.*, with respect to the affect of stronger electron–donor and withdrawing groups on the photophysical properties of the different thiophene heterocycle derivatives.

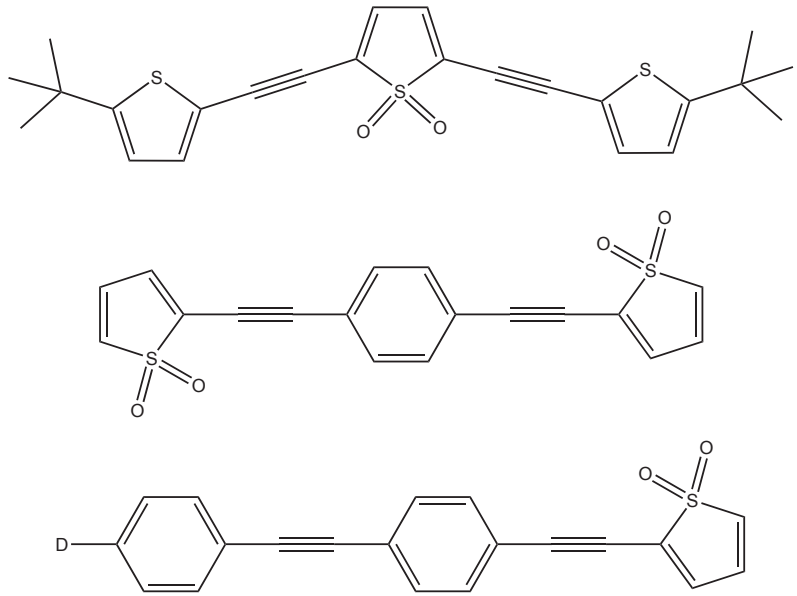

Figure 5.1: Thiophene-1,1-dioxide derivatives for potential future work.

The central position of the electron–deficient thiophene-1,1-dioxide in the oligomer resulted in a charge transfer, from the peripheral rings *in* towards the centre. The reverse process – thiophene-1,1-dioxide as the external ring in the three–ring motif – was not investigated. Equally, preparation of an asymmetric system – where one end of the oligomer features the electron withdrawing species and the other end features an electron–rich species – would enable investigation into what length the charge in these types of systems was able to transfer (see Figure 5.1). Also, use of thio-

phene and thiophene-1,1-dioxide in the same molecule would enable an appreciation of how the oxidised derivative behaves with its parent when separated by acetylene linkages – similar to work performed by Barbarella and co-workers who have already examined these compounds when directly bonded [77, 79], and for comparison with work performed by an earlier group member, Dr S R Rutter, who reported studies on 2,5-bis(thienylethynyl)thiophene in his thesis.

In light of the conjugation break across **BPEantXTT.tBu** and **BPEsynTT** it would be interesting to see whether, and indeed how well, charge could be transferred across the fused thiophene groups from a donor (D) to an acceptor (A) type moiety (see Figure 5.2). The appendage of an electron–donator on one end and an electron–withdrawing substituent on the opposite end would be a relatively trivial synthesis. Preliminary calculations indicate that the HOMO and LUMO would be localised over opposing halves of the molecule, suggesting extensive charge separation in the excited state.

For the molecules containing thiophene-1,1-dioxide, and thus subject to charge transfer, DFT calculations using the CAM-B3LYP functional should be performed, as this has been shown [196] to provide more accurate results for this type of system. This functional was not employed during the course of this work as the process is computationally intensive and the routine use of this functional has only recently become available on commercial packages (Gaussian–09).

5.1.2 Oxadiazole derivatives

An improved synthetic methodology is required for the preparation of **BPEOx** in order to allow for study of this system in greater detail. The 4 % yield in generating the final product needs to be circumvented; a substantial amount of the acyl hydrazide was left unreacted, believed to be due to a deactivating effect of the alkynyl group. Furthermore, preparation of methoxy– and cyano–substituted acylhydrazides and acylbenzotriazoles would enable a study on the effect of electron–donating and withdrawing substituents on this system's excited state properties. Ideally a crystal would be obtained for analysis using X–ray diffraction methods.

The isolated benzofurazan derivatives constitute a well–rounded series. Prepara-

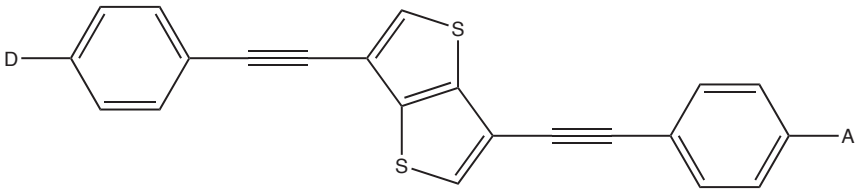

(a) **BPEantXTT** featuring donor and acceptor groups. D = donor group. A = acceptor group.

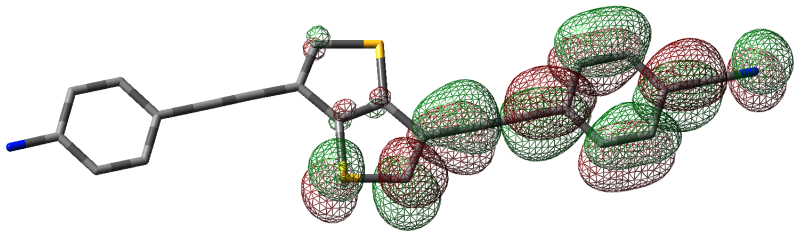

(b) **BPEantXTT** LUMO using GaussView.

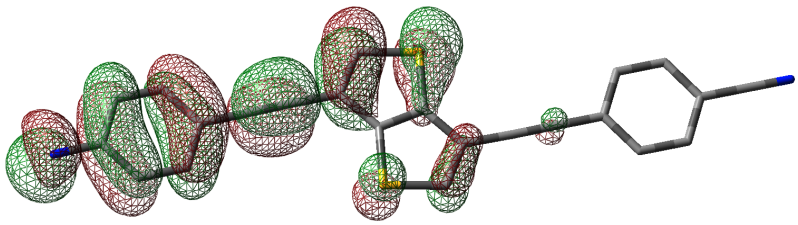

(c) **BPEantXTT** HOMO using GaussView.

Figure 5.2: Conceptual **BPEantXTT** derivative featuring donor and acceptor groups. TD–DFT calculations indicate localised HOMO and LUMO electron densities.

tion of new asymmetrical derivatives to complement the **PEBf.R** series, for instance with an electron–withdrawing ester, is being considered to see the effect of pulling electron–density away from the already electron–deficient benzofurazan moiety. Furthermore, preparation of a three–heterocycle system (see Figure 5.3) would allow examination of electron–deficiency over the whole species and would also remove the localisation effect of the electron–poor heterocycles, as all rings would experience the same electron deficiency. Preparation of other terminally substituted benzofurazan systems (see Figure 5.3) would enable observations as to the effect of stronger charge–injection on the inverted system **BBfEB**.

Additionally, as in the case for several of the thiophene derivatives mentioned above, the electron–deficient benzofurazan induces a charge transfer nature to the excited state of the systems, and as such the CAM–B3LYP functional should be

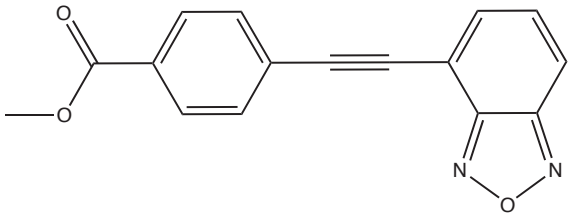

(a) **PEBf.R** derivative featuring an electron–withdrawing ester substituent.

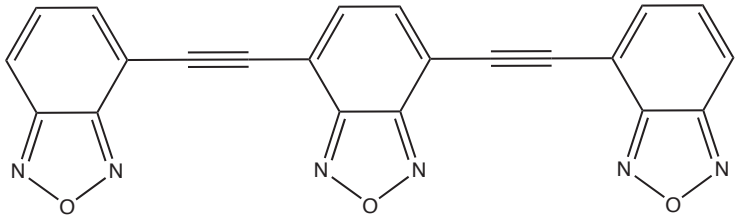

(b) All three ring positions featuring the benzofurazan heterocycle, **BBfEBf**.

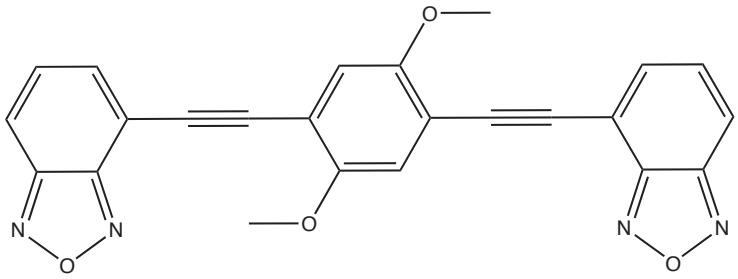

(c) Methoxy–substituted derivative of **BBfEB**.

Figure 5.3: Three potential novel benzofurazan–containing arylethynylenes.

used for further calculations on these systems.

The electrochemical characterisation of these materials can be more thoroughly investigated, to explore any possible oxidation process on those derivatives appended with R = NH_2 and OMe, as well as in different solvents to widen the solvent window. Also, use of a faster spectrometer for the UV–vis spectroelectrochemical analysis may allow for a fully reversible reduction, as it is believed that prolonged periods of applied potential caused deterioration of the products. Calculations should be performed on the anion of the compounds, to assess where the reduction occurs for these systems, and to consider what transitions are responsible for the absorption profiles shown for the reduction of **BPEBf.OMe** and **BPEBf.CO_2Me**.

The potential uses for these types of molecules have already been shown (see section 4.3.2, from page 129), but for these novel benzofurazan–derivatives, their

application as a DNA sensor could be considered, and compared to observations made for the benzothiadiazole derivatives by Neto *et al.*. [178] Furthermore, due to their absorption characteristics ($\lambda_{max} \sim 400$ nm for **BPEBf**), their application as a laser dye could be pursued.

5.2 Conclusion and summary

So far, the arylethynylenes have been divided on the basis of the heterocycle they contain. Here the unsubstituted parent systems (or with *t*-butyl where necessary), for which k_f was determined, are compared with each other and to the parent system 1,4-bis(phenylethynyl)benzene, **BPEB**.

As demonstrated in Figure 5.4, there is a distinct difference between the spectral profiles of the top five molecules and the bottom three. The oxadiazole, benzene, thiophene, EDOT and *anti*-thienothiophene derivatives all exhibit relatively narrow profiles, with some fine structure in the emission spectra due to the Franck Condon excited states rapidly relaxing to a planarized geometry. This is in contrast to the thiophene-1,1-dioxide, benzofurazan and benzothiadiazole derivatives, which exhibit broad, featureless absorption and emission spectra. This is characteristic of some degree of ICT, from the relatively electron–rich phenyl rings into the central core. This does not account for the spectra observed for **BPEOx**, as oxadiazole is known for its electron–deficiency.

Furthermore, the benzofurazan and benzothiadiazole derivatives are alone in featuring two distinct absorption bands, separated by $\sim$ 8790 cm^{-1}. Using TD–DFT calculations the lower absorption bands have been assigned to excitation in to the first excited state, attributed to the LUMO←HOMO transition, and the higher energy bands have been attributed to transitions into various upper excited states, S_n←S_0.

At low temperature, all systems exhibit a significant enhancement of vibrational structure in their absorption, excitation and emission spectral profiles, as the low temperature enforces the low energy planar state.

The quantum yields for the oxadiazole, benzofurazan and benzothiadiazole species are substantially higher ($\phi_f \geq 0.57$) than those for the thiophene derivatives ($0.12 \leq \phi_f \leq 0.43$). **BPEBf** and **BPEBtd** exhibit the longest fluorescence lifetimes, although **BPETO$_2$** displays a substantially longer lifetime than the other thiophene derivatives. **BPEantXTT.tBu** is alone in displaying phosphorescent decay at low temperature. This is highly unusual for an aryleneethynylene.

From this it can be shown that for those systems featuring electron density

	R–group	λ_{max} abs/nm	ε/ $M^{-1}cm^{-1}$	λ_{max} ex/nm	λ_{max} em/nm	Stokes' shift/cm^{-1}	PLQY ϕ_f (± 10 %)	lifetime τ_f / ns (± 0.1 ns)	Calculated k_f / ns^{-1} (± 14 %)
BPEB$^{\heartsuit}$	H	320	58 400	n/a	344	2180	0.85	0.53	1.6
BPET$^{\spadesuit}$	H	350	33 000	n/a	382	2390	0.20	0.24	0.83
BPEEDOT	H$^{\clubsuit}$	361	45 200	362	395	2380	0.12	0.13	0.92
BPETO$_2$	H	415	21 000	409	519	4830	0.24	1.1	0.22
BPEantTT	tBu	371	62 300	371	402	2080	0.43	0.38	1.13
BPEOx	H	304	31 900	303	357	4990	0.57$^{\diamondsuit}$	0.81$^{\diamondsuit}$	0.71
BPEBf	H	411	27 800	407	470	3290	0.80	3.1	0.26
BPEBtd	H	303/413	44 900	302/411	483	3630	0.85	4.1	0.21

Measurements recorded in toluene unless otherwise stated.
$^{\heartsuit}$ = data taken from work by Dr K S Findlay, previous group member. Recorded in cyclohexane.
$^{\spadesuit}$ = data taken from work published by Siddle *et al.* [114]
$^{\clubsuit}$ = compound prepared by Dr S R Rutter, previous group member.
$^{\diamondsuit}$ = measurements recorded in DCM.

Table 5.1: Arylethynylenes' photophysical properties.

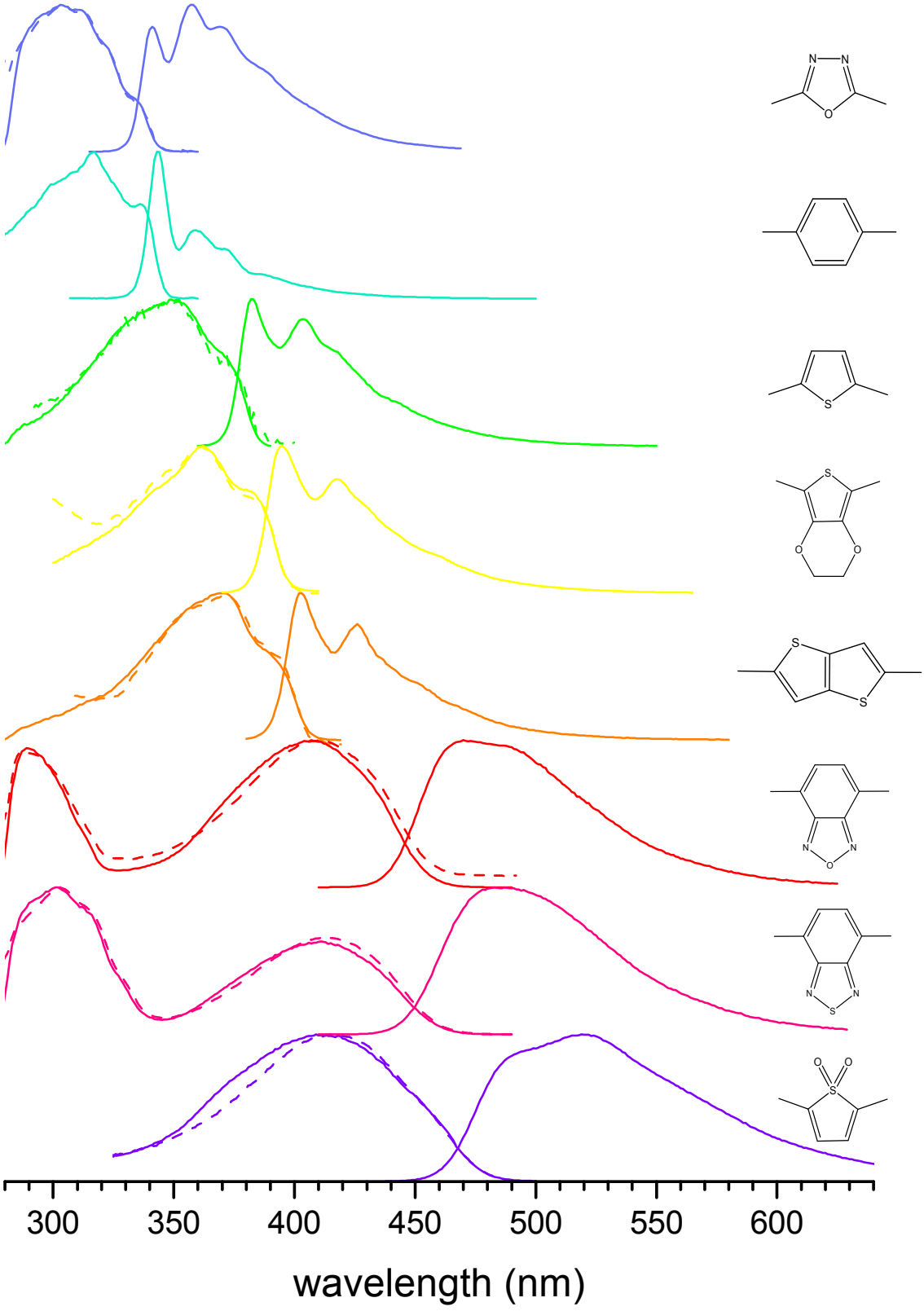

Figure 5.4: Arylethynylenes' absorption, excitation and emission spectra. Arranged to descend with decreasing energy of absorption.

delocalised evenly over the whole molecule in both the HOMO than the LUMO (as determined by using GaussView), *i.e.* systems without electron rich or deficient regions, such as **BPEB** and **BPEantTT.tBu**, the rates of radiative decay are high ($0.83 \leq k_f \leq 1.6$ ns^{-1}), and the absorption and emission profiles are relatively narrow. For the systems featuring a partially localised electron density in the LUMO, with electron deficient heterocycles, the radiative decay rates are comparatively low (see Table 5.1) and the spectral profiles are broader and unstructured.

The gratification comes in the doing, not in the results.

James Dean

6

Experimental

Introduction

All experiments were conducted in standard Quickfit© glassware. Where necessary, reactions were performed under an atmosphere of dry nitrogen using standard Schlenk techniques. Dry solvents were obtained dry from an Innovative Technologies Solvent Purification System and deoxygenated (bubbled through with N_2 or freeze–pump–thaw) prior to use (diethyl ether and tetrahydrofuran) and triethylamine was provided by the research group Prof. PJ Low. Starting materials were obtained from Sigma Aldrich, Acros Organics and Lancaster and used without further purification. The catalyst bis(triphenylphosphine)palladium (II) dichloride ($PdCl_2(PPh_3)_2$) was provided by the research group of Professor TB Marder and tetrakis(triphenylphosphine) palladium (0) ($Pd(PPh_3)_4$) was prepared from chemicals kindly provided by the research group of Prof. PJ Low.

Laboratory coat, safety spectacles and gloves were worn in accordance with the University of Durham Department of Chemistry safety policies. Synthetic experiments were performed in an efficient fume–hood, and COSHH assessments were completed on all chemicals. Waste materials were disposed after separation in accordance with the Department's and HSE regulations.

GC MS analyses were performed on an Agilent Technologies 6890 N gas chromatograph equipped with a 5973 inert mass selective detector and a 10 m fused silica capillary column (5 % cross-linked phenylmethylsilicone) using the following operating conditions: Injector temperature 250 °C, detector temperature 300 °C, the oven temperature was ramped from 70 °C to 280 °C at 20 °C min^{-1}. UHP helium was used as the carrier gas. MALDI mass spectrometry was performed on an Autoflex II ToF/ToF mass spectrometer (Bruker Daltonik GmBH), equipped with a 337 nm nitrogen laser, with analysis performed by a reflectron. *trans*-2-[3-(4-*tert*-Butylphenyl)-2-methyl-2-propenylidene]malonitrile (DCTB) was used as the matrix. Accurate mass analyses were performed on a Xevo QToF mass spectrometer (Waters Ltd., UK) equipped with an Agilent 7890 GC (Agilent Technologies UK Ltd., UK), set up to perform atmospheric pressure of solids analysis probe ionisation (ASAP) of positive ions. MS data was processed using MassLynx 4.1. Exact mass measurements utilised a lock–mass correction to provide < 3 mDa precision.

Exact mass measurement used Elemental Composition version 4.0 embedded within MassLynx 4.1 (Waters Ltd., UK).

Routine NMR spectra were collected using either a Varian Unity 300, Mercury 400, Avance 400 MHz Bruker, Varian Inova 500 or Varian 700 MHz instrument, and spectra analysed using Varian NMR software and MestReNova version 5.2.5. Chemical shifts are referenced to the residual protio impurities in the deuterated solvent (^{1}H) or the ^{13}C shift of the solvent (^{13}C). Solvent proton shifts (ppm); $CDCl_3$, 7.27 (s); CD_2Cl_2, 5.34 (t); $(CD_3)_2SO$, 2.50 (s); $C_2D_2Cl_4$, 5.91 (s).Solvent carbon shifts (ppm): $CDCl_3$, 77.2 (t); CD_2Cl_2, 54.0 (quin); $(CD_3)_2SO$, 39.5 (s); $C_2D_2Cl_4$, 73.3 (t).

Elemental analyses were performed by the Analytical Services of the Department of Chemistry University of Durham, using an Exeter Analytical Inc. CE-440 Elemental Analyser (C, H, N).

Melting points are reported uncorrected.

A full assignment of the NMR spectroscopic characterisation of the aryleneethynylenes is provided. 2D NMR spectroscopic techniques (COSY, HSQC and HMBC) were used to facilitate assignment of ^{1}H and ^{13}C chemical shifts. The intermediates prepared for this work which have already been reported in the literature have been characterised (^{1}H NMR spectroscopy and mass spectrometry and ^{13}C where available) and shown to agree with literature data. As such a full assignment of their NMR spectra is not provided here.

6.1 Thiophene Derivatives

6.1.1 2,5-bis(Trimethylsilyl)thiophene

Synthesis adapted from work by Furukawa *et al.* [127]

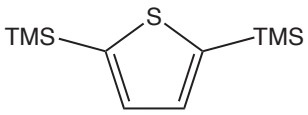

$C_{10}H_{20}SSi_2$

Mol. Wt.: 228.50 $gmol^{-1}$

Thiophene (0.8 mL, 10 mmol) was dissolved in dry THF (50 mL) and stirred at -78 °C for 30 minutes. *n*-Butyllithium (*n*-BuLi) (15.6 mL, 1.6M in hexanes, 25 mmol) was added dropwise *via* syringe, and the solution warmed to -20 °C and stirred for a further 30 minutes under N_2. After cooling back to -78 °C, chlorotrimethylsilane (TMSCl) (4 mL, 31 mmol) was added dropwise. After 10 minutes of stirring the solution was allowed to warm to room temperature. Water (3 mL) was added and the organic solvent was removed *in vacuo*. More water (10 mL) was added and the product was extracted with DCM. The organic layer was dried over $MgSO_4$ and the solvent removed *in vacuo* to yield a yellow-brown viscous oil (1.7 g). Preliminary NMR spectroscopic analysis of this material revealed it to be a mixture of both the mono- and bis-trimethylsilylated thiophene compounds. The oil was re-dissolved in THF (40 mL), and reacted with additional n-BuLi (6.5 mL, 1.6M in hexanes, 10 mmol) and TMSCl (4 mL, 31 mmol) under the original conditions. The reaction was quenched and the product was isolated as a yellow oil (1.7 g, 75 %).
^{1}H NMR ($CDCl_3$, 300 MHz): δ 7.30 (2 H, s), 0.34 (18 H, s). MS (EI): (m/z) 228 [M], 213 [M - CH_3].

6.1.2 2,5-bis(Trimethylsilyl)thiophene-1,1-dioxide

Synthesis adapted from work by Furukawa *et al.* [127]

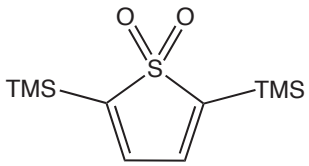

$C_{10}H_{20}O_2SSi_2$

Mol. Wt.: 260.50 $gmol^{-1}$

2,5-bis-(Trimethylsilyl)thiophene (500 mg, 2.27 mmol) was dissolved in DCM (20 mL) and, separately, *m*-CPBA (1.2 g, 7 mmol) was dissolved in DCM (20 mL). The two solutions were combined by dropwise addition of the *m*-CPBA solution and the resulting solution was stirred at room temperature. After 3 h the solution turned an opaque creamy colour. After stirring overnight, saturated aqueous K_2CO_3 solution was added to quench the reaction and neutralise the solution. The organic layer was separated and washed with more aqueous K_2CO_3, extracted with DCM and dried over anhydrous $MgSO_4$. The solvent was reduced *in vacuo* to yield a light brown solid (420 mg), which was purified using column chromatography on silica gel, eluting with hexane and DCM (1:1) to yield **2,5-bis(trimethylsilyl)thiophene-1,1-dioxide** (330 mg, 56 %) as a cream/brown solid.
^{1}H NMR ($CDCl_3$, 400 MHz): δ 6.74 (2 H, s), 0.34 (18 H, s). MS (EI): (m/z) 260 [M], 245 [M - CH_3].

6.1.3 2,5-Dibromothiophene-1,1-dioxide

Synthesis adapted from work by Furukawa *et al.* [127]

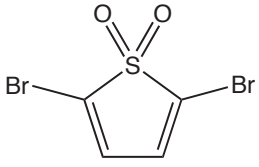

$C_4H_2Br_2O_2S$

Mol. Wt.: 273.93 $gmol^{-1}$

A solution of bromine in DCM (0.4M solution, 0.76 mmol, 1.9 mL) was added carefully to 2,5-bis(trimethylsilyl)thiophene-1,1-dioxide (100mg, 0.38 mmol) and $AgBF_4$ (220 mg, 1.14 mmol) dissolved in DCM (20 mL), in a aluminium foil–covered vessel.

Fumes were evolved during this step, necessitating slow addition. After complete addition of the bromine solution, the reactants were stirred at 0 °C for 1 h after which DCM (10 mL) was added, and the solution was filtered through a silica plug, eluting with DCM. The resulting solution was reduced *in vacuo* to afford **2,5-dibromothiophene-1,1-dioxide** (66 mg, 60 %) as a light beige solid.
^{1}H NMR ($CDCl_3$, 300 MHz): δ 6.90 (s). $^{13}C\{^{1}H\}$NMR ($CDCl_3$, 75 MHz): δ 128.5, 119.5. MS (EI): (m/z) 272-274-276 [M *including splitting characteristic of isotopic abundances of dibrominated species* $C_4H_2Br_2O_2S$].

6.1.4 2,5-bis(Phenylethynyl)thiophene-1,1-dioxide [$\mathbf{BPETO_2}$]

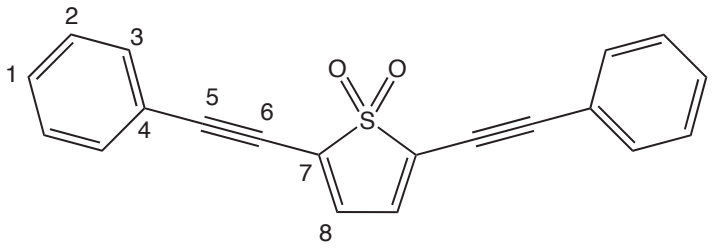

$C_{20}H_{12}O_2S$

Mol. Wt.: 316.37 $gmol^{-1}$

2,5-Dibromothiophene-1,1-dioxide (550 mg, 2 mmol) and phenylacetylene (2.5 equivalents, 0.6 mL, 5 mmol) were dissolved in dry THF (15 mL), and the solution degassed through four freeze-pump-thaw cycles. Under a flow of N_2, dry Et_3N (0.7 mL, 5 mmol), CuI (50 mg, 13 mol%) and $PdCl_2(PPh_3)_2$ (180 mg, 13 mol%) were added, and the mixture stirred for 30 minutes. The solvent of the resulting suspension was removed under reduced pressure and the solid product purified by column chromatography, eluting with hexane/DCM (1:1) on silica gel. The product was recrystallised from warmed ether/ cold hexane to yield **2,5-bis(phenylethynyl)thiophene-1,1-dioxide [$\mathbf{BPETO_2}$]** as orange needles (365 mg, 58 %). M.P.: 178 – 179 °C.
^{1}H NMR ($CDCl_3$, 500 MHz): δ 7.61 (4 H, d, ^{3}J 7.5 Hz, **3**), 7.16 (6 H, m, **1 and 2**), 6.69 (2 H, s, **8**). $^{13}C\{^{1}H\}$NMR ($CDCl_3$, 126 MHz): δ 132.3 (**3**), 130.1 (**1**), 128.5 (**2**),

128.1 (**8**), 126.8 (**6**), 121.05 (**4**), 104.1 (**5**), 77.4 (**7**). Acc. MS (ES^+): (m/z) calcd. for $[M + H]^+$ 317.06308, for $[M + Na]^+$ 339.04502; found for $[M + H]^+$, 317.06310, for $[M + Na]^+$ 339.04501. Elemental analysis: expected ($C_{20}H_{12}O_2S$): C, 75.93 %; H, 3.82 %; found: C, 75.78 %, H, 3.76 %.

Crystal data for **$BPETO_2$** (06SRV345): $C_{20}H_{14}O_2S$ (see Figure 3.29, page 79), M = 318.37, monoclinic, space group $P21/c$ (No. 14), a = 14.1518(4), b = 6.29430(10), c = 18.7696(5) Å, β = 109.7410(10) °, V = 1573.65(7) Å^3, Z = 4, D_c = 1.344 g/cm^3, F_{000} = 664, CuKα radiation, λ = 1.54178 Å, T = 120(2) K, $2\theta_{max}$ = 121.1 °, 5822 reflections collected, 2146 unique (R_{int} = 0.0470). Final *GooF* = 1.049, *R1* = 0.0633, *wR2* = 0.1693, R indices based on 1773 reflections with I > 2σ(I) (refinement on F^2), 244 parameters, 0 restraints. Lp and absorption corrections applied, μ = 1.877 mm^{-1}.

6.1.5 2,5-bis(4-Methoxyphenylethynyl)thiophene-1,1-dioxide [$BPETO_2$.OMe]

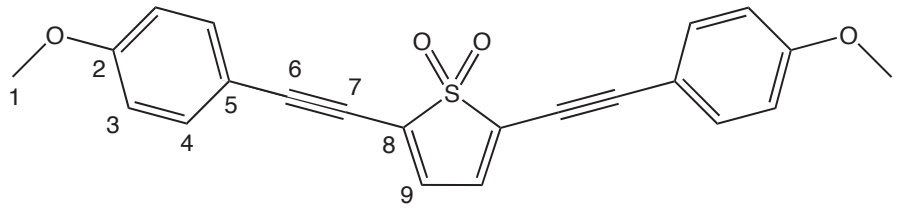

$C_{22}H_{16}O_4S$

Mol. Wt.: 376.43 gmol^{-1}

2,5-Dibromothiophene-1,1-dioxide (550 mg, 2 mmol) was placed in a Schlenk flask and the reaction procedure from **6.1.4** was followed, using 4-ethynylanisole (2.5 equivalents, 0.6 mL, 5 mmol). The resultant suspension was reduced *in vacuo* and the solid product purified initially by column chromatography, eluting with hexane/DCM (2:1) on silica gel, and secondly by Chromatotron chromatography on 4 mm silica/gypsum plates, eluting with hexane/DCM (1:1). The red powder (product) was recrystallised from diethyl ether to yield **2,5-bis(4-ethynylanisole)thiophene-1,1-dioxide [$BPETO_2$.OMe]** as orange needles (300 mg, 40 %). M.P.: 156 – 158 °C.

^{1}H NMR ($CDCl_3$, 500 MHz): δ 7.51 (4 H, d, ^{3}J 9 Hz, **4**), 6.89 (4 H, d, ^{3}J 9 Hz, **3**), 6.82 (2 H, s, **9**), 3.84 (6 H, s, **1**). $^{13}C\{^1H\}$NMR ($CDCl_3$, 126 MHz): δ 161.3 (**2**), 134.3 (**4**), 127.5 (**9**), 126.8 (**7**), 114.5 (**3**), 113.4 (**5**), 104.8 (**6**), 77.1 (**8**), 55.7 (**1**). Acc. MS. (AP+): (m/z) calcd. for $[M + H]^+$ 377.0834; found for $[M + H]^+$ 377.0848. Elemental analysis: expected ($C_{22}H_{16}O_4S$): C, 70.20%; H, 4.28%; found: C, 69.4%, H, 5.03%.

Crystal data for **BPETO$_2$.OMe** (06SRV367): $C_{22}H_{16}O_4S$ (see Figure 3.30, page 80), M = 376.41, monoclinic, space group $C2/c$ (No. 15), $a = 32.2351(18)$, $b = 6.1529(3)$, $c = 9.1323(5)$ Å, $\beta = 94.304(2)$ °, $V = 1806.19(17)$ Å^3, $Z = 4$, $D_c = 1.384$ g/cm^3, $F_{000} = 784$, MoKα radiation, $\lambda = 0.71073$ Å, $T = 293(2)$ K, 2 $\theta_{max} = 58.3$ °, 10247 reflections collected, 2414 unique ($R_{int} = 0.0345$). Final $GooF = 1.052$, $R1 = 0.0367$, $wR2 = 0.0964$, R indices based on 2170 reflections with $I > 2\sigma(I)$ (refinement on F^2), 124 parameters, 0 restraints. Lp and absorption corrections applied, $\mu = 0.205$ mm^{-1}.

6.1.6 2,5-bis(4-methylester phenylethynyl)thiophene-1,1-dioxide [BPETO$_2$.CO$_2$Me]

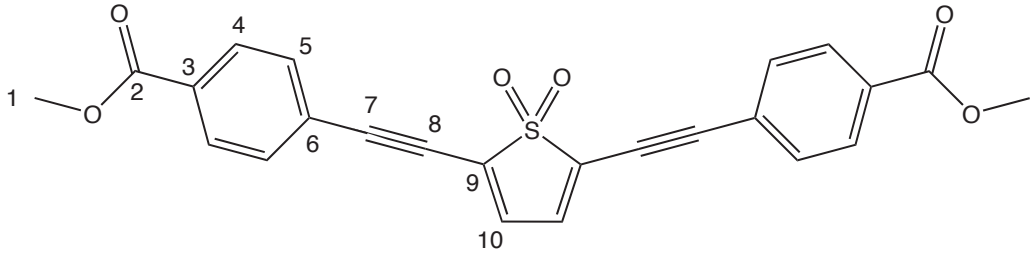

$C_{24}H_{16}O_6S$

Mol. Wt.: 432.45 gmol^{-1}

2,5-Dibromothiophene-1,1-dioxide (176 mg, 0.64 mmol) was placed in a Schlenk flask and the reaction procedure from **6.1.4** was followed with 4-(methylester)phenylacetylene (225 mg, 1.4 mmol). No precipitate had formed after 1 h, so the reaction was stirred at 60 °C over night. TLC analysis indicated no starting material after 12 h. The resultant suspension was chromatographed through a silica gel plug, with ether eluant, and then DCM eluant. The DCM fraction was slightly luminous

and was therefore reduced *in vacuo* and the remaining solid was chromatographed further using a ether/DCM gradient elution. At 3:1 DCM/ether (v/v) a yellow fraction was collected. This was evaporated under reduced pressure. **2,5-bis(4-methylester phenylethynyl)thiophene-1,1-dioxide [$BPETO_2.CO_2Me$]** was isolated as a yellow/orange solid (25 mg, 9 %).

^{1}H NMR ($CDCl_3$, 400 MHz): δ 8.05 (4 H, d, ^{3}J 8 Hz, **5 or 4**), 7.65 (4 H, d, ^{3}J 8 Hz, **4 or 5**), 6.97 (2 H, s, **2**), 3.94 (6 H, s, **1**).

No other characterisation was performed on this sample, see results and discussion (section 3.3.1, page 80).

6.1.7 2,5-bis(4-Cyanophenylethynyl)thiophene-1,1-dioxide [$BPETO_2.CN$]

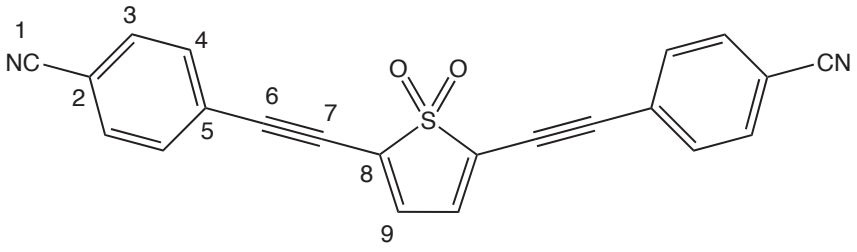

$C_{22}H_{10}N_2O_2S$

Mol. Wt.: 366.39 $gmol^{-1}$

In a Schlenk flask were placed 2,5-dibromothiophene-1,1-dioxide (274 mg, 1 mmol) and 4-ethynylbenzonitrile (2.2 equivalents, 277 mg, 2.2 mmol). The reaction procedure from **6.1.4** was followed. No precipitation was present after 1 h, and TLC analysis indicated presence of starting material after 1 h, so the reaction was heated to 60 °C and allowed to stir over night. After 15 h the resultant suspension was reduced *in vacuo* and the black, crude product eluted through a silica gel plug with ether (150 mL). Column chromatography on silica gel and ether elutant, with increasing proportions of DCM, was initiated. A red powder, **2,5-bis(4-cyanophenylethynyl)thiophene-1,1-dioxide [$BPETO_2.CN$]**, was isolated when the solvent was removed under reduced pressure (20 mg, 5 %).

^{1}H NMR ($CDCl_3$, 400 MHz): δ 7.70 (4 H, m, **3 or 4**), 7.37 (6 H, m, **4 or 3 and**

9). MS (MALDI+): (m/z) 389.1 $[M + Na]^+$, 339 $[M - CN]^+$.

For more information regarding this compound see results and discussion (section 3.3.1, page 80).

6.1.8 2,5-Diiodo-3,4-ethylenedioxythiophene

Method adapted from work by Zotti *et al.*. [117]

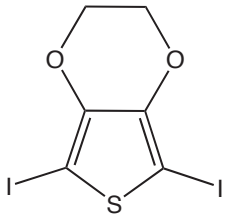

$C_6H_4I_2O_2S$

Mol. Wt.: 393.97 $gmol^{-1}$

Under an atmosphere of nitrogen, 3,4-ethylenedioxy thiophene (2.7 g, 19 mmol) and N-iodosuccinimide (9.0 g, 40 mmol) were dissolved in dry DMF (100 mL), and stirred at room temperature for 3 h. The resulting solution was poured into distilled water (200 mL) and extracted with DCM (4 × 30 mL aliquots). The organic fractions were collected and dried over $MgSO_4$, and then reduced *in vacuo*. The isolated solid was eluted through a silica plug (chloroform eluant) and evaporated to dryness to afford **2,5-diiodo-3,4-ethylenedioxy thiophene** (5.3 g, 70 %) as an off–white solid.

^{1}H NMR ($CDCl_3$, 400 MHz): δ 4.26 (4 H, s). MS (EI): m/z 394 [M].

6.1.9 2,5-bis(4-Methoxyphenylethynyl)-3,4-ethylenedioxythiophene [BPEEDOT.OMe]

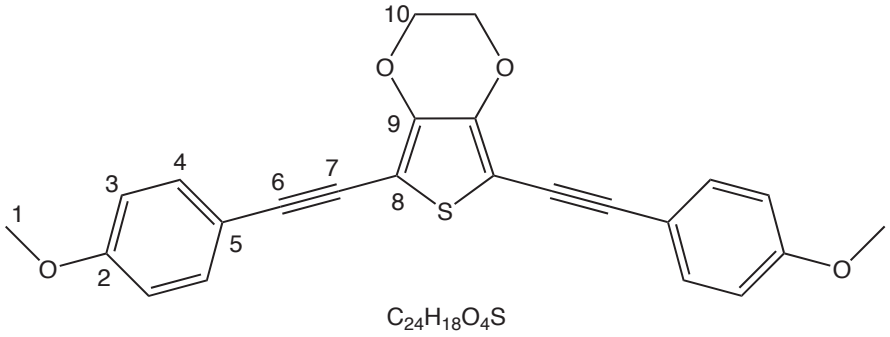

$C_{24}H_{18}O_4S$

Mol. Wt.: 402.46 $gmol^{-1}$

2,5-Diiodo-3,4-ethylenedioxy thiophene (930 mg, 2.36 mmol) and 4-ethynylanisole (0.65 mL, 4.8 mmol) were dissolved in a mixture of Et_3N (20 mL) and THF (15 mL) in a Schlenk flask. The mixture was degassed through five freeze-pump-thaw cycles and back filled with nitrogen. Under a blanket of N_2, CuI (4.5 mg, 1 mol%) and $Pd(PPh_3)_4$ (55 mg, 2 mol%) were added and the mixture allowed to stir overnight. The reaction was monitored by TLC for presence of starting materials. After 48 h the solvent was removed under reduced pressure and the residue eluted with diethyl ether through a silica plug. The ether fractions were combined and reduced *in vacuo*. The remaining solid was absorbed on to silica and chromatographed on silica gel (hexane/ether 1:5 – 5:2 gradient elution according to optimized separation as determined by TLC analysis). This afforded product **2,5-bis(4-methoxyphenylethynyl)-3,4-ethyldioxythiophene [BPEEDOT.OMe]** (410 mg, 43%) as a red/orange solid. M.P. = 162 – 164 °C.

^{1}H NMR ($CDCl_3$, 700 MHz): δ 7.46 (4 H, d, ^{3}J 7 Hz, **4**), 6.86 (4 H, d, ^{3}J 7 Hz, **3**), 4.31 (4 H, s, **10**), 3.82 (6 H, s, **1**). $^{13}C\{^1H\}$NMR ($CDCl_3$, 176 MHz): δ 159.8 (**2**), 142.7 (**9**), 133.1 (**4**), 114.9 (**5**), 114.0 (**3**), 99.7 (**7 or 8**), 96.7 (**6**), 78.3 (**8 or 7**), 64.8 (**10**), 55.3 (**1**). Acc. MS (AP+): (m/z) calcd. for $[M + H]^+$ 403.1004; found for $[M + H]^+$ 403.1012. Elemental analysis: expected ($C_{24}H_{18}O_4S$): C, 71.62 %; H, 4.51 %; found: C, 71.01 %; H, 5.11 %.

Crystal data for **BPEEDOT.OMe** (09SRV340): $C_{24}H_{18}O_4S$ (see Figure 3.31, page 81), M = 402.44, colourless block, 0.40 × 0.36 × 0.12 mm^3, triclinic, space group

P-1 (No. 2), a = 8.1324(5), b = 8.8069(5), c = 14.2035(8) Å, α = 99.4190(10), β = 93.8120(10), γ = 96.7300(10) °, V = 992.82(10) Å^3, Z = 2, D_c = 1.346 g/cm^3, F_{000} = 420, Bruker SMART 1 K CCD Detector, MoKα radiation, λ = 0.71073 Å, T = 120(2) K, $2\theta_{max}$ = 56.6 °, 11037 reflections collected, 4873 unique (R_{int} = 0.0210). Final *GooF* = 1.043, $R1$ = 0.0372, $wR2$ = 0.0908, R indices based on 4047 reflections with I > 2σ(I) (refinement on F^2), 264 parameters, 0 restraints. Lp and absorption corrections applied, μ = 0.191 mm¹.

6.1.10 2,5-bis(4-Cyanophenylethynyl)-3,4-ethylenedioxythiophene [BPEEDOT.CN]

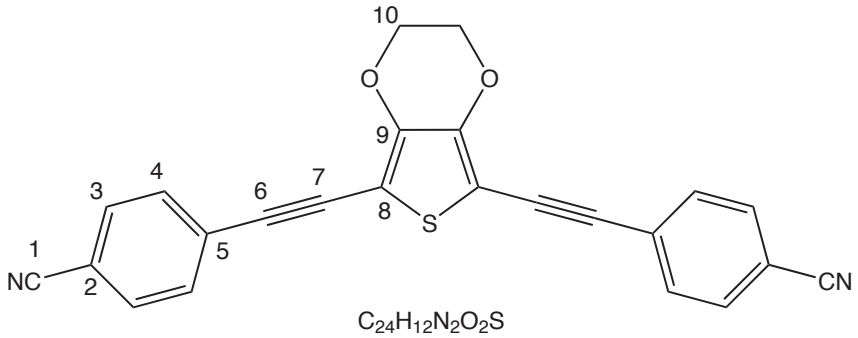

$C_{24}H_{12}N_2O_2S$

Mol. Wt.: 392.43 gmol^{-1}

2,5-Diiodo-3,4-ethylenedioxythiophene (423 mg, 1.1 mmol) and 4-ethynylbenzonitrile (300 mg, 2.36 mmol) were dissolved in a mixture of Et_3N (15 mL) and THF (10 mL) in a Schlenk flask. The mixture was degassed through three freeze-pump-thaw cycles and back filled with nitrogen. Under a blanket of N_2 CuI (2 mg, 1 mol%) and $PdCl_2(PPh_3)_2$ (15 mg, 2 mol%) were added and the mixture allowed to stir at 60 °C. After 48 h the suspension was filtered through a silica plug, eluting with hexane (200 mL) and then ether (500 mL). The fractions were evaporated to dryness and redissolved in a minimum of hot hexane, from which precipitated a highly luminescent yellow solid, **2,5-bis(4-cyanophenylethynyl)-3,4-ethyldioxythiophene [BPEEDOT.CN]** (200 mg, 55 %). M.P. = 258 – 260°C.

^{1}H NMR ($CDCl_3$, 500 MHz): δ 7.60 (8 H, dd, ^{3}J 8.8 Hz, **3 and 4**), 4.35 (4 H, s, **10**).

^{13}C{^{1}H}NMR ($CDCl_3$, 126 MHz): δ 144.4 (**9**), 132.3 (**3 or 4**), 132.0 (**4 or 3**), 127.7 (**1, 2, 5 or 6**), 118.7 (**1, 2, 5 or 6**), 111.9 (**1, 2, 5 or 6**), 100.2 (**8**), 95.6 (**1, 2, 5 or**

6), 84.3 (**7**), 65.1 (**10**). Acc. MS (AP+): (m/z) calcd. for $[M + H]^+$ 393.0698; found for $[M + H]^+$ 393.0715. Elemental analysis: expected ($C_{24}H_{12}N_2O_2S$): C, 73.45 %; H, 3.08 %; N, 7.13 %; found: C, 73.96 %; H, 3.07 %; N, 7.33 %.

Crystal data for **BPEEDOT.CN** (09SRV344): $C_{24}H_{12}N_2O_2S$ (see Figure 3.32, page 82), M = 392.42, orange needle, 0.40 × 0.12 × 0.08 mm^3, triclinic, space group *P*-1 (No. 2), a = 5.0890(9), b = 13.626(2), c = 14.075(2) Å, α = 79.036(3), β = 82.199(4), γ = 81.678(3) °, V = 942.2(3) $Å^3$, Z = 2, D_c = 1.383 g/cm^3, F_{000} = 404, Bruker SMART 1K CCD Detector, MoKα radiation, λ = 0.71073 Å, T = 120(2) K, $2\theta_{max}$ = 50.1 °, 8263 reflections collected, 3304 unique (R_{int} = 0.0573). Final *GooF* = 1.018, $R1$ = 0.0579, $wR2$ = 0.1308, R indices based on 2126 reflections with I > 2σ(I) (refinement on F^2), 262 parameters, 0 restraints. Lp and absorption corrections applied, μ = 0.195 mm^{-1}.

6.1.11 2,5-Dibromo-3,4-ethylenedioxythiophene

Following method by Tran-Van *et al.* [131]

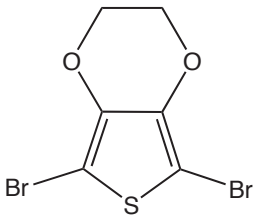

$C_6H_4Br_2O_2S$

Mol. Wt.: 299.97 $gmol^{-1}$

3,4-Ethylenedioxythiophene (3.0 g, 21 mmol) and N-bromosuccinimide (8.0 g, 45 mmol) were dissolved in chloroform and glacial acetic acid (1:1 v/v, 100 mL), and stirred at room temperature for 3 h. The resulting solution was poured into distilled water (200 mL) and neutralised by addition of $NaHCO_3$. The solution was extracted into DCM (4 × 30 mL aliquots), the organic fractions collected, combined and dried over $MgSO_4$, and then reduced *in vacuo*. The isolated solid was eluted through a silica plug with chloroform and evaporated to dryness to afford **2,5-dibromo-3,4-ethylenedioxy thiophene** (4.4 g, 70 %) as a cream solid.

^{1}H NMR ($CDCl_3$, 400 MHz): δ 4.27 (4 H, s). MS (EI): (m/z) 298-300-302 [M

including splitting characteristic of isotopic abundances for dibrominated species $C_6H_4Br_2O_2S$].

6.1.12 2,5-Dibromo-3,4-ethylenedioxy thiophene-1,1-dioxide

Following method by Berlin *et al.* [89]

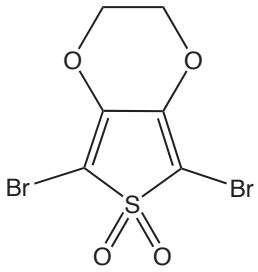

$C_6H_4Br_2O_4S$

Mol. Wt.: 331.97 $gmol^{-1}$

2,5-Dibromo-3,4-ethylenedioxythiophene (1.6 g, 5.3 mmol) and *m*-CPBA (2.3 g, 13.5 mmol) were dissolved in CH_2Cl_2 (40 mL) and stirred at room temperature over night. The reaction mixture was filtered and the filtrate washed with aqueous sodium bicarbonate (2 × 50 mL) and then water (2 × 50 mL). The organic layer was dried over $MgSO_4$, filtered, and reduced *in vacuo* to leave an orange residue. Analysis by TLC revealed multiple spots so the isolated solid was chromatographed on silica, eluting with DCM/Petroleum ether (4:1 v/v). **2,5-dibromo-3,4-ethylenedioxy thiophene-1,1-dioxide** was collected as a yellow solid (420 mg, 40 %). The compound was found to decompose at room temperature and hence was stored under nitrogen in the freezer.

^{1}H NMR ($CDCl_3$, 400 MHz): δ 4.49 (4 H, s). MS (EI): (m/z) 330-332-334 [M *including splitting characteristic of isotopic abundances of dibrominated species* $C_6H_4Br_2O_4S$]

6.1.13 2,5-bis(Phenylethynyl)-3,4-ethylenedioxy thiophene-1,1-dioxide [BPEEDOTO$_2$.tBu]

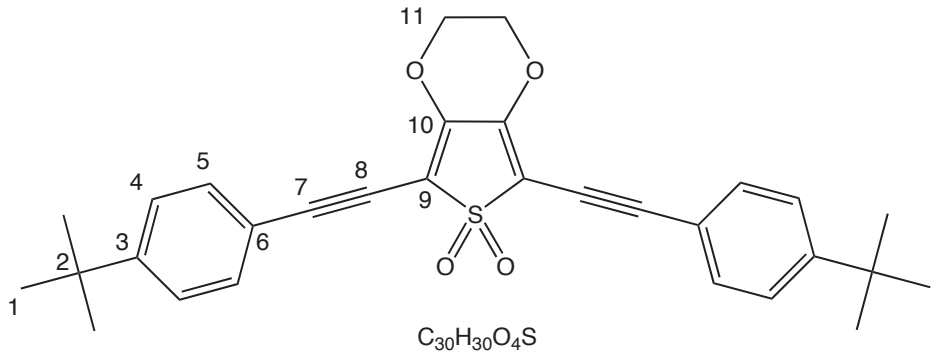

$C_{30}H_{30}O_4S$

Mol. Wt.: 486.62 gmol^{-1}

In an oven-dried Schlenk flask 2,5-dibromo-3,4-ethylenedioxythiophene-1,1-dioxide (250 mg, 0.75 mmol) and 4-*t*-butylphenylacetylene (240 mg, 0.28 mL, 1.5 mmol) were dissolved in Et_3N (15 mL) and THF (10 mL) and degassed through 4 freeze-pump-thaw cycles. The reaction vessel was back-filled with nitrogen, and the solution heated to 50 °C. Under a blanket of N_2 CuI (3 mg, 2 mol%) and $Pd(PPh_3)_4$ (18 mg, 2 mol%) were added and the reaction mixture heated to 70 °C and allowed to stir for 24 h. The deep red suspension was evaporated to dryness and the residue remaining was eluted through a silica plug with ether. The orange solid isolated was absorbed onto silica and chromatographed on silica gel, eluting initially with 1:1 hexane/ether and finally with 3:2 ether/hexane. Product **2,5-bis(4-*t*-butylphenylethynyl)-3,4-ethylenedioxythiophene-1,1-dioxide** [**BPEEDOTO$_2$.tBu**] was isolated as a yellow powder (40 mg, 11 %).

^{1}H NMR (CD_2Cl_2, 700 MHz): δ 7.46 (4 H, d, ^{3}J 7 Hz, **5**), 7.39 (4 H, d, ^{3}J 7 Hz, **4**), 4.51 (4 H, s, **11**), 1.30 (18 H, s, **1**). ^{13}C{^{1}H}NMR (CD_2Cl_2, 176 MHz): δ 153.6 (**3**), 149.2 (**10**), 131.8 (**5**), 125.9 (**4**), 118.7 (**6**), 103.8 (**7, 8 or 9**), 103.7(**7, 8 or 9**), 73.5 (**8 or 9**), 66.7 (**11**), 35.1 (**2**), 31.0 (**1**). Acc. MS (AP+): (m/z) Calcd. for [M + H]$^+$ 487.1945; Found for [M + H]$^+$ 487.1943.

There was insufficient material for elemental analysis of this compound after completion of the photophysical analysis.

Crystal data for **BPEEDOTO$_2$.tBu** (09SRV317): $C_{30}H_{30}O_4S$, M = 486.60, orange

needle, 0.40 × 0.10 × 0.08 mm^3, monoclinic, space group $P21/n$ (No. 14), a = 16.4620(8), b = 7.2069(3), c = 23.1514(14) Å, β = 107.172(6) °, V = 2624.2(2) $Å^3$, Z = 4, D_c = 1.232 g/cm^3, F_{000} = 1032, Xcalibur, Sapphire3, Gemini ultra, MoKα radiation, λ = 0.71073 Å, T = 120(2) K, $2\theta_{max}$ = 50.1°, 19062 reflections collected, 4640 unique (R_{int} = 0.0789). Final $GooF$ = 0.865, $R1$ = 0.0508, $wR2$ = 0.0696, R indices based on 2544 reflections with I > 2σ(I) (refinement on F^2), 322 parameters, 0 restraints. Lp and absorption corrections applied, μ = 0.156 mm^{-1}.

6.2 Thienothiophene Derivatives

6.2.1 3-(Carboxymethylsulfanyl)thiophene

Synthesis adapted from work by Frère *et al.* [134]

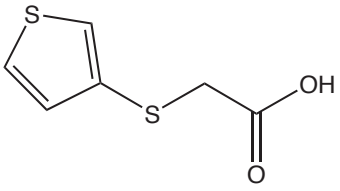

$C_6H_6O_2S_2$

Mol. Wt.: 174.24 $gmol^{-1}$

3-Bromothiophene (4.76 g, 30.7 mmol) was dissolved in dry diethyl ether (40 mL), and stirred at -78 °C under a nitrogen atmosphere. To this was added *n*-BuLi (12.9 mL, 2.5 M in hexane, 32.2 mmol), and stirring continued for 20 mins during which time the lithium salt was seen to have precipitated. Elemental sulfur (0.99 g, 32.2 mmol) was added and stirring continued, under N_2 at -78 °C for 30 mins. The reaction mixture quickly turned an opaque yellow. Separately a solution of potassium bromoacetate was prepared: bromoacetic acid (4.85 g, 35.2 mmol) was dissolved in THF (15 mL) and potassium carbonate (4.85 g, 35.2 mmol) was dissolved in water (20 mL) and the two solutions combined slowly. The potassium bromoacetate was added to the main reaction vessel over 30 mins. A white salt had precipitated by completion of the addition, and the reaction vessel was stirred for an hour at 55 °C. The reaction mixture was allowed to cool, and water was added until the salt had

dissolved. The organic layer was separated and the aqueous layer acidified by 2 M HCl. This aqueous layer was washed with several aliquots of diethyl ether and the organic fractions combined and dried over $MgSO_4$ and reduced *in vacuo* to afford **3-(carboxymethylsulfanyl)thiophene** as a brown oil (5 g, 98 %).
^{1}H NMR ($CDCl_3$, 400 MHz): δ 9.12 (1H, broad s), 7.31 (2H, m), 7.08 (1H, d, ^{4}J 3.2 Hz), 3.55 (2H, m). ^{13}C{^{1}H}NMR ($CDCl_3$, 125 MHz): δ 176.23, 130.52, 130.02, 126.61, 126.4, 37.78. MS (EI): (m/z) 174 [M].

6.2.2 Thieno[3,2-*b*]thiophen-4[5H]-one

Synthesis adapted from work by Frère *et al.* [134]

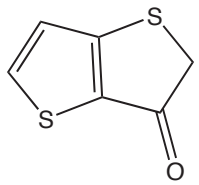

$C_6H_4OS_2$

Mol. Wt.: 156.23 gmol^{-1}

3-(Carboxymethylsulfanyl)thiophene (2 g, 11.6 mmol), under a nitrogen atmosphere, was dissolved in dry diethyl ether (50 mL). To this was added thionyl chloride (4.15 g, 35 mmol) and the solution stirred at reflux for 4 h. Solvent and any excess thionyl chloride were subsequently removed under reduced pressure, and the residue re-dissolved in 1,2-dichloroethane (60 mL). To this mixture was added $AlCl_3$ (1.6 g, 12 mmol). The mixture was refluxed over night, cooled to room temperature and poured over ice (50 g) and concentrated hydrochloric acid (100 mL). The aqueous phase was extracted with several aliquots of DCM, and the organic fractions collected, combined, and dried over $MgSO_4$. The solvent was removed *in vacuo* to yield the crude product, brown solid **thieno[3,2-*b*]thiophen-4[5H]-one** (1.2 g, 41 %).
^{1}H NMR ($CDCl_3$, 400 MHz): δ 7.93 (1H, d, ^{3}J 4.8 Hz), 6.95 (1H, d, ^{3}J 4.8 Hz), 4.08 (2H, s). MS (EI): (m/z) 156 [M].

6.2.3 Thieno[3,2-*b*]thiophene

Synthesis adapted from work by Frère *et al.* [134]

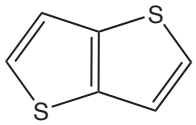

$C_6H_4S_2$

Mol. Wt.: 140.23 $gmol^{-1}$

$NaBH_4$ (0.1 g, 2.56 mmol) was added to a cold solution (0 °C) of thieno[3,2-*b*]thiophen-4[5H]-one (0.40 g, 2.56 mmol) dissolved in a mixture of methanol and DCM (v/v 10 mL) under nitrogen. The reaction mixture was allowed to stir at room temperature for 2 h, after which it was diluted with DCM (50 mL) and poured into 1M HCl (50 mL). This mixture was stirred for 30 mins, the organic layer was separated, washed with several aliquots of water and the organic fractions reduced *in vacuo* to yield **thieno[3,2-*b*]thiophene** as a white solid (270 mg, 75 %).
^{1}H NMR ($CDCl_3$, 400 MHz): δ 7.42 (2H, d, ^{3}J 4.8 Hz), 7.32 (2H, d, ^{3}J 4.8 Hz). ^{13}C{^{1}H}NMR ($CDCl_3$, 101 MHz): δ 139.74, 127.67, 119.68. MS (EI): (m/z) 140 [M].

6.2.4 2,5-Dibromothieno[3,2-*b*]thiophene

Synthesis adapted from work by Raithby *et al.* [197]

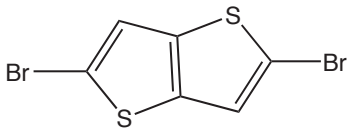

$C_6H_2Br_2S_2$

Mol. Wt.: 298.02 $gmol^{-1}$

Thieno[3,2-*b*]thiophene (300 mg, 2.1 mmol) was dissolved in DMF (8 mL) and stirred at 0 °C. To this was added a solution of NBS (747 mg, 4.2 mmol) in DMF (10 mL) and the combined mixture stirred at 0 °C for 3 h. Crushed ice was added to quench the reaction mixture and then extracted with DCM. The organic fraction was washed

with several aliquots of water, dried over $MgSO_4$ and reduced *in vacuo* to yield **2,5-dibromothieno[3,2-*b*]thiophene** (600 mg, 96 %).

^{1}H NMR ($CDCl_3$, 400 MHz): δ 7.17 (1H, s). MS (EI): (m/z) 296-298-300 [M *including splitting characteristic of isotopic abundances of dibrominated species* $C_6H_2Br_2S_2$].

6.2.5 3-Bromothiophene-2-carbaldehyde

Synthesis adapted from work by Iddon *et al.* [135]

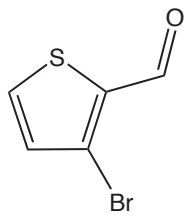

C_5H_3BrOS

Mol. Wt.: 191.05 $gmol^{-1}$

Under a nitrogen atmosphere diisopropylamine (6.33 g, 8.75 mL, 62.5 mmol) was dissolved in dry THF (100 mL) and cooled to -78 °C. To this stirred solution was added *n*-BuLi (25 mL, 2.5 M in hexane, 62.5 mmol) and the resulting solution stirred for 30 mins. The solution was then warmed up to 0 °C with ice cooling and 3-bromothiophene (10.2 g, 5.9 mL, 62.5 mmol) was added dropwise and stirring continued for a further 30 mins. N-Formylpiperidine (7.10 g, 6.9 mL, 62.5 mmol) was added and the solution allowed to stir at room temperature for 3 h, during which time a precipitate formed. Aqueous ammonium chloride (20 %, 50 mL) was added and the volatile solvent was removed under reduced pressure. The product was extracted with diethyl ether, dried over $MgSO_4$, and evaporated to dryness to yield the crude product as a brown oil. Fractional distillation was performed to purify the material (Kugelrohr apparatus, 80 °C, 2 $\times$ 10^{-4} bar) and afforded **3-bromothiophene-2-carbaldehyde** (9.2 g, 76 %) as a dark yellow oil.

^{1}H NMR ($CDCl_3$, 400 MHz): δ 9.96 (1 H, s), 7.70 (1 H, d, ^{3}J 4.8 Hz) 7.13 (1 H, d, ^{3}J 5.2 Hz). ^{13}C{^{1}H}NMR ($CDCl_3$, 50 MHz): δ 183.2, 135.1, 132.2, 68.1, 25.8. MS (EI): (m/z) 191 [M].

6.2.6 Ethyl thieno[3,2-*b*]thiophene-5-carboxylate

Synthesis adapted from work by Iddon *et al.* [135]

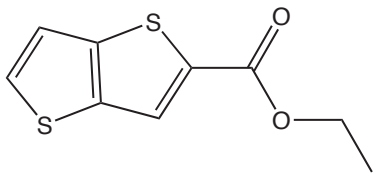

$C_9H_8O_2S_2$

Mol. Wt.: 212.29 gmol^{-1}

Ethyl thioglycolate (3 mL, 27 mmol) and potassium carbonate (5 g) were dissolved in DMF (50 mL) and 3-bromothiophene-2-carbaldehyde (5.2 g, 26.8 mmol) was added dropwise over 5 minutes. The mixture was allowed to stir at room temperature for 24 h, after which it was poured into water (100 mL) and the product extracted with DCM, dried over $MgSO_4$ and concentrated *in vacuo*. The crude oil was purified by fractional distillation (Kugelrohr apparatus, 160 – 180 °C, 2×10^{-4} bar) to a light orange oil, **ethyl thieno[3,2-*b*]thiophene-5-carboxylate** (4.5 g, 85 %).
^{1}H NMR ($CDCl_3$, 400 MHz): δ 7.99 (1 H, s), 7.58 (1 H, d, ^{3}J 5.2 Hz), 7.28 (1 H, d, ^{3}J 5.2Hz), 4.38 (2 H, q, ^{3}J 7.2 Hz), 1.4 (3 H, t, ^{3}J 7.2 Hz). MS (AP+): (m/z) 213 $[M + H]^+$.

6.2.7 Thieno[3,2-*b*]thiophene-5-carboxylic acid

Synthesis adapted from work by Iddon *et al.* [135]

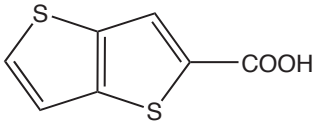

$C_7H_4O_2S_2$

Mol. Wt.: 184.24 gmol^{-1}

Ethyl thieno[3,2-*b*]thiophene-5-carboxylate (4.0 g, 19 mmol) was stirred in THF (40 mL) with aqueous lithium hydroxide (40 mL, 1 M) added slowly. The mixture was stirred at reflux for 12 h. The solution was concentrated *in vacuo* and 5M HCl acid was added, which precipitated a white solid. The precipitate was isolated by

filtration, washed with water and ether, and dried under vacuum to give **thieno[3,2-*b*]thiophene-5-carboxylic acid** (3.1 g, 90 %).

^{1}H NMR (DMSO, 400 MHz): δ 13.2 (1 H, broad s), 8.1 (1 H, s), 7.91 (1 H, d, ^{3}J 5.6 Hz), 7.49 (1 H, d, ^{3}J 5.6 Hz). MS (AP+): (m/z) 185 $[M + H]^+$.

6.2.8 2,5-Dibromothieno[3,2-*b*]thiophene

Synthesis adapted from work by Campbell *et al.* [138]

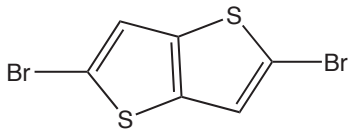

$C_6H_2Br_2S_2$

Mol. Wt.: 298.02 gmol^{-1}

A solution of NBS (2.3 g, 13 mmol) in water (15 mL) was added added portionwise to thieno[3,2-*b*]thiophene-5-carboxylic acid (1.0 g, 5.6 mmol) dissolved in nMP (100 mL) over 1h. The mixture was allowed to stir for 18 h and then water (100 mL) was added, whereupon a solid precipitated. The precipitate was isolated by filtration and dried under vacuum as a white solid **2,5-dibromothieno[3,2-*b*]thiophene** (1.4 g, 83 %).

^{1}H NMR ($CDCl_3$, 400 MHz): δ 7.17 (s). ^{13}C{^{1}H}NMR ($CDCl_3$, 400 MHz): δ 138.3, 121.8, 113.6. MS (EI): (m/z) 296-298-300 [M *including splitting characteristic of isotopic abundances of dibrominated species* $C_6H_2Br_2S_2$].

6.2.9 2,5-bis(4-*tert*-Butylphenylethynyl)thieno[3,2-*b*]thiophene [BPEantTT.tBu]

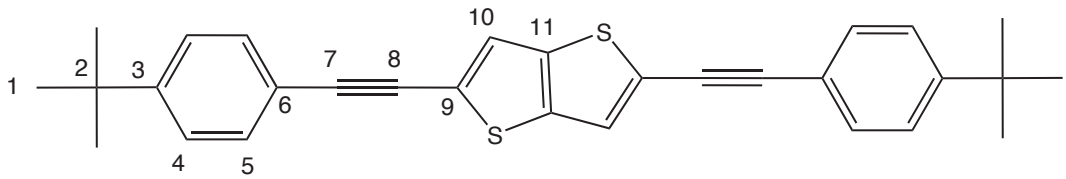

$C_{30}H_{28}S_2$

Mol. Wt.: 452.67 gmol^{-1}

Under a nitrogen atmosphere using Schlenk-line apparatus, 2,5-dibromothieno[3,2-*b*]thiophene (540 mg, 1.8 mmol) was dissolved in Et_3N (20 mL) and THF (15 mL). The mixture was degassed *via* five freeze-pump-thaw cycles. Under a flow of N_2 4-*t*-butylphenylacetylene (0.81 mL, 4.5 mmol) was added, followed by $Pd(PPh_3)_4$ (100 mg, 5 mol%) and CuI (10 mg, 3 mol%). The mixture was stirred at 65 °C for 24 h after which it was reduced *in vacuo* and filtered through a silica plug, eluting with ether. The ether fraction was reduced *in vacuo*. Column chromatography on silica gel was performed, eluting with hexane, and then ether. **2,5-bis(4-*tert*-Butylphenylethynyl)thieno[3,2-*b*]thiophene [BPEantTT.tBu]** was isolated as a fluffy yellow powder (490 mg, 60 %). M.P. = 303 – 305 °C.

^{1}H NMR ($CDCl_3$, 700 MHz): δ 7.47 (4 H, d, ^{3}J 6.8 Hz, **5**), 7.39 (4 H, d, ^{3}J 6.8 Hz, **4**), 7.35 (2 H, s, **10**), 1.33 (18 H, s, **1**). ^{13}C{^{1}H}NMR ($CDCl_3$, 176 MHz): δ 152.3 (**3**), 139.2 (**11**), 131.4 (**5**), 126.9 (**9**), 125.7 (**4**), 123.9 (**10**), 119.7 (**6**), 95.9 (**7**), 82.7 (**8**), 35.1 (**2**), 31.4 (**1**). Acc. MS (AP+): (m/z) calcd. for $[M + H]^+$ 453.1711; found 453.1703. Elemental analysis: expected ($C_{30}H_{28}S_2$): C, 79.60 %; H, 6.23 %: found: C, 79.49 %; H, 6.15 %.

Crystal data for **BPEantTT.tBu** (08SRV340) (see Figure 3.35, page 85): $C_{30}H_{28}S_2$, M = 452.64, colourless block, 0.34 × 0.22 × 0.20 mm^3, triclinic, space group *P*-1 (No. 2), a = 6.0263(4), b = 8.1335(5), c = 13.0125(7) Å, α = 87.992(2), β = 77.1150(10), γ = 74.0720(10) °, V = 597.64(6) Å^3, Z = 1, D_c = 1.258 g/cm^3, F_{000} = 240, Bruker SMART 6K CCD Detector, MoKα radiation, λ = 0.71073 Å, T = 120(2) K, $2\theta_{max}$ = 56.5 °, 8056 reflections collected, 2949 unique (Rint = 0.0261). Final $GooF$ = 1.122, $R1$ = 0.0412, $wR2$ = 0.1122, R indices based on 2571 reflections with I > 2σ(I) (refinement on F^2), 148 parameters, 0 restraints. Lp and absorption corrections applied, μ = 0.239 mm^{-1}.

6.2.10 2,5-bis(4-Methoxyphenylethynyl)-thieno[3,2-b]thiophene [BPEantTT.OMe]

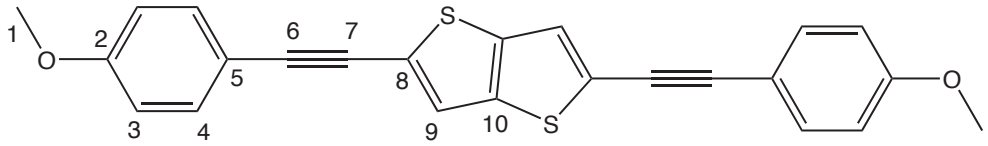

$C_{24}H_{16}O_2S_2$

Mol. Wt.: 400.51 $gmol^{-1}$

The procedure of **6.2.9** was followed using 2,5-dibromothieno[3,2-*b*]thiophene (540 mg, 1.8 mmol) and 4-ethynylanisole (0.58 mL, 4.5 mmol) with stirring at 65 °C for 24 h. The solvent was reduced *in vacuo* and the residue filtered through a silica plug, eluting with ether. The isolated dark orange solid was further chromatographed on silica gel, eluting with hexane and ether. **2,5-bis(4-Methoxyphenylethynyl)-thieno[3,2-b]thiophene [BPEantTT.OMe]** was isolated (100 mg, 14 %) as a flaky yellow solid .

^{1}H NMR ($CDCl_3$, 700 MHz): δ 7.47 (4 H, d, ^{3}J 7 Hz, **4**), 7.32 (2 H, s, **9**), 6.89 (4 H, s, ^{3}J 7 Hz, **3**), 3.84 (6 H, s, **1**). ^{13}C{^{1}H}NMR ($CDCl_3$, 176 MHz): δ 160.0 (**2**), 138.8 (**10**), 133.0 (**4**), 126.6 (**8**), 123.4 (**9**), 114.6 (**5**), 114.1 (**3**), 95.5 (**6**), 81.8 (**7**), 55.3 (**1**). Acc. MS (AP+): (m/z) calcd. for $[M + H]^+$ 401.0670; found 401.0660.

There was insufficient material for elemental analysis of this compound after completion of the photophysical analysis.

6.2.11 2,3,5,6-Tetrabromothieno[3,2-*b*]thiophene

Synthesis adapted from work by Iddon *et al.* [135]

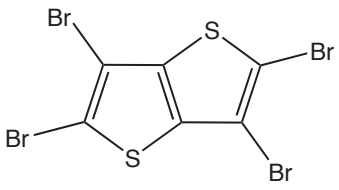

$C_6Br_4S_2$

Mol. Wt.: 455.81 $gmol^{-1}$

2,5-Dibromothieno[3,2-*b*thiophene (see **6.2.8**) (4 g, 22 mmol) was dissolved in acetic acid (300 mL) with stirring, and bromine (1.13 mL, 22 mmol) added slowly. After stirring for 1 h at room temperature, water (80 mL) was added, causing precipitation. The mixture was then heated at reflux and another portion of bromine added (1.13 mL, 22 mmol). After 4 h excess bromine (4.5 mL, 80 mmol) was added, and the solution stirred for a further 12 h at 65 °C. The white precipitate formed was filtered, washed with water and isolated as a pink solid. **2,3,5,6-Tetrabromo thieno[3,2-*b*]thiophene** was recrystallised from THF as white needle-shaped crystals (7.5 g, 75 %).

MS(EI): (m/z) 455 [M *including splitting characteristic of isotopic abundances of tetrabrominated species* $C_6Br_4S_2$]. Elemental analysis: expected ($C_6Br_4S_2$): C, 15.81%; found: C, 15.83 %.

6.2.12 3,6-Dibromothieno[3,2-*b*]thiophene

Synthesis adapted from work by Iddon *et al.* [135]

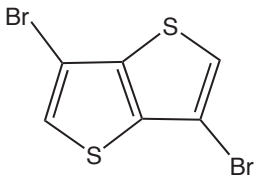

$C_6H_2Br_2S_2$

Mol. Wt.: 298.02 $gmol^{-1}$

2,3,5,6-Tetrabromothieno[3,2-*b*]thiophene (640 mg, 1.4 mmol) was dissolved in acetic acid (100 mL) with stirring at reflux. Zinc dust (96 mg, 1.5 mmol) was added and stirring continued for 30 mins. A second portion of zinc dust (96 mg, 1.5 mmol) was added, and heating at reflux was continued for a further 30 mins. At this time the solution was cooled to ambient temperature, water added, and the precipitate isolated by filtration and vacuum dried. NMR spectroscopy revealed the isolated solid to be a combination of the dibrominated and tribrominated species. Consequently, the solid was redissolved in acetic acid (100 mL) and stirred at reflux whilst excess zinc dust (∼300 mg) was added. The mixture was allowed to stir for 1.5 h, after which time it was quenched and worked up as previously described,

enabling isolation of pure **3,6-dibromothieno[3,2-*b*]thiophene** (250 mg, 60 %). ^{1}H NMR ($CDCl_3$, 400 MHz): δ 7.34 (s). $^{13}C\{^1H\}$NMR ($CDCl_3$, 400 MHz): δ 139.8, 125.1, 103.0. MS (EI): (m/z) 296-298-300 (M *including splitting characteristic of isotopic abundances of dibrominated species* $C_6H_2Br_2S_2$).

6.2.13 3,6-bis(4-*tert*-Butylphenylethynyl)-thieno[3,2-*b*]thiophene [BPEantXTT.tBu]

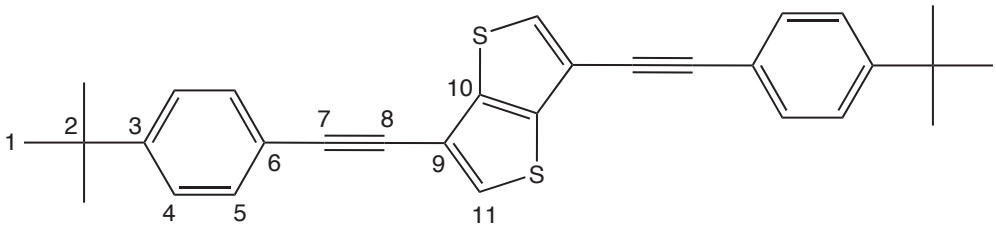

$C_{30}H_{28}S_2$

Mol. Wt.: 452.67 gmol^{-1}

3,6-Dibromothieno[3,2-*b*]thiophene (160 mg, 0.53 mmol) was dissolved in dry Et_3N (20 mL) using Schlenk-line apparatus under N_2, and five freeze-pump-thaw cycles were performed. Under a flow of N_2 4-*t*-butylphenylacetylene (1.6 mL, 3.7 mmol) was added, followed by $Pd(PPh_3)_4$ (15 mg, 2 mol%) and CuI (2 mg, 2 mol%). The mixture was stirred at reflux for 40 h, after which it was reduced in volume *in vacuo* and filtered through a silica plug, eluting with ether. The crude residue isolated here was dissolved in DCM, and any insoluble solid removed. The DCM was removed under reduced pressure and the residue taken into hot ether. From this a light brown solid precipitated. This was washed in cold ether, affording **3,6-bis(4-tert-butylphenylethynyl)thieno[3,2-*b*]thiophene [BPEantXTT.tBu]** as a lustrous, light brown solid (96 mg, 40 %). This was further recrystallised from DCM/cyclohexane to afford colourless plate-like crystals. M.P. = 278 – 280 °C.

^{1}H NMR ($CDCl_3$, 700 MHz): δ 7.58 (2 H, s, **11**), 7.49 (4 H, d, ^{3}J 7 Hz, **5**), 7.38 (4 H, d, ^{3}J 7 Hz, **4**), 1.33 (18 H, s, **1**). $^{13}C\{^1H\}$NMR ($CDCl_3$, 176 MHz): δ 152.0 (**3**), 140.0 (**9 or 10**), 131.4 (**5**), 130.5 (**11**), 125.4 (**4**), 119.6 (**6**), 115.8 (**10 or 9**),

91.9 (**7**), 81.4 (**8**), 34.8 (**2**), 31.1 (**1**). Acc. MS (AP+): (m/z) calcd. for $[M + H]^+$ 453.1711; found 453.1711. Elemental analysis: expected ($C_{30}H_{28}S_2$): C, 79.6 %; H, 6.23 %; found: C, 80.29 %, H, 6.41 %.

Crystal data for **BPEantXTT.tBu** 08SRV338 (see Figure 3.36, page 87): $C_{30}H_{28}S_2$, $M = 452.64$, colourless plate, 0.30 × 0.20 × 0.04 mm^3, triclinic, space group P-1 (No. 2), $a = 6.2158(4)$, $b = 7.6037(5)$, $c = 13.2115(10)$ Å, $\alpha = 102.290(2)$, $\beta = 93.687(2)$, $\gamma = 97.016(2)$ °, $V = 602.91(7)$ Å^3, $Z = 1$, $D_c = 1.247$ g/cm^3, $F_{000} = 240$, Bruker SMART 6K CCD Detector, MoKα radiation, $\lambda = 0.71073$ Å, $T = 120(2)$ K, $2\theta_{max} = 52.7$ °, 6903 reflections collected, 2468 unique ($R_{int} = 0.0374$). Final $GooF = 1.092$, $R1 = 0.0492$, $wR2 = 0.1354$, R indices based on 2056 reflections with $I > 2\sigma(I)$ (refinement on F^2), 148 parameters, 0 restraints. Lp and absorption corrections applied, $\mu = 0.237$ mm^{-1}.

6.2.14 3,4-Dimethylthieno[2,3-*b*]thiophene-2,5-dicarboxylate

Synthesis adapted from work by Kirsch *et al.* [145]

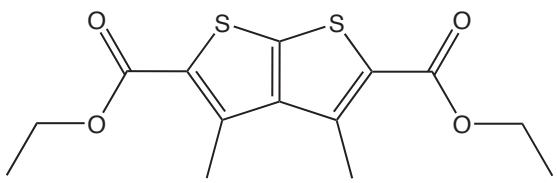

$C_{14}H_{16}O_4S_2$

Mol. Wt.: 312.40 gmol^{-1}

A solution of pentane-2,4-dione (10.2 mL, 0.1 mol) and CS_2 (9 mL, 0.15 mol) in DMF (15 mL) was added dropwise to a solution of potassium carbonate (41.5 g, 0.3 mol) in DMF (60 mL), with vigorous stirring. After 30 mins the mixture was cooled to 0 °C and ethyl bromoacetate (22 mL, 0.2 mol) in DMF (5 mL) was added dropwise over 30 mins. The reaction mixture was then allowed to stir at room temperature for 12 h, after which it was poured into cold water (200 mL). The precipitate was collected by filtration, washed with cold water (3 × 100 mL aliquots) and allowed to dry to give a white solid of **3,4-dimethylthieno[2,3-*b*]thiophene-2,5-dicarboxylate** (30 g, 93 %).

^{1}H NMR ($CDCl_3$, 400 MHz): δ 4.36 (4 H, q, ^{3}J 7.2 Hz), 2.88 (6 H, s), 1.39 (6 H, t, ^{3}J 6.8 Hz). MS (EI): (m/z) 312 [M].

6.2.15 3,4-Dimethylthieno[2,3-*b*]thiophene-2,5-dicarboxylic acid

Synthesis adapted from work by Kirsch *et al.* [145]

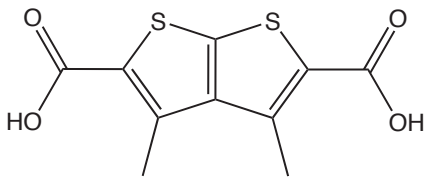

$C_{10}H_8O_4S_2$

Mol. Wt.: 256.30 gmol^{-1}

3,4-Dimethylthieno[2,3-*b*]thiophene-2,5-dicarboxylate (12.5 g, 40 mmol) was heated at reflux with an excess of potassium hydroxide (11.2 g, 200 mmol) in ethanol (50 mL) and water (10 mL) for 24 h. The solvent was removed *in vacuo* and the residue acidified with 5M HCl. The crude acid precipitated out and was isolated by filtration to afford **3,4-dimethylthieno[2,3-*b*]thiophene-2,5-dicarboxylic acid** as a tacky white solid (8.7 g, 85 %).

^{1}H NMR ($CDCl_3$, 400 MHz): δ 3.4 (v. broad s), 2.8 (6 H, s). ^{13}C{^{1}H}NMR ($CDCl_3$, 100 MHz): δ 164.3, 147.8, 144.3, 140.5, 131.3, 14.5. MS (AP+): (m/z) 257 [M + H]$^+$.

6.2.16 2,5-Dibromo-3,4-dimethylthieno[2,3-*b*]thiophene

Synthesis adapted from work by Campbell *et al.* [138]

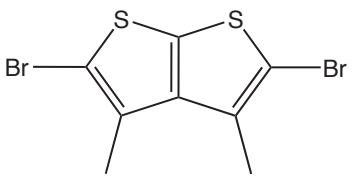

$C_8H_6Br_2S_2$

Mol. Wt.: 326.07 gmol^{-1}

NBS (1.96 g, 11 mmol) in water (20 mL) was added portionwise over 30 minutes to 3,4-dimethylthieno[2,3-*b*]thiophene-2,5-dicarboxylic acid (1.2 g, 4.7 mmol) dissolved in NMP (100 mL). The mixture was then allowed to stir for 18 h. Water (100 mL) was added and the white solid that precipitated was isolated and dried under vacuum to afford **2,5-dibromo-3,4-dimethyl thieno[2,3-*b*]thiophene** (1.4 g, 90 %) as a cream/white solid.

^{1}H NMR ($CDCl_3$, 400 MHz): δ 2.4 (s). ^{13}C{^{1}H}NMR ($CDCl_3$, 101 MHz): δ 143.2, 133.4, 130.6, 110.5, 14.4. MS (EI): (m/z) 324-326-328 [M *including splitting characteristic of isotopic abundances of dibrominated species* $C_8H_6Br_2S_2$].

6.2.17 2,5-bis(phenylethynyl)-3,4-dimethylthieno[2,3-*b*] thiophene [BPEsynTT]

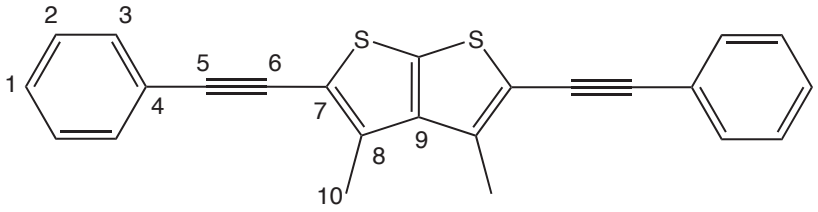

$C_{24}H_{16}S_2$

Mol. Wt.: 368.51 gmol^{-1}

Under a nitrogen atmosphere using Schlenk line apparatus, 2,5-dibromo-3,4-dimethyl thieno[2,3-*b*]thiophene (1.28 g, 3.9 mmol) was dissolved in dry Et_3N (75 mL) and five freeze-pump-thaw cycles were performed. Under a flow of N_2 phenylacetylene (0.9 mL, 8.2 mmol) was added, followed by $Pd(PPh_3)_4$ (900 mg, 20 mol%) and CuI (70 mg, 10 mol%). The mixture was stirred under reflux conditions for 12 h after which it was reduced *in vacuo* and filtered through a silica plug, eluting with ether. The crude product isolated was purified further on silica gel eluting with toluene, affording the product **2,5-bis(phenylethynyl)-3,4-dimethyl thieno[2,3-*b*]thiophene [BPEsynTT]** as a yellow solid upon concentration *in vacuo* (500 mg, 35 %). Recrystallisation from hot toluene afforded plate–like yellow crystals. M.P. = 200 – 201 °C.

^{1}H NMR ($CDCl_3$, 500 MHz): δ 7.54 (4 H, d, ^{3}J 6.5 Hz, **3**), 7.37 (6 H, m, **1 and 2**),

2.62 (6 H, s, **10**). $^{13}C\{^1H\}$NMR ($CDCl_3$, 100 MHz): δ 144.8 (**7,8 or 9**), 137.6 (**1 or 4**), 135.9 (**7, 8 or 9**), 131.6 (**3**), 128.7 (**2**), 123.1(**1 or 4**), 121.4 (**7, 8 or 9**), 96.6 (**5**), 82.8 (**6**), 14.7 (**10**). Acc. MS. (AP+): (m/z) calcd. for $[M + H]^+$ 369.0772; found 369.0779. Elemental analysis: expected ($C_{24}H_{16}S_2$): C, 78.20 %; H, 4.38 %. found: C, 78.48 %; H, 4.45 %.

Crystal data for **BPEsynMTT** 08SRV184 (see Figure 3.36, page 87): $C_{24}H_{16}S_2$, M = 368.49, yellow block, 0.40 × 0.22 × 0.20 mm^3, triclinic, space group P-1 (No. 2), a = 8.7833(4), b = 14.8444(6), c = 15.8708(7) Å, α = 64.8500(10), β = 80.0040(10), γ = 81.0040(10) °, V = 1836.74(14) Å^3, Z = 4, D_c = 1.333 g/cm^3, F_{000} = 768, Bruker SMART 1K CCD Detector, MoKα radiation, λ = 0.71073 Å, T = 120(2) K, $2\theta_{max}$ = 52.7 °, 18265 reflections collected, 7475 unique (R_{int} = 0.0504). Final $GooF$ = 1.075, $R1$ = 0.0463, $wR2$ = 0.1229, R indices based on 5371 reflections with I > 2σ(I) (refinement on F^2), 553 parameters, 243 restraints. Lp and absorption corrections applied, μ = 0.294 mm^{-1}.

6.3 Oxadiazole Derivatives

6.3.1 Phenyl propiolic ethyl ester

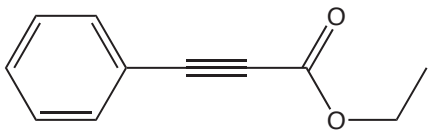

$C_{11}H_{10}O_2$

Mol. Wt.: 174.20 gmol^{-1}

Concentrated hydrochloric acid (approx. 1 mL) was added to phenylpropiolic acid (3.25 g, 22 mmol) dissolved in ethanol (50 mL) and the solution heated at reflux for 3 h. The solution was subsequently reduced *in vacuo*, water added, and then extracted with DCM (3 × 25 mL). The organic fraction was dried with anhydrous $MgSO_4$. **Phenyl propiolic ethyl ester** was obtained upon removal of the solvent under reduced pressure (3.45 g, 90 %).

^{1}H NMR ($CDCl_3$, 400 MHz): δ 7.59 (2 H, d, ^{3}J 7.2 Hz), 7.42 (1 H, m), 7.38 (2 H, m), 4.30 (2 H, q, ^{3}J 7.2 Hz), 1.36 (3 H, t, ^{3}J 7.2 Hz). MS (EI): (m/z) 174 [M].

6.3.2 Phenylethynyl acylhydrazide

Synthesis adapted from work by Al Jallo. [190]

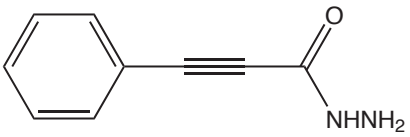

$C_9H_8N_2O$

Mol. Wt.: 160.17 $gmol^{-1}$

Ester phenylpropiolic ethanoate (1.1 g, 6.1 mmol) was dissolved in ethanol and stirred with ice cooling. Hydrazine monohydrate was added (0.3 mL, 6.1 mmol) and the solution was stirred at 0 °C for 3 h. The solvent was removed at room temperature under high vacuum and the remaining residue dried over 48 h to a tacky light brown/orange solid. This was washed with DCM and the white/cream powder isolated by filtration was product **phenylethynyl acyl hydrazide** (750 mg, 77 %).

^{1}H NMR (DMSO, 400 MHz): δ 10.0 (broad s), 7.66 (2 H, d, ^{3}J 7.6 Hz), 7.40 (2 H, t, ^{3}J 8 Hz), 7.29 (1 H, t, ^{3}J 7.2 Hz), 5.89 (1 H, s). MS (AP+): (m/z) 161 $[M + H]^+$.

6.3.3 1-Benzotriazol-1-yl-3-phenylpropynone

Synthesis adapted from work by Katritzky *et al.* [189]

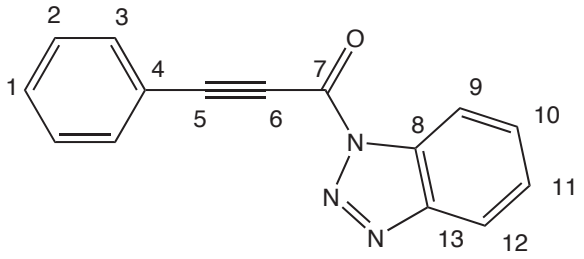

$C_{15}H_9N_3O$

Mol. Wt.: 247.25 $gmol^{-1}$

Phenylpropiolic acid (1.2 g, 8.3 mmol) and benzotriazole (3 g, 25 mmol) were dissolved in DCM (20 mL) and thionyl chloride (5.6 mL, 21 mmol) added *via* syringe. The mixture was stirred at room temperature for 18 h, after which solvent was

removed under reduced pressure and the subsequent residue redissolved in ethyl acetate. The organic fraction was washed with water, aqueous sodium hydroxide and brine (3 × 25 mL aliquots of each). The organic solvent was removed under reduced pressure to yield **1-benzotriazol-1-yl-3-phenylpropynone** (1.4 g, 70 %) as a white solid.

^{1}H NMR ($CDCl_3$, 700 MHz): δ 8.30 (1 H, d, ^{3}J 8.2 Hz, **9 or 12**) 8.2 (1 H, d, ^{3}J 8.2 Hz, **12 or 9**), 7.80 (2 H, d, ^{3}J 7.7 Hz, **3**), 7.69 (1 H, t, ^{3}J 7 Hz, **10 or 11**), 7.54 (2 H, m, **1 and 11 or 10**), 7.45 (2 H, t, ^{3}J 7.7 Hz, **2**). ^{13}C{^{1}H}NMR ($CDCl_3$, 176 MHz): δ 150.4 (**7**), 146.3 (**8 or 13**), 133.6 (**3**), 131.6 (**1**), 130.9 (**13 or 8**), 130.6 (**11 or 10**), 128.7 (**2**), 126.6 (**10 or 11**), 120.4 (**11 or 12**), 119.0 (**4**), 114.3 (**12 or 9**), 96.0 (**5**), 81.3 (**6**). MS (AP+): (m/z) 248.1 $[M + H]^{+}$. Elemental analysis: expected $C_{15}H_{11}N_0O$: C, 72.28 %; H, 4.45 %; N, 16.86 %; found: C, 71.78 %; H, 3.73 %; N, 16.95 %.

6.3.4 2,5-bis(Phenylethynylene)-1,3,4-oxadiazole [BPEOx]

Method adapted from work by Katritzky *et al.* [188]

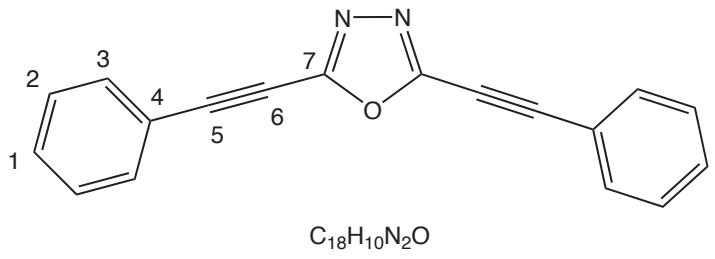

$C_{18}H_{10}N_2O$

Mol. Wt.: 270.28 $gmol^{-1}$

Sodium hydride (60 % in mineral oil, 180 mg, 4.25 mmol) was added to a stirred solution of 1-benzotriazol-1-yl-3-phenylpropynone (470 mg, 1.7 mmol) and phenylpropiolhydrazide (270 mg, 1.7 mmol) in DCM (25 mL). This mixture was allowed to stir for 12 h, after which carbon tetrabromide (1.12 g, 3.4 mmol) and triphenylphosphine (890 mg, 3.4 mmol) were added and stirring continued for a further 12 h. The resulting mixture was reduced *in vacuo* and chromatographed on silica gel eluting with DCM. **2,5-bis(phenylethynyl)-1,3,4-oxadiazole [BPEOx]** was isolated as

a white solid (18 mg, 4 %).

^{1}H NMR ($CDCl_3$, 700 MHz): δ 7.63 (4 H, d, ^{3}J 7 Hz, **3**), 7.49 (2 H, t, ^{3}J 7 Hz, **1**), 7.42 (4 H, t, ^{3}J 7 Hz, **2**). ^{13}C{^{1}H}NMR ($CDCl_3$, 176 MHz): δ 150.8 (**7**), 132.4 (**3**), 130.8 (**1**), 128.7 (**2**), 119.5 (**4**), 97.6 (**5 or 6**), 72.6 (**6 or 5**). Acc. MS. (AP+): (m/z) calcd. for $[M + H]^+$ 271.0871; found 271.0864.

There was insufficient material for elemental analysis of this compound after completion of the photophysical analysis.

6.4 Benzofurazan Derivatives

6.4.1 4,7-Dibromobenzofurazan

Synthesis adapted from work by Blouin *et al.*. [177]

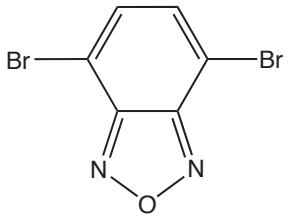

$C_6H_2Br_2N_2O$

Mol. Wt.: 277.90 gmol^{-1}

Benzofurazan (2.41 g, 20.1 mmol) and iron powder (230 mg, 4 mmol) were placed in a round bottom flask and the materials heated to 90 °C. Elemental bromine (9.6 g, 60 mmol) was added dropwise over an hour, and upon complete addition the reaction mixture was heated at reflux for 2 h. The reaction mixture was allowed to cool, which caused it to solidify. The residue was dissolved in DCM (20 mL) and washed with brine (50 mL). The organic fraction was separated and washed with saturated sodium bicarbonate solution (4 × 50 mL), with brine (3 × 50 mL) and with water (3 × 50 mL). The organic fraction was dried over magnesium sulfate and reduced *in vacuo*. The brown crude product was chromatographed on silica gel (hexane/ethyl acetate 9:1 eluant) to afford 4,7-dibromobenzofurazan (4.4 g, 78 %) as a cream powder.

^{1}H NMR ($CDCl_3$, 400 MHz): δ 7.51 (s). ^{13}C{^{1}H}NMR ($CDCl_3$, 101 MHz): δ 149.4,

134.2, 108.7. GCMS (EI): m/z 276-278-280 [M *including splitting characteristic of isotopic abundances of dibrominated species* $C_6H_2Br_2N_2S$].

6.4.2 4,7-bis(Phenylethynyl)benzofurazan [BPEBf]

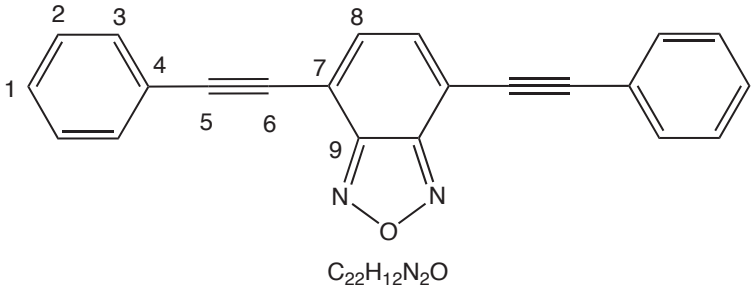

$C_{22}H_{12}N_2O$

Mol. Wt.: 320.34 $gmol^{-1}$

4,7-Dibromobenzofurazan (380 mg, 1.37 mmol) was placed in an oven–dried Schlenk flask, followed by addition of Et_3N (10 mL) and THF (20 mL) and the reaction mixture sonicated to ensure dissolution. The mixture was then degassed *via* three freeze–pump–thaw cycles and back–filled with nitrogen. Phenylacetylene (0.33 mL, 3 mmol) was added and the mixture was heated to 65 °C. $Pd(PPh_3)_4$ (50 mg, 5 mol%) and CuI (15 mg, 5 mol%) were added under a flow of nitrogen, and the mixture allowed to stir for 24 h. The resulting suspension was filtered through silica gel (ether eluant) and the filtrate reduced *in vacuo*. The brown solid residue was further purified by absorbing the compound onto silica and dry–loading onto a longer silica–gel column for chromatography, using gradient elution (initially 100 % hexane, but polarity increased with ether; product isolated at hexane/ether 6:1). The isolated yellow powder was further recrystallised out of hot ethanol and allowed to cool slowly, forming dark yellow crystals of **4,7-bis(phenylethynyl)benzofurazan [BPEBf]** (160 mg, 36 %). M.P. = 205 – 206 °C.

^{1}H NMR ($CDCl_3$, 700 MHz): δ 7.63 (4 H, d, ^{3}J.6 7 Hz, **3**), 7.57 (2 H, s, **8**), 7.40 (6 H, m, **1 and 2**). $^{13}C\{^1H\}$NMR ($CDCl_3$, 176 MHz): δ 149.5 (**7 or 9**), 134.1(**8**), 132.0 (**3**), 129.5 (**1**), 128.5 (**2**), 122.0 (**4**), 112.6 (**9 or 7**), 99.1 (**5**), 83.73 (**6**). Acc. MS. (AP+): (m/z) calcd. for $[M + H]^+$ 321.1028; found 321.1031.

Repeated attempts to obtain accurate elemental analysis failed. Consistency was also not obtained. There was insufficient material for repeated elemental analysis of this compound.

Crystal data for **BPEBf** (09SRV273) (see Figure 4.20, page 144): $C_{22}H_{12}N_2O$, M = 320.34, orange plate, 0.38 × 0.36 × 0.08 mm^3, monoclinic, space group $P2_1/c$ (No. 14), a = 11.9834(9), b = 10.8146(8), c = 12.4346(9) Å, β = 98.906(7) °, V = 1592.0(2) Å^3, Z = 4, D_c = 1.336 g/cm^3, F_{000} = 664, Xcalibur, Sapphire3, Gemini ultra, MoKα radiation, λ = 0.71073 Å, T = 100(2) K, $2\theta_{max}$ = 52.7 °, 7147 reflections collected, 3245 unique (R_{int} = 0.0356). Final $GooF$ = 0.832, $R1$ = 0.0374, $wR2$ = 0.0752, R indices based on 2008 reflections with I > 2σ(I) (refinement on F^2), 226 parameters, 0 restraints. Lp and absorption corrections applied, μ = 0.083 mm^{-1}.

6.4.3 4,7-bis(4-*t*-Butylphenylethynyl)benzofurazan [BPEBf.tBu]

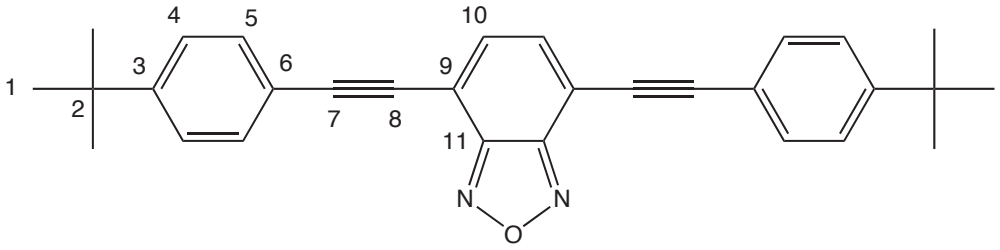

$C_{30}H_{28}N_2O$

Mol. Wt.: 432.56 gmol^{-1}

The procedure for **6.4.2** was followed, using 4,7-dibromobenzofurazan (415 mg, 1.51 mmol) and 4-*t*-butylphenylacetylene (0.7 mL, 3.78 mmol) with stirring at 65 °C for 48 h. The resulting suspension was filtered through a silica plug, eluting with ether. The solvent was reduced *in vacuo*, and the residue taken into hot ether. This was filtered and the filtrate allowed to cool very slowly. **4,7-bis(4-*t*-Butylphenylethynyl)benzofurazan [BPEBf.tBu]** crystallised out as bright yellow plate-like crystals, which were isolated by filtration (375 mg, 57 %). M.P. = 210 – 212 °C.

^{1}H NMR ($CDCl_3$, 700 MHz): δ 7.57 (4 H, d, ^{3}J 8.5 Hz, **5**), 7.54 (2 H, s, **10**), 7.41 (4 H, d, ^{3}J 8.5 Hz, **4**). ^{13}C{^{1}H}NMR ($CDCl_3$, 176 MHz): δ 152.9 (**3**), 149.5 (**9 or 11**), 133.9 (**10**), 131.8 (**5**), 125.5 (**4**), 119.0 (**6**), 112.6 (**11 or 9**), 99.4 (**7**), 83.4 (**8**), 34.9 (**2**), 31.1 (**1**). Acc. MS. (AP+): (m/z) calcd. for $[M + H]^+$ 433.2280, found 433.2261. Elemental analysis: expected ($C_{30}H_{28}N_2O$): C, 83.30 %; H, 6.52 %; N, 6.48 %; found: C, 83.03 %; H, 6.56 %; N, 6.37 %.

6.4.4 4,7-bis(4-Methoxyphenylethynyl)benzofurazan [BPEBf.OMe]

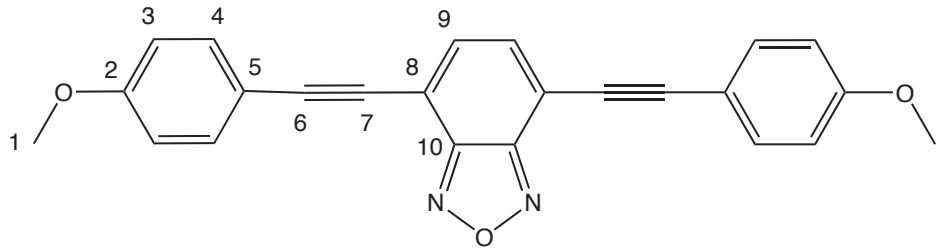

$C_{24}H_{16}N_2O_3$

Mol. Wt.: 380.40 gmol^{-1}

The procedure for **6.4.2** was followed, using 4,7-dibromobenzofurazan (405 mg, 1.46 mmol) and 4-ethynylanisole (0.4 mL, 3.2 mmol) with stirring at 65 °C for 48 h. The resulting suspension was filtered through a silica plug, eluting with ether and DCM. The solvents were evaporated, leaving an orange residue. This was redissolved in hot ether. Hot filtration was performed on this mixture, with an orange precipitating on standing overnight. The solid was isolated by filteration and washed with cold ether. **4,7-bis(4-ethynylanisole)benzofurazan [BPEBf.OMe]** was collected as a bright orange solid (350 mg, 66 %). A small amount of this solid was taken into a minimum amount of warm DCM, and cyclohexane layered over, in attempts to grow a single crystal for X-ray crystallographic analysis. M.P. = 236 – 237 °C.
^{1}H NMR ($CDCl_3$, 700 MHz): δ 7.59 (4 H, dd, ^{3}J 8.4 Hz, **4**), 7.52 (2 H, s, **9**), 6.92 (4 H, dd, ^{3}J 8.4 Hz, **3**). ^{13}C{^{1}H}NMR ($CDCl_3$, 176 MHz): δ 160.5 (**2**), 149.5 (**10 or 8**), 133.62 (**4**), 133.61 (**9**), 114.2 (**3**), 114.1 (**5**), 112.4 (**8 or 10**), 99.3 (**6**), 83.0 (**7**), 55.4 (**1**). Acc. MS. (AP+): (m/z) calcd. for $[M + H]^+$ 381.1239; found 381.1224.

Elemental analysis: expected ($C_{24}H_{16}N_2O_3$): C, 75.78 %; H, 4.24 %; N, 7.36 %; found: C, 75.57 %; H, 4.19 %; N, 7.16 %.

Crystal data for **BPEBf.OMe** (09SRV339) (see Figure 4.21, page 145): $C_{24}H_{16}N_2O_3$, $M = 380.39$, orange needle, $0.40 \times 0.20 \times 0.04$ mm^3, monoclinic, space group $P2_1/c$ (No. 14), $a = 14.7083(2)$, $b = 9.78930(10)$, $c = 12.76830(10)$ Å, $\beta = 93.08$ °, $V = 1835.77(3)$ Å^3, $Z = 4$, $D_c = 1.376$ g/cm^3, $F_{000} = 792$, CuKα radiation, $\lambda = 1.54178$ Å, $T = 100(2)$ K, $2\theta_{max} = 133.1$ °, 9247 reflections collected, 3122 unique ($R_{int} = 0.0239$). Final $GooF = 1.061$, $R1 = 0.0332$, $wR2 = 0.0914$, R indices based on 2921 reflections with $I > 2\sigma(I)$ (refinement on F^2), 264 parameters, 0 restraints. Lp and absorption corrections applied, $\mu = 0.747$ mm^{-1}.

6.4.5 4,7-bis(4-Aminophenylethynyl)benzofurazan [BPEBf.NH$_2$]

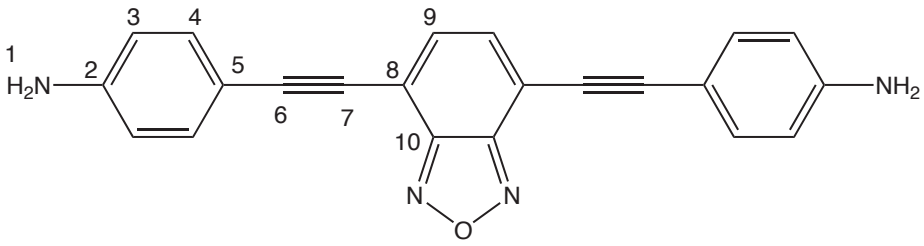

$C_{22}H_{14}N_4O$

Mol. Wt.: 350.37 gmol^{-1}

In an oven–dried Schlenk flask were placed 4,7-dibromobenzofurazan (160 mg, 0.57 mmol) and 4-ethynylaniline (170 mg, 1.45 mmol). These were dissolved in Et_3N (15 mL) and THF (15 mL) and the reaction mixture sonicated to ensure dissolution. The mixture was then degassed *via* three freeze-pump-thaw cycles and back filled with nitrogen. The reaction vessel was heated to 65 °C, $Pd(PPh_3)_4$ (35 mg, 5 mol%) and CuI (5 mg, 5 mol%) were added under a flow of nitrogen, and the mixture allowed to stir for 48 h. The resulting suspension was filtered through a silica plug (ether eluant) and the filtrate reduced *in vacuo*. The isolated brown solid was further purified by absorbing the compound onto silica and dry-loading onto a longer silica-gel column for chromatography, using a gradient elution (starting with

hexane increasing polarity with addition of ether; product isolated at hexane/ether 1:3). Solvent was evaporated to yield **4,7-bis(4-ethynylaniline)benzofurazan [BPEBf.NH$_2$]** (124 mg, 62 %) as a very dark red powder. M.P. = decomposes at 190 °C.

^{1}H NMR (DMSO, 700 MHz): δ 7.63 (2 H, s, **9**), 7.30 (4 H, d, ^{3}J 8.6 Hz, **4**), 6.60 (4 H, d, ^{3}J 8.6 Hz, **3**), 5.82 (4 H, s, **1**). ^{13}C{^{1}H}NMR (DMSO, 176 MHz): δ 151.1 (**2 or 5**), 149.8 (**8 or 10**), 134.3 (**9**), 133.6 (**4**), 114.1 (**3**), 111.2 (**10 or 8**), 107.1 (**5 or 2**), 101.7 (**6**), 82.8 (**7**). Acc. MS. (AP+): (m/z) calcd. for [M + H]$^+$ 351.1246; found 351.1255. Elemental analysis: expected ($C_{22}H_{14}N_4O$): C, 75.42 %; H, 4.03 %; N, 15.99 %; found: C, 74.67 %; H, 4.79 %; N, 14.16 % - indicative of 2[BPEBf.NH$_2$]:1[Ether].

6.4.6 4,7-bis(4-Methylesterphenylethynyl)benzofurazan [BPEBf.CO$_2$Me]

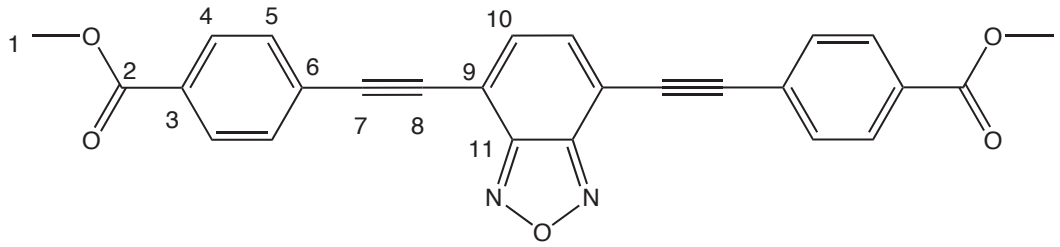

$C_{26}H_{16}N_2O_5$

Mol. Wt.: 436.42 gmol^{-1}

The procedure for **6.4.5** was followed, using 4,7-dibromobenzofurazan (278 mg, 1 mmol) and 4-ethynylmethylbenzoate (368 mg, 2.5 mmol) with stirring at 65 °C for 48 h. The resulting suspension was filtered through a silica plug, eluting with ether, followed by DCM. Evaporation of the DCM–containing fractions yielded a highly coloured yellow solid. This was subsequently redissolved in a minimum of hot DCM. Hot filtration was performed on the mixture, and overnight a highly luminescent yellow solid precipitated from the filtrate, which was collected by filtration and washed with cold DCM. **4,7-bis(4-ethynylmethylbenzoate)benzofurazan [BPEBf.CO$_2$Me]** was collected as a highly luminescent yellow solid (290 mg, 67

%). M.P. = 256 – 258 °C.

^{1}H NMR ($CDCl_3$, 700 MHz): δ 8.08 (4 H, d, ^{3}J 8.5 Hz, **4**), 7.72 (4 H, d, ^{3}J 8.5 Hz, **5**), 7.63 (2 H, s, **10**), 3.95 (6 H, s, **1**). ^{13}C{^{1}H}NMR ($CDCl_3$, 176 MHz): δ 166.3 (**2**), 149.3 (**9 or 11**), 134.5 (**10**), 131.9 (**5**), 130.7 (**3**), 129.6 (**4**), 126.4 (**6**), 112.7 (**11 or 9**), 98.3 (**7**), 86.1 (**8**), 52.3 (**1**). Acc. MS. (AP+): (m/z) calcd. for $[M + H]^+$ 437.1137; found 437.1135. Elemental analysis: expected ($C_{26}H_{16}N_2O_5$): C, 71.56 %; H, 3.70 %; N, 6.42 %; found: C, 71.07 %; H, 3.65 %; N, 6.15 %.

6.4.7 4,7-bis(4-Cyanophenylethynyl)benzofurazan [BPEBf.CN]

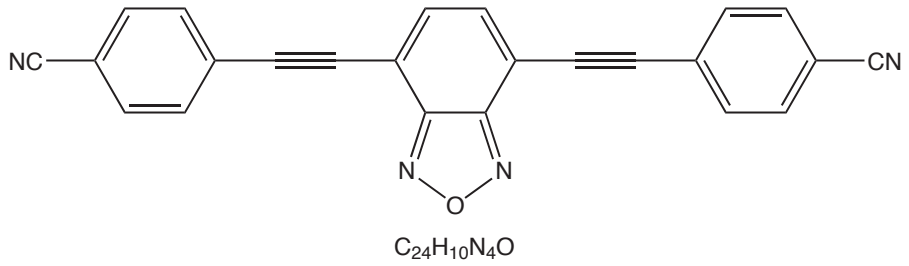

$C_{24}H_{10}N_4O$

Mol. Wt.: 370.36 gmol^{-1}

The procedure for **6.4.5** was followed, using 4,7-dibromobenzofurazan (140 mg, 0.5 mmol) and 4-ethynylbenzonitrile (190 mg, 1.5 mmol) with stirring at 75 °C for 48 h. The resulting suspension was filtered through a silica plug eluting with ether and DCM. The organic fractions were evaporated to dryness and absorbed onto silica for further chromatographic purification. A gradient elution of 100% ether—100% DCM in 10% increments allowed isolation of the desired product (at 100 % DCM), **4,7-bis(4-ethynylbenzonitrile)benzofurazan [BPEBf.CN]** as a largely insoluble yellow solid (22 mg, 12 %). M.P. = decomposes at 240 °C. NMR spectroscopy was performed on a saturated solution of this sample in hot DMSO, but the spectrum was noisy and peaks were indescernible.

Acc. MS. (AP+): (m/z) calcd. for $[M + H]^+$ 370.0855; found 370.0854.

There was insufficient material for elemental analysis of this compound.

6.4.8 4,7-bis(4-Nitrophenylethynyl)benzofurazan [BPEBf.NO_2]

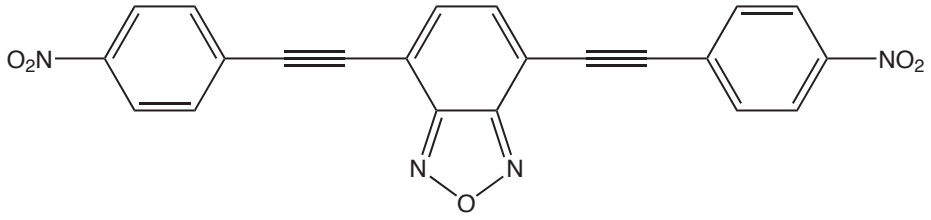

$C_{22}H_{10}N_4O_5$

Mol. Wt.: 410.34 $gmol^{-1}$

The procedure for **6.4.5** was followed, using 4,7-dibromobenzofurazan (278 mg, 1 mmol) and 4-ethynylnitrobenzene (368 mg, 2.5 mmol) with stirring at 65 °C for 48 h. The resulting suspension was filtered through a silica plug (ether and DCM eluants, separately) and the solvent evaporated *in vacuo*. Attempts to further purify this product consistently failed. Consquently there is no NMR of a pure species. Accurate mass (below) provides evidence of its synthesis.

Acc. MS. (AP+): (m/z) calcd. for $[M + H]^+$ 411.0729; found 411.0718.

6.4.9 4-Bromobenzofurazan

Synthesis adapted from work by Salvati *et al.* [192]

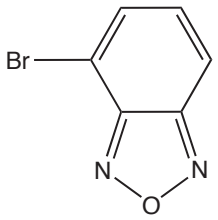

$C_6H_3BrN_2O$

Mol. Wt.: 199.00 $gmol^{-1}$

2,6-Dibromoaniline (1 g, 5 mmol) was dissolved in DCM (10 mL), to which was added a solution of m-CPBA (2.76 g, 75 % w/w, 12 mmol) in DCM (20 mL). The reaction mixture was allowed to stir at room temperature overnight. After 12 h TLC indicated no starting material was remaining, and the green solution was diluted by

addition of DCM (50 mL). The organic fraction was washed with sodium thiosulfate, sodium bicarbonate (until neutral as determined by pH indicator paper), brine (2 × 50 mL) and then water (2 × 50 mL). The organic product was dried over $MgSO_4$ and evaporated to dryness. The crude intermediate was taken into DMSO (20 mL) and NaN_3 (360 mg, 5.5 mmol) dissolved in DMSO (15 mL) was added. The mixture was allowed to stir overnight. It was then poured onto ice (immediately causing precipitation of a cream solid) and left to stand for 30 mins. The precipitate was collected, dried, and TLC analysis indicated two products. The crude product was taken into a small amount of hexane and the impurity was removed by eluting through a silica plug with hexane. The product remained on the silica and was subsequently eluted with ether, and the solvent removed under reduced pressure. **4-Bromobenzofurazan** was isolated as a brown solid (690 mg, 87 %).
^{1}H NMR ($CDCl_3$, 400 MHz): δ 7.78 (1 H, d, ^{3}J 8.8 Hz), 7.61 (1 H, m), 7.30 (1 H, d, ^{3}J 6.8 Hz). MS (EI): (m/z) 198-200 [M *including splitting characteristic of isotopic abundances of brominated species* $C_6H_3BrN_2S$].

6.4.10 4-(Phenylethynyl)benzofurazan [PEBf]

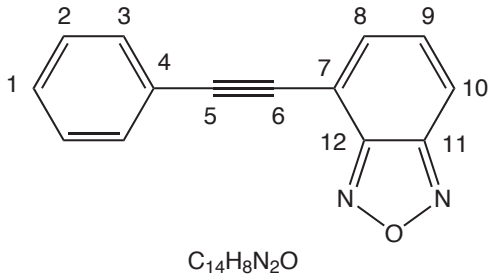

$C_{14}H_8N_2O$

Mol. Wt.: 220.23 $gmol^{-1}$

The procedure for **6.4.2** was followed, using 4-bromobenzofurazan (390 mg, 2.0 mmol) and phenylacetylene (0.22 mL, 2.0 mmol) with stirring at 40 °C for 48 h. The resulting suspension was filtered through a silica plug (ether eluant) and the solvent evaporated *in vacuo*. This solid was purified using column chromatography with gradient elution (hexane/ether, isolated at 5:1 v/v). **4-(Phenylethynyl)benzofurazan [PEBf]** was obtained as a yellow powder in very low yield ($\sim$ 20 mg, $<$ 5 % after

chromatography).

^{1}H NMR ($CDCl_3$, 700 MHz): δ 7.80 (1 H, d, ^{3}J 9.8 Hz, **10**), 7.64 (2 H, m, **3**), 7.57 (1 H, d, ^{3}J 6.3 Hz, **8**), 7.42 (1 H, dd, ^{3}J 9.1 Hz, ^{4}J 2.8 Hz, **9**), 7.39 (3 H, m, **1 and 2**). ^{13}C{^{1}H}NMR ($CDCl_3$, 176 MHz): δ 149.8 (**12**), 149.2 (**11**), 134.4 (**8**), 132.2 (**3**), 131.6 (**9**), 129.6 (**1**), 128.7 (**2**), 122.3 (**4**), 116.4 (**10**), 113.5 (**7**), 97.7 (**5**), 83.6 (**6**). Acc. MS. (AP+): (m/z) calcd. for $[M + H]^+$ 221.0705; found 221.0715.

There was insufficient material for elemental analysis of this compound after completion of the photophysical analysis.

6.4.11 4-(4-Aminophenylethynyl)benzofurazan [PEBf.NH$_2$]

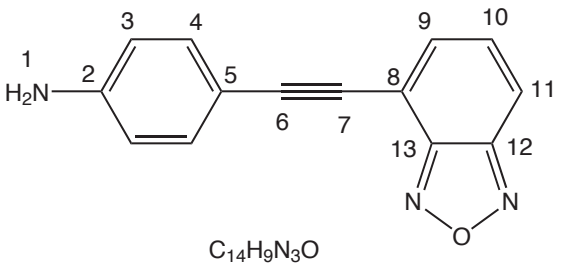

$C_{14}H_9N_3O$

Mol. Wt.: 235.24 gmol^{-1}

The procedure for **6.4.5** was followed, using 4-bromofurazan (200 mg, 1.0 mmol) and 4-ethynylaniline (130 mg, 1.1 mmol), with stirring at 65 °C for 55 h. The resulting suspension was filtered through a silica plug (ether eluant) and the solvent evaporated *in vacuo*. The brown/red residue was recrystallised out of hot cyclohexane to yield **4-(4-ethynylaniline)benzofurazan [PEBf.NH$_2$]** as short red needle-type crystals (70 mg, 30 %). M.P. = 155 – 157 °C.

^{1}H NMR ($CDCl_3$, 400 MHz): δ 7.75 (1 H, d, ^{3}J 9.1 Hz, **11**), 7.50 (1 H, d, ^{3}J 6.8 Hz, **9**), 7.45 (2 H, d, ^{3}J 6.3 Hz, **4**), 7.40 (1 H, dd, ^{3}J 6.3 Hz, ^{4}J 2.8 Hz, **10**), 6.67 (2 H, d, ^{3}J 8.4 Hz, **3**), 3.91 (bs, **1**). ^{13}C{^{1}H}NMR ($CDCl_3$, 176 MHz): δ 149.9 (**13**), 149.2 (**12 or 8**), 147.8 (**2**), 133.8 (**4**), 133.3 (**9**), 131.7 (**10**), 115.4 (**11**), 114.9 (**3**), 114.1 (**8 or 12**), 111.5 (**5**), 99.2 (**6**), 82.2 (**7**). Acc. MS. (AP+): (m/z) calcd. for $[M + H]^+$ 236.0824; found 236.0813.

Repeated attempts to obtain accurate elemental analysis failed, and consistency was

not obtained. There was insufficient material for repeated elemental analysis of this compound.

Crystal data for **PEBf.NH$_2$** (09SRV341) (see Figure 4.23, page 147): $C_{14}H_9N_3O$, M = 235.24, orange needle, 0.40 × 0.12 × 0.12 mm^3, monoclinic, space group $P2_1/c$ (No. 14), a = 6.6693(6), b = 11.9492(11), c = 14.1875(13) Å, β = 98.125(2) °, V = 1119.29(18) Å^3, Z = 4, D_c = 1.396 g/cm^3, F_{000} = 488, Bruker SMART 1K CCD Detector, MoKα radiation, λ = 0.71073 Å, T = 120(2) K, $2\theta_{max}$ = 56.6 °, 7443 reflections collected, 2765 unique (R_{int} = 0.0355). Final $GooF$ = 1.029, $R1$ = 0.0504, $wR2$ = 0.1083, R indices based on 1844 reflections with I > 2σ(I) (refinement on F^2), 163 parameters, 0 restraints. Lp and absorption corrections applied, μ = 0.092 mm^{-1}.

6.4.12 1,4-bis(4-Ethynylbenzofurazan)benzene [BBfEB]

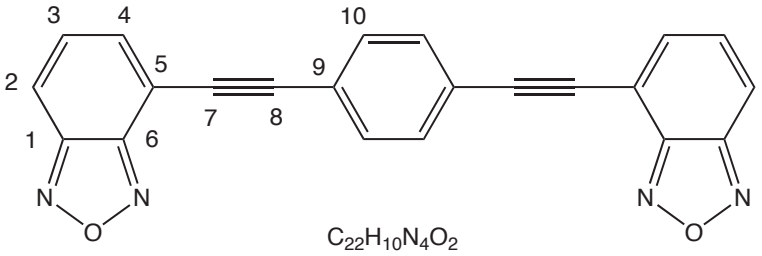

$C_{22}H_{10}N_4O_2$

Mol. Wt.: 362.34 gmol^{-1}

The procedure for **6.4.5** was followed, using 4-bromofurazan (400 mg, 2.0 mmol) and 1,4-diethynylbenzene (101 mg, 0.8 mmol), with stirring at 65 °C for 55 h. The resulting suspension was filtered through a silica plug (ether eluant) and the solvent evaporated *in vacuo*. The cream/light brown residue was recrystallised from cyclohexane to yield **4,7-bis(4-ethynylbenzofurazan)benzofurazan [BBfEBf]** as a dark yellow solid (160 mg, 55 %). M.P. = decomposes at 240 °C

^{1}H NMR ($CDCl_3$, 500 MHz): δ 7.86 (2 H, d, ^{3}J 9.0 Hz,), 7.70 (4 H, s, **10**), 7.62 (2 H, d, ^{3}J 6.4 Hz, **4**), 7.50 (2 H, dd, ^{3}J 9.0 Hz and 6.7 Hz, **3**). ^{13}C{^{1}H}NMR ($CDCl_3$, 126 MHz): δ 149.7 (**1,5 or 6**), 149.2 (**1,5 or 6**), 134.7 (**4**), 132.3 (**10**), 131.6 (**3**), 123.2 (**9**), 116.8 (**2**), 113.1 (**1,5 or 6**), 97.0 (**8**), 85.8 (**7**). Acc. MS.

(AP+): (m/z) calcd. for $[M + H]^+$ 363.0882; found 363.0880. Elemental analysis: expected ($C_{22}H_{10}N_4O_2$): C, 72.98 %; H, 2.78 %; N, 15.45 %; found: C, 71.87 %; H, 2.97 %; N, 14.07 %.

6.5 Benzothiadiazole Derivatives

6.5.1 4,7-Dibromobenzothiadiazole

Synthesis adapted from work by Neto *et al.* [184]

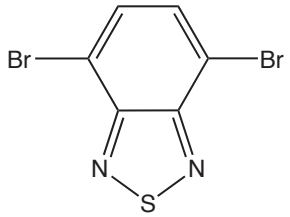

$C_6H_2Br_2N_2S$

Mol. Wt.: 293.97 $gmol^{-1}$

o-Phenyldiamine (5 g, 46 mmol) was added to a mixture of DCM and Et_3N (220 mL, v/v 10:1) and the solid totally dissolved by sonication. Thionyl chloride (6.7 mL, 92 mmol) was added drop–wise and the mixture refluxed for 3 h. The solvent was removed *in vacuo* and water was added (100 mL). Hydrochloric acid (5 M) was added slowly to achieve a pH of 1, and then the product was extracted with DCM and the organic layer dried over magnesium sulfate. The solvent was removed under reduced pressure, and the crude product purified by recrystallisation from hot hexane to yield an orange crystalline solid (5.3 g, 85 %). A portion of this product (1.5 g, 11 mmol) was reacted on immediately by taking into HBr (48 %, 30 mL), then bromine (2 mL) in HBr (30 mL) was added slowly. The reaction mixture was refluxed for 3 h. An orange solid precipitated during the reaction. The mixture was allowed to cool and the solid removed by filtration. The filtrate was washed with aqueous sodium bisulfite, and the product extracted with DCM. The organic layer was dried over $MgSO_4$ and the solvent was removed under reduced pressure, affording 4,7-dibromobenzothiadiazole as a light brown solid (2.9 g, 90 %).

^{1}H NMR ($CDCl_3$, 400 MHz): δ 7.72 (s). MS (EI): (m/z) 292-294-296 [M *including splitting characteristic of isotopic abundances of dibrominated species* $C_6H_2Br_2N_2S$].

6.5.2 4,7-bis(Phenylethynyl)benzothiadiazole [BPEBtd]

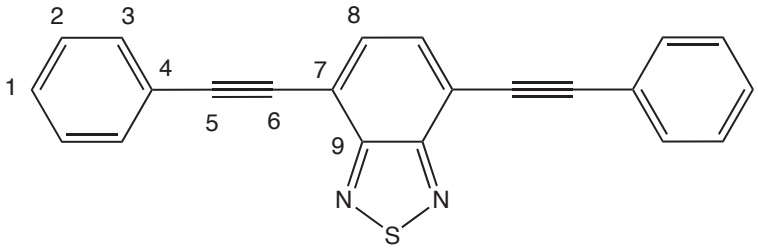

$C_{22}H_{12}N_2S$

Mol. Wt.: 336.41 gmol^{-1}

The procedure for **6.4.2** was followed, using 4,7-Dibromobenzothiadiazole (310 mg, 1.05 mmol) and phenylacetylene (0.25 mL, 2.2 mmol) with stirring at 75 °C for 48 h. The resulting suspension was filtered and the filtrate reduced *in vacuo*. The residue was chromatographed through a silica plug (eluting with hexane/ether 1:1), and the isolated brown solid was further purified by absorbing the compound onto silica and dry-loading onto a longer silica–gel (hexane eluant) column for chromatography, using gradient elution (product isolated at hexane/ether 5:1). The isolated dark orange powder **4,7-bis(phenylethynyl)benzothiadiazole [BPEBtd]** (220 mg, 62 %) was further purified by recrystallisation from hot ethanol, affording dark orange short needle–like crystals. M.P. = 168 – 170 °C.

^{1}H NMR ($CDCl_3$, 700 MHz): δ 7.80 (2 H, s, **8**), 7.67 (4 H, m, **3**), 7.40 (6 H, m, **1 and 2**). $^{13}\{^1H\}$ NMR ($CDCl_3$, 176 MHz): δ 154.6 (**7 or 9**), 132.7 (**8**), 132.2 (**3**), 129.3 (**1**), 128.7 (**2**), 122.7 (**4**), 117.4 (**9 or 7**), 97.7 (**5**), 85.5 (**6**). Acc. MS. (AP+): (m/z) calcd. for $[M + H]^+$ 337.0766; found 337.0782. Elemental analysis: expected $C_{22}H_{12}N_2S$: C, 78.56 %; H, 3.60 %; N, 8.33 %; found: C, 77.99 %; H, 3.68 %; N, 8.23 %.

6.5.3 4,7-bis(4-*t*-Butylphenylethynyl)benzothiadiazole [BPEBtd.tBu]

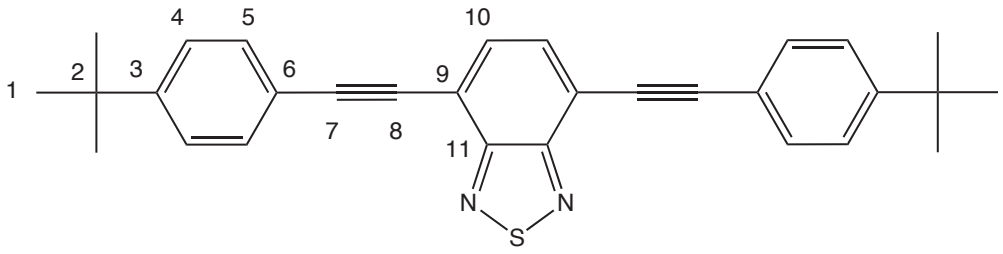

$C_{30}H_{28}N_2S$

Mol. Wt.: 448.62 $gmol^{-1}$

The procedure for **6.4.2** was followed, using 4,7-dibromobenzothiadiazole (280 mg, 0.95 mmol) and 4-*t*-butylphenylacetylene (0.37 mL, 2.4 mmol) with stirring at 65 °C for 48 h. The resulting suspension was filtered through silica–gel (ether eluant). The solvent was reduced *in vacuo* and the residue absorbed onto silica and chromatographed on silica–gel, with a gradient elution of hexane/ether (product isolated at 2:3 hexane/ether v/v). **4,7-Bis(4-*t*-butylphenylethynyl)benzothiadiazole [BPEBtd.tBu]** was isolated (290 mg, 70 %) as an orange solid. M.P. = decomposes at 260 °C.

^{1}H NMR ($CDCl_3$, 700 MHz): δ 7.76 (2 H, s, **10**), 7.59 (4 H, d, ^{3}J 8.6 Hz, **5**), 7.41 (4 H, d, ^{3}J 8.6 Hz, **4**), 1.35 (18 H, s, **1**). ^{13}C{^{1}H} NMR ($CDCl_3$, 176 MHz): δ 154.7 (**9 or 11**), 152.7 (**3**), 132.5 (**10**), 132.0 (**5**), 125.7 (**4**), 119.7 (**6**), 117.4 (**11 or 9**), 98.0 (**7**), 85.1 (**8**), 35.1 (**2**), 31.3 (**1**). Acc. MS. (AP+): (m/z) calcd. for $[M + H]^+$ 449.2051; found 449.2048.

Repeated attempts to obtain accurate elemental analysis failed. Consistency was also not obtained.

6.5.4 4,7-bis(4-Aminophenylethynyl)benzothiadiazole [BPEBtd.NH_2]

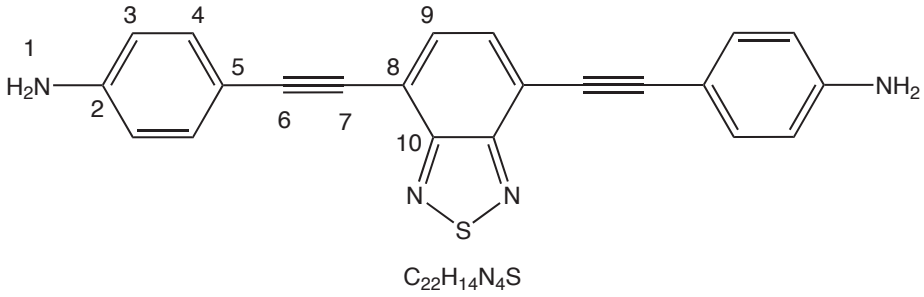

$C_{22}H_{14}N_4S$

Mol. Wt.: 366.44 $gmol^{-1}$

The procedure for **6.4.2** was followed, using 4,7-dibromobenzothiadiazole (300 mg, 0.97 mmol) and 4-ethynylaniline (280 mg, 2.4 mmol) with stirring at 65 °C for 60 h. The resulting suspension was filtered through silica–gel (ether eluant) and the solvent removed *in vacuo*. The brown residue was taken into a minimum amount of hot ether, and cold cyclohexane was added. This caused precipitation of **4,7-bis(4-ethynylaniline)benzothiadiazole [BPEBtd.NH_2]** as a bright red solid (110 mg, 31 %). M.P. = decomposes at 230 °C.

^{1}H NMR ($CDCl_3$, 700 MHz): δ 7.69 (2 H, s, **9**), 7.46 (4 H, d, ^{3}J 8.6 Hz, **4**), 6.66 (4 H, d, ^{3}J 8.6 Hz, **3**), 3.89 (4 H, s, **1**). ^{13}C{^{1}H} NMR ($CDCl_3$, 176 MHz): δ 154.7 (**8 or 10**), 147.5 (**2**), 133.7 (**4**), 132.0 (**9**), 117.3 (**10 or 8**), 114.9 (**3**), 112.1 (**5**), 90.6 (**6**), 84.10 (**7**). Acc. MS. (AP+): (m/z) calcd. for $[M + H]^+$ 367.1017; found 367.1002. Elemental analysis: expected $C_{22}H_{14}N_4S$: C, 72.11 %; H, 3.85 %; N, 15.29 %; found: C, 70.80%; H, 3.86 %; N, 15.64 %.

6.5.5 4,7-bis(4-Methylesterphenylethynyl)benzothiadiazole [BPEBtd.CO_2Me]

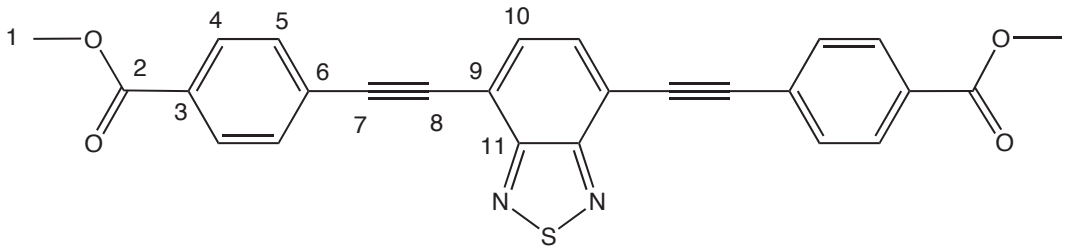

$C_{26}H_{16}N_2O_4S$

Mol. Wt.: 452.48 $gmol^{-1}$

The procedure for **6.4.5** was followed, using 4,7-dibromobenzothiadiazole (168 mg, 0.57 mmol) and 4-methylester phenylacetylene (204 mg, 1.4 mmol), with stirring at 60 °C for 48 h. The resulting suspension was filtered through a silica gel plug (ether eluant) and reduced *in vacuo*. A brown residue remained, which was dry loaded on to silica, and purified by column chromatography on silica gel with gradient elution starting at 100 % hexane (upto 3:2 ether/hexane v/v). **4,7-bis(4-Methylesterphenylacetylene)benzothiadiazole [BPEBtd.CO_2Me]** was isolated as an orange solid (122 mg, 47 %). M.P. = decomposes at 210 °C.

^{1}H NMR ($C_2D_2Cl_4$, 700 MHz): δ 7.99 (4 H, d, ^{3}J 8.4 Hz, **4**), 7.79 (2 H, s, **10**), 6.68 (4 H, d, ^{3}J 8.4 Hz, **5**), 3.86 (6 H, s, **1**). ^{13}C{^{1}H} NMR ($C_2D_2Cl_4$, 176 MHz): δ 166.7 (**2**), 154.5 (**11 or 9**), 133.2 (**10**), 132.3 (**5**), 130.5 (**6**), 129.9 (**4**), 127.3 (**3**), 117.3 (**9 or 11**), 97.0 (**7**), 88.4 (**8**), 52.8 (**1**). Acc. MS. (AP+): (m/z) calcd. for $[M + H]^+$ 453.0909; found 453.0908.

Repeated attempts to obtain accurate elemental analysis failed. Consistency was also not obtained. There was insufficient material for repeated elemental analysis of this compound.

Notes and References

[1] C. K. Chiank, C. R. Fincher, Y. W. Park, A. J. Heeger, H. Shirikawa, E. J. Louis, S. C. Gau and A. G. MacDiarmid, *Phys. Rev. Lett.*, 1977, **39**, 1098–1101.

[2] P. Atkins and J. de Paula, *Atkins' Physical Chemistry*, Oxford University Press, 7^{th} edn., 2002.

[3] G. Moore, *Electronics*, 1965, **38**, 114–117.

[4] R. Carroll and C. Gorman, *Angew. Chem. Int. Ed.*, 2002, **41**, 4379–4400.

[5] U. Bunz, *Chem. Rev.*, 2000, **100**, 1605–1644.

[6] D. T. McQuade, A. E. Pullen and T. M. Swager, *Chem. Rev.*, 2002, **100**, 2537–2574.

[7] S. W. Thomas III, G. D. Joly and T. M. Swager, *Chem. Rev.*, 2007, **107**, 1339–1386.

[8] P. Schwab, M. Levin and J. Michl, *Chem. Rev.*, 1999, **99**, 1863–1933.

[9] K. Sanechika, T. Yamamoto and A. Yamamoto, *Bull. Chem. Soc. Jpn.*, 1984, **57**, 752–755.

[10] J. H. Burroughes, D. D. C. Bradley, A. R. Brown, R. N. Marks, K. Mackay, R. H. Friend, P. L. Burns and A. B. Holmes, *Nature*, 1990, **347**, 539–541.

[11] A. Beeby, S. Bettington, I. Samuel and Z. Wang, *J. Mater. Chem.*, 2003, **13**, 80–83.

[12] A. R. Brown, D. D. C. Bradley, J. H. Burroughes, R. H. Friend, N. C. Greenham, P. L. Burn, A. B. Holmes and A. Kraft, *Appl. Phys. Lett.*, 1992, **61**, 2793–2795.

[13] Q. Zhou and T. M. Swager, *J. Org. Chem.*, 1995, **60**, 7096–7100.

[14] L. Zhao, I. F. Perepichka, F. Turksoy, A. S. Batsanov, A. Beeby, K. S. Findlay and M. R. Bryce, *New J. Chem.*, 2004, **28**, 912–918.

[15] G. Mao, A. Orita, L. Fenenko, M. Yahiro, C. Adachi and J. Otera, *Mater. Chem. Phys.*, 2009, **115**, 378–384.

[16] Y. J. Cheng, S. H. Yang and C. S. Hsu, *Chem. Rev.*, 2009, **109**, 5868–5923.

[17] D. Mühlbacher, M. Scharber, M. Morana, Z. Zhu, D. Waller, R. Gaudiana and C. Brabec, *Adv. Mater.*, 2006, **18**, 2884–2889.

[18] Q. Liu, J. Mao, L. Z, N. Zhang, Y. Wang, L. Yang, S. Yin and Y. Chen, *Nanotechnology*, 2008, **19**, 115601.

[19] Q. Zhou and T. M. Swager, *J. Am. Chem. Soc.*, 1995, **117**, 12593–12602.

[20] J. Yang and T. Swager, *J. Am. Chem. Soc.*, 1998, **120**, 11864–11873.

[21] J. Yang and T. Swager, *J. Am. Chem. Soc.*, 1998, **120**, 5321–5322.

[22] J. Tour, *Acc. Chem. Res.*, 2000, **33**, 791–804.

[23] L. A. Bumm, J. J. Arnold, M. T. Cygan, T. D. Dunbar, T. P. Burgin, L. Jones II, D. L. Allara, J. M. Tour and P. S. Weiss, *Science*, 1996, **271**, 1705–1707.

[24] M. A. Reed, C. Zhou, C. J. Muller, T. P. Burgin and J. M. Tour, *Science*, 1998, **278**, 252–254.

[25] M. Reed, J. Chen, A. Rawlett, D. Price and J. Tour, *Appl. Phys. Lett.*, 2001, **78**, 3735–3737.

[26] A. Beeby, K. S. Findlay, P. J. Low, T. B. Marder, P. Matousek, A. W. Parker, S. R. Rutter and M. Towrie, *Chem. Commun.*, 2003, 2406–2407.

[27] A. Beeby, K. S. Findlay, A. E. Goeta, L. Porrès, S. R. Rutter and A. L. Thompson, *Photochem. Photobiol. Sci.*, 2007, **6**, 982–986.

[28] M. I. Sluch, A. Godt, U. H. F. Bunz and M. A. Berg, *J. Am. Chem. Soc.*, 2001, **123**, 6447–6448.

[29] J. Cornil, Y. Karzazi and J. L. Brédas, *J. Am. Chem. Soc.*, 2002, **124**, 3516–3517.

[30] A. M. Moore, A. A. Dameron, B. A. Mantooth, R. K. Smith, D. J. Fuchs, J. W. Cizwek, F. Maya, Y. Yao, J. M. Tour and P. S. Weiss, *J. Am. Chem. Soc.*, 2006, **128**, 1959–1967.

[31] N. J. Turro, V. Ramamurthy and J. C. Scaiano, *Principles of Modern Photochemistry*, University Science Books, Sausalito, California, 1st edn., 2009.

[32] G. Salvato-Vallverdu, *The perrin–jablonski diagram*, http://www.texample.net/tikz/examples/the-perrin-jablonski-diagram/, 2009.

[33] J. R. Lakowicz, *Principles of Fluorescence Spectroscopy*, Springer, 3rd edn., 2006.

[34] K. S. Findlay, Ph.D. thesis, *A photophysical study of substituted arylethynylenes*, University of Durham, 2007.

[35] G. Drefahl and G. Plötner, *Chem. Ber.*, 1958, **91**, 1280–1285.

[36] C. E. Castro and R. D. Stephens, *J. Org. Chem.*, 1963, **28**, 3313–3315.

[37] C. E. Castro and R. D. Stephens, *J. Org. Chem.*, 1963, **28**, 2163.

[38] K. Sonogashira, Y. Tohda and N. Hagihara, *Tetrahedron Lett.*, 1975, 4467–4470.

[39] P. Nguyen, Z. Yuan, G. Lesley, L. Agocs and T. Marder, *Inorg. Chim. Acta*, 1994, **220**, 289–296.

[40] R. Chinchilla and C. Najera, *Chem. Rev.*, 2007, **107**, 874–922.

[41] P. Bertus, F. Fecourt, C. Bauder and P. Pale, *New J. Chem.*, 2004, **28**, 12–14.

[42] S. R. Rutter, Ph.D. thesis, *Effects of conformation on the electronic and optical properties of aryleneethynylenes*, Durham University, 2007.

[43] P. Bäuerle, *Adv. Mater.*, 1992, **4**, 102–107.

[44] *Oxford instruments dn 1704 optical cryostat*, http://www.oxford-instruments.com/products/low-temperature/opticaland-spectroscopy/optistatdn/PublishingImages/OptistatDN-liquid-nitrogen-LN2-optical-spectroscopy-cryostat-cutaway.jpg, June 2010.

[45] Horiba, *A guide to recording fluorescence quantum yields*, http://www.horiba.com/fileadmin/uploads/Scientific/Documents/Fluorescence/quantumyieldstrad.pdf, July 2010.

[46] L. Porrès, A. Holland, L. Palsson, A. Monkman, C. Kemp and A. Beeby, *J. Fluoresc.*, 2006, **16**, 267–273.

[47] M. J. Frisch, G. W. Trucks, H. B. Schiegel, G. E. Scuseria, M. A. Robb, J. R. Cheeseman, J. A. Montgomery Jr, T. Vreven, K. N. Kudin, J. C. Burant, J. M. Millam, S. S. Iyengar, J. Tomasi, V. Barone, B. Mennucci, M. Cossi, G. Scalmani, N. Rega, G. A. Petersson, H. Nakatsuji, M. Hada, M. Ehara, K. Toyota, R. Fukuda, J. Hasegawa, M. Ishida, T. Nakajima, Y. Honda, O. Kitao, H. Nakai, M. Klene, X. Li, J. E. Knox, R. E. Stratmann, O. Yazyev, A. J. Austin, R. cammi, C. Pomelli, J. W. Ochterski, P. Y. Ayala, K. Morokuma, G. A. Voth, P. Salvador, J. J. Dannenberg, V. G. Zakrzewski, S. Dapprich, A. D. Daniels, M. C. Strain, O. Farkas, M. D. K, A. D.

Rabuck, K. Raghavachari, J. B. Foresman, J. V. Ortiz, Q. Cui, A. G. Baboul, S. Clifford, J. Cioslowski, B. B. Stefanov, G. Liu, A. Liashenko, P. Piskorz, I. Komaromi, R. L. Martin, D. J. Fox, T. Keith, M. A. Al-Laham, C. Y. Peng, A. Nanayakkara, M. Challacombe, P. M. W. Gill, B. Johnson, W. Chen, M. W. Wong, C. Gonzalez and J. A. Pople, *Gaussian 03, revision c.02.*, Gaussian, Inc., Wallingford CT, 2004.

[48] A. D. Becke, *J. Chem. Phys.*, 1993, **98**, 5648–5652.

[49] A. D. Becke, *Phys. Rev. A*, 1988, **38**, 3098–3100.

[50] C. Lee, W. Yang and R. G. Parr, *Phys. Rev. B*, 1988, **37**, 785–789.

[51] S. H. Vosko, L. Wilk and M. Nusair, *Can. J. Phys.*, 1980, **58**, 1200–1211.

[52] P. J. Stephens, F. J. Devlin, C. F. Chabalowski and M. J. Frisch, *J. Phys. Chem.*, 1994, **98**, 11623–11627.

[53] G. Barbarella, M. Melucci and G. Sotgiu, *Adv. Mater.*, 2005, **17**, 1581–1593.

[54] A. Tsumara, H. Koezuka and T. Ando, *Appl. Phys. Lett.*, 1986, **49**, 1210–1212.

[55] A. Assadi, C. Svensson, M. Willander and I. Inganäs, *Appl. Phys. Lett.*, 1988, **53**, 195–197.

[56] D. Fichou, J. M. Nunzi, F. Charra and N. Pfeffer, *Adv. Mater.*, 1994, **6**, 64–67.

[57] D. Fichou, G. Horowitz, B. Xu and F. Garnier, *Synth. Met.*, 1990, **39**, 243–259.

[58] C. D. Dimitrakopoulos and D. J. Mascaro, *IBM J. Res. Dev.*, 2001, **45**, 11–27.

[59] Z. Bao, A. Dodabalapur and A. J. Lovinger, *Appl. Phys. Lett.*, 1996, **69**, 4108–4110.

[60] J. Paloheimo, P. Kuivalainen, H. Stubb, E. Vuorimaa and P. Ylilahti, *Appl. Phys. Lett.*, 1990, **56**, 1157–1159.

[61] F. Garnier, R. Hajlaoui, A. Yassar and P. Srivastava, *Science*, 1994, **265**, 1684–1686.

[62] F. Garnier, A. Yassar, R. Hajlaoui, G. Horowitz, F. Deloffre, B. Servet, S. Ries and P. Alnot, *J. Am. Chem. Soc.*, 1993, **115**, 8716–8721.

[63] S. A. Jenekhe, P. T. Wu, H. Xin, F. S. Kim and G. Ren, *Macromolecules*, 2009, **42**, 8817–8826.

[64] H. Fuchigami, A. Tsumura and H. Koezuka, *Appl. Phys. Lett.*, 1993, **63**, 1372–1374.

[65] A. Dodabalapur, L. Torsi and H. E. Katz, *Science*, 1995, **268**, 270–271.

[66] H. Sirringhaus, R. H. Friend, X. C. Li, S. C. Moratti, A. B. Holmes and N. Feeder, *Appl. Phys. Lett.*, 1997, **71**, 3871–3873.

[67] L. Qiu, W. H. Lee, X. Wang, J. S. Kim, J. A. Lim, D. Kwak, S. Lee and K. Cho, *Adv. Mater.*, 2009, **21**, 1349–1353.

[68] H. Sirringhaus, N. Tessler and R. H. Friend, *Science*, 1998, **280**, 1741–1744.

[69] T. M. Swager and M. J. Marsella, *Adv. Mater.*, 1994, **6**, 595–597.

[70] H. A. Ho, H. Brisset, E. H. Elandaloussi, P. Frere and J. Roncali, *Adv. Mater.*, 1996, **8**, 990–994.

[71] R. H. Friend, S. C. Moratti, R. Cervini, A. B. Holmes, D. R. Baigent, N. C. Greenham, J. Gruner and P. J. Hamer, *Synth. Met.*, 1995, **71**, 2117–2120.

[72] G. Barbarella, L. Favaretto, M. Zambianchi, O. Pudova, C. Arbizzani, A. Bongini and M. Mastragostino, *Adv. Mater.*, 1998, **10**, 551–554.

[73] M. S. Raasch, *J. Org. Chem.*, 1980, **45**, 856–867.

[74] S. Gronowitz, A. Hallberg and G. Nikitidis, *Tetrahedron*, 1987, **43**, 4793–4802.

[75] A. Tsirk, S. Gronowitz and A. Hornfeldt, *Tetrahedron*, 1998, **54**, 9529–9558.

[76] W. J. Bailey and E. W. Cummins, *J. Am. Chem. Soc.*, 1954, **76**, 1932–1936.

[77] G. Barbarella, L. Favaretto, G. Sotgiu, M. Zambianchi, L. Antolini, O. Pudova and A. Bongini, *J. Org. Chem.*, 1998, **63**, 5497–5506.

[78] T. Granlund, M. Theander, M. Berggren, M. Andersson, A. Ruzeckas, V. Sunderström, G. Björk, M. Granström and O. Inganäs, *Chem. Phys. Lett.*, 1998, **288**, 879–884.

[79] G. Gigli, G. Barbarella, L. Favaretto, F. Cacialli and R. Cingolani, *Appl. Phys. Lett.*, 1999, **75**, 439–441.

[80] G. Gigli, O. Inganas, M. Anni, M. De Vittorio, R. Cingolani, G. Barbarella and L. Favaretto, *Appl. Phys. Lett.*, 2001, **78**, 1493–1495.

[81] N. Camaioni, G. Ridolfi, V. Fattori, L. Favaretto and G. Barbarella, *Appl. Phys. Lett.*, 2004, **84**, 1901–1903.

[82] G. Ridolfi, N. Camaioni, P. Samori, M. Gazzano, G. Accorsi, N. Armaroli, L. Favaretto and G. Barbarella, *J. Mater. Chem.*, 2005, **15**, 895–901.

[83] B. Groenendaal, F. Jonas, D. Freitag, H. Pielartzik and J. Reynolds, *Adv. Mater.*, 2000, **12**, 481–494.

[84] S. Oyston, C. Wang, I. Perepichka, A. Batsanov, M. Bryce, J. Ahn and M. Petty, *J. Mater. Chem.*, 2005, **15**, 5164–5173.

[85] K. T. Kamtekar, C. Wang, S. Bettington, A. S. Batsanov, I. F. Perepichka, M. R. Bryce, J. H. Ahn, M. Rabinal and M. C. Petty, *J. Mater. Chem.*, 2006, **16**, 3823–3835.

[86] V. N. Gogte, L. G. Shah, B. D. Tilak, K. N. Gadekar and M. B. Sahasrabudhe, *Tetrahedron*, 1967, **23**, 2437–2441.

[87] J. R. Reynolds, G. A. Sotzing and S. P. J, *Chem. Mater.*, 1996, **8**, 882–889.

[88] J. R. Reynolds, D. J. Irvin and C. J. Dubois Jr, *Chem. Commun.*, 1999, 2121–2222.

[89] A. Berlin, G. Zotti, S. Zecchin, G. Schiavon, M. Cocchi, D. Virgili and C. Sabatini, *J. Mater. Chem.*, 2003, **13**, 27–33.

[90] J. Casado, G. Zotti, A. Berlin, V. Hernandez, R. P. Ortiz and J. T. L. Navarrete, *J. Mol. Struct.*, 2005, **744-747**, 551–556.

[91] V. P. Litvinov and Y. L. Gol'dfarb, *Adv. Heterocyc. Chem.*, 1976, **19**, 123–214.

[92] A. Berlin, G. A. Pagani and F. Sannicolo, *J. Chem. Soc. Chem. Comm.*, 1986, 1663–1664.

[93] K. Kobayashi and Y. Mazaki, *Tetrahedron Lett.*, 1989, **30**, 3315–3318.

[94] W. Wu, Y. Liu and D. Zhu, *Chem. Soc. Rev.*, 2010, **39**, 1489–1502.

[95] X. C. Li, H. Sirringhaus, F. Garnier, A. B. Holmes, S. C. Moratti, N. Feeder, W. Clegg, S. J. Teat and R. H. Friend, *J. Am. Chem. Soc.*, 1998, **120**, 2206–2207.

[96] I. McCulloch, M. Heeney, M. L. Chabinyc, D. DeLongchamp, R. J. Kline, M. Coelle, W. Duffy, D. Fischer, D. Gundlach, B. Hamadani, R. Hamilton, L. Richter, A. Salleo, M. Shkunov, D. Sporrowe, S. Tierney and W. Zhong, *Adv. Mater.*, 2009, **21**, 1091–1109.

[97] O. K. Kim, A. Fort, M. Barzoukas, M. Blanchard-Desce and J. M. Lehn, *J. Mater. Chem.*, 1999, **9**, 2227–2232.

[98] M. Heeney, C. Bailey, K. Genevicius, M. Shkunov, D. Sparrowe, S. Tierney and I. McCulloch, *J. Am. Chem. Soc.*, 2005, **127**, 1078–1079.

[99] I. McCulloch, M. Heeney, C. Bailey, K. Genevicius, I. Macdonald, M. Shkunov, D. Sparrowe, S. Tierney, R. Wagner, W. Zhang, M. L. Chabinyc, R. J. Kline, M. D. McGehee and M. F. Toney, *Nat. Mater.*, 2006, **4**, 328–333.

[100] B. M. Medina, A. Van Vooren, P. Brocorens, J. Gierschner, M. Shkunov, M. Heeney, I. McCulloch, R. Lazzaroni and J. Cornil, *Chem. Mater.*, 2007, **19**, 4949–4956.

[101] K. H. Kim, Z. Chi, M. J. Cho, J.-I. Jin, M. Y. Cho, S. J. Kim, J.-S. Joo and D. H. Choi, *Chem. Mater.*, 2007, **19**, 4925–4932.

[102] C. C. Ko, W. H. Lam and V. W. W. Yam, *Chem. Commun.*, 2008, 5203–5205.

[103] D. F. Perepichka, A. Dadvand, F. Cicoira, K. Y. Chernichenko, E. S. Balenkova, R. M. Osuna, F. Rosei and V. G. Nenajdenko, *Chem. Commun.*, 2008, 5254–5356.

[104] D. R. Rutherford and J. K. Stille, *Macromolecules*, 1988, **21**, 3530–3532.

[105] M. Takagi, K. Kizu, Y. Miyazaki, T. Maruyama, K. Kubota and T. Yamamoto, *Chem. Lett.*, 1993, 913–916.

[106] T. Yamamoto, M. Takagi, K. Kizu, T. Maruyama, K. Kubota, H. Kanbara, T. Kurihara and T. Kaino, *J. Chem. Soc. Chem. Comm.*, 1993, 797–798.

[107] T. Yamamoto, W. Yamada, M. Takagi, K. Kizu, T. Maruyama, N. Ooba, S. Tomaru, T. Kurihara, T. Kaino and K. Kubota, *Macromolecules*, 1994, **27**, 6620–6626.

[108] K. Thomas and J. Lin, *J. Organomet. Chem.*, 2001, **637**, 139–144.

[109] S. H. Eichorn, A. J. Paraskos, K. Kishikawa and T. M. Swager, *J. Am. Chem. Soc.*, 2002, **124**, 12742–12751.

[110] J. G. Rodgriguez, L. A, R. L and E. J, *Tetrahedron Lett.*, 2004, **45**, 7061–7064.

[111] N. Tanifuji, M. Irie and K. Matsuda, *J. Am. Chem. Soc.*, 2005, **127**, 13344–13353.

[112] T. Yasuda, T. Imase, Y. Nakamura and T. Yamamoto, *Macromolecules*, 2005, **38**, 4687–4697.

[113] J. G. Rodgriguez, E. J, L. A and R. L, *Tetrahedron*, 2006, **62**, 3112–3122.

[114] J. S. Siddle, R. M. Ward, J. C. Collins, S. R. Rutter, L. Porrès, L. Applegarth, A. Beeby, A. S. Batsanov, A. L. Thompson, J. A. K. Howard, A. Boucekkine, K. Costuas, J.-F. Halet and T. B. Marder, *New J. Chem.*, 2007, **31**, 841–851.

[115] P. Lind, M. Carlsson, B. Eliasson, E. Glimsdal, M. Lindgren, C. Lopes, L. Boman and P. Norman, *Mol. Phys.*, 2009, **107**, 629–641.

[116] J. Tour, R. Wu, J. S. Schumm and D. L. Pearson, *J. Org. Chem.*, 1996, **61**, 6906–6921.

[117] G. Zotti, G. Schiavon, S. Zecchin and A. Berlin, *Synth. Met.*, 1998, **97**, 245–254.

[118] T. Yamamoto, I. Nurulla, H. Hayashi and H. Koinuma, *Synth. Met.*, 1999, **107**, 137–141.

[119] D. P. Lydon, L. Porrès, A. Beeby, T. B. Marder and P. J. Low, *New J. Chem.*, 2005, **29**, 972–976.

[120] S. J. Greaves, E. L. Flynn, E. L. Futcher, E. Wrede, D. P. Lydon, P. J. Low, S. R. Rutter and A. Beeby, *J. Phys. Chem. A*, 2006, **110**, 2114–2121.

[121] A. Beeby, K. S. Findlay, P. J. Low and T. B. Marder, *J. Am. Chem. Soc.*, 2002, **124**, 8280–8284.

[122] Y. Miyahara and T. Inazu, *Tetrahedron Lett.*, 1990, **31**, 5955–5958.

[123] J. Nakayama, H. Nagasawa, Y. Sugihara and A. Ishii, *J. Am. Chem. Soc.*, 1997, **119**, 9077–9078.

[124] J. Nakayama, H. Nagasawa, Y. Sugihara and A. Ishii, *Heterocycles*, 2000, **52**, 365–382.

[125] R. Ballini, E. Marcantoni and M. Petrini, *Tetrahedron Lett.*, 1992, **33**, 4835–4838.

[126] V. Nenajdenko, A. Gavryushin and E. Balenkova, *Tetrahedron Lett.*, 2001, **42**, 4397–4399.

[127] N. Furukawa, H. Hoshiai, T. Shibutani, M. Higaki, F. Iwasaki and H. Fujihara, *Heterocycles*, 1992, **34**, 1085–1088.

[128] S. Rozen and Y. Bareket, *J. Chem. Soc. Chem. Comm.*, 1994, 1959.

[129] S. Rozen and Y. Bareket, *J. Org. Chem.*, 1997, **62**, 1457—1462.

[130] E. Amir and S. Rozen, *Angew. Chem. Int. Ed.*, 2005, **44**, 7374—7378.

[131] F. Tran-Van, S. Garreau, G. Louarn, G. Froyer and C. Chevrot, *J. Mater. Chem.*, 2001, **11**, 1378–1382.

[132] H. J. Spencer, P. J. Skabara, M. Giles, I. McCulloch, S. J. Coles and M. B. Hursthouse, *J. Mater. Chem.*, 2005, **15**, 4783–4792.

[133] H. Meng, D. F. Perepichka, M. Bendikov, F. Wudl, G. Z. Pan, W. Yu, W. Dong and S. Brown, *J. Am. Chem. Soc.*, 2003, **125**, 15151–15162.

[134] P. Frère, P. Leriche, J.-M. Raimundo, M. Turbiez, V. Monroche, F.-X. Sauvage, J. Roncali and P. Skabara, *J. Mater. Chem.*, 2003, **13**, 1324–1332.

[135] B. Iddon, L. Fuller and K. Smith, *J. Chem. Soc. Perkin Trans.*, 1997, 3465–3470.

[136] S. Jung, H. Kim, S. Kim, Y. Kim, S. Jeoung and D. Kim, *Macromolecules*, 2000, **33**, 9277–9288.

[137] E. Lim, B. J. Jung and H. K. Shim, *Macromolecules*, 2003, **36**, 4288–4293.

[138] A. Campbell, M. Gather, M. Heeney, W. Zhang, K. Whitehead, D. Bradley and I. McCulloch, *Chem. Commun.*, 2008, 1079–1081.

[139] A. J. Matzger, L. San Miguel and W. W. Porter III, *Org. Lett.*, 2007, **9**, 1005–1008.

[140] M. Turbiez, P. Frére, P. Leriche, N. Mercier and J. Roncali, *Chem. Commun.*, 2005, 1161–1163.

[141] L. De Cremer, T. Verbiest and G. Koeckelberghs, *Macromolecules*, 2008, **41**, 568–578.

[142] S. Gronowitz and B. Persson, *Acta Chem. Scand.*, 1967, **21**, 812–813.

[143] R. L. P. de Jong and L. Brandsma, *J. Chem. Soc. Chem. Comm.*, 1983, 1056–1057.

[144] T. Otsubo, Y. Kono, N. Hozo, Y. A. Miyamoto, F. Ogura, T. Tanaka and M. Sawada, *Bull. Chem. Soc. Jpn.*, 1993, **66**, 2033–2041.

[145] G. Kirsch and A. Comel, *J. Heterocyclic Chem.*, 2001, **38**, 1167–1171.

[146] C. Wang, L. Pålsson, A. Batsanov and M. Bryce, *J. Am. Chem. Soc.*, 2006, **128**, 3789–3799.

[147] A. Pace and P. Pierro, *Org. Biomol. Chem.*, 2009, **7**, 4337–4348.

[148] C. W. Tang and S. A. VanSlyke, *Appl. Phys. Lett.*, 1987, **51**, 913–915.

[149] C. Adachi, S. Tokito, T. Tsutsui and S. Saito, *Jpn. J. Appl. Phys.*, 1988, **27**, L269–L271.

[150] S. Saito, C. Adachi and T. Tsutsui, *Appl. Phys. Lett.*, 1989, **55**, 1489–1491.

[151] C. Adachi, T. Tsutsui and S. Saito, *Appl. Phys. Lett.*, 1990, **56**, 799–801.

[152] S. Aratini, C. Zhang, K. Pakbaz, F. Wudi, S. Höger and A. J. Heeger, *J. Electron. Mater.*, 1993, **22**, 745–749.

[153] C. Zhang, S. Höger, K. Pakbaz, F. Wudl and A. J. Heeger, *J. Electron. Mater.*, 1994, **23**, 453–458.

[154] M. Yoshida, H. Kawahara, A. Fujii, Y. Ohmori and K. Yoshino, *Jpn. J. Appl. Phys.*, 1995, **34**, L1237–L1240.

[155] W. Huang, H. Meng, W. Yu, J. Gao and A. Heeger, *Adv. Mater.*, 1998, **10**, 593–596.

[156] C. Wang, G. Jung, Y. Hua, C. Pearson, M. Bryce, M. Petty, A. Batsanov, A. Goeta and J. Howard, *Chem. Mater.*, 2001, **13**, 1167–1173.

[157] C. Wang, G. Jung, A. Batsanov, M. Bryce and M. Petty, *J. Mater. Chem.*, 2002, **12**, 173–180.

[158] G. Hughes and M. R. Bryce, *J. Mater. Chem.*, 2005, **15**, 94–107.

[159] T. Yasuda, T. Imase, S. Sasaki and T. Yamamoto, *Macromolecules*, 2005, **38**, 1500–1503.

[160] P. B. Ghosh and M. W. Whitehouse, *Biochem. J.*, 1968, **108**, 155–156.

[161] A. Chattopadhyay, *Chem. Phys. Lipids.*, 1990, **52**, 1–15.

[162] I. Dufau and H. Mazarguil, *Tetrahedron Lett.*, 2000, 6063–6066.

[163] E. Pazos, O. Vázquez, M. as J L and M. E. Vázquez, *Chem. Soc. Rev.*, 2009, **38**, 3348–3359.

[164] A. Pexa, K. Fischer, A. Deussen and T. Henle, *Eur. Food. Res. Technol.*, 2008, **226**, 933–935.

[165] R. Haselberg, C. Hempen, S. van Leeuwen, M. Vogel and U. Karst, *J. Chromatogr. B*, 2006, **830**, 47–53.

[166] N. C. Price and M. Cohn, *J. Biol. Chem.*, 1975, **250**, 644–652.

[167] K. K. Sadhu, B. Bag and P. K. Bharadwaj, *Inorg. Chem.*, 2007, **46**, 8051–8058.

[168] B. Bag and P. K. Bharadwaj, *Inorg. Chem.*, 2004, **43**, 4626–4630.

[169] M. Boiocchi, L. Fabbrizzi, M. Licchelli, D. Sacchi, M. Vázquez and C. Zampa, *Chem. Commun.*, 2003, 1812–1813.

[170] S. H. Kim, J. S. Kim, S. M. Park and S. K. Chang, *Org. Lett.*, 2006, **8**, 371–374.

[171] G. Ambrosi, S. Ciattini, M. Formica, V. Fusi, L. Giorgi, E. Macedi, M. Micheloni, P. Paulo, P. Rossi and G. Zappia, *Chem. Commun.*, 2009, 7039–7041.

[172] N. Wanichacheva, M. Siriprumpoonthum, A. Kamkaew and K. Grudpan, *Tetrahedron Lett.*, 2009, **50**, 1783–1786.

[173] M. Bernius, M. Inbasekaran, E. Woo, W. Wu and L. Wujkowski, *J. Mater. Sci.- Mater. Electron.*, 2000, **11**, 111–116.

[174] M. T. Bernius, M. Inbasekaran, J. O'Brien and W. Wu, *Adv. Mater.*, 2000, **12**, 1737–1750.

[175] X. Zhang, H. Gorohmara, M. Kadowaki, T. Kobayashi, T. Ishi-i, T. Thiemann and S. Mataka, *J. Mater. Chem.*, 2004, **14**, 1901–1904.

[176] S. Kato, T. Matsumoto, T. Ishi-i, T. Thiemann, M. Shigeiwa, H. Gorohmara, S. Maeda, Y. Yamashita and S. Mataka, *Chem. Commun.*, 2004, 2342–2343.

[177] N. Blouin, A. Michaud, D. Gendron, S. Wakim, E. Blair, R. Neagu-Plesu, M. Belletete, G. Durocher, Y. Tao and M. Leclerc, *J. Am. Chem. Soc.*, 2008, **130**, 732–742.

[178] B. A. D. Neto, A. A. M. Lapis, F. S. Manchilha, I. B. Vasconcelos, C. Thum, L. A. Basson, D. S. Santos and J. Dupont, *Org. Lett.*, 2007, **9**, 4001–4004.

[179] C. Kitamura, S. Tanaka and Y. Yamashita, *Chem. Mater.*, 1996, **8**, 570–578.

[180] J. Bouffard and T. M. Swager, *Macromolecules*, 2008, **41**, 5559–5562.

[181] C. G. Bangcuyo, U. Evans, M. L. Myrick and U. H. F. Bunz, *Macromolecules*, 2001, **34**, 7592–7594.

[182] M. Akhtaruzzaman, M. Tomura, M. B. Zaman, J. I. N. Nishida and Y. Yamashita, *J. Org. Chem.*, 2002, **67**, 7813–7818.

[183] M. J. Edelmann, J.-M. Raimundo, N. F. Utesch and F. Diederich, *Helv. Chim. Acta*, 2002, **85**, 2195–2213.

[184] B. Neto, A. Lopes, G. Ebeling, R. Goncalves, V. Costa, F. Quina and J. Dupont, *Tetrahedron*, 2005, **61**, 10975–10982.

[185] A. A. Vieira, R. Cristiano, A. J. Botoluzzi and H. Gallardo, *J. Mol. Struct.*, 2008, **875**, 364–371.

[186] T. Agou, T. Kojima, J. Kobayashi and T. Kawashima, *Org. Lett.*, 2009, **11**, 3534–3537.

[187] E. Hamciuc, M. Bruma, T. Kopnick, Y. Kaminorz and B. Schulz, *Polymer*, 2001, **42**, 1809–1815.

[188] A. R. Katritzky, P. P. Mohapatra and L. Huang, *Arkivoc*, 2008, 62–68.

[189] A. R. Katritzky, J. W. Rogers, R. M. Witek and S. K. Nair, *Arkivoc*, 2004, 52–60.

[190] H. N. Al-Jallo, *Tetrahedron Lett.*, 1970, 875–876.

[191] A. J. Boulton, P. B. Ghosh and A. R. Katritzky, *J. Chem. Soc. (B)*, 1966, 1004–1011.

[192] M. E. Salvati, J. A. Balog, D. A. Pickering, S. Giese, A. Fura, W. Li, R. N. Patel, R. L. Hanson, T. Mitt, J. Y. Roberge, J. R. Corte, S. H. Spergel and R. A. Rampulla, *Fused heterocyclic succinimide compounds and analogs thereof, modulators of nuclear hormone receptor function*, Patent PCT/US02/40598, 2001.

[193] F. S. Mancilha, B. A. DaSilveira Neto, A. S. Lopes, J. Moreira Paulo F., F. H. Quina, R. S. Goncalves and J. Dupont, *Eur. J. Org. Chem.*, 2006, 4924–4933.

[194] B. Neto, A. Lopes, M. Wust, V. Costa, G. Ebeling and J. Dupont, *Tetrahedron Lett.*, 2005, **46**, 6843–6846.

[195] P. Zanello, *Inorganic electrochemistry: theory, practice and application*, RSC, 2003.

[196] P. Wiggins, J. Williams and D. Tozer, *J. Chem. Phys.*, 2009, **131**, 091101.

[197] P. Raithby, P. Li, B. Athrens, N. Feeder, S. Teat and M. Khan, *Dalton Trans.*, 2005, 874–883.

Appendix A

Throughout this thesis compounds have been assigned a short code, derived in a similar manner to that for 1,4-bis(phenylethynyl)benzene - **BPEB**. This is the standard short–hand nomenclature for this three–ring oligomer. As such, given the nature of the systems prepared for this work, the final compounds have been assigned similar short–hand abbreviations (see left hand column).

* denotes literature compounds.

CODE	STRUCTURE	NAME
BPEB*	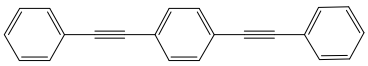	1,4-bis(phenylethynyl) benzene [34, 121]
BPET*	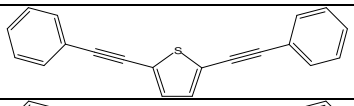	2,5-bis(phenylethynyl) thiophene [114]
BPETO$_2$	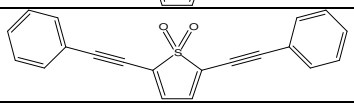	2,5-bis(phenylethynyl) thiophene-1,1-dioxide
BPETO$_2$.OMe	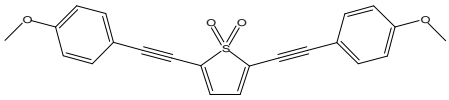	2,5-bis(4-methoxy phenylethynyl)thiophene-1,1-dioxide
BPEEDOT*	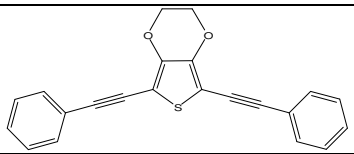	2,5-bis(phenylethynyl)-3,4-ethylenedioxythiophene [42]
BPEEDOT.OMe	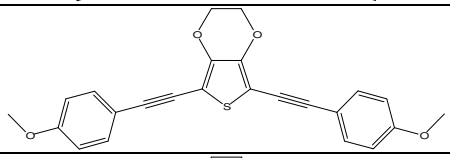	2,5-bis(4-methoxyphenylethynyl) -3,4-ethylenedioxy thiophene
BPEEDOT.CN	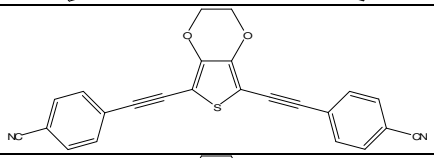	2,5-bis(4-cyanophenylethynyl) -3,4-ethylenedioxy thiophene
BPEEDOTO$_2$. tBu	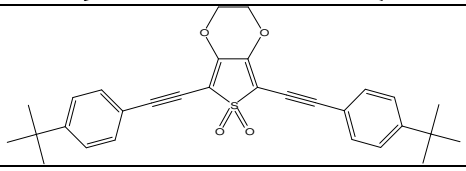	2,5-bis(phenylethynyl)-3,4-ethylenedioxy thiophene-1,1-dioxide
BPEantTT.tBu	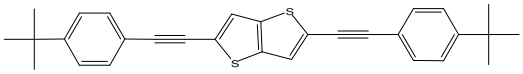	2,5-bis(4-*t*-butylphenylethynyl) thieno[3,2-*b*] thiophene
BPEantTT.OMe	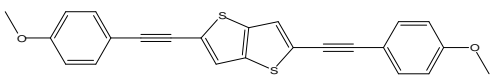	2,5-bis(4-methoxyphenylethynyl) thieno[3,2-*b*] thiophene
BPEantXTT.tBu	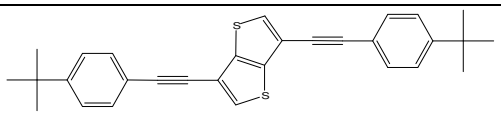	3,6-bis(4-*t*-butyl phenylethynyl) thieno[3,2-*b*] thiophene
BPEsynTT	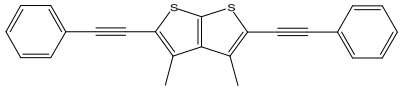	2,5-bis(phenylethynyl)-3,4-dimethylthieno [2,3-*b*]thiophene

Appendix A

CODE	STRUCTURE	NAME
BPEOx	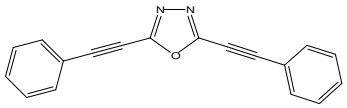	2,5-bis(phenylethynyl)-1,3,4-oxadiazole
BPETd*	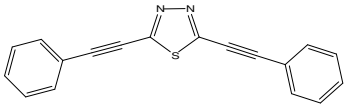	2,5-bis(phenylethynyl)-1,3,4-thiadiazole [159]
BPEBf	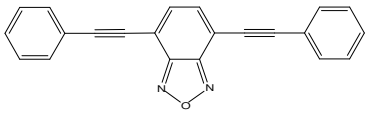	4,7-bis(phenylethynyl) benzofurazan
BPEBf.tBu	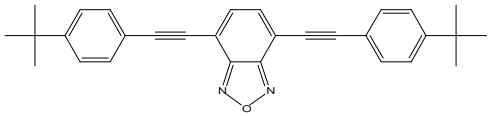	4,7-bis(4-*t*-butylphenylethynyl) benzofurazan
BPEBf.OMe	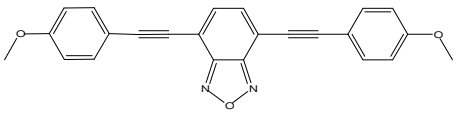	4,7-bis(4-methoxyphenylethynyl) benzofurazan
BPEBf.NH_2	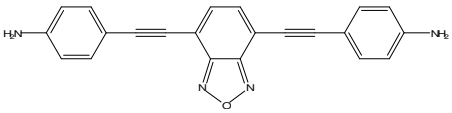	4,7-bis(4-aminophenylethynyl) benzofurazan
BPEBf.CO_2Me	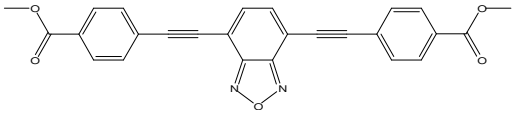	4,7-bis(4-methylester phenylethynyl) benzofurazan
PEBf	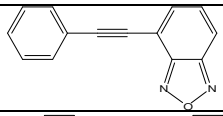	4-(phenylethynyl) benzofurazan
PEBf.NH_2	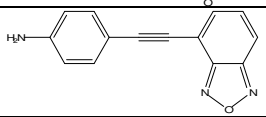	4-(4-aminophenylethynyl) benzofurazan
BBfEB	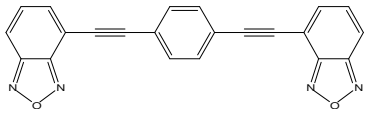	1,4-bis(phenylethynyl) benzene
BPEBtd*	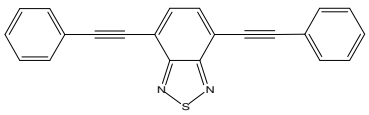	4,7-bis(phenylethynyl) benzothiadiazole [183]
BPEBtd.tBu	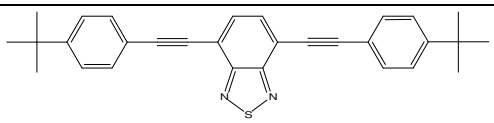	4,7-bis(phenylethynyl) benzothiadiazole
BPEBtd.NH_2	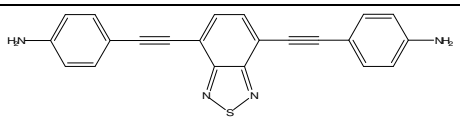	4,7-bis(4-aminophenylethynyl) benzothiadiazole
BPEBtd.CO_2Me	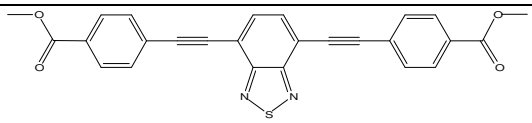	4,7-bis(4-methylesterphenylethynyl) benzothiadiazole

NB. **BPEBtd** has been reported previously in the literature but was prepared for study in the course of this work.